UNIVERSITE MONTPELLIER II
SCIENCES ET TECHNIQUES DU LANGUEDOC

THESE

pour obtenir le grade de

DOCTEUR DE L'UNIVERSITE MONTPELLIER II

Discipline : Biologie Intégrative des Plantes

Spécialité complémentaire : Modélisation

Ecole Doctorale : SIBAGHE

Flux d'Auxine et Ramification Racinaire chez Arabidopsis thaliana : Vers une Racine Virtuelle.

présentée et soutenue publiquement

par

Mikaël LUCAS

Soutenue le 03 juillet 2008

JURY

M.	Jan TRAAS	Président
M.	Christian JAY-ALLEMAND	Directeur de Thèse
M.	Christophe GODIN	Directeur de Thèse
M.	Michel MORVAN	Rapporteur
M.	Tom BEECKMAN	Rapporteur
M.	Alain GOJON	Examinateur
M.	Laurent LAPLAZE	Invité

« *As Above, So Below* »

Emerald Tablet of Hermes Trismegistus

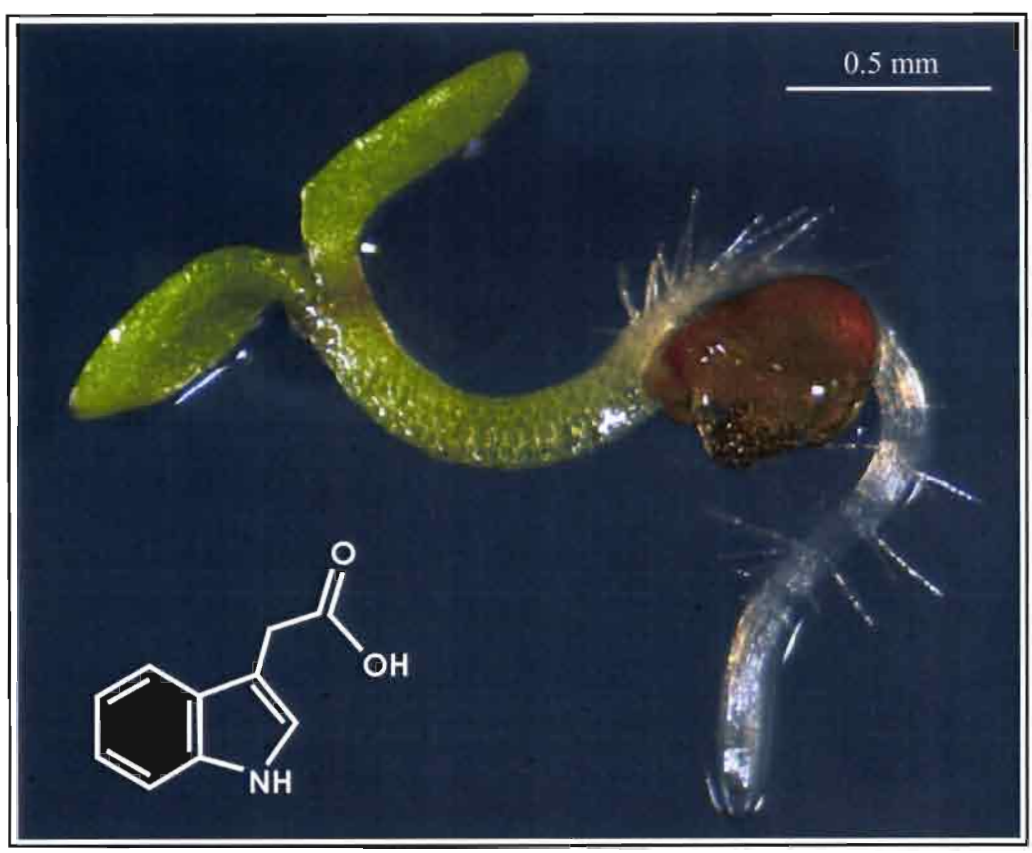

Figure 1. ***Arabidopsis thaliana*** **seedling**
The red-brown seed is still visible. In the corner is represented the chemical formula of one of the main plant hormone, auxin or 3-indol-acetic acid (IAA).

A Charlène, ma Dame de Cœur,

Une chance formidable qui ne manque pas de piment.

Acknowledgments

Mon premier merci est avant tout et sans aucun doute pour Laurent. Merci de ta gentillesse, de ta disponibilité, et de ton enthousiasme. S'il m'est donné d'être un jour chercheur, j'espère pouvoir me montrer digne de ton exemple et te faire honneur.

Mes deux mercis suivants vont à Christophe et Christian. Il n'a pas toujours été aisé de trouver un moment pour discuter, mais même si le temps vous manquait, vous l'avez toujours pris pour moi, ce dont je vous suis profondément reconnaissant. Sans vous ce projet n'aurait jamais pu voir le jour, et pour cela encore un immense merci à tous les deux.

Merci à Jan Traas, Michel Morvan, Tom Beckmann, et Alain Gojon d'avoir accepté de faire partie de mon jury et de juger mes travaux. Votre présence m'honore et j'espère que vous m'en trouverez digne.

Merci à tous les membres de l'Université pour leur accueil chaleureux et pour toutes les discussions que nous avons pu avoir. Merci à Christine, merci à Yves, merci à Marc, merci à Luc, merci à Pascal et à tous ceux que j'ai pu croiser un jour au détour d'un couloir.

Merci à tous les membres de l'équipe Rhizogenèse pour leur gentillesse, leur aide, leur camaraderie. Merci à Didier de m'avoir accueilli au sein de l'équipe, merci à Claudine, Valérie, Florence, Hassen, Sergio, Patrick, Benjamin, Mame, Mariana et à tous les stagiaires pour tous les bons moments que nous avons pu passer ensemble.

Merci à toute l'équipe VirtualPlants, que j'ai eu la chance de voir naître et grandir. Le bébé est beau, les premiers pas arrivent, souhaitons que beaucoup d'autres suivent. Merci donc à Jérome, Szymon, Fréderic, Samuel, David, Florence, Vincent, Romain, Damien, Valérie, Annie, Christophe P., Yan et Evelyne.

Merci également à toute l'équipe avec qui j'ai agréablement partagé la folle aventure de l'enseignement. Merci à Michel, Lydia, Pierre, Laurence, Cécile R., Cécile M., et ceux que j'oublie. Merci aussi à tous ces élèves qui m'ont subi pendant ces 3 années, je pense que nous en aurons tous tiré quelque chose…

Un simple mais non moins profond merci à tous mes amis et à ma famille, sans qui je ne serais pas celui que je suis aujourd'hui. Merci à mes parents et à mes frères pour leur affection et leur présence. Merci enfin à toi ma Dame de Cœur, pour tous ces instants de bonheur passé, présent et à venir.

Du fond du cœur, à tous, merci.

Table of Contents

Index of Figures

DVD Contents

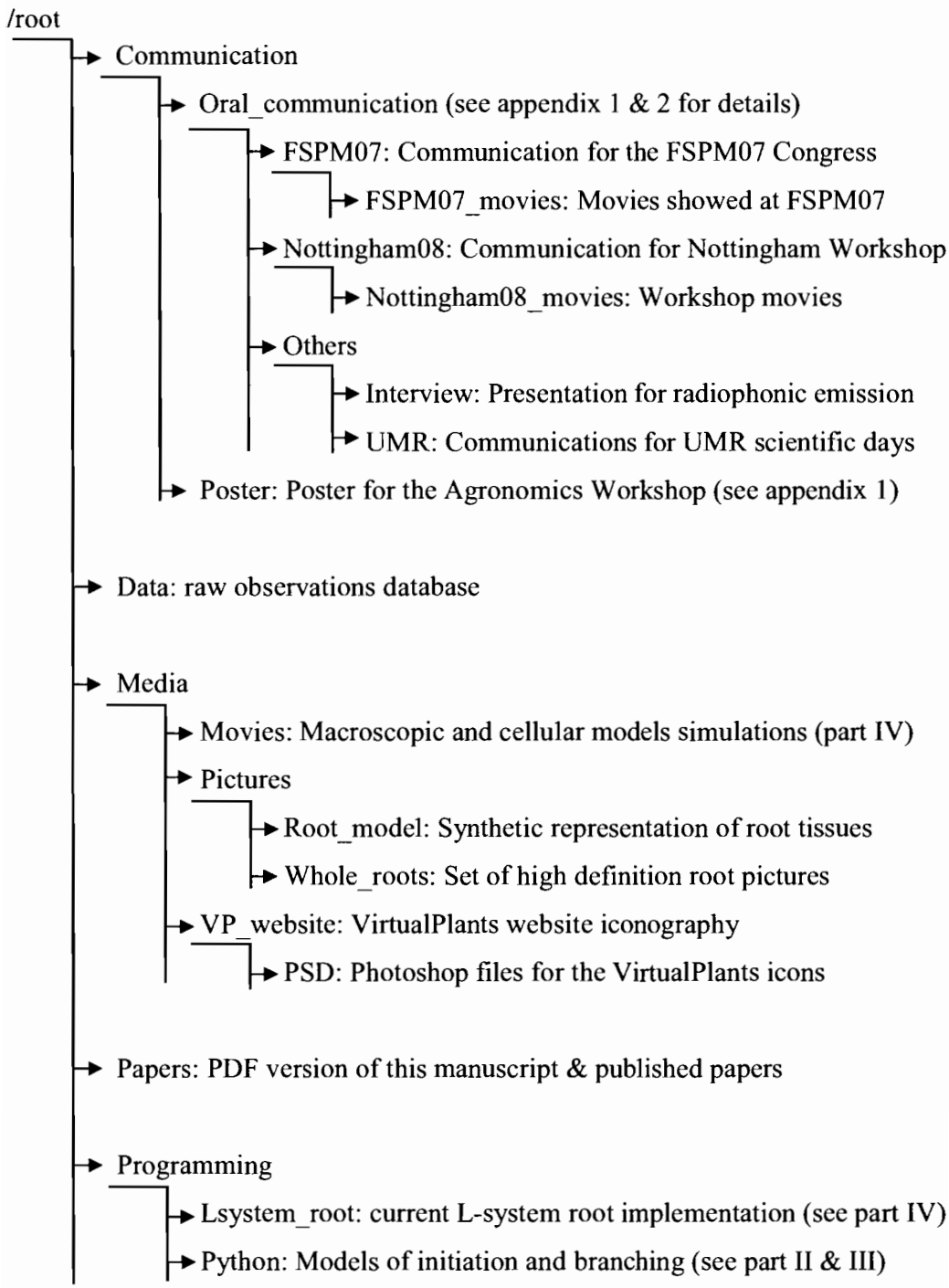

Main Abbreviations

	2,4,5T	**2,4,5 T**richlorophenoxyacetic acid - an auxin analogue
	2,4D	**2,4 D**ichlorophenoxyacetic acid - an auxin analogue
A		
	AIB	3-**I**ndol-5-**B**utyric **A**cid - an auxin analogue
	ARF(s)	**A**uxin **R**esponse **F**actor(s)
	Aux/IAA	**Aux**in/**I**ndole-3-**A**cetic **A**cid transcription factor
	AUX1 / aux1	***AUX1** gene / mutant* - auxin influx carrier
	aux1-22	a null mutant of ***AUX1***
	AuxRE	**Aux**in **R**esponse **E**lement
	AXR3 / axr3	**AuX**in **R**esistant 3 *gene / mutant*
C		
	Col-0	**Col**umbia ecotype of *Arabidopsis thaliana*
D		
	DMF	**D**i**M**ethyl**F**ormamide
	DNA	**D**eoxyribo**N**ucleic **A**cid
	DR5	synthetic promoter formed by tandem repetitions of **AuxRE**
	$(DS)^2$	**D**ynamical **S**ystem in **D**ynamical **S**tructure
E		
	EDTA	**E**thylen-**D**iamine **T**etra-**A**cetic acid
G		
	GUS	β-glucuronidase
I		
	IAA	**I**ndole **A**cetic **A**cid - auxin
	IAA^-	Ionic form of **IAA**
	IAAH	Protonated form of **IAA**
J		
	J0951	GAL4 line specific of the root epidermis and lateral root cap
L		
	LAX1-3 / lax1-3	**L**ike **AUX1** *gene / mutant* - a family of auxin influx carriers
	LR	**L**ateral **R**oot (emerged)
	LRI	**L**ateral **R**oot **I**nitiation
	LRP	**L**ateral **R**oot **P**rimordium
M		
	M0013	GAL4 line specific of the lateral root cap
	MDR/PGP	**M**ulti **D**rug **R**esistant / **P**-**G**lyco**P**rotein – auxin efflux carrier
N		
	NAA	1-**N**apthalene**A**cetic **A**cid - an auxin analogue
P		
	PIN1-7 / pin1-7	***PIN** gene / mutant* - a family of auxin efflux carriers
	Pro_{CYCB1}	promoter specific of **CYC**lin **B1**
S		
	SCF^{TIR1}	proteinubiquitin ligase complex
T		
	TIR1	F-Box protein - intracellular receptor of auxin
U		
	UAS-GAL4	System of gene transactivation based on **U**pstream **A**ctivating **S**equence and their interaction with the Yeast transcription factor **GAL4**
	uidA	β-glucuronidase

Preface

Unlike animal development, plant development is essentially post-embryonic. The mature form of plants is not pre-existent from the start, but rather arises from complex interactions between growing plants and their environment. Environmental cues can be either biotics, ranging from micro-organisms to herbivorous predators, or abiotics, such as light, temperature, hygrometry or gravity. As plants are sessile and cannot escape from their predators or search for resources by simply moving around, all responses to the environment must come either from biochemical/physiological adaptations or from alteration of the developmental pathways. The latter alterations can affect pre-existing organs, bending or reinforcing them through differential cell growth or differentiation. They can also occur upstream of organ formation, inhibiting or promoting the creation of new organs.

In all cases, plants integrate stimuli at a microscopic level, and tune their development through complex signaling systems. One of the main components of these signaling systems is auxin. This hormone has been extensively studied in the last decades for its roles in the control of plant development. It has been shown to affect a large array of apparently unrelated processes, sometime in contradictory fashions. For example, auxin promotes cell growth in the stem, while inhibiting it in the root.

As genetic and molecular studies progress, the precise action mode of auxin is starting to appear more and more clearly. The regulation of auxin production and transport throughout the plant now appears as the principal determinant of auxin-controlled development. One of the most important

advances in the field of auxin study was the invention of molecular markers of auxin presence such as the DR5 promoter, allowing biologist to directly observe sites of auxin perception in developing plants. Combined with the molecular knowledge acquired on auxin transporters, it led to the design of complex conceptual models of fluxes seeking to explain how auxin regulates organ formation and growth at the cellular level, and how this regulation give rise to complex macroscopic forms.

The complexity of these concepts is often an obstacle for their full comprehension. Fortunately, the abstractive power of mathematics and computer sciences can be used to simplify these concepts, integrate them in true logical or dynamical models, and study the specific properties of these models, gaining hindsight on the biological processes they represent.

Here, we will present a study of root development in *Arabidopsis thaliana*, and its interaction with auxin. We used a mix of biology to investigate physiological processes and mathematical / *in silico* modelling to rationalize our findings, and finally conceive an integrated view of root branching and its auxin regulation.

- PART I -

General Introduction

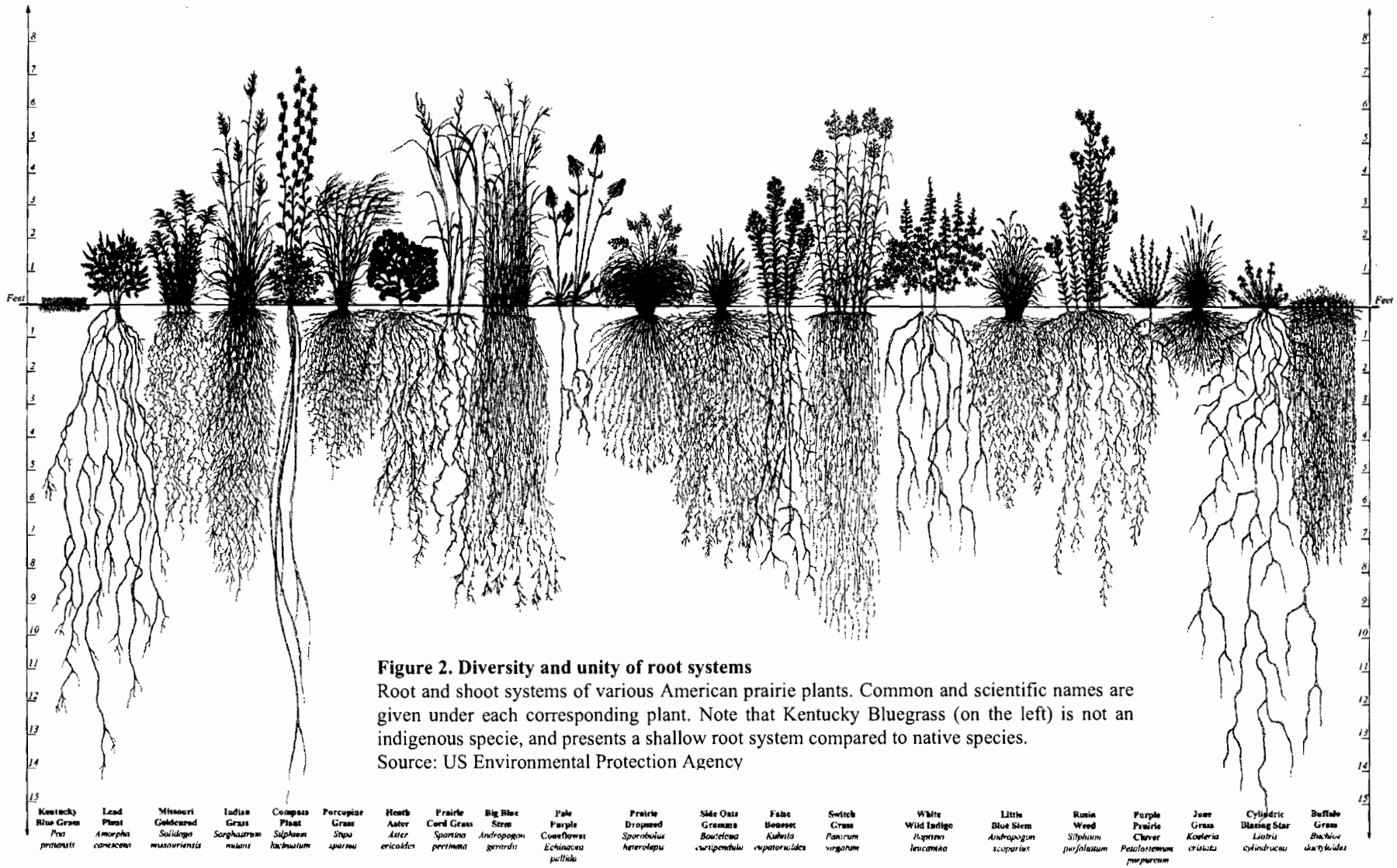

Figure 2. Diversity and unity of root systems

Root and shoot systems of various American prairie plants. Common and scientific names are given under each corresponding plant. Note that Kentucky Bluegrass (on the left) is not an indigenous specie, and presents a shallow root system compared to native species.

Source: US Environmental Protection Agency

In this first chapter, we will present the current understanding of root structure and development, of their relationship with auxin, and how this understanding came to be. Whenever possible, we will compare root and stem development in order to draw the parallels and differences between those two systems, both controlled by auxin.

I) Root Superstructure and Anatomy

I.A) Nature and roles of root systems

Wondering about the nature of the root system can appear as a rather superficial question at first, as one simple way to define the root system would be to consider that it is the sum of plant organs growing underground, while the stem is the sum of organs growing in the open air. However, some plants present aerial roots growing above the ground, or aerating roots growing upward and emerging from the soil, while others support stems growing underground, such as rhizomes.

The best way to define the root system then would be to resume it to its two major functions. The first one is the absorption of water and inorganic nutrients. The second major function of roots is to provide anchorage for the plant, be it underground or over other hard surfaces (for example ivy aerial roots clinging to walls). Roots can assume other functions in specific cases, such as for example the previously evoked aerating roots (a.k.a. pneumatophores) assuring gas exchange in mangrove, haustorial roots of parasitic plants (such as mistletoe) absorbing water and nutrient from another plant, or storage roots modified for water and nutrient storage (for example in carrots and beets).

In all cases, the efficiency of the root system in his role is mainly determined by a single factor: its architecture. As in the stem system, architecture is the key to exploration of neighboring space and gathering of available resources while in competition with other organisms.

I.B) Root systems as branching structures

As illustrated in Figure 2, root architecture appears outwardly as extremely diverse. Moreover, while stems present repetitive nodes defined by the presence of leaves and axillaries buds and called phytomers, roots appear devoid of such repetitive patterns, seeming almost chaotic (Figure 3).

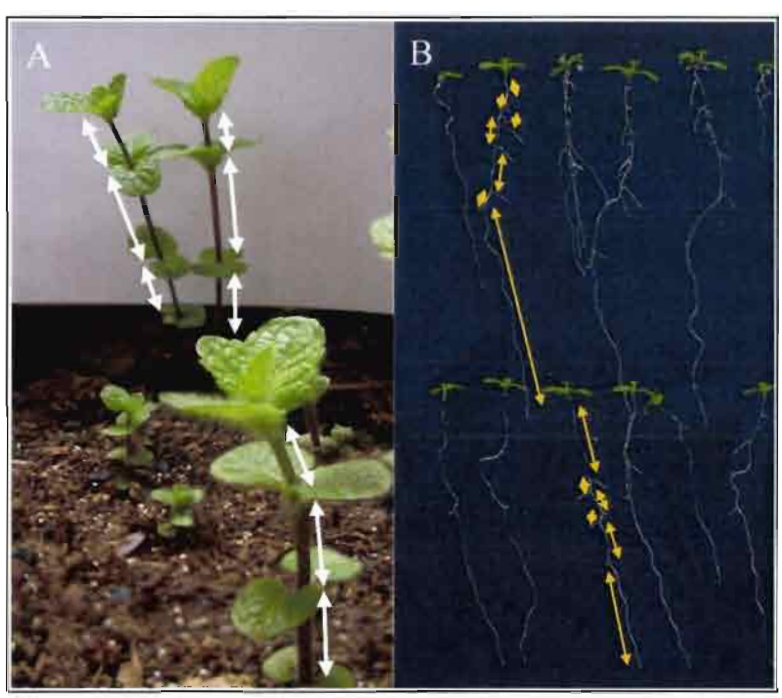

Figure 3. Comparison of stem and root architectures
A – Mint stem shows a highly regular and modular organisation while growing in wilderness. White arrows mark the phytomers.
B – Arabidopsis root architecture is highly variable despite homogenous growth conditions *in vitro*. Orange arrows mark root segment defined by the successive lateral roots.

Lateral roots, the root system rough equivalent to the axillaries buds present at the level of each phytomers in stems, appear dispersed without order

or regularity along the longitudinal root axis. One feature is however common between the root and stem systems: they are both ramified, iterative structures. The basic element of branching, whether lateral branch or lateral root, is repeated throughout the architecture and this repetition defines successive branching scales. Thus, the architecture of stem and root, however complex it may appear, can be fully characterized using two types of information: the topology and the geometry of the basic elements of structure. Biologist and mathematicians alike have exploited these properties of modularity and iteration to propose various classifications and views of plant stems architectures (Hallé and Oldeman 1970; Prusinkiewicz and Remphrey 2000). While roots exhibit the same iterative structure as stem, no equivalent classification was ever proposed for root architecture. One possible reason for this is purely practical. Root systems are not easily observed in the wilderness as they are hidden underground, away from curious researchers. Persistent researchers may however took up the task to uproot a plant to have a direct look to its roots, but such attempts often damage the structure of the root system and can only give a general idea of the whole functional structure. Another possibility is to use rhizotrons, clear-walled chambers through which one can observe roots as they grow. However only the roots growing along the clear interface will be visible, and the major part of the root system will remained hidden from view. For these reasons, the design of *in vitro* systems allowing plant culture in clear medium and controlled conditions was a major milestone for the understanding of root development regulation and of the resulting architecture. The second major step in root developmental study was the adoption of *Arabidopsis thaliana* as a model plant in 1964. *Arabidopsis* is a small dicotyledonous angiosperm of the Brassica family. It can be easily

grown and propagated in controlled conditions *in vitro*, and has the invaluable advantage of possessing an almost transparent and fairly simple root system whose anatomy is constant and has been fully described (Figure 4). In addition, *Arabidopsis* genome is the smallest angiosperm genome known (~157 Mb for five chromosomes). Roots in general came into major scrutiny at the cellular and molecular level in the 1980s (Schiefelbein and Benfey 1991), and molecular analyses of root development gained major momentum since the publication of the full genome of *Arabidopsis* on December 2000 (The Arabidopsis Genome Initiative 2000). For all these reasons, we choose to centre our work on the model plant *Arabidopsis thaliana*. We will present here what is known of the anatomy and development of the *Arabidopsis* root system and the current understanding of its regulation by the plant hormone auxin.

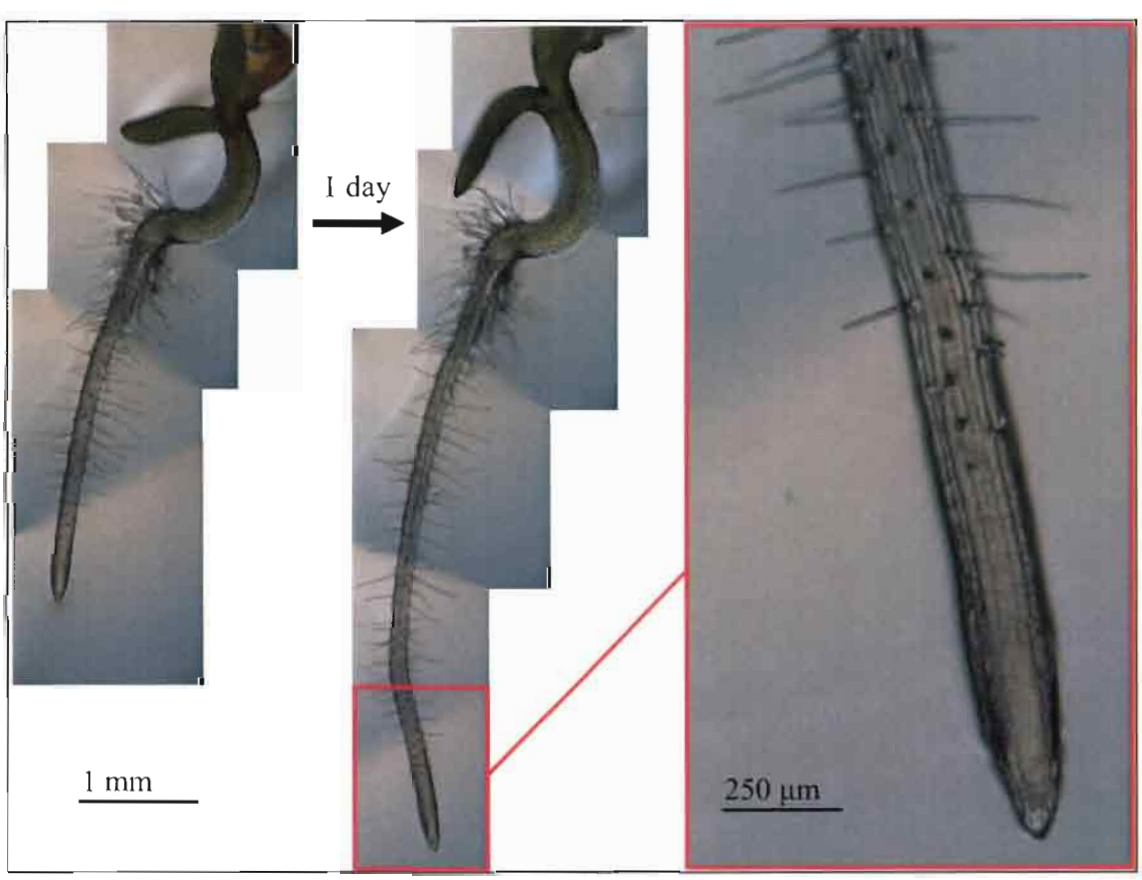

Figure 4. In vitro growth and observation of the *Arabidopsis* root system
The root of *Arabidopsis thaliana* is devoid of pigments, allowing direct observation of the cellular superstructure and its evolution during root development.

I.C) Arabidopsis root anatomy

The anatomy of the *Arabidopsis* root was formally described in full details in the 1990s (Dolan et al. 1993). From a general point of view, roots can be considered as an ensemble of concentric cylinders organized around a cylindrical core of vascular tissue. In *Arabidopsis*, each of those peripheral cylinders corresponds to a single cell layer. From the outer layers to the most central ones, the *Arabidopsis* root is radially organized as follow: epidermis, cortex, endodermis, and pericycle. The xylem and phloem cell files are located within the cylinder defined by the pericycle. *Arabidopsis* possess four alternating poles of xylem and phloem. Each of those layers presents a constant number of cells in *Arabidopsis*. This global organization is presented in Figure 5.

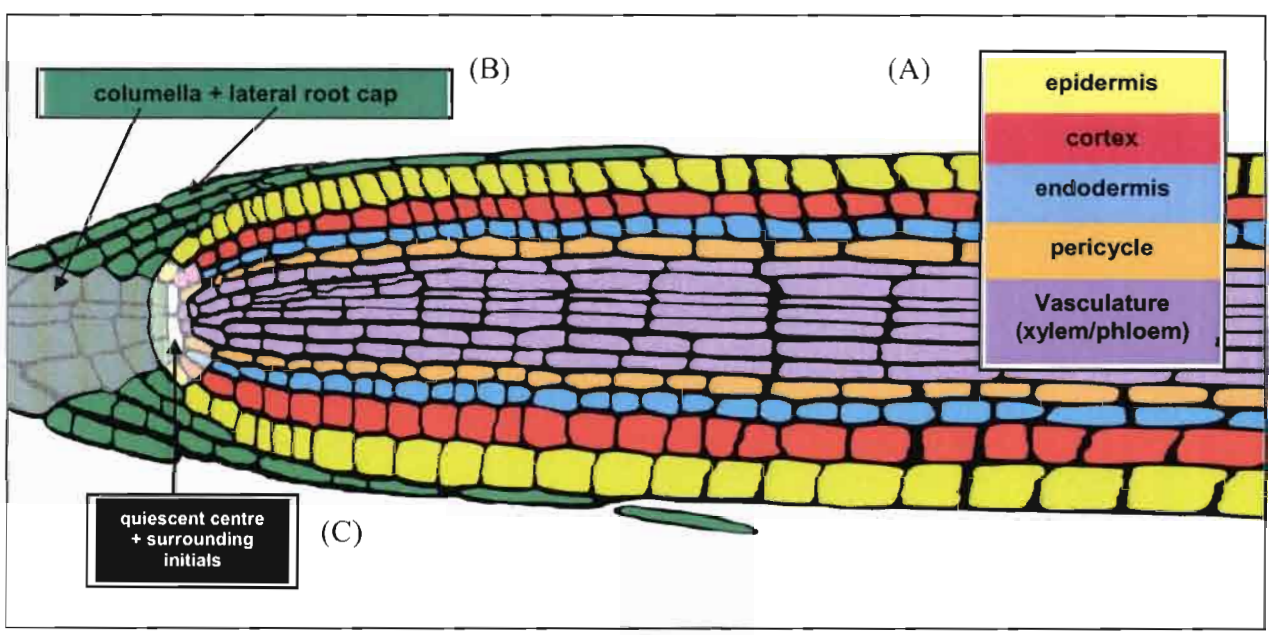

Figure 5. Anatomy of *Arabidopsis* root
(A) Cell layers constituting the main root body, colour-coded. Each cell layer takes its origin at the root apex, inside the root apical meristem.
(B) The root cap is composed of the columella (central zone of the root cap) and lateral root cap and protects the apical meristem during root growth.
(C) The root apical meristem is formed by the quiescent centre (here in white) and the surrounding founder cells of the root tissues, called initials.

This organization is constant longitudinally along the root axis, from the base of the root through the apex. Each tissue layer is however subject to differentiation as the root ages, resulting in a gradient of differentiation with young, undifferentiated tissues located at the apex (Figure 6).

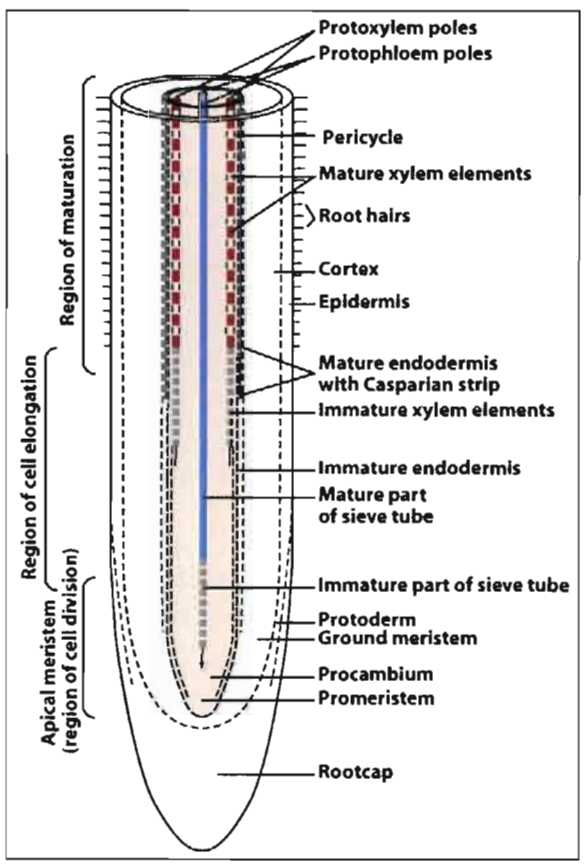

Figure 6. Gradient of differentiation along the root axis
From outer layers to inner layers, the main differentiation events are:
- apparition of root hair (epidermis)
- formation of the Casparian strip (endodermis)
- maturation of vascular elements (central cylinder)
Mature cell length is acquired through the elongation zone, overlapping the first differentiation events.
From "Biology of Plants", 7th Ed., W.H.Freeman and Company.

Figure 7. Embryonic organization of the root apical meristem

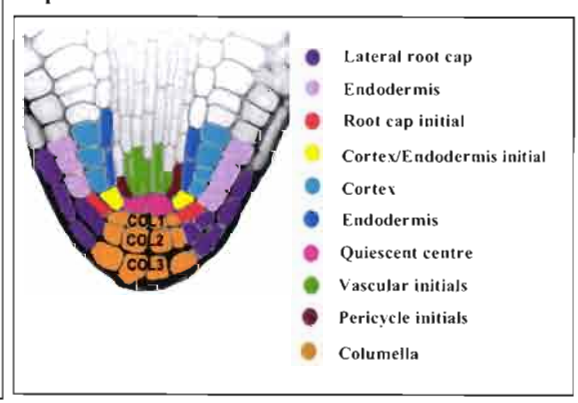

The root apex itself is a slightly more complex structure (Figure 7). It comprises the apical meristem, which is defined as the quiescent centre surrounded by the initials. As its name implies, the cells forming the quiescent centre hardly divide, while the surrounding initials do so to adjoin new cells to each of the cell layers we described previously. The apical meristem however maintains its integrity and structure at all time during root development. Due to the specific dynamics of cell division and growth in this zone, the root apex is

conceptually divided into three domains which are, starting from the root tip (Figure 8):

- the root cap, divided between the columella in its centre and the lateral root cap along the apex. The root cap plays a dual role, protecting the apical meristem and secreting mucilage to ease the movements of the root through soil, and simultaneously being the site of perception for specific environmental cues such as gravity.

- the meristematic zone. It is defined as the ensemble formed by the apical meristem and the mitotically active cells created by division of the initials.

- the elongation zone, in which cells start to elongate and acquire their mature length. Its start corresponds roughly to the end of the lateral root cap, and its end is defined by the end of cell elongation. The cells going through the elongation zone also start to differentiate, and may continue to do so along the differentiation zone until all root tissues have acquired their mature phenotypes.

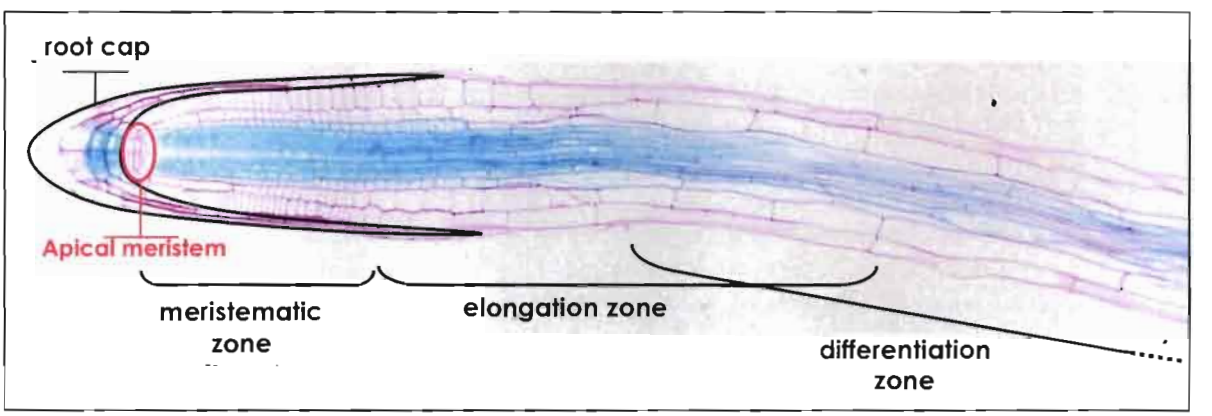

Figure 8. Functional zonation of the root apex
The frontiers between each zone are purely conceptual, as the zones themselves are dynamics and constantly moving along the root axis with each cell division occurring in the meristematic zone.

The mitotic activity of the root apical meristem is the source of all the root tissues. As we will now see, its functioning has been extensively described and analyzed at the cellular and molecular levels during the past 20 years.

II) *Arabidopsis* root system development

Like for the stem, root development depends on the activity of an apical meristem, small mass of mitotically active undifferentiated cells. However, the mechanisms of ramification in the root differ strongly from those governing root branching. While the shoot apical meristem produces the future lateral organs and the stem tissues simultaneously, the formation of lateral organs in the root system appears spatially and temporally disjointed from the functioning of the root apical meristem. We will thus distinguish two developmental processes in *Arabidopsis*: the development of the primary root of embryonic origin, and the formation of lateral roots along the mature primary root.

II.A) *Arabidopsis* primary root development

The primary root is set up during embryogenesis. The contribution of each embryonic cell to the primary root final structure was historically analyzed through clonal analysis. This technique is based on the marking of a single cell using a visible genetic marker that can be subsequently scored. This genetic marker is inherited by all descendants of the original marked cell, and this group of marked cells constitutes a clone. The clone dimensions and localization quantify the contribution of the progenitor cell to the mature organism. For the root embryo analyses, clones were marked with the *uid A* gene (glucuronidase gene) that catalyses the formation of a blue precipitate in cells expressing the gene when incubated with the proper substrate. More precisely, studies of embryonic root territories were done using genetic constructs based on mobile genetic elements called transposons. The principle of these studies was to use a

genetic construct in which the *uid A* was disrupted by a transposon, and would only activate when a rare transposition event occurs, removing the transposon and restoring the gene. Such an event would only occurs in one or two cells at a time during embryonic development, creating the sought after cell-specific marking. Screening for plants in which the transposition event occurred allowed isolating marked clones and analyzing their boundaries. This permitted the construction of maps depicting the probable fate of each embryonic cell. It was possible to demonstrate that the origin of the quiescent centre and the columella root cap can be traced back to a single cell, the hypophysis (Scheres et al. 1994). This cell derives from the basal daughter cell of the first zygotic division, and is the only contribution of the basal cell to the embryo. The cells that will form the primary root derive from the apical daughter cell of the zygote (Figure 9).

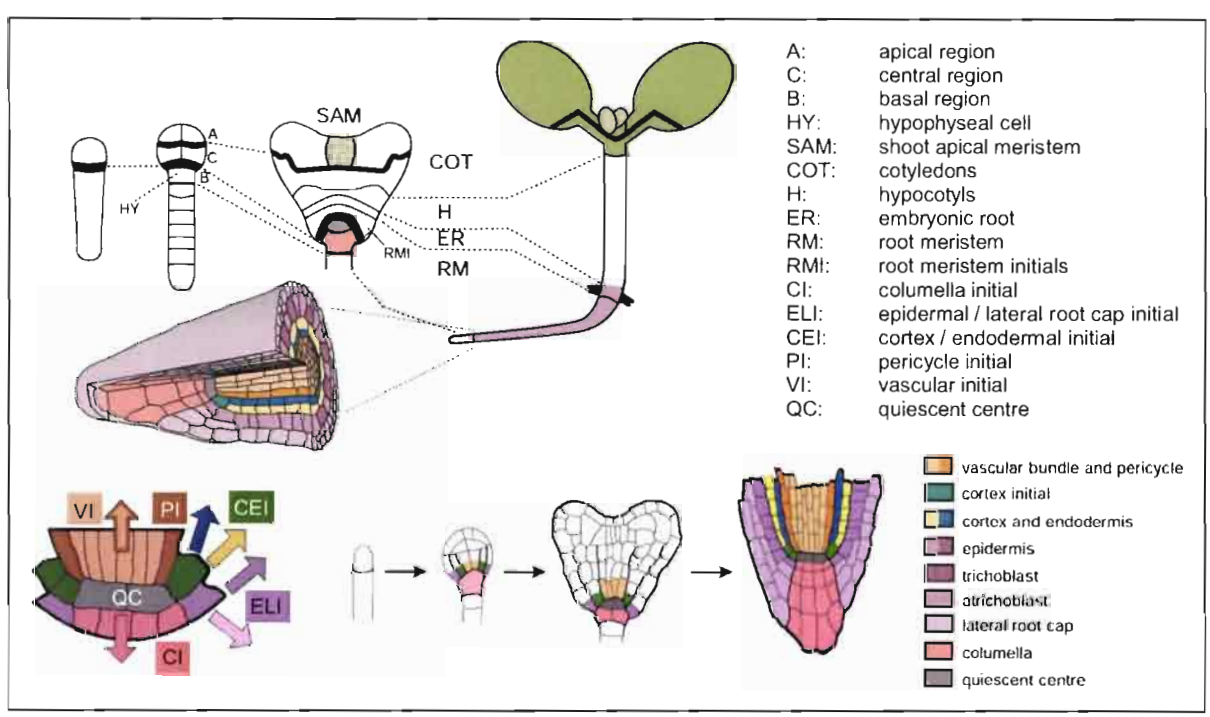

Figure 9. Embryonic origin of the *Arabidopsis* root
Top, from left to right:
first zygotic division; octant stage embryo; heart stage embryo; seedling with enlarged root meristem region.
Bottom:
Root apical meristem & Meristem specific correspondence between embryonic cells and mature root meristem.
Adapted from "The *Arabidopsis* Book"

The primary root apical meristem formed in the embryo will starts its development at germination. The precise sequences of mitotic divisions assuring the constitution of new tissues at the root apex have been well described (Scheres, Benfey, and Dolan 2000; Benfey and Scheres 2000).

The epidermal/lateral root cap initials give rise to the epidermis and the outer portion of the root cap known as the lateral root cap. The central portion of the root cap, the columella, has its own set of initials. Cortex and endodermis are generated by division of the cortex/endodermal initials. Finally, the vascular tissue and pericycle have their own sets of initials. Division of initials can be either solely anticlinal (orthogonal to the axis of growth) resulting in a single file of cells or first anticlinal then periclinal (parallel to the axis of growth) resulting in two or more cell layers. The columella initials generally divide only anticlinally and their progeny undergo rapid cell expansion and then differentiate, producing the starch-containing amyloplasts that play a role in gravity sensing. The other three types of initials generally undergo both anticlinal and periclinal divisions, resulting in the distinct cell lineages. For example the cortex/endodermal initials divide first anticlinally to regenerate the initial cell and a basal daughter cell. The basal daughter then undergoes a periclinal division to form the first cells of the cortex and endodermal lineages. These cells will undergo a small number of anticlinal divisions during which time they will acquire their specific fates.

The maintenance of a coherent meristem structure despite the active divisions of initials throughout the primary root development implies the existence of identity conservation mechanisms. Laser ablation experiments were used to determine whether these mechanisms depend on signals exchanged

between the quiescent centre and the initials (van den Berg et al. 1995; van den Berg et al. 1997; van den Berg, Weisbeek, and Scheres 1998; Berger et al. 1998). The principle of these studies is to specifically destroy one cell with a high-energy laser pulse, inducing a reorganisation of the targeted tissue. Neighbors of the destroyed cell will re-arrange to occupy the void formed by the cell ablation. Thus a neighbor cell will finally occupy the actual position of the destroyed cell (Figure 10).

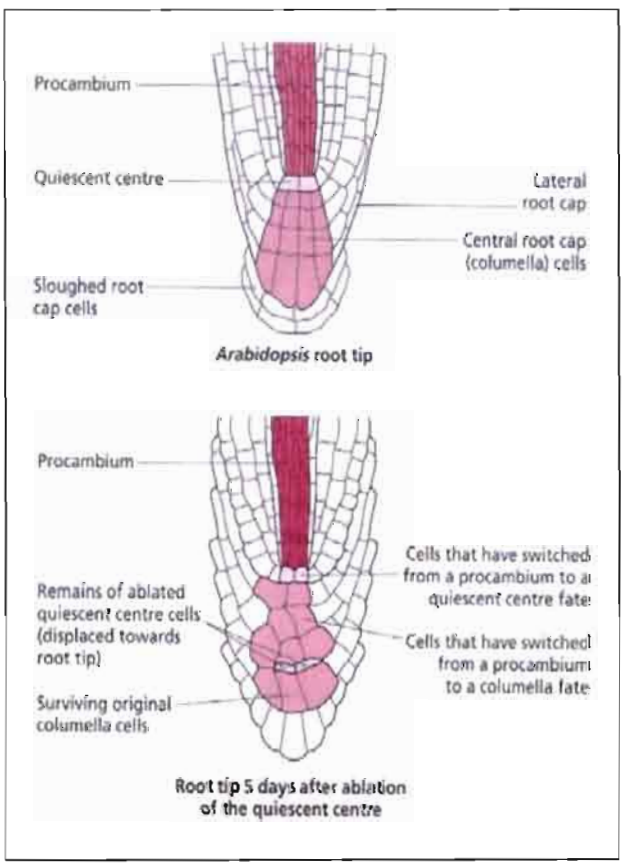

Figure 10. Laser ablation experiment in the root apical meristem
The quiescent centre was specifically targeted, and was replaced by cells coming from division of the vascular initials.

These studies revealed that the fate of meristematic cells depends on their position within the meristem rather than on their origins. Ablation and subsequent reallocation of meristematic cells along the radial axis and along the apical-basal axis resulted in appropriate cell fate changes. This suggested that

cell fates depend on both radial and apical-basal positional signaling, continuously interpreted by the meristematic cells. The precise nature of the signal promoting positional cell fate determination was investigated, and it was shown that re-specification does not occur when the fluxes of auxin were altered in the root apex, or when meristematic cells could not perceive auxin (Sabatini et al. 1999).

The meristematic activities we described "build" the primary root by adding new cells at its tip. These cells will then undergo longitudinal cellular growth when passing through the elongation zone (see Figure 4 for an illustration of the root elongation). As such, primary root growth is the combination of cellular divisions in the meristematic zone and cellular elongation within the elongation zone. In this regard, primary root development appears conceptually similar to shoot development. However, whereas the shoot apical meristem directly create future lateral organs in the form of primordia, lateral root primordia formation appears to be disconnected from the activity of the root apical meristem.

II.B) Root branching in *Arabidopsis*

Root branching can be defined as the occurrence of lateral roots along a longitudinal root axis. As evoked earlier, it is an iterative process, in the sense that lateral roots may themselves support lateral roots. The classical terminology is to name lateral root orders by reference to the primary root. As such, lateral root forming on the primary root are named "secondary roots", lateral roots of the secondary roots are named "tertiary roots", etc.

In *Arabidopsis*, lateral roots of different orders all present the same anatomy as the primary root. They possess an apical meristem responsible for their growth, and the functioning of this meristem occurs in identical ways as for the primary root apical meristem. This is another parallel between the shoot and the root system. In the shoot, axillaries buds also reproduce the structure and function of the shoot apical meristem during shoot branching. The difference between root and shoot branching lies in the respective origins of these lateral organs. As mentioned before, lateral roots can be considered at first glance as created without specific order or logic along the root axis. While in the stem axillaries buds are neatly organized, always present and visible at the base of each leaf, lateral roots appear dispersed and in a fashion unpredictable by simple macroscopic observation of the root system.

This conclusion is however based on a misconception. It appeared through fine scale anatomic observations that the lateral roots where not the exact equivalents of the axillaries buds, but rather of the branches that can arise from those buds. The true equivalents of the axillaries buds are lateral root primordia. Those cellular structures arise from one of the inner root tissue layer, the pericycle. The sequence of events leading from the first cell division to the fully organized primordium as been well described and codified in *Arabidopsis* (Casimiro et al. 2003; Benková et al. 2003).

The first morphological event related to primordia initiation occurs in the three pericycle cell files adjacent to one of the xylem poles (Figure 11). Two adjacent cells from each pericyclic cell file will become founder cells for the future lateral root primordia (for a total of 6 founder cells). One of the first

perceivable events of initiation is the migration of founder cells nucleus toward the transversal junction between founder cells of the same pericycle cell file.

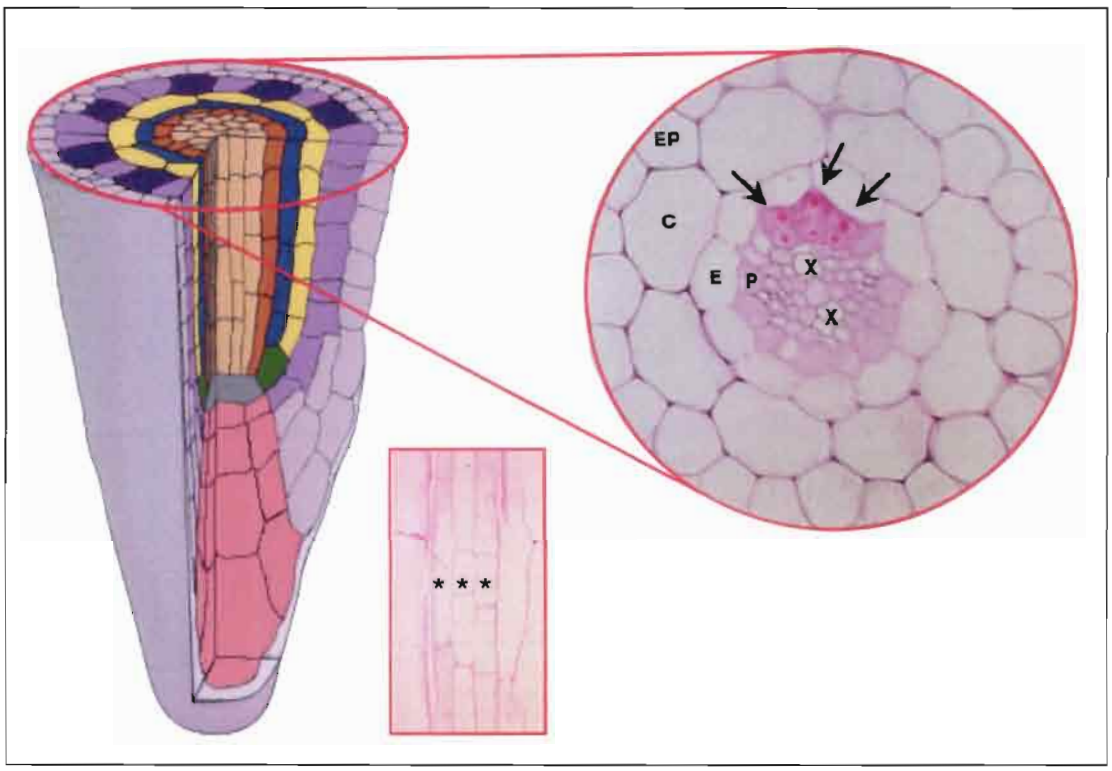

Figure 11. Lateral root primordia initiation occurs in front of xylem poles
Right insert: transversal view of the root. EP – epidermis; C – cortex; E – endodermis; P – phloem pole; X – xylem pole. Black arrows point to the developing primordium.
Bottom insert: front view of the 6 founder cells. Stars mark the small cells born from the first asymmetric division.
Adapted from Casimiro et al. 2003

Founder cells then undergo almost simultaneous polarized asymmetric transverse divisions, creating two short cells flanked by two longer cells. The daughter cells continue to divide symmetrically and asymmetrically, from the centre upwards and downwards. The structures resulting from these divisions are a constant (Malamy and Benfey 1997). The founder cells first give rise to a primordium composed of inner and outer cell layers, defined as stage II. With subsequent divisions, the primordium passes through stages III to VII, as defined by the number of cell layers existing in each stage. This ultimately leads to stage VIII, at which time the primordium has acquired the same cellular structure as

the root apical meristem (Figure 12). Stage VIII corresponds to the time of emergence when the primordium undergoes a noticeable expansion and pierce through the outer tissue layer of the root. Once emerged, the primordium act as the apical meristem of the young lateral root, creating new cells in the same way the primary root apical meristem does.

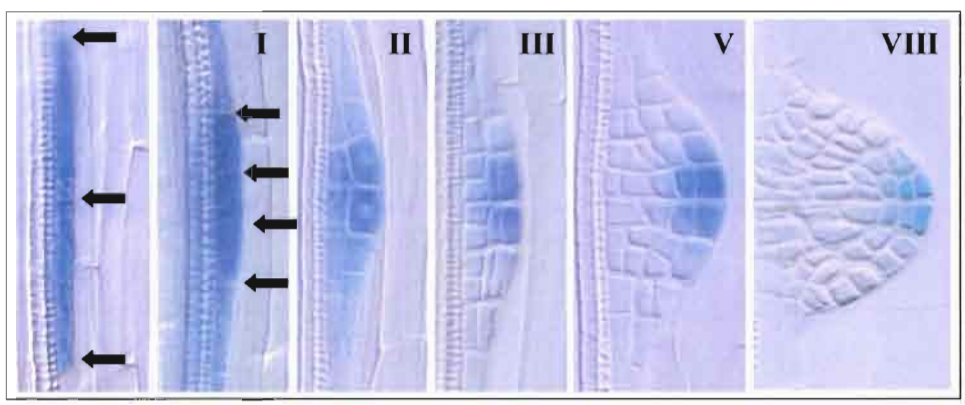

Figure 12. Lateral root primordia developmental sequence
The first panel shows the founder pericycle cells previous the first asymmetric division (revealed by the blue coloration). The ladder-like structure on the left of the pericycle corresponds to the xylem file. The successive developmental stages are named according to the number of cell layer constituting the primordia. Arrows point to the cell walls. Adapted from Benkova et al. 2003.

It has been shown that the developmental sequence leading from the first asymmetric division to emergence presents a number of important checkpoints (Laskowski et al. 1995; Celenza, Grisafi, and Fink 1995; J G Dubrovsky et al. 2001; J G Dubrovsky et al. 2006). These checkpoints correspond to stages when a specific signal is needed to pursue development, this signal often being the hormone auxin. It is possible to distinguish three main checkpoints:

1 – Initiation *stricto sensu*, as defined by the first asymmetric division.

2 – Emergence of the fully organized, mature primordium.

3 – Development and growth of the young emerged lateral root.

Each of these checkpoints is controlled by auxin. One important consequence of these checkpoints is the fact that not all primordia will emerge.

This phenomenon can be directly compared to the regulation of axillaries buds development in the shoot system. In shoots, not all axillaries buds give rise to a new branch and this developmental process is also regulated by auxin.

The fact that not all primordia emerge implies that the observed macroscopic architecture of the root system does not necessarily represent the microscopic organization existing within the root, and that inherent regularities in primordium initiation may be masked by randomness of emergence.

As evoked earlier, environment has its role in this potential randomness (Drew 1975; Robinson 1994; Hodge 2006). Indeed, in soils or media with patchy nutrient distributions, lateral roots appear to proliferate preferentially in nutrient rich zones. It has been shown that regulation of root branching by environment can occur at different levels (Zhang et al. 1999; Zhang and Forde 2000; Malamy and Ryan 2001). For example high sucrose to nitrogen ratio in the environment inhibits primordia initiation, while high levels of nitrate affect the lateral root development after emergence, blocking the activation of the lateral root meristem. These effects of environment on root development were proven to be essentially mediated by hormones such as abscisic acid or auxin. Auxin in particular plays an important role in the global regulation of root development, as we will see now.

III) Auxin and root development

III.A) A brief history of auxin

From a historical point of view, understanding of plant development is closely linked with the plant hormone auxin. At the beginning of the 18th

century, Dodart and Astruc took note of the vertical orientation of numerous vegetal organs, and formulated the hypothesis that this orientation was linked with gravity. Indeed, a root growing according to gravity and then rotated to be perpendicular to it will quickly curve and reorient its apex in its former direction. The same is true for shoot, albeit in the opposite direction. The causal relationship between gravity and plant organ growth was demonstrated almost one century later, in 1806, by Sir Thomas Andrew Knight. Growing seedlings at the periphery of a horizontal rotating wheel, he showed that roots and shoot re-oriented themselves according to the centrifugal forces (Figure 13).

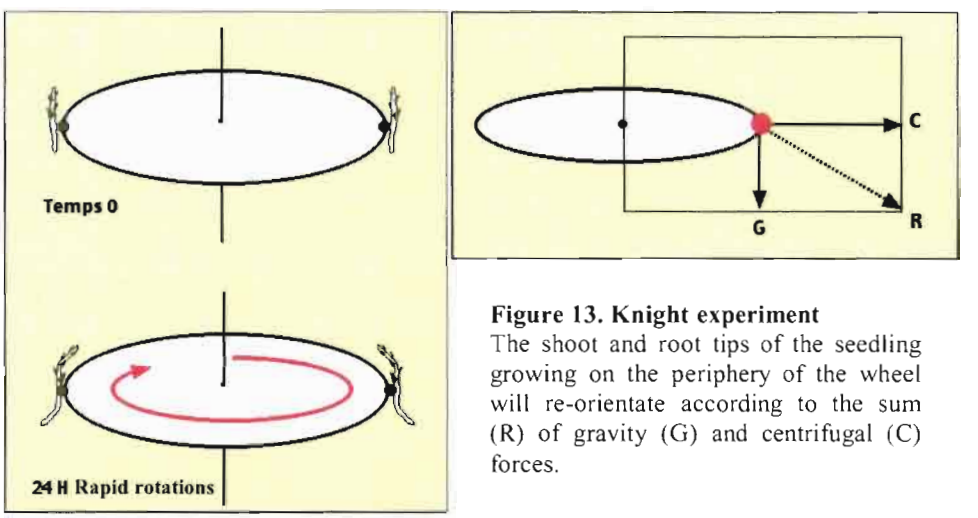

Figure 13. Knight experiment
The shoot and root tips of the seedling growing on the periphery of the wheel will re-orientate according to the sum (R) of gravity (G) and centrifugal (C) forces.

In 1868, Dr. A. B. Franck showed in "Beitrage zur Pflanzenphysiologie" that the re-orientation of roots in response to gravity was linked with a differential elongation of the epidermis cell between the two sides of the root: the epidermis cells within root turn appeared shorter than normal while cell on the outside of root turn presented normal length. This differential elongation happens within the elongation zone and induces a curvature reorienting the root apex. Franck introduced the term geotropism to characterize this reorientation of the

root toward the earth. This term was later replaced by the term gravitropism, as roots re-orientate according to any gravity-field.

As many biological processes, gravitropism is not an instantaneous mechanism, and there is usually a delay between the change in gravity direction and the reorientation of the plant organs. This delay varies from species to species, and *Arabidopsis* root needs approximately four hours to be fully re-oriented after a change of gravity field (or gravistimulation). In "The power of movement in plants" (C Darwin and G Darwin 1880), Charles Darwin and his son repeated Theophil Cielsielski experiments (Ciesielski 1872) to determine the site of gravity perception in maize and bean roots. Through root dissection combined with gravistimulation, they showed that gravity is perceived in the root cap, at the level of the columella, and also drawn conclusion on the gravitropic and phototropic re-orientation of the shoot. They suggested that the apex perceived environmental variation (such as changes in gravity or light) and issued a molecular signal which diffused to the sub-apical zone, where it induced the re-orientation (Figure 14).

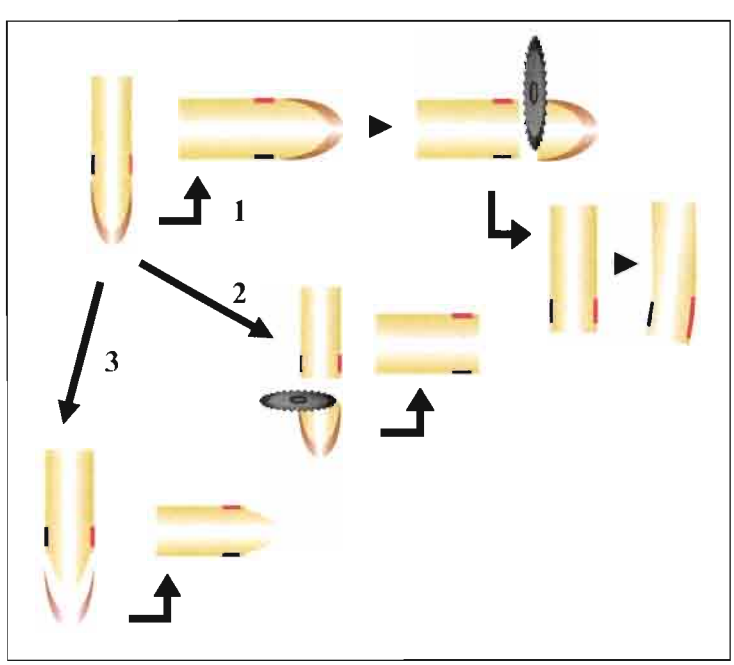

Figure 14. Cielsielski / Darwins experiments
1 – Roots were gravistimulated (90° rotations). After a time, the apex (up to the end of the lateral root cap) was cut off and the roots were rotated back to the original orientation. Differential elongation was observed then.
2 – The root apex was first cut and the root was gravistimulated afterward. No differential elongation was observed.
3 – Only the root cap was ablated before gravistimulation. No differential elongation was observed.

The physical existence of this compound was demonstrated in 1915 by Frits W. Went (as a reference, the notion of hormone was introduced in plant science in 1909). Went used agar blocks to capture the diffusive factor from oat coleoptiles tips, and showed that applying the blocks on other coleoptiles induced differential elongation (Figure 15). He proceeded to name this compound auxin, from the Greek word auxano (to grow).

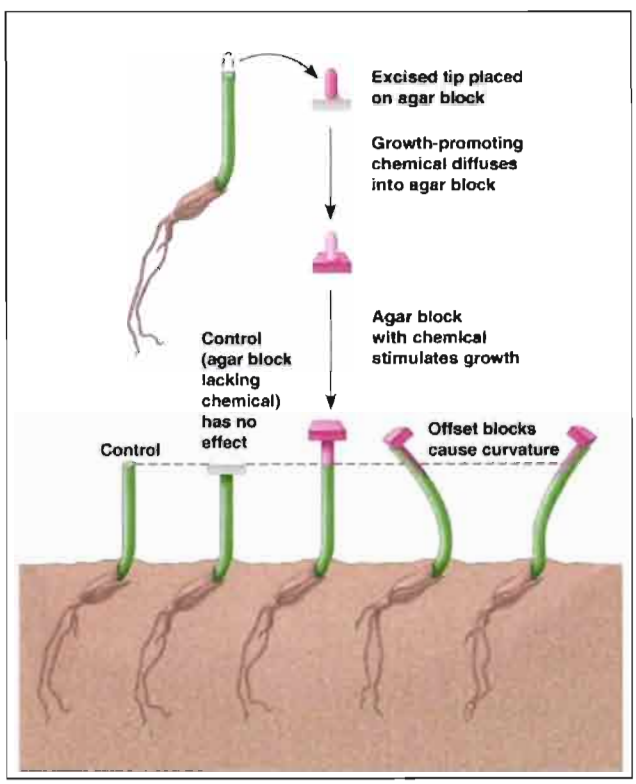

Figure 15. Went experiment
The diffusive chemical compound mediating environment perception was shown to induce elongation in oat coleoptile.

This chemical compound was isolated in 1934 from human urine by Fritz Kögel and Arie Jan Haagen-Smit, who characterized auxin as indol-3-acetic acid (IAA). Incidentally, IAA was independently characterized in 1935 from culture medium of the fungus *Rhizopu* by Kenneth V.Thimann. IAA was not isolated from higher plants until 1946. During the 1930s, Arie Jan Haagen-Smit and Frits W. Went proceeded to synthesize compounds chemically similar to IAA and able to mimic its effect on plants (Figure 16). Others natural auxins such as 3-indol-5-butyric acid (AIB) were described during the last decades (Ludwig-Müller 2000).

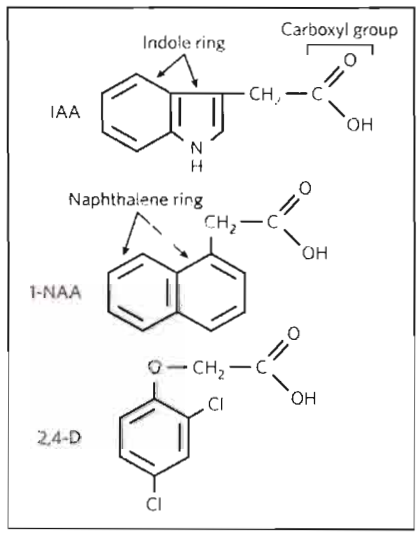

Figure 16. Chemical structure of natural auxin and two of its analogues
Both 1-naphtalene acetic acid (1-NAA) and 2,4-dichlorophenoxyacetic acid (2,4-D) are synthetic auxins able to mimic the effect of indol-3-acetic acid (IAA – natural auxin) *in vivo*.
The military defoliant Agent Orange used during Vietnam War is a high concentration mixture of 2,4-D and 2,4,5-trichlorophenoxyacetic acid (2,4,5-T), another synthetic auxin.

III.B) Auxin physiology

Discovered thanks to its simple capacity to induce differential tissue growth, auxin (and its synthetics analogues) in fact regulates highly complex physiological responses in plants. Auxin can promote both generic mechanisms such as cell division and differentiation throughout the whole plant, and at the same time induce strong tissue-specific responses. For example, auxin promotes cell elongation in shoot, and inhibits it in roots, due to a higher sensitivity of root tissues to auxin (Figure 17).

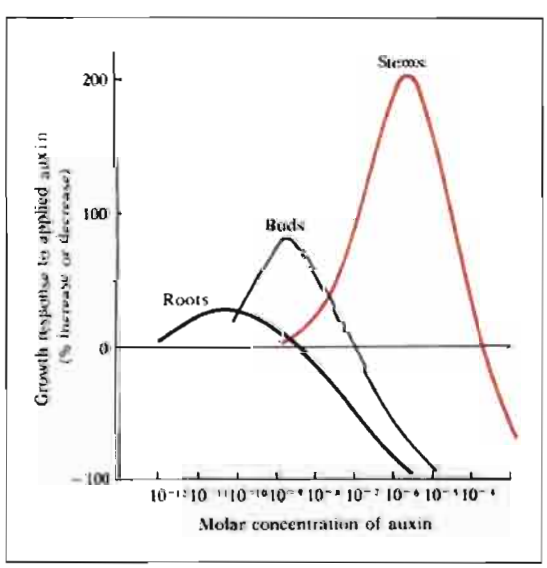

Figure 17. Dose dependent auxin-response of different plant tissues
All plant tissues exhibit similar dose-dependent auxin-responses. At low concentration ranges, increasing auxin concentration causes an increase in growth relative to controls, whereas, after an optimum is reached, any further increase auxin concentration then causes decreasing growth. Due to higher sensitivity of root tissues as compared to shoot tissues, physiological auxin doses appear to promote cell elongation in stem while inhibiting it in roots.
From K. Thimann, *Plant Growth Hormones. In: The Hormones, Vol. 1.*[24]

More generally, auxin appears necessary to regulate a wide range of developmental processes such as:

- lateral root development (Reed, Brady, and G K Muday 1998; Casimiro et al. 2001; Bhalerao et al. 2002)
- vascular patterning (Mattsson, Sung, and Berleth 1999), phyllotaxis (D Reinhardt, T Mandel, and C Kuhlemeier 2000; Stieger, Didier Reinhardt, and Cris Kuhlemeier 2002; Didier Reinhardt et al. 2003)
- embryonic axis development (Jirí Friml et al. 2003) and tropisms (Jirí Friml et al. 2002)

The combination of auxin concentration and tissue sensitivity determine what type of response is induced (Cholodny 1927; Thimann 1948; Thimann 1977; Weyers et al. 1995; Davies 1995). Intracellular auxin concentration itself depends on a dynamic equilibrium between four processes: biosynthesis, conjugation, degradation and transport.

The most abundant natural auxin is IAA, and though its base structure is derived from tryptophan, it can also be synthesized from indolic tryptophan precursor in tryptophan-independent pathways (Bartel 1997; Woodward and Bartel 2005). *Arabidopsis* seedlings can synthesize IAA in leaves, cotyledons and roots. Young leaves appear to have the highest biosynthetic capacity (Ljung, Bhalerao, and Göran K Sandberg 2001; Ljung et al. 2005).

Plants can store IAA within their cells in the form of IAA conjugates and indole-3-butyric acid (IBA), which can provide free IAA upon hydrolysis or β-oxidation, respectively. IAA can also be ester-linked to sugars or amide-linked to amino acids and peptides. These conjugates have been proposed to play a role in

storage, transport and compartmentalization of IAA, as well as permitting excess IAA detoxification, or acting as protection against peroxidative degradation of IAA. Certain IAA conjugates appear to be active in auxin bioassays, and several plants store IAA conjugates in seeds to provide IAA to developing seedlings by hydrolysis of the conjugate during germination.

Contrary to the described storage conjugation pathways which temporarily "remove" IAA from the cell cytoplasm, some conjugation systems are akin to catabolic pathways and can definitively inactivate IAA. For example, Arabidopsis permanently inactivates IAA by ring oxidation to oxIAA, which is then conjugated to hexose. In addition, IAA can be conjugated to amino-acid such as Asparagine, Glutamate and Glutamine and/or to Glucose, forming conjugates that Arabidopsis seedlings do not appreciably hydrolyze. The balance between catabolic and storage conjugation pathways is determined by the level of IAA present in the cells. For example, catabolic conjugation is up-regulated and storage conjugation down-regulated in response to elevated IAA levels.

Auxin transport is complex and highly regulated, involving purely physical mechanisms such as diffusion or vascular convection, as well as active protein transporters. The regulation of plant development by IAA strongly depends on the different IAA fluxes going through the plant tissues (Figure 18). As mentioned earlier, IAA is mainly produced in the shoot, at the level of young leaves and developing primordia (Ljung, Bhalerao, and Göran K Sandberg 2001), and is transported toward the shoot apical meristem, where it regulates phyllotaxis. It is then transported basipetally through the vascular tissues of the shoot (Lomax, Gloria K Muday, and Rubery 1995) and act as the mediator of apical dominance by indirectly inhibiting axillaries buds growth (Skoog and

Thimann 1934). Within roots, IAA is transported acropetally in the central cylinder (Scott and Wilkins 1969), controlling lateral root primordia development and emergence (Celenza, Grisafi, and Fink 1995). Arriving at the root apex, IAA is redirected through the outer cellular layers and transported basipetally in the epidermis (Davies and Mitchell 1972; Tsurumi and Ohwaki 1978). This basipetal transport controls cell elongation in the elongation zone and has been shown to control lateral root primordia initiation (Celenza, Grisafi, and Fink 1995). The full extend of the basipetal transport in the epidermis is still unknown.

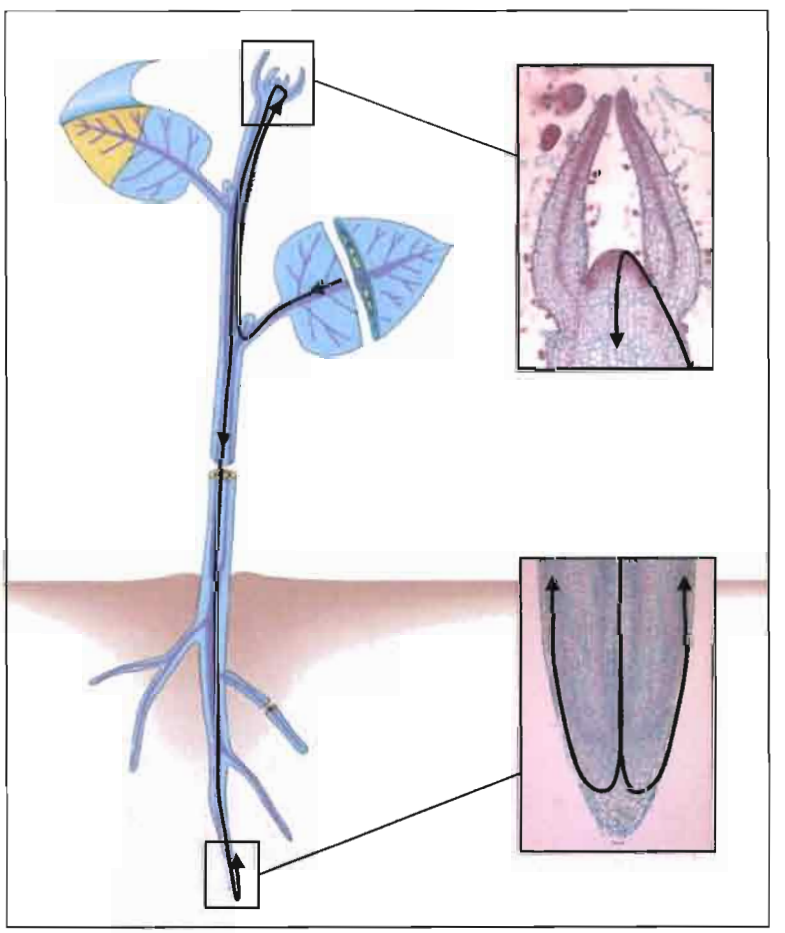

Figure 18. Global auxin fluxes in the plant
Top insert: auxin fluxes in the shoot apical meristem determine primordia positioning before leaving the epidermis through the vascular tissues.
Bottom insert: auxin fluxes in the root apex are directed through the meristem, pass in the root cap and flow back into the epidermis toward the elongation zone.

III.C) Molecular basis of auxin active transport

The long distance auxin transport between leaves, shoots and roots is mainly vascular, depending on auxin being loaded into the phloem. Where there is no mature vasculature (embryo, shoot apical meristem, young lateral buds, lateral root primordia and root apical meristem), auxin cellular transport depends mainly on specific proteins that will actively create coordinated fluxes through the tissues. The term "polar transport" is used to describe these fluxes, and a conceptual model was proposed in 1974 (Rubery and Sheldrakke 1974) to explain the mechanisms driving this transport. Thanks to molecular and genetics analysis on *Arabidopsis*, this model has since then been greatly refined (Figure 19).

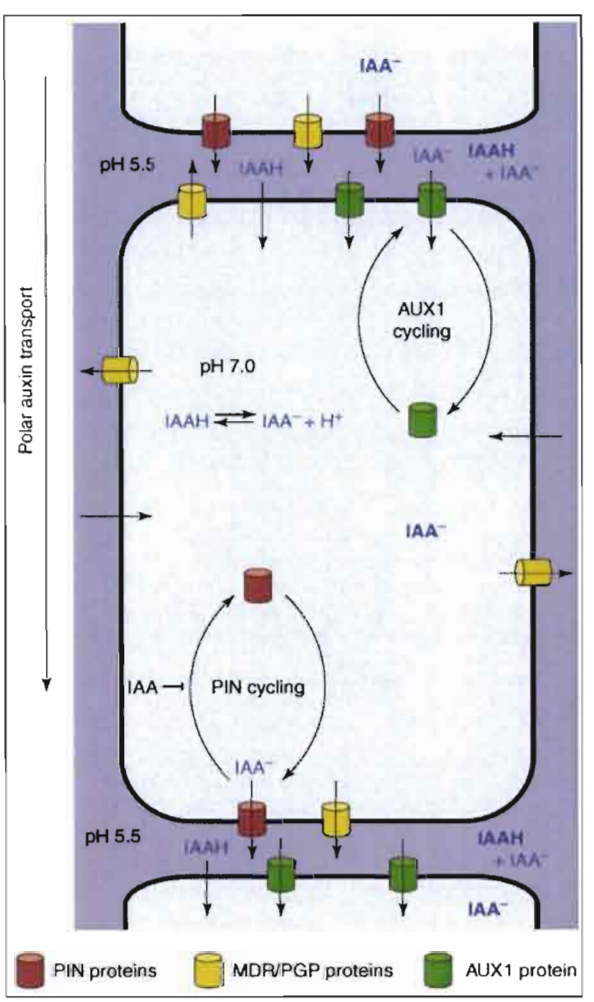

Figure 19. Cellular model for polar, cell-to-cell auxin transport
According to the chemiosmotic hypothesis, a pH gradient across the plasma membrane leads to the accumulation of IAA in the cell. A higher pH inside the cell causes protonated auxin molecules (IAAH) to dissociate, making them unable to pass passively back through the cell membrane. Auxin efflux carrier (PINs, some MDR/PGPs) are needed to transport auxin out of the cell. In addition, auxin influx carriers (AUX1 here, LAX1/2/3 not shown) can import auxin anions (IAA^-) directly from the cell wall into the cytoplasm.
Polar localisation of the carriers directs coordinated auxin fluxes through the plant tissues. The carriers themselves are subject to constant endocytic cycling. Auxin has been shown to inhibit the endocytosis of PINs, increasing their levels at the cell surface.
From Vieten et al. 2007

The chemiosmotic hypothesis at the base of this model states that as a weak acid, IAA can be either ionic (IAA^-) or protonated (IAAH) depending on the pH, and that only the protonated form IAAH can diffuse freely through the plasmic membrane. Once inside the cell, IAAH is dissociated into IAA^-, and is trapped inside the cytoplasm. Auxin entry can also be promoted by an influx carrier, and its exit from the cell will only be possible thanks to active efflux carriers. The polar transport model was notably refined by the analysis of *Arabidopsis* mutants resistant to auxin: applying exogenous auxin on such mutants does not induce specific auxin response such as stem cells elongation or strong lateral roots initiation. Those mutants were often found to be defective in proteins mediating auxin transport. Among the earliest genes cloned that were defective in auxin-resistant mutants was *AUX1*, which encodes a transmembrane protein similar to amino acid permeases (Bennett et al. 1996). AUX1 mediates the influx of IAA into cells (Marchant et al. 2002). AUX1 can be localized asymmetrically in the plasma membrane of certain cell files, facilitating directional auxin transport (Swarup et al. 2001; Swarup et al. 2004). Since the discovery of *AUX1*, three homologous genes coding for putative auxin influx carriers were identified in *Arabidopsis*, and named *LAX1* to *3* (Like AUX1 genes). It was recently shown that *LAX3* plays an important role in lateral root emergence (Swarup et al. 2008, Nature Cell Biology. *In press*).

The pin-formed (*pin1*) *Arabidopsis* mutant is another auxin transport mutant, characterized by shoot meristem defects causing inflorescences to terminate in pin-shaped points generally lacking lateral organs (Okada et al. 1991). *PIN1* was identified as a member of a multigene family including the genes later named *PIN2* to *PIN7*. The *PINs* genes expression appears to be

extremely tissue-specific in wild-type plants, but observation of *PIN*-knocked-out mutants revealed that the expression of the other members of the *PIN* family can change to compensate for the loss of activity from the knocked-out gene (Vieten et al. 2005). *PINs* have been found to encode transmembrane auxin efflux facilitator proteins with homology to bacterial efflux carriers (Chen et al. 1998; Gälweiler et al. 1998; Luschnig et al. 1998; Müller et al. 1998; Utsuno et al. 1998). PINs appear more often asymmetrically localized in the cell than AUX1, and their polar localization is highly dynamic. For example, PIN3 is expressed in columella cells and does not usually present a polarized membrane localization. However upon gravistimulation, PIN3 quickly moves from all sides of columella cells specifically to the lateral side newly oriented toward gravity (Jirí Friml et al. 2002). This directs the majority of auxin fluxes toward the lower side of the root (Ottenschläger et al. 2003). The large amount of auxin flowing through the lateral root cap and epidermis then inhibits cell elongation more strongly on this side of the root, which induces a bend re-orienting the root apex parallel to the gravity vector. This mechanism of flux redirection is the one responsible for the differential elongation observed by Cielsielski & Darwin during the gravitropic response. More generally, PINs have been found to rapidly cycle between the plasma membrane and unidentified endosomal compartments. PINs membrane localization responds to cues from the PINOID serine-threonine kinase. Overexpressing or disrupting PINOID alters the polar localization of PINs proteins in the cell (Jirí Friml et al. 2004). PINs recycling appears to be actin-dependent (Geldner et al. 2001), and links between actin, polar auxin transport and gravitropism have been reported in several plants. Auxin has been

shown to inhibit the recycling of PINs, reinforcing the polar localization of PINs existing in cells (Paciorek et al. 2005).

AUX1/LAX and PINs expression and localization have been extensively studied in *Arabidopsis* using gene reporter strategies, antibodies, protein-fusion techniques and confocal microscopy (Jirí Friml et al. 2002; Benková et al. 2003; Blilou et al. 2005; Tanaka et al. 2006; Wisniewska et al. 2006). This allowed the compilation of "transporter maps" describing the expression patterns and positioning of auxin carriers during *Arabidopsis* development. Those maps are available for almost all *Arabidopsis* root tissues and for lateral root primordia as illustrated by Figure 20 and Figure 21.

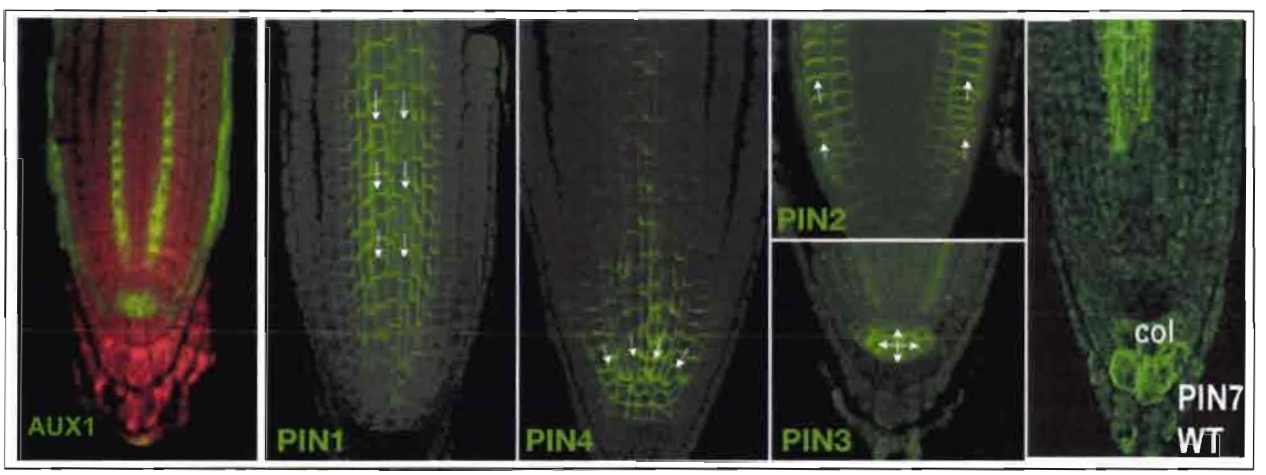

Figure 20. Auxin transporters present in the root apex of *Arabidopsis*
Auxin efflux carriers were genetically fused with the green fluorescent protein GFP and their localization was determined in confocal microscopy. AUX1 was localized in confocal microscopy through immunolabelling. White arrows indicate the global direction of auxin flows mediated by the corresponding carrier.
AUX1 is expressed specifically in the protophloem, lateral root cap, epidermis and apical meristem, with a strong polar localization within the protophloem (on the basal membrane).
PIN1 is expressed in the stele tissues, directed toward the root apical meristem.
PIN4 present a complementary expression to PIN1, being expressed at the lower end of the stele and at the level of the initials and quiescent centre. PIN4 in the stele is directed toward the meristem, but does not exhibit specific polarity in the meristem.
PIN3 is expressed in the columella, and does not exhibit a specific polarity outside of gravistimulation.
PIN2 is expressed in the lateral root cap, epidermis and cortex. Polar localization of PIN2 is extremely tissue specific, with basal localization in the lateral root cap and epidermis, and dual localization in the cortex: apical from the initials to the elongation zone, then basal localization from the start of the elongation zone and upward (Abas et al. 2006)

Adapted from Swarup et al. 2001, Tanaka et al. 2006

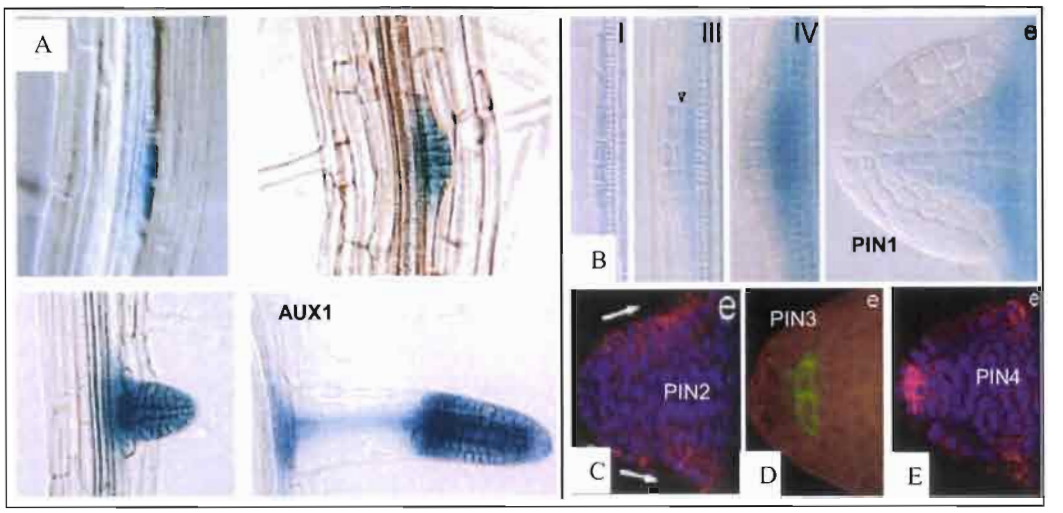

Figure 21. Auxin transporters present in lateral root primordia of *Arabidopsis*
(A) Localization of AUX1 expression (revealed by GUS marker in blue) during the development of lateral root primordia.
(B) Localization of PIN1 expression during lateral root primordia development.
(C) to (E) Localization of PIN2/3/4 proteins in emerging lateral root primordia.
Adapted from Marchant et al. 2002, Benkova et al. 2003.

We will adopt the following convention to describe the sub-cellular localization of auxin carriers: basal localization will design polarization toward the collet, and apical localization will design polarization toward the apex of the considered plant organ (shoot or root apex).

Lateral root primordia strongly express AUX1 as early as developmental stage I. They also express the same PINs as the root apex, and the localization of those PINs also mimics the localization of PINs in the root apex, suggesting the existence of common developmental processes for the embryonic root and the laterals root primordia.

Synthesizing the information available on the localization of auxin carrier, it is possible to describe how auxin will flows within the plant and directs its development at the cellular level (Figure 22).

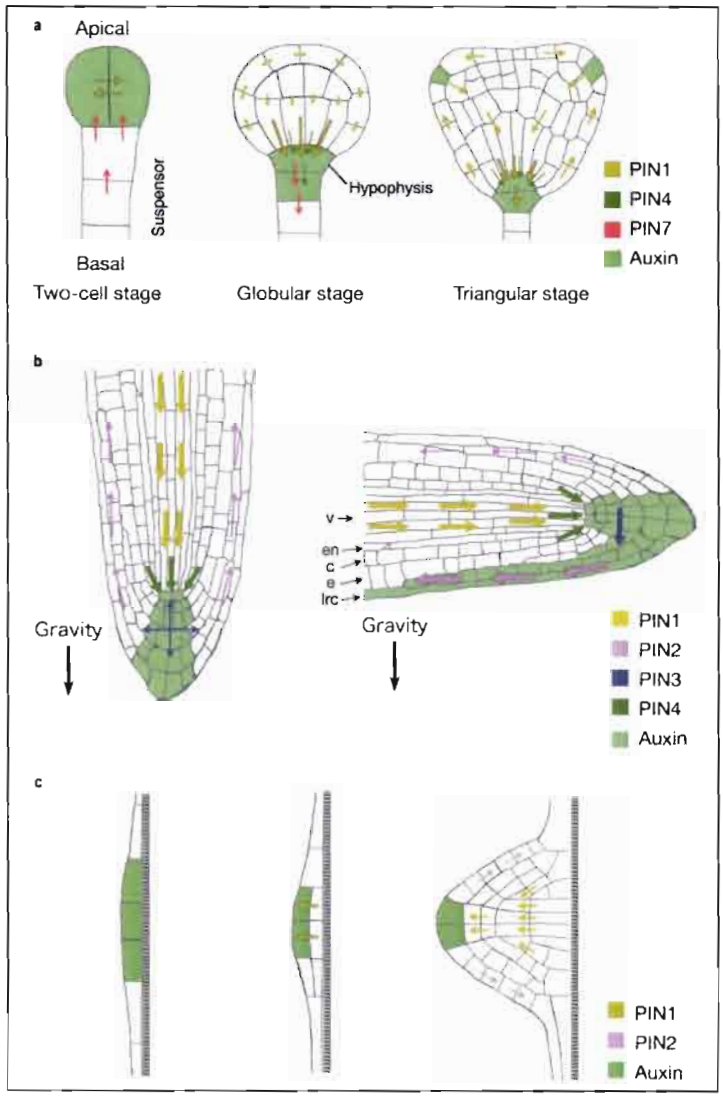

Figure 22. Coordinated auxin flows direct plant development
(a) Developing embryo exhibit strong PIN patterns shaping the future seedling.
(b) Auxin flows within the mature root apex maintain the meristem identity and mediate tropic response such as gravitropism.
(c) PIN-directed auxin flows control lateral root initiation, development and emergence.
The polarity of PIN proteins and presumptive directions of auxin flow are indicated by arrows. The place of perceivable auxin accumulation is highlighted in green. Lrc, lateral root cap; e, epidermis; c, cortex; en, endodermis; v, vascular bundle.
From Tanaka et al. 2006

III.D) Molecular basis of auxin signaling

Genetic and molecular components of the cellular auxin response have been vastly studied, and a large number of genes and proteins related to auxin signaling have been characterized in the past decades (Ulmasov et al. 1997; Guilfoyle, Ulmasov, and Hagen 1998; Guilfoyle et al. 1998; Okushima et al. 2007; Tan et al. 2007).

One of the principal effects of auxin perception in cells is a rapid increase in gene transcription. This transcriptional response is regulated by genes from two multigenic families: ARFs (Auxin Response Factors) and Aux/IAA (Auxin/Indole-acetic acid) genes. ARFs are transcription factors, able to bind to

specific promoter sequences named AuxRE (Auxin Response Element), inducing the expression of genes sensitive to auxin. Aux/IAA are transcriptional repressors of those same auxin sensitive genes. However, Aux/IAA do not possess DNA-binding domains, and they regulate transcription by inhibiting the action of ARFs. This inhibition is mediated by direct protein/protein interaction and creation of ARF/Aux/IAA complexes. Aux/IAA have short half-lives, and their turn-over has been estimated to be around 10 minutes. Auxin has been shown to reduce this even further, inducing degradation of existing Aux/IAA proteins, and allowing ARFs to induce gene activation.

The precise mechanism of auxin signaling has been partially elucidated in 2005, with the identification of the auxin intracellular receptor as being the F-box protein TIR1 (transport inhibitor response 1). TIR1 is a component of a cellular proteic complex known as SCF^{TIR1}. Upon auxin binding, TIR1 can recruit Aux/IAA proteins and poly-ubiquitine them. This poly-ubiquitination targets the Aux/IAA to the proteasome for proteolytic destruction, and the ARFs are then free to induce gene expression by binding with AuxRE (Figure 23).

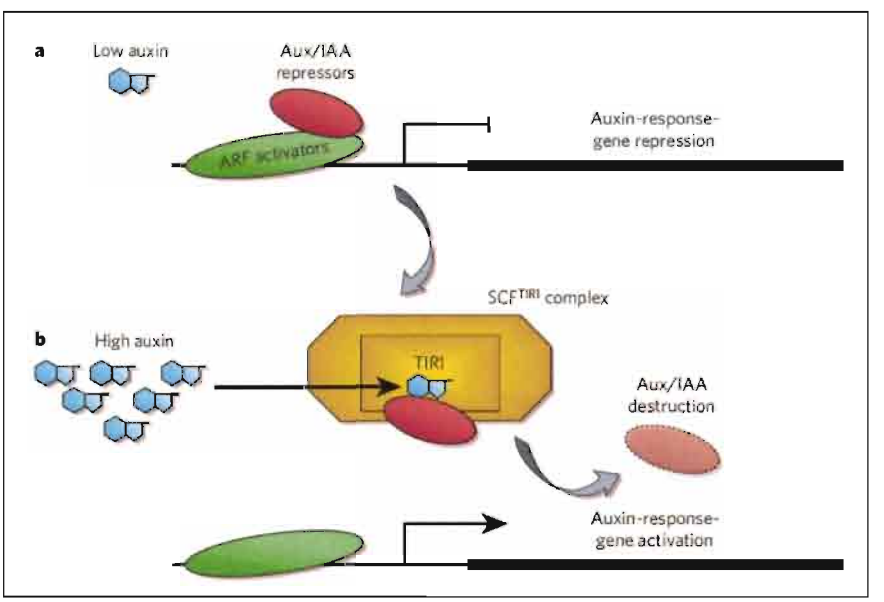

Figure 23. Auxin signaling pathway
ARFs activators bind to auxin-response elements in promoters of auxin-response genes.
(a) When auxin concentrations are low, Aux/IAA repressors associates with the ARF activators and repress gene expression.
(b) When auxin concentration increase, auxin binds to the TIR1 receptor in the SCF^{TIR1} complex, leading to recruitment of Aux/IAA in the SCF^{TIR1} complex. Once recruited, Aux/IAA are targeted for proteasomic destruction through poly-ubiquitination. The subsequently liberated ARFs then activate gene transcription.
From Guilfoyle 2007.

ARFs induce the expression of a wide array of genes, including various cell-cycle regulation genes, cell-wall remodeling enzymes, and even Aux/IAA genes. The expression of Aux/IAA genes following the degradation of Aux/IAA proteins creates a feedback loop which dampens the auxin signal.

Of important note, the fact that AuxRE respond specifically to auxin signaling was used to design a critical tool for the study of auxin fluxes (Ulmasov et al. 1997). The artificial promoter DR5 was constructed based on tandem repetitions of the AuxRE motif, and is now widely used as a marker of auxin perception (Figure 24).

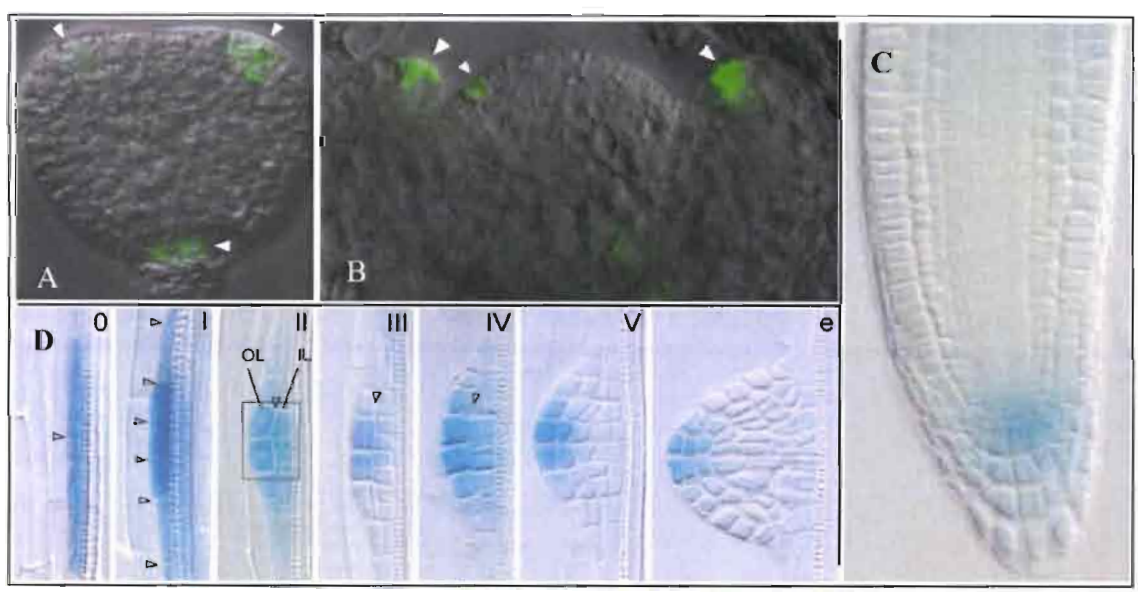

Figure 24. Auxin accumulation revealed by the DR5 artificial promoter in *Arabidopsis*
DR5 can be used to detect auxin accumulation and sensitivity through expression of direct markers such as the green fluorescent protein, or indirect one such as the glucorunidase enzyme (GUS) which is revealed through an enzymatic reaction generating a blue coloration.
Auxin accumulates at the apex of the future cotyledons and the future primary root of the embryo (A – white arrows). Accumulation also occurs at the level of developing leaves primordia in the shoot apical meristem (B – white arrows). The main accumulation site in root is located at the level of the root apical meristem and columella (C). During lateral root primordia development, auxin accumulate at the location of the future lateral root apical meristem (D – OL, outer layer of cells; IL, inner layer of cells; 0, I, II, III, IV, V, e, developmental stages of the lateral root primordia).
Adapted from Benkova et al. 2003.

The pathways of auxin signaling are now well understood at the cellular level. We know how auxin may enter or leave cells, what its receptor is, the genetic consequences of their binding, and the precise metabolism and catabolism of auxin molecules in cells (Delker, Raschke, and Marcel Quint 2008) (Figure 25). We still lack biological data about potential extracellular or intracellular auxin "sensors" such as ABP1 (auxin binding protein 1) and about the regulation of auxin carrier trafficking by auxin itself.

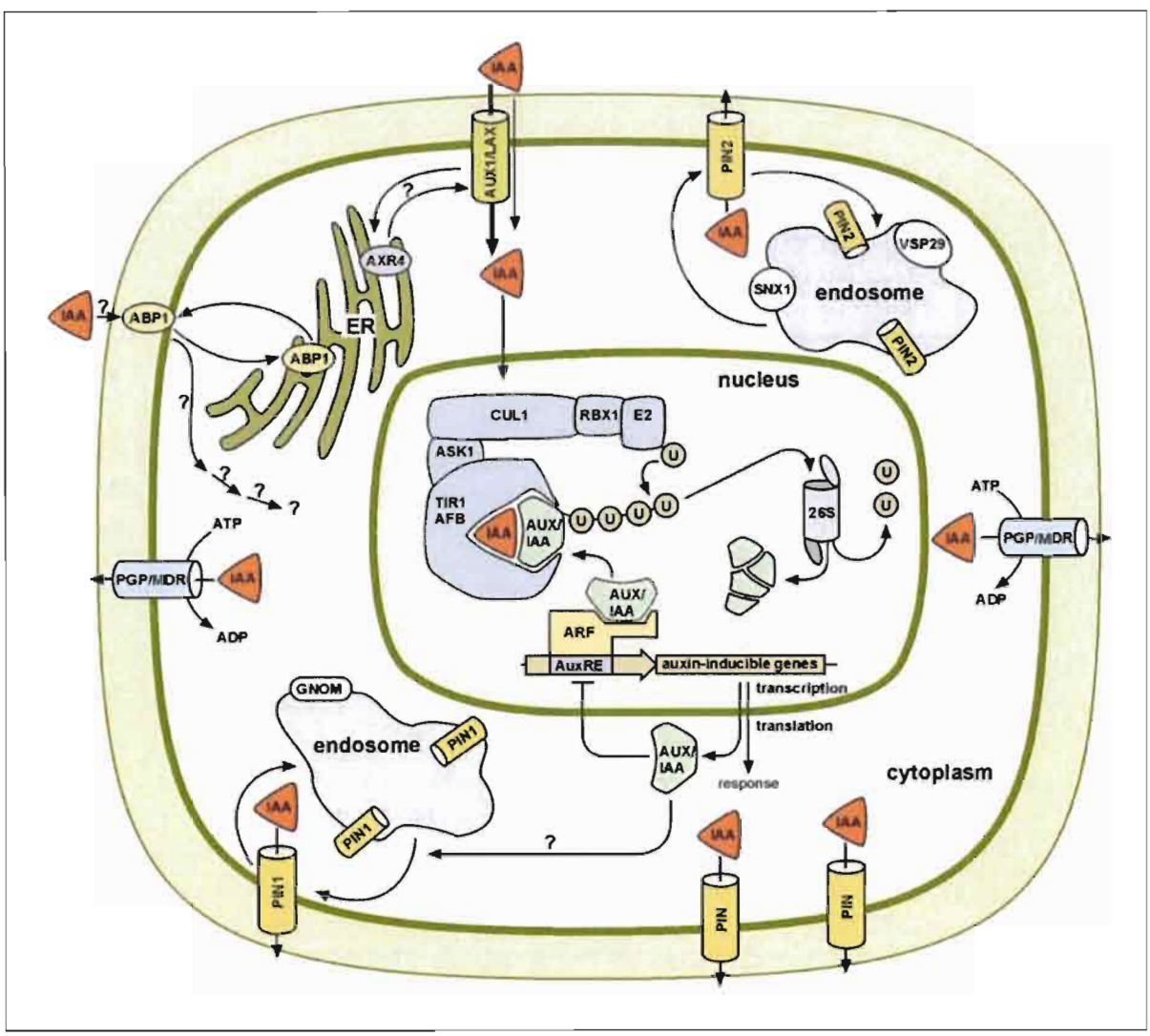

Figure 25. Synthetic overview of cellular active auxin transport and signaling
Auxin may enter cells through AUX1/LAX activities, and leave cells through PIN/PGP activities. There is a constant turnover of PINs protein at the membrane, which may be regulated by auxin perception. This perception is mediated by the proteic complex SCF^{TIR1}, which upon binding auxin will polyubiquitinate AUX/IAA proteins. AUX/IAA will then be destroyed by the proteasome (identified here by its 26S subunit tag), and ARF transcription factors, freed from the AUX/IAA inhibition, will bind to promoter presenting auxin response element (AuxRE) sequences. This will in turn induce the expression of downstream genes and the global auxin response.
From Delker et al. 2008

In the same way, macroscopical knowledge of auxin flows, accumulations and effects has been increasingly refined in the last few years. Once only considered to be related to plant growth, auxin now appears as a critical factor at all stages of plant development and growth (Figure 26). The range of its perceived effects and of the processes it appears to regulate is so large that auxin can be considered as a holy grail for plant developmental biology, coordinating and controlling (almost) everything during plant development (Jones 1998; Swarup, Marchant, and Bennett 2000; Swarup and Bennett 2003; Jirí Friml et al. 2003; Blilou et al. 2005; Ottoline Leyser 2005; Ottoline Leyser 2006; Scheres and Xu 2006; Kramer and Bennett 2006; Guilfoyle 2007).

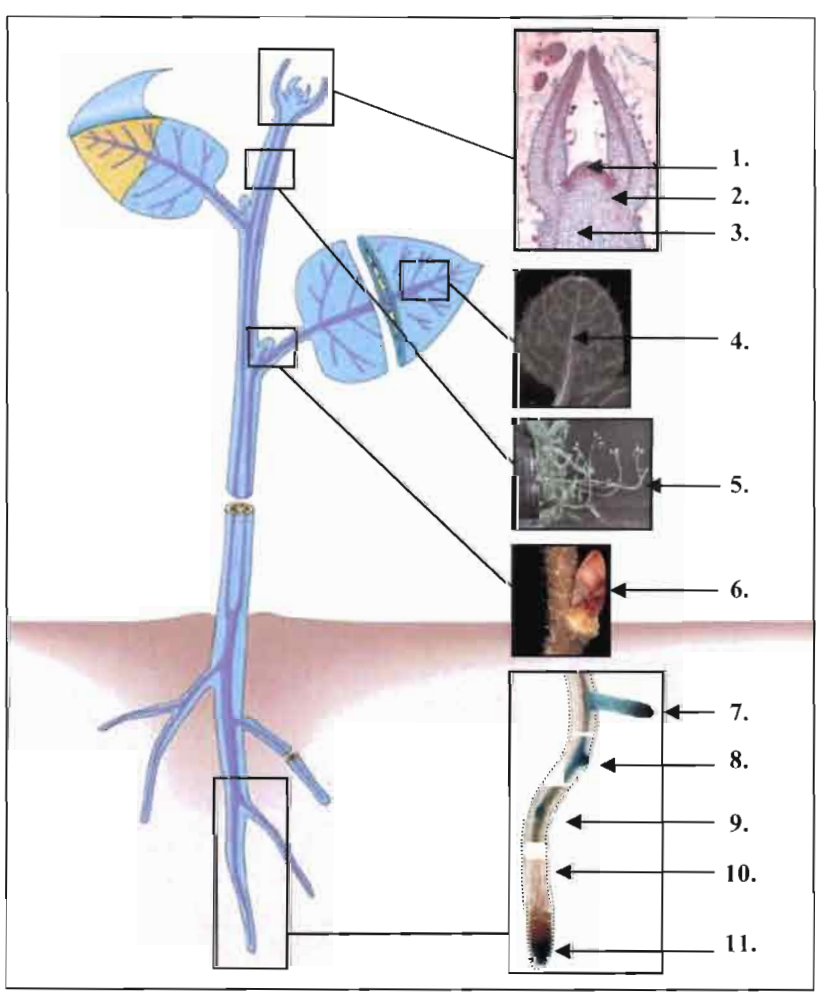

Figure 26. Roles of auxin in plant development
Auxin controls a wide range of developmental processes such as:
1. Phyllotaxis
2. Leaves primordia development
3. Vasculature patterning in stem
4. Vasculature patterning in leaves
5. Stem tropisms
6. Apical dominance and axillaries buds development
7. Lateral root emergence & development
8. Lateral root primordia development
9. Lateral root primordia initiation
10. Root tropisms
11. Maintenance of root apical meristem identity

- THESIS PROJECT -

This PhD project was born from a collaboration between the INRIA Project Virtual Plants and the Rhizogenesis IRD/University Montpellier II laboratory, enlisting both biologists and computers scientists. Benefiting from the experience of a previous thesis based on study and modelling of the shoot apical meristem (de Reuille et al. 2005; de Reuille et al. 2006), our main objective was to understand and model how auxin may control secondary root morphogenesis at the macroscopic and cellular scale.

We aimed to elucidate the regulation of ramification processes by auxin fluxes along the primary root of the model plant *Arabidopsis thaliana*, and to investigate the parallel and differences between shoot and root branching. We were particularly interested to test whether or not the inhibitory field theory used to describe shoot phyllotaxis and branching could be applied to root development (Hofmeiester 1868; M Snow and R Snow 1962) (Figure 27).

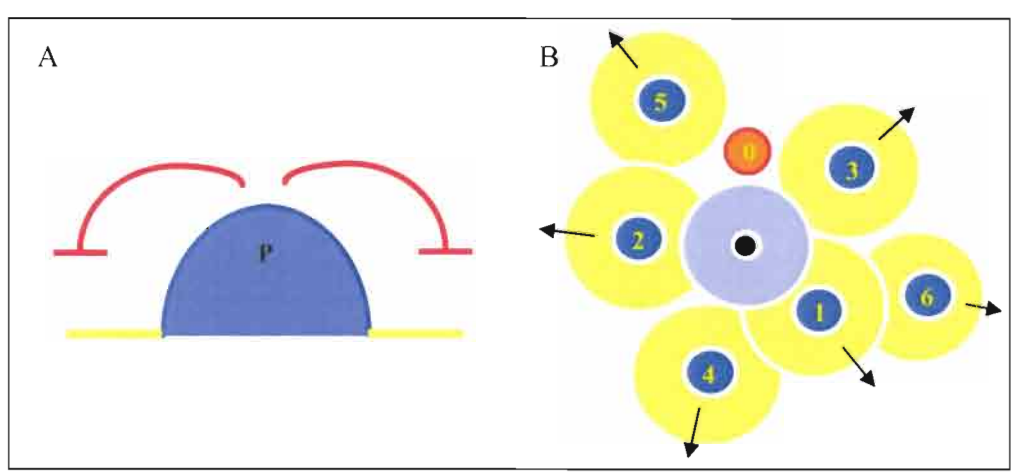

Figure 27. Inhibitory field and phyllotaxis
A – Schematic side view of a leaf primordium (P). The inhibitory field theory states that primordia inhibit the formation of nearby primordia within a certain radius (yellow) by emission of an "inhibitory signal" (red). This signal can correspond physically to the depletion of a local resource by the developing primordia. New primordia will not appear while this local resource does not become available again.
B – Schematic top view of a shoot apical meristem. Primordia (dark blue) appear in sequence (from oldest 6 to youngest 1) at the margin of the central competence zone (light blue) and progressively drift away from the centre (black) by cellular divisions. The conjugation of inhibition radius of the drifting primordia (yellow) defines a place on the border of the competence zone where inhibition is minimal (orange dot). This is where the next primordia (n° 0) will appear. The ratio of primordia inhibition radius and competence zone radius will determine the type of phyllotactic pattern emerging from these interactions.

Main steps of this project were:

i) To integrate available knowledge on lateral root positioning and development to pin-point black-boxes for which biological knowledge was absent or deficient

ii) To analyze homogeneous *Arabidopsis thaliana* seedling grown in controlled conditions *in vitro* and search for developmental regularities or specific developmental patterns, in order to exhibit some intrinsic regulation of root development

iii) To design structure-function models of developing roots and test hypothesis concerning the control of root ramification, at macroscopic and microscopic scales

iv) To investigate the black-boxes through biological experimentation and use perturbations of root morphogenesis to validate model predictions

The first black-box we encountered concerned the positioning of primordia along the primary root axis. While auxin has been identified as responsible for lateral root primordia initiation, and while auxin fluxes in the root were globally well understood, no mechanism was ever proposed to explain how auxin fluxes positioned lateral roots along the longitudinal root axis.

We studied this positioning mechanism on the basis that lateral root initiation appeared correlated to root waving, another phenomenon controlled by auxin. The results are presented in Chapter II of the present manuscript. We were able to demonstrate a formal link between the auxin fluxes controlling gravitropism and those inducing initiation. We proposed a predictive mechanistic model for the regulation of primordia initiation.

We were then interested in the regulation of root branching at the level of the whole primary root, taking into account initiation, development and emergence of lateral roots, as all these processes were known to be regulated by auxin fluxes (Figure 28). The results of this study are presented in Chapter III. We were able to show that root branching is regulated by mechanisms akin to inhibitory fields, and we designed a predictive mechanistic model of root branching.

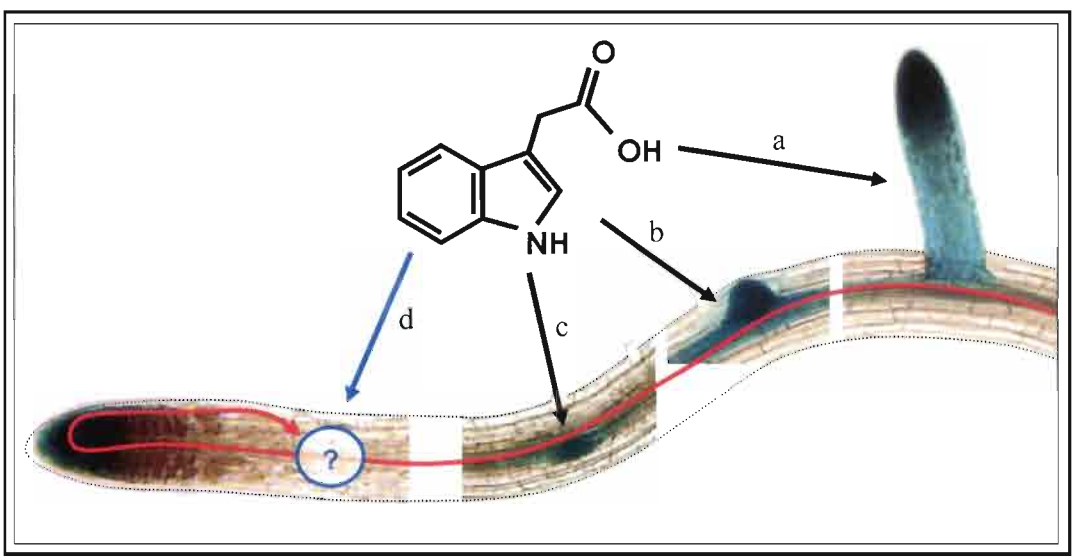

Figure 28. Auxin fluxes and root branching
Auxin has been shown to regulate lateral root development (a), lateral root emergence (b), lateral root primordia development (c), and lateral root primordia positioning (d). We investigated here the mechanisms of primordia positioning along the root axis, and the interactions between primordia initiation and development, on the basis of auxin fluxes (red arrow).

In parallel to those two previous studies, we designed a macroscopic model of root development and auxin fluxes based on L-system as a tool to feed biological reflection. As a complementary approach, and to investigate the precise cellular events of lateral root primordia initiation, we also built an *in silico* representation of the root tissue at the cellular scale. We proceeded to analyze the auxin fluxes occurring within this virtual root, and the results we obtained are presented in Chapter IV. The main results we obtained will be put into perspective and discussed in Chapter V.

- PART II -

Auxin fluxes in the root apex co-regulate gravitropism and lateral root initiation.

I) Introduction

As discussed earlier, lateral root formation has been well described in *Arabidopsis thaliana* (Casimiro et al. 2003; De Smet et al. 2006). Lateral root initiation has been shown to occur within the pericycle, in front of the xylem poles and in a zone close to the root apex (J G Dubrovsky et al. 2000; J G Dubrovsky et al. 2006). The precise longitudinal site of primordia initiation is still unknown, but it can be roughly located between the start of the elongation zone and the differentiation zone. It has also been shown that initiation only occurs sequentially in this zone, and that no new primordia can occur between existing primordia.

Here, we were interested in the mechanisms controlling primordia initiation. It was known that lateral root initiation is regulated by auxin, and correlation existed between primordia positioning and root bending, another phenomenon controlled by auxin fluxes (Fortin, Pierce, and Poff 1989; De Smet et al. 2007). Using gravistimulation as a tool to induce root bending, we studied the relationship between the fluxes controlling primordia initiation and root bending.

II) Results summary

We demonstrated that a gravistimulus quickly leads to lateral root initiation at the site of reorientation of root growth. Using gravistimulation to perturb the pattern of lateral root initiation, we were able to show that lateral root

initiation follows a plastic endogenous rhythm. This initiation rhythm appeared to be biologically constrained, with both a minimum and a maximum time between two successive lateral root initiations. We used our data to generate a mathematical model that could predict the effects of gravistimulations on lateral root initiation density. Moreover, we observed that the auxin flux responsible for lateral root initiation follows the same tissular pathway as the auxin responsible for gravitropism thus explaining the co-regulation of these two processes. Finally, a simple mathematical model suggested that the co-regulation of root bending and branching may optimize soil exploration by the root system.

The results we obtained were published in the Journal of Experimental Botany in January 2008, within a special issue on Transport of Plant Growth Regulators.

Research Article

Auxin fluxes in the root apex co-regulate gravitropism and lateral root initiation

Running title: Co-regulation of root gravitropism and branching by auxin transport

Lucas, M.[1,2], Godin, C.[2], Jay-Allemand, C.[3], and Laplaze L.[1,*]

[1] IRD, UMR DIA-PC (Agro.M/INRA/IRD/UM2), Equipe Rhizogenèse, 911 avenue Agropolis, 34394 Montpellier cedex 5, France

[2] INRIA, UMR DAP (Agro.M/Cirad/INRIA/INRA/UMII), Virtual Plants, TA40/02, Cirad, Avenue Agropolis 34398 Montpellier cedex 5, France

[3] Université Montpellier II, UMR DIA-PC (Agro.M/INRA/IRD/UM2), Equipe Rhizogenèse, Laboratoire de Biochimie et Physiologie Végétale, case 024, 34095 Montpellier cedex 5, France

Corresponding author: Laurent Laplaze, IRD, UMR DIA-PC, Equipe Rhizogenèse, 911 avenue Agropolis, 34394 Montpellier cedex 5, France, Tel: +33 (0)4 67 41 62 02, Fax: +33 (0)4 67 41 62 22, E-mail: laplaze@mpl.ird.fr

Date of submission: 27 June 2007

6 figures

6 supplementary figures

Published in Journal of Experimental Botany Special Issue "Transport of Plant Growth Regulators" in January 2008

ABSTRACT

Root architecture plays an important role in water and nutrient acquisition and in the ability of the plant to adapt to the soil. Lateral root development is the main determinant of the shape of the root system and is controlled by external factors such as nutrient concentration. Here we show that lateral root initiation and root gravitropism, two processes that are regulated by auxin, are co-regulated in *Arabidopsis*. We generated a mathematical model that can predict the effects of gravistimulations on lateral root initiation density and suggests that lateral root initiation is controlled by an inhibitory fields mechanism. Moreover, gene transactivation experiments suggest a mechanism involving a single auxin transport route for both responses. Finally, co-regulation may offer a selective advantage by optimizing soil exploration as supported by a simple quantitative analysis.

Keywords: AUX1, auxin transport, AXR3, GAL4, pericycle, root meristem.

INTRODUCTION

Exploration and exploitation of soil resources by plants depend on the development of the root system. Lateral root formation, which occurs throughout the life of the plant, is a main determinant of the shape of the root system and of its ability to adapt to a heterogeneous and changing environment (Malamy, 2005; Hodge, 2006).

The events leading to lateral root formation have been well described in *Arabidopsis thaliana* (Casimiro *et al.*, 2003; De Smet *et al.*, 2006). Lateral root development starts with asymmetric cell divisions in two adjacent pericycle cells, a process referred to as lateral root initiation (Malamy and Benfey, 1997; Dubrovsky *et al.*, 2000; De Smet *et al.*, 2006). Only pericycle cells that are in contact with the xylem poles are competent for lateral root initiation (Dubrovsky *et al.*, 2001). Lateral root formation takes place according to an acropetal gradient with lateral root initiation occurring in the differentiation zone of the root close to the root apex (Dubrovsky *et al.*, 2000, 2006; De Smet *et al.*, 2006). Subsequently, initiation can no longer occur between existing primordia (Dubrovsky *et al.*, 2006). In addition, lateral root initiation has a strong tendency toward alternation between the two xylem poles (Dubrovsky *et al.*, 2006). After initiation, the lateral root primordium goes through a series of well-characterised cell divisions that give rise to a root meristem (Malamy and Benfey, 1997; Casimiro *et al.*, 2003). The lateral root primordium then emerges from the parent root mostly by cell elongation (Malamy and Benfey, 1997).

Little is known about the mechanisms that control root branching. However, it is known that lateral root initiation, the establishment of the meristem, and lateral

root emergence are regulated independently. The plant hormone auxin plays a central role in lateral root development. It is the key signal that controls lateral root initiation (Casimiro *et al.*, 2003; De Smet *et al.*, 2006). Auxin is also involved in the growth and organisation of lateral root primordia (Benková *et al.*, 2003; Casimiro *et al.*, 2003) and in the emergence of lateral roots from the parent root (Laskowski *et al.*, 2006).

This work is part of a project combining mathematical and *in silico* modelling with experimental biology to better understand the mechanisms of root branching in *Arabidopsis*. Since lateral root initiation in *Arabidopsis* only occurs close to the root tip and since auxin is the key signal that controls this process, we decided to focus our efforts on auxin fluxes in the root apex. Auxin fluxes have already been studied in the apical root meristem (Blilou *et al.*, 2005) but little is known about the fluxes that are responsible for lateral root initiation. Interestingly, data suggests a link between root waving, which depends on gravitropism/thigmotropism, and lateral root initiation (De Smet *et al.*, 2007; Fortin *et al.*, 1989). Reorientation of primary root growth according to the gravity vector (gravitropism) depends on auxin fluxes in the root apical meristem, which have already been well described (Ottenschläger *et al.*, 2003; Swarup *et al.*, 2005).

Here we show that a gravistimulus quickly leads to lateral root initiation at the site of reorientation of root growth. We used gravistimulation to analyze the pattern of lateral root initiation. Our results indicate that lateral root initiation is rather plastic and that it is not strictly controlled by an internal rhythm. However, the existence of a minimum and a maximum time between two successive lateral root initiations demonstrate that there is a form of endogenous

control. We used our data to generate a mathematical model that can predict the effects of gravistimulations on lateral root initiation density. Moreover, we observed that the auxin flux responsible for lateral root initiation goes through the same route as the auxin responsible for gravitropism thus explaining the co-regulation of these two processes. Finally, mathematical modelling suggests that the co-regulation of root bending and branching optimize soil exploration by the root system.

MATERIAL AND METHODS

Plant Material and Growth

Wild type (Col-0) seeds were obtained from the NASC. *Pro$_{CYCB1}$:GUS* (Col-0 background) seeds were provided by Dr P. Doerner (University of Edinburgh, UK). J0951, M0013, UAS-axr3 lines in wild-type (Col-0) background and J0951, M0013, UAS-AUX1 lines in *aux1-22* mutant background were kindly provided by Dr. R. Swarup (University of Nottingham, UK). Plants were grown on vertical plates as previously described (Laplaze *et al.*, 2005). Plates were then subjected to 90° gravistimulations. For additional details on the periodical gravistimulation, see Figure S1. All gravistimulation and transactivation experiments were repeated twice independently.

Root lengths were measured from scans of the roots with the UTHSCSA ImageTool open-source software, available at http://ddsdx.uthscsa.edu/dig/itdesc.html. Lateral root development stages were

scored using an optical microscope according to Malamy and Benfey (1997). Data were analyzed using the Excel statistical package.

Microscopy

Seedlings were collected and incubated in a solution containing 50 mM sodium phosphate buffer, pH 7.0, 0.5 mM $K_3Fe(CN)_6$ and $K_4Fe(CN)_6$, 0.05% (v/v) Triton X-100, 0.05% (v/v) DMF, 0.02% (v/v) EDTA, and 1 mM 5-bromo-4-chloro-3-indolyl-β-glucuronic acid and incubated at 37°C for several hours. Seedlings were then cleared in 70% (v/v) ethanol for 24 hours, before being immersed for 2 hours in 10% (v/v) glycerol 50% (v/v) ethanol; 2h in 30% (v/v) glycerol 30% (v/v) ethanol; 2h in 50% (v/v) glycerol. Seedlings were mounted in 50% (v/v) glycerol and visualized using a DMRB microscope (Leica).

Design of a mechanistic model of lateral root initiation

The mechanistic model of lateral root initiation we introduced (Fig. 3A) was formalized and transcribed in the python programming language as a logical algorithm (Fig S4). Parameter T1 (spontaneous initiation threshold) was estimated directly from the observed data as the mean time between two successive initiations in the control. The two other parameters T2 (induced initiation threshold) and G (cost of gravistimulation) were inferred from observed data, using Python-scripts to explore the parameters-space. Over 1800 parameter combinations of T2 and G were tested. The parameter combination corresponding to the best fit of lateral root initiation densities to the observed

values was selected for subsequent model prediction. The Python stand-alone module is available from the authors.

Lateral dissymmetry of soil exploitation along the primary root

As primary roots do not grow straight, successive bends induce geometric dissymmetry between the inner and outer parts of a root turn. We quantified the effect of such dissymmetry in terms of the availability of local resources using simple mathematical modelling. As *Arabidopsis thaliana* lateral root initiation takes place in a plane defined by the two protoxylem strands, this analysis was made in a 2-dimensional space. In addition, we made a number of simplification hypotheses. The number of root hairs (n) is considered equal between each side of a root turn. As a consequence, due to the differential growth of epidermal cells under gravistimulation, the density of root hairs on the external side is lower than on the internal side (Fig. 5B). We consider that each root hair harvests a fixed pool of resource (a) and that resources diffuse passively in the soil (i.e. resources flow toward the root as they become locally depleted). According to these assumptions, overall soil exploitation, defined as the volume of resources harvested per time unit, is equivalent on both sides of the root. Working in a 2-dimensionnal space, here we consider the corresponding exploited surfaces, s_1 on the inner side and s_2 on the outer side (Fig. 5C). We also assume that each root turn corresponds to a portion of a circle of radius ρ. Considering an infinitesimal portion of root turn defined by the angle $d\alpha$, soil exploitation takes place over dl_1 (inner side) and dl_2 (outer side; Fig. 5B). If (b) represents the thickness of the root (assumed to be constant in the zone concerned), we have:

(1) $dl_1 = (\rho - b / 2) \, . \, d\alpha$

(2) $dl_2 = (\rho + b / 2) \, . \, d\alpha$

The surface of soil exploited on each side can be written as:

(3) $s_1 \propto dl_1 \, . \, h_1$

(4) $s_2 \propto dl_2 \, . \, h_2$

where $\propto$ stands for proportional and h_1 and h_2 are the respective depth of exploitation on each side (not to be confounded with root hair length – see Fig. 5C). Under our hypotheses, these surfaces are proportional to the number of root hairs (n) and their harvesting power (a). These parameters being the same on each side of the root, we have:

(5) $s_1 = s_2 = s \propto n \, . \, a$

From (3), (4) and (5) we obtain:

(6) $dl_1 \, . \, h_1 = dl_2 \, . \, h_2$

And from (1), (2) and (6) we get:

(7) $h_1 / h_2 = (\rho + b / 2) / (\rho - b / 2)$

This equation gives the ratio between the depth of exploration on each side as a function of ρ (Fig. S6A). If ρ tends toward infinity, i.e. the root becomes completely straight (infinite curve radius), then the ratio h_1/h_2 tends to 1. This corresponds to an equal depth of exploration on each side of straight roots. By contrast, if ρ tends to ($b/2$), h1 becomes much greater than h2. The equation (7) is not valid for ρ inferior to ($b/2$) as this is a biological impossibility (root turn with an inner side of negative length dl_1).

Using pictures of gravistimulated root turn and waving roots, we were able to estimate various values for ρ (Fig. S6B, C). These values correspond to a ratio h_1/h_2 varying between 1.4 and 3 (Fig. S6D). Extrapolating these results to the

whole root and in three dimensions leads to an asymmetric profile of soil exploration (Fig. 5A, D) and corresponding resource depletion (Fig. 5E).

Root hair length analysis

Wild type (Col-0) seeds were grown on vertical plates as previously described (Laplaze *et al.*, 2005). Plates were then subjected to three 90° gravistimulations at 12h time intervals, starting 30h after germination. Pictures of the plants were obtained using a MZFLIII (Leica) dissecting microscope equipped with a digital camera. Root hair length was measured with the UTHSCSA ImageTool open-source software. Data were analyzed using the Excel statistical package.

RESULTS

Gravistimulation leads to local lateral root initiation

Recent studies indicate that lateral root formation is correlated with root waving in an AUX1-dependent way (De Smet *et al.*, 2007). In order to test whether gravitropism and lateral root initiation are co-regulated, we tested the effect of gravistimuli on lateral root initiation. Transgenic *Arabidopsis* plants carrying a Pro_{CYCB1}*:GUS* marker for cell division were grown on vertical plates for 30 hours after germination and then subjected to a gravistimulus (90° rotation) every 12h for 3.5 days. Two different patterns of gravistimulation were used leading to stair- or crenel-shaped root growth (see Fig. S1). Plants were then left to grow for an extra 60h before testing for GUS activity. Roots were then cleared and

lateral root initiation, i.e. the presence of a lateral root primordium from the first asymmetric cell divisions in the pericycle (stage I) on, was scored under a light microscope.

We observed that lateral root initiation occurred in more than 90% of the gravistimulated zones where the root apex was reorientating its growth toward the new gravity vector (thereafter called turns; Fig. 1A, B). By contrast, only a limited number of lateral root initiations were observed between turns (<10%; Fig. 1A, B). This cannot be explained by the relative length of the gravistimulated zone versus the non-gravistimulated zone because the straight (non-gravistimulated) zone was longer than the curved (gravistimulated) zone (data not shown). Moreover, we observed that it took four hours in our growth conditions for all root apexes to reorient their growth direction after a 90° gravistimulus (data not shown) in agreement with previous studies (Swarup *et al.*, 2005). In our experiment, we therefore had about four hours of gravistimulated growth followed by about eight hours of non-gravistimulated root growth. If lateral root initiation occurs randomly or regularly, we would expect about 2/3 of the LRP to occur in the non-gravistimulated zone. We therefore conclude that lateral root initiation is induced in response to gravitropic root bending.

We next analyzed the timing of lateral root initiation following a gravistimulus. Six batches of *Pro$_{CYCB1}$:GUS* plants were grown for 30h after germination on vertical Petri dishes then subjected to a 90° gravistimulus every six hours with a one hour delay between each batch. This was done for 24h and plants were then harvested and stained for GUS activity. This enabled us to observe gravistimulated zones every hour from 0 to 25h after stimulation. The

occurrence and stage of development of lateral root primordia at root turns were scored (Malamy and Benfey, 1997). The first occurrence of stage I lateral root primordia was found seven hours after gravistimulation (Fig. 1C). All the gravistimulated zones showed lateral root initiation 13 hours after gravistimulation (Fig. 1C). Stage II and III of lateral root development occurred six and 12 hours after lateral root initiation respectively (Fig. 1D). Our data therefore indicate that lateral root initiation occurs rapidly after gravistimulation.

We observed that lateral root primordia always appeared on the external side of the bend (100%, n=2677 LRP observed; Fig. S2). Previous studies observed a left-right alternation of lateral root formation (De Smet *et al.*, 2007). This was indeed the case in stair-shaped roots. In contrast, the crenel-shaped roots had two initiations on one side followed by two initiations on the other side (Fig. S2). In this case we observed that lateral root initiation occurred twice along the same protoxylem pole (data not shown). This indicates that lateral root initiation is not constrained to a left-right alternation but that lateral root primordia always appear on the external part of a gravistimulus-initiated root bend. This is in agreement with previous results showing that emerged lateral roots occur preferentially on the convex side of a curved root (Fortin *et al.*, 1989).

The rhythm of lateral root initiation is modified by external clues

We showed that lateral root initiation can be initiated by gravistimuli applied every 12 hours. Studies by De Smet et al. (2007) suggest that lateral root initiation sites are predetermined by an endogenous rhythm with a period of about 15 hours. In order to test whether lateral root initiation was strictly

controlled by an internal rhythm, we used the experimental design previously described applying gravistimuli every 1, 3, 6, 12 or 24 hours (Fig. 2A, Fig. S3A). Similar results were obtained for stair- and crenel-shaped roots (Fig. 2 and Fig. S3 respectively). For periods of 6, 12 and 24 hours between gravistimuli, lateral root initiation was found in more than 90% of root turns (gravistimulated zones; Fig. 2B). This value was reduced to about 50% for roots gravistimulated every three hours (Fig. 2B). For roots stimulated every hour, the roots did not have enough time to reorientate their growth and we were therefore unable to measure the percentage of turns showing lateral root initiation. Lateral root initiation occurred between turns only in roots subjected to gravistimulation at 12 hour (less than 10%) or 24h intervals (more than 35%; Fig. 2C). This confirms that lateral root initiation is induced by gravistimulation independently of the period between stimulations. As previously observed, lateral root primordia always formed on the external part of the bend.

We then determined the effect of the gravistimuli on the density of lateral root initiation. We first observed that gravistimuli had no significant effect on the growth of the primary root (Fig. 2D). Moreover within gravistimulated roots the gravistimulated and non-gravistimulated segments displayed similar root growth (Fig. 2D). We then observed that gravistimulation changed lateral root density with an optimum for gravistimulation at 6-hour intervals (Fig. 2E). Taken together our results indicate that lateral root initiation is not strictly controlled by an internal biological rhythm and that the rhythm of lateral root initiation can vary according to environmental clues such as gravity or touch. However, we also show that, in our experimental conditions, two subsequent lateral root initiations cannot occur at too short intervals. Indeed, when the interval between

two successive gravistimulations was equal to or less than three hours, the percentage of turns with LRI dropped and LRP density returned to non stimulated level. Moreover, our data also suggest that, on the contrary, two lateral root initiations cannot be separated by too long a time interval. Accordingly, lateral root initiations between turns increased with the time between gravistimulations and LRP density cannot be reduced below a minimal level that is close to non-stimulation conditions. We conclude from our experiments and previous data (De Smet *et al.*, 2007) that there is an endogenous regulatory system controlling lateral root initiation that is responsible for regular lateral root initiation in a homogeneous medium. However this regulatory system is influenced by external clues such as gravitropism.

The effect of gravistimulations suggests a mechanism of inhibitory fields controlling root branching

These first results on gravistimulation showed a global consistent rationale that we attempted to capture quantitatively through the design of a simple mechanistic model. This model was based on an auxin budget system (Fig. 3A) and aimed to explain the effects of gravistimulations on lateral root initiation. When a root grows unperturbed it initiates new lateral root primordia regularly. We model this phenomenon as the progressive filling of an exploitable auxin pool. The filling is assumed to take place at a constant rate (P). When the quantity of auxin in the pool is greater than the threshold value T1, lateral root initiation occurs and the auxin pool is entirely consumed. This mechanism

controls spontaneous initiation (Fig. 3A, white arrows). We estimated the threshold value T1 to be equivalent to 12 hours of auxin production/accumulation in our conditions, as initiation density in our control corresponds to a 12 hours period between lateral root initiations.

When a 90° gravistimulation is applied, it either enhances the perception of auxin at the future initiation sites, or locally concentrates auxin at these points by changing auxin distribution without changing the global auxin quantity in the root. Both hypotheses are strictly equivalent at an abstract level, and can be expressed in the model by introducing a new threshold. We thus distinguish in our model the spontaneous lateral root initiation threshold T1 and the lower threshold T2 corresponding to gravistimulation-induced initiation. In addition, each gravistimulation induces an auxin consumption (G) from the auxin pool. Two cases must then be distinguished: either the remaining auxin level is higher than T2, or it is lower. In the first case, a lateral root initiation occurs and the auxin pool is flushed (Fig. 3A, grey arrows). In the second case, no initiation occurs, and the system runs its course (Fig. 3A, black arrows).

We designed a computer algorithm implementing the above mechanistic model controlling lateral root initiation in time as described in figure 3A. This model takes as an input parameter T1, estimated from observed data (T1=12h, which corresponds to the mean time between two successive initiations in the control), and a gravistimulation pattern, corresponding to a series of time intervals between gravistimulations on a given individual. The algorithm returns the predicted sequence of lateral root initiations over the time length of the gravistimulation pattern, depending on the value of T2 and G. To estimate the values of these two parameters, we proceeded to an extensive exploration of the

parameter space and compared the number of lateral root initiations of the returned initiation patterns to the observed number of lateral root initiations of gravistimulated roots. The values of T2 and G giving the best fit were T2 ~ 0.4 T1 and G ~ 0.05 T1. The output of the model obtained using those values closely follows the observed number of lateral root initiations (Fig. 3B).

In order to validate the model, we designed a new experiment to evaluate its predictive power. We selected 6 new gravistimulation patterns (Fig. S5) not previously tested, with either regular or irregular spacing between gravistimulations. Based on direct pattern observation, it was not possible to guess the total number of lateral root initiations that would be produced. Those patterns were applied on *Pro$_{CYCB1}$:GUS* seedlings for 48h, according to the previously described protocol of gravistimulation. The total number of lateral root initiations for the various seedlings groups were scored and compared to the total number of lateral root initiations predicted by the model (Fig. 3C). This experiment was repeated twice independently.

We found that the total number of lateral root initiations is not governed by the number of gravistimulations (Fig. 3D). The quantitative model was able to predict with accuracy the total number of LRI for each pattern, over a large range of total number of lateral root initiations without loss of accuracy (Fig. 3C,E) thus showing that the total number of lateral root initiations is actually a function of the structure of the gravistimulation pattern. Similarly to the inhibitory field models for the shoot apical meristem (Douady and Couder, 1996; Smith *et al.*, 2006), the proposed model suggests that lateral root initiations are submitted to inhibition fields (here represented by auxin consumption) that control their patterning.

Common auxin fluxes regulate gravitropism and lateral root initiation

Gravitropism and lateral root initiation are both regulated by auxin (Casimiro *et al.*, 2001; Swarup *et al.*, 2005). Gravity is perceived in the central part of the root cap and gravitropism relies on an AUX1-dependent acropetal auxin flux from the root apex through the lateral root cap and the elongating root epidermis where it induces changes in cell elongation (Ottenschläger *et al.*, 2003; Swarup *et al.*, 2005). AUX1 encodes a high-affinity auxin influx carrier (Yang *et al.*, 2006). On the other hand, very little is known about the auxin fluxes that are responsible for lateral root initiation in the root pericycle. However, the *aux1* mutant is perturbed in both lateral root initiation and root gravitropism and recent studies suggest a common auxin transport pathway for gravitropism and lateral root initiation (De Smet *et al.*, 2007).

Since we found that gravitropism and lateral root initiation are co-regulated we tested whether both processes were dependent on the same auxin transport route. We used a transactivation strategy to complement the *aux1* mutant in different tissues at the root apex as described by De Smet *et al.* (2007) and to test the effect on lateral root initiation. Plants expressing *UAS:AUX1* under the control of the GAL4 enhancer trap lines M0013 (root cap) or J0951 (root cap and expanding root epidermis) in an *aux1-22* mutant background (Swarup *et al.*, 2005) were grown for 10 days on vertical plates. They were then harvested and scored for gravitropism and lateral root primordia density. Our results on lateral root initiation (Fig. 4A) were similar to those obtained by De Smet *et al.* (2007)

on lateral root density. We therefore conclude that the auxin necessary for lateral root initiation and gravitropic root growth has to be transported through the same route in the lateral root cap and the elongating root epidermis.

We next tested whether auxin needs to be perceived in the tissues through which it flows for lateral root initiation. We transactivated a dominant negative version of the AXR3 protein (axr3-1) that was previously shown to inhibit auxin response in different root tissues (Swarup *et al.*, 2005) and tested the effects on gravitropism and lateral root initiation. F1 plants were grown for 10 days on vertical plates before analysis. Our results on gravitropism were similar to those of Swarup *et al.* (2005). When axr3-1 was transactivated in the root cap, using ET line M0013, it had no effect on gravitropism or lateral root initiation (Fig. 4B). When axr3-1 was transactivated in both the root cap and the root epidermis using enhancer trap line J0951, it abolished the gravitropic response of the root but did not perturb lateral root initiation (Fig. 4B). Thus our results suggest that in contrast to gravitropism, auxin does not need to be perceived in the root epidermis in order to direct lateral root formation.

Does co-regulation of gravitropism and lateral root initiation optimize soil exploration?

Our results indicated that lateral root initiation and gravitropism/thigmotropism are, at least in part, co-regulated. We next wondered if co-regulation could have some selective advantage. We used simple geometrical considerations to evaluate the potential effect of co-regulation on resource exploitation (Fig. 5). We estimated the volume of soil explored by a

root (see Material and Methods for details) using three simplifying assumptions: 1) the volume of soil exploited by a given root segment is proportional to the number of root hairs, 2) resources (water and nutrients) diffuse in the soil according to their concentration gradient, and 3) all root hairs have the same absorption potential. Since gravitropism/thigmotropism is due to changes in cell elongation in the root epidermis, the number of root hairs is the same on the internal as on the external side of a curved root, and root hair density (per root length) is lower on the external side (Fig. 5B). This means a greater depth of soil is exploited on the internal side (h1, Fig. 5C) than on the external side (h2). Extrapolating these results to the whole root and in three dimensions leads to an asymmetric profile of soil exploration (Fig. 5A,D). This suggests that lateral root formation on the outer parts of the turns may optimize soil exploitation (Fig. 5E). We considered in our model that root hair length was identical on both side of the bend. On the other hand, auxin is known to increase root hair length (Pitts *et al.*, 1998) and auxin preferentially accumulates on the lower side of roots during gravitropic curvature. Accordingly, we found that root hairs were significantly longer on the inside and shorter on the outside of a bend than control root hairs (Fig. S6E,F). This will therefore increase the depletion effect that observed in our model on the inside of the bend.

DISCUSSION

Our study shows that gravistimuli induce lateral root initiation. Lateral root formation in gravistimulation experiments is not due to bending itself because the root of the *aux1* mutant or J0951>>axr3 plants showed many turns without

increasing lateral root initiation. The co-regulation of lateral root initiation and root gravitropism explains why there is such a good correlation between root waving and lateral root initiation (De Smet et al., 2007). This is also in agreement with the fact that many mutants are perturbed in both processes. Simple mathematical modelling suggests that this co-regulation of gravitropism/thigmotropism and lateral root initiation leading to formation of lateral root primordia on the external side of a bend might offer some selective advantage by optimizing soil exploration.

Our data suggest that the regulatory system responsible for lateral root initiation is sensitive to external clues perceived at the root apex such as gravity. Indeed we were able to change root architecture simply by applying gravistimulations at different intervals. Our data also point out to internal characteristics of the regulatory system such as the minimum/maximum time between two successive initiations. We used these results to create a mathematical model that can explain and predict the effects of gravistimulations on lateral root initiation density. Our model suggests that by creating a asymmetric distribution of auxin in the apex using gravistimulations, one is able to reduce the amount of auxin necessary for lateral root initiation. Interestingly this simple mechanistic model suggests that lateral root initiation is controlled by inhibition fields (auxin consumption) in the root apex like lateral organ formation in the shoot apical meristem (Douady and Couder, 1996; Smith *et al.*, 2006).

Because it is impossible to predict the position of lateral root initiation and because initiation is a relatively rapid process, little is known about the cellular events that precede it, i.e. the very first division that occurs during lateral root development. Our results indicate that it is possible to use gravistimuli to induce

lateral root initiation locally with almost 100% success. Such a system can thus be used to monitor the course of cellular events that occur before lateral root initiation. It offers an alternative approach to auxin-based lateral root induction systems (Himanen *et al.*, 2002) to study cellular processes such as nucleus movement or changes in cellular trafficking or in the organization of the cytoskeleton that might prepare the first cell division i.e. lateral root initiation.

Finally, our experimental data suggest a mechanism for co-regulation of gravitropism and lateral root initiation (Fig. 6). Auxin, the key signal that controls both processes, is produced in leaf primordia and transported to the root via the vascular basipetal flow (Friml *et al.*, 2006). Root meristems and lateral root primordia can also produce auxin (Ljung *et al.*, 2005). An auxin maximum is generated in the root columella (Sabatini *et al.*, 1999) and auxin is redistributed in the meristem from the columella in a PIN3-dependent way. Upon gravistimulation, PIN3 is retargeted to the lower face of columella cells thus creating an asymmetric auxin distribution (Friml *et al.*, 2002). Auxin is transported from the root tip through the lateral root cap and in the elongating root epidermis in an AUX1/PIN2-dependent way thus generating an acropetal auxin flux (Swarup *et al.*, 2005). Auxin perception in the epidermis is then responsible for root gravitropism by changing the relative elongation of epidermal cells (Swarup *et al.*, 2005). Our transactivation experiments together with previous results (De Smet *et al.*, 2007) indicate that the same acropetal flux is responsible for lateral root initiation further up the root. This is consistent with previous data indicating that acropetal auxin transport from the root tip is responsible for lateral root initiation (Casimiro *et al.*, 2001; Bhalerao *et al.*, 2002). Moreover, our axr3 transactivation data suggest that while gravitropism

requires AUX/IAA-dependent auxin perception in the root epidermis, lateral root initiation does not. This suggests that the root epidermis only acts as a passive auxin transport route in lateral root initiation. Since the dynamic changes in PIN protein cellular localization in response to changes in auxin concentration in the root depend on the AUX/IAA-ARF pathway (Sauer *et al.*, 2006), this suggests that lateral root initiation does not require such auxin-dependent PIN relocalisation at least in the epidermis.

Later stages of lateral root development depend on basipetal auxin transport from the shoot (Casimiro *et al.*, 2001; Bhalerao *et al.*, 2002) until lateral root primordia become independent of external auxin between stage III and V (Laskowski *et al.*, 1995) when auxin synthesis may start (Ljung *et al.*, 2005). As a consequence the position of lateral root primordia is partially controlled by gravitropism/thigmotropism but the later development of these primordia is independent of these two processes and may be regulated by other factors such as water or nutrient availability (Malamy, 2005). How an asymmetric auxin distribution in the epidermis leads to lateral root initiation in the pericycle is still unknown. Interestingly, during gravitropism the auxin maximum occurs on the internal side of the bend while lateral root initiation occurs on the external side. We are currently building an *in silico* model based on this and previous studies (Blilou *et al.*, 2005; Swarup *et al.*, 2005) to try to understand how the redistribution of auxin in the root apex controls root branching.

SUPPLEMENTARY DATA

Fig. S1. Gravistimulation protocols. Seedlings were grown on vertical plates and gravistimulated by a periodic (period T) 90° rotation of the growth plates. Two different rotation protocols were used to generate either crenel-shaped or stair-shaped roots. Roots subjected to these protocols were grown under stimulation for 3.5 days and with no stimulation for an additional 2.5 days before harvesting.

Fig. S2. Localisation of lateral root initiation in a gravistimulated root. A Pro_{CYCB1}::GUS seedling was subjected to crenel gravistimulation at 12-h intervals. Lateral root initiations were localized and their development scored.

Fig. S3. Influence of varying gravistimulation on lateral root initiation density (crenel-shaped roots). (A) Vertically grown Pro_{CYCB1}::GUS seedlings were left to grow (control; n=20) or were subjected to gravistimulation at intervals of 1 h (n = 24), 3 h (n = 20), 6 h (n = 21), 12 h (n = 21) or 24 h (n= 24) over a period of 3.5 days (1), then left to grow for 2.5 days without stimulation (2). Bars = 1 cm. (B) Occurrence of LRI in root turns. (C) Occurrence of lateral root initiation between root turns. Due to the particular configuration of roots subjected to gravistimulation at 1-h and 3-h intervals (respectively presenting no visible turns and only turns), some values were not determined (na = not applicable). (D) Effect of gravistimulation on root growth. Length of the gravistimulated root segments (first 5 days of growth) and non-gravistimulated root segments (last 2.5 days of growth) were also determined. (E) Lateral root initiation densities were determined in gravistimulated and non-gravistimulated root segments. Different

letters indicate significantly different results as tested by a Student T-test ($P < 0.01$).

Fig. S4. The RootInit algorithm corresponding to the mechanistic model. The pseudo-code is expressing the mechanisms described in Fig. 3A in discrete time.

Fig. S5. Gravistimulation patterns used for the evaluation of our model. Six previously non-tested gravistimulation patterns were applied to seedlings over a 48h period starting 30 hours after germination. Gravistimulation are indicated by black dots. The total number of gravistimulation for each pattern varies between 10 and 25. After the last gravistimulus, seedlings were left to grow undisturbed for 24h before harvest and observation.

Fig. S6. Curve radius, depth of exploration and root hair length. (A) Curve of the function $h_1 / h_2 = (\rho + b / 2) / (\rho - b / 2)$. (see figure 4 for additional details on the parameters) (B) Curve radius estimated for a portion of a gravistimulated root (90° re-orientation). b and ρ are the thickness and the curve radius of the chosen root portion respectively. (C) Curve radius estimated for various root turns of a waving root. (D) Ratio of exploration depths (h_1 / h_2) for various values of (ρ). (E) Direct visualization of root hair on both sides of a root turn. (F) Root hair length was measured on both sides of root turns (n=20) and straight roots. Different letters indicate significantly different results as tested by a Student T-test ($P < 0.01$).

ACKNOWLEDGEMENTS

We thank Dr P. Doumas and Dr D. Bogusz (Equipe Rhizogenèse) for critical reading of the manuscript. This work was supported by IRD and INRIA (Virtual Plants project). M.L. is the recipient of a PhD grant from the French *Ministère de l'Enseignement Supérieur, de la Recherche et de la Technologie.*

REFERENCES

Benková E, Michniewicz M, Sauer M, Teichmann T, Seifertová D, Jürgens G, Friml J. 2003. Local, efflux-dependent auxin gradients as a common module for plant organ formation. *Cell* **115,** 591-602

Bhalerao RP, Eklöf J, Ljung K, Marchant A, Bennett MJ, Sandberg G. 2002. Shoot-derived auxin is essential for early lateral root emergence in Arabidopsis seedlings. *The Plant Journal* **29,** 325-332

Blilou I, Xu J, Wildwater M, Willemsen V, Paponov I, Friml J, Heidstra R, Aida M, Palme K, Scheres B. 2005. The PIN auxin efflux facilitator network controls growth and patterning in Arabidopsis roots. *Nature* **433,** 39-44

Casimiro I, Beeckman T, Graham N, Bhalerao R, Zhang H, Casero P, Sandberg G, Bennett MJ. 2003. Dissecting Arabidopsis lateral root development. *Trends in Plant Sciences* **8,** 165-171

Casimiro I, Marchant A, Bhalerao RP, Beeckman T, Dhooge S, Swarup R, Graham N, Inzé D, Sandberg G, et al.. 2001. Auxin transport promotes Arabidopsis lateral root initiation. *The Plant Cell* **13,** 843-852

De Smet I, Tetsumura T, De Rybel B, Frei Dit Frey N, Laplaze L, Casimiro I, Swarup R, Naudts M, Vanneste S, et al.. 2007. Auxin-dependent regulation of lateral root positioning in the basal meristem of Arabidopsis. *Development* **134, 681-690**

De Smet I, Vanneste S, Inzé D, Beeckman T. 2006. Lateral root initiation or the birth of a new meristem. *Plant Molecular Biology* **60,** 871-887

Douady S, Couder Y. 1996. Phyllotaxis as a dynamical self organizing process .1. The spiral modes resulting from time-periodic iterations. *Journal of Theoretical Biology* **178,** 255-274

Dubrovsky JG, Doerner PW, Colón-Carmona A, Rost TL. 2000. Pericycle cell proliferation and lateral root initiation in Arabidopsis. *Plant Physiology* **124,** 1648-1657

Dubrovsky JG, Gambetta GA, Hernández-Barrera A, Shishkova S, González I. 2006. Lateral Root Initiation in Arabidopsis: Developmental Window, Spatial Patterning, Density and Predictability. *Annals of Botany (Lond)* **97,** 903-915

Dubrovsky JG, Rost TL, Colón-Carmona A, Doerner P. 2001. Early primordium morphogenesis during lateral root initiation in *Arabidopsis thaliana. Planta* **214,** 30-36

Fortin MC, Pierce FJ, Poff KL. 1989. The pattern of secondary root formation in curving roots of *Arabidopsis thaliana* (L.) Heynh. *Plant Cell & Environment* **12,** 337-339

Friml J, Benfey P, Benková E, Bennett MJ, Berleth T, Geldner N, Grebe M, Heisler M, Hejátko J, et al.. 2006. Apical-basal polarity: why plant cells don't standon their heads. *Trends in Plant Sciences* **11,** 12-14

Friml J, Wiśniewska J, Benková E, Mendgen K, Palme K. 2002. Lateral relocation of auxin efflux regulator PIN3 mediates tropism in Arabidopsis. *Nature* **415,** 806-809

Himanen K, Boucheron E, Vanneste S, de Almeida Engler J, Inzé D, Beeckman T. 2002. Auxin-mediated cell cycle activation during early lateral root initiation. *The Plant Cell* **14,** 2339-2351

Hodge A. 2006. Plastic plants and patchy soils. *Journal of Experimental Botany* **57,** 401-411

Laplaze L, Parizot B, Baker A, Ricaud L, Martinière A, Auguy F, Franche C, Nussaume L, Bogusz D, Haseloff J. 2005. GAL4-GFP enhancer trap lines for genetic manipulation of lateral root development in Arabidopsis thaliana. *Journal of Experimental Botany* **56,** 2433-2442

Laskowski M, Biller S, Stanley K, Kajstura T, Prusty R. 2006. Expression Profiling of Auxin-Treated Arabidopsis Roots: Toward a Molecular Analysis of Lateral Root Emergence. *Plant Cell Physiology* **47,** 788-792

Laskowski MJ, Williams ME, Nusbaum HC, Sussex IM. 1995. Formation of lateral root meristems is a two-stage process. *Development* **121,** 3303-3310

Ljung K, Hull AK, Celenza J, Yamada M, Estelle M, Normanly J, Sandberg G. 2005. Sites and regulation of auxin biosynthesis in Arabidopsis roots. *The Plant Cell* **17,** 1090-1104

Malamy JE, Benfey PN. 1997. Organization and cell differentiation in lateral roots of Arabidopsis thaliana. *Development* **124,** 33-44

Malamy JE. 2005. Intrinsic and environmental response pathways that regulate root system architecture. *Plant Cell & Environment* **28,** 67-77

Ottenschläger I, Wolff P, Wolverton C, Bhalerao RP, Sandberg G, Ishikawa H, Evans M, Palme K. 2003. Gravity-regulated differential auxin transport from columella to lateral root cap cells. *Proceedings of the National Academy of Sciences U S A* **100,** 2987-2991

Pitts RJ, Cernac A, Estelle M. 1998. Auxin and ethylene promote root hair elongation in Arabidopsis. *The Plant Journal* **16,** 553-560

Sabatini S, Beis D, Wolkenfelt H, Murfett J, Guilfoyle T, Malamy J, Benfey P, Leyser O, Bechtold N, et al.. 1999. An auxin-dependent distal organizer of pattern and polarity in the Arabidopsis root. *Cell* **99,** 463-472

Sauer M, Balla J, Luschnig C, Wisniewska J, Reinöhl V, Friml J, Benková E. 2006. Canalization of auxin flow by Aux/IAA-ARF-dependent feedback regulation of PIN polarity. *Genes & Development* **20,** 2902-2911

Smith RS, Guyomarc'h S, Mandel T, Reinhardt D, Kuhlemeier C, Prusinkiewicz P. 2006. A plausible model of phyllotaxis. *Proceedings of the National Academy of Sciences USA* **103,** 1301-1306

Swarup R, Kramer EM, Perry P, Knox K, Leyser HM, Haseloff J, Beemster GT, Bhalerao R, Bennett MJ. 2005. Root gravitropism requires lateral root cap and epidermal cells for transport and response to a mobile auxin signal. *Nature Cell Biology* **7,** 1057-1065

Yang Y, Hammes UZ, Taylor CG, Schachtman DP, Nielsen E. 2006. High-Affinity Auxin Transport by the AUX1 Influx Carrier Protein. *Current Biology* **160,** 1123-1127

FIGURE LEGENDS

Fig. 1. Influence of gravistimulation on lateral root initiation (LRI). (A) Segmentation of the root between gravistimulated (turn) and non-gravistimulated (straight) zones used for determination of the position of LRI. (B) Percentage of lateral root initiations in the gravistimulated and non-gravistimulated zone of crenel-shaped (n = 23) and stair-shaped (n = 24) roots gravistimulated at 12-hour intervals (see supplementary figure 1 for additional details on the gravistimulation protocol). (C) Kinetic of lateral root initiation after gravistimulation. Six batches of roots (n = 40) were gravistimulated every 6 hours over a 24-hour period before harvest and GUS staining, with a one-hour shift between each batch. This led to the formation of root turns aged from 0 to 25 hours, which were scored for lateral root initiation. (D) Kinetic of LRP development after gravistimulation. Arrows indicate the period of time over which the different developmental stages were observed.

Fig. 2. Influence of the gravistimulation interval on lateral root initiation density. (A) Vertically grown *Pro$_{CYCB1}$:GUS* seedlings were left to grow (control; n=20) or were subjected to gravistimulation at intervals of 1 h (n = 24), 3 h (n = 20), 6 h (n = 21), 12 h (n = 21) or 24 h (n= 24) over a period of 3.5 days (1), then left to grow for 2.5 days without stimulation (2). Bars = 1 cm. (B) Occurrence of lateral root initiation in root turns. (C) Occurrence of lateral root initiation between root turns. Due to the particular configuration of roots subjected to gravistimulation at intervals of 1 h and 3 h (respectively presenting no visible turns and only turns), some values were not determined (na = not applicable). (D)

Effect of gravistimulation on root growth. The length of the gravistimulated root segments (first 5 days of growth) and non-gravistimulated root segments (last 2.5 days of growth) was also determined. (E) Lateral root initiation densities were determined in the gravistimulated and non-gravistimulated root segments. Different letters indicate significantly different results as tested by a Student T-test ($P < 0.01$).

Fig. 3. Model of lateral root initiation regulation. (A) Logical circuit of the model. Auxin accumulates with a production rate P, and when its level is above the threshold T1 a lateral rot initiation (LRI) occurs. Initiations cause a flush of the auxin pool. Gravistimulations induce an auxin consumption (G) and an initiation if the remaining auxin level is higher than a second threshold T2. (B) Comparison of observed LRI densities and of the best fit output of the logical model. The parameters corresponding to the best fit were determined by extensive automated parameters space exploration. (C) Evaluation of the predictive power of the logical model. The predicted LRI densities and the LRI densities observed for each gravistimulation treatment were compared (n = 20, see figure S4 for additional details on the treatments). The control is a non-gravistimulated seedlings lot grown in the same condition as the gravistimulated seedlings (n = 20). (D) There is no relation between the number of gravistimulations and the number of LRI. Each point corresponds to one of the treatments presented in (B) or (C), as identified by the corresponding tag. TBR: time between rotations. E) Number of observed LRI as a function of the predicted number of LRI. Each point corresponds to one of the treatments

presented in (B) or (C). This graph shows that the values observed match closely the predicted value.

Fig. 4. Effect of *AUX1* and *axr3* transactivation on lateral root initiation. LRP densities were determined for the AUX1 complementation crosses (A) and the axr3 transactivation (B). Different letters indicate significantly different results as tested by a Student T-test ($P < 0.01$).

Fig. 5. Influence of root bending on resource exploitation. (A) Exploitation of soil resources by a bent root (grey zone). (B) Infinitesimal portion of root turn. Parameters are (n), number of root hairs; (ρ), curve radius of selected zone; (b), thickness of the root; ($d\alpha$), angle made by selected zone; (dl_1) and (dl_2), length of curved zone on each side of the root turn. (C) Area of soil exploited. Parameters are (s_1) and ($s2$), area of soil exploited each side of the root turn; (a), absorption strength of a single root hair ; (h_1) and (h_2), depth of soil exploited on each side of the root turn. (D) Transversal profile of soil exploitation at a root turn. (E) Corresponding depletion of resources.

Fig. 6. Model of gravitropism and lateral root initiation signaling pathways. Auxin fluxes responsible for gravitropism (A) pass through the lateral root cap and are perceived in the epidermal cells via the AUX/IAA molecular pathway, eliciting auxin response (B). Auxin fluxes responsible for lateral root initiation pass through the lateral root cap and the epidermis, but do not require interaction with the AUX/IAA molecular pathway, suggesting a more direct influence on internal tissues further along the root.

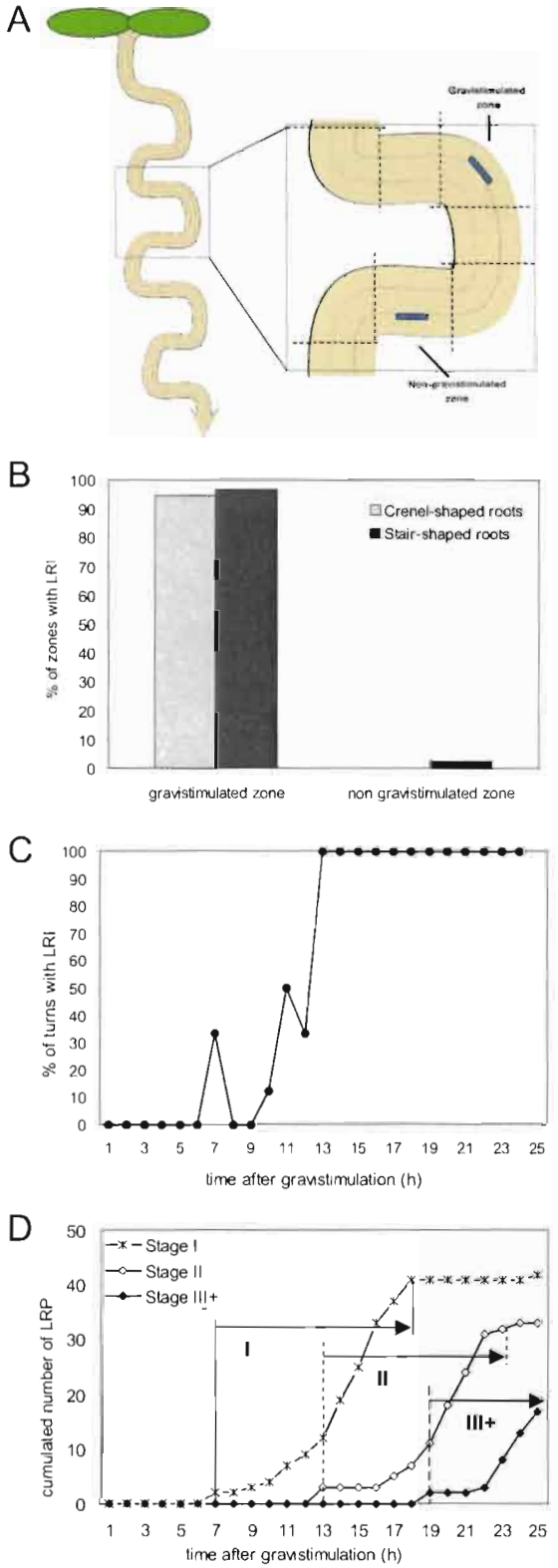

Figure 1. Influence of gravistimulation on lateral root initiation (LRI). (A) Segmentation of the root between gravistimulated (turn) and non-gravistimulated (straight) zones used for determination of the position of LRI. (B) Percentage of lateral root initiations in the gravistimulated and non-gravistimulated zone of crenel-shaped (n = 23) and stair-shaped (n = 24) roots gravistimulated at 12-hour intervals (see supplementary figure 1 for additional details on the gravistimulation protocol). (C) Kinetic of lateral root initiation after gravistimulation. Six batches of roots (n = 40) were gravistimulated every 6 hours over a 24-hour period before harvest and GUS staining, with a one-hour shift between each batch. This led to the formation of root turns aged from 0 to 25 hours, which were scored for lateral root initiation. (D) Kinetic of LRP development after gravistimulation. Arrows indicate the period of time over which the different developmental stages were observed.

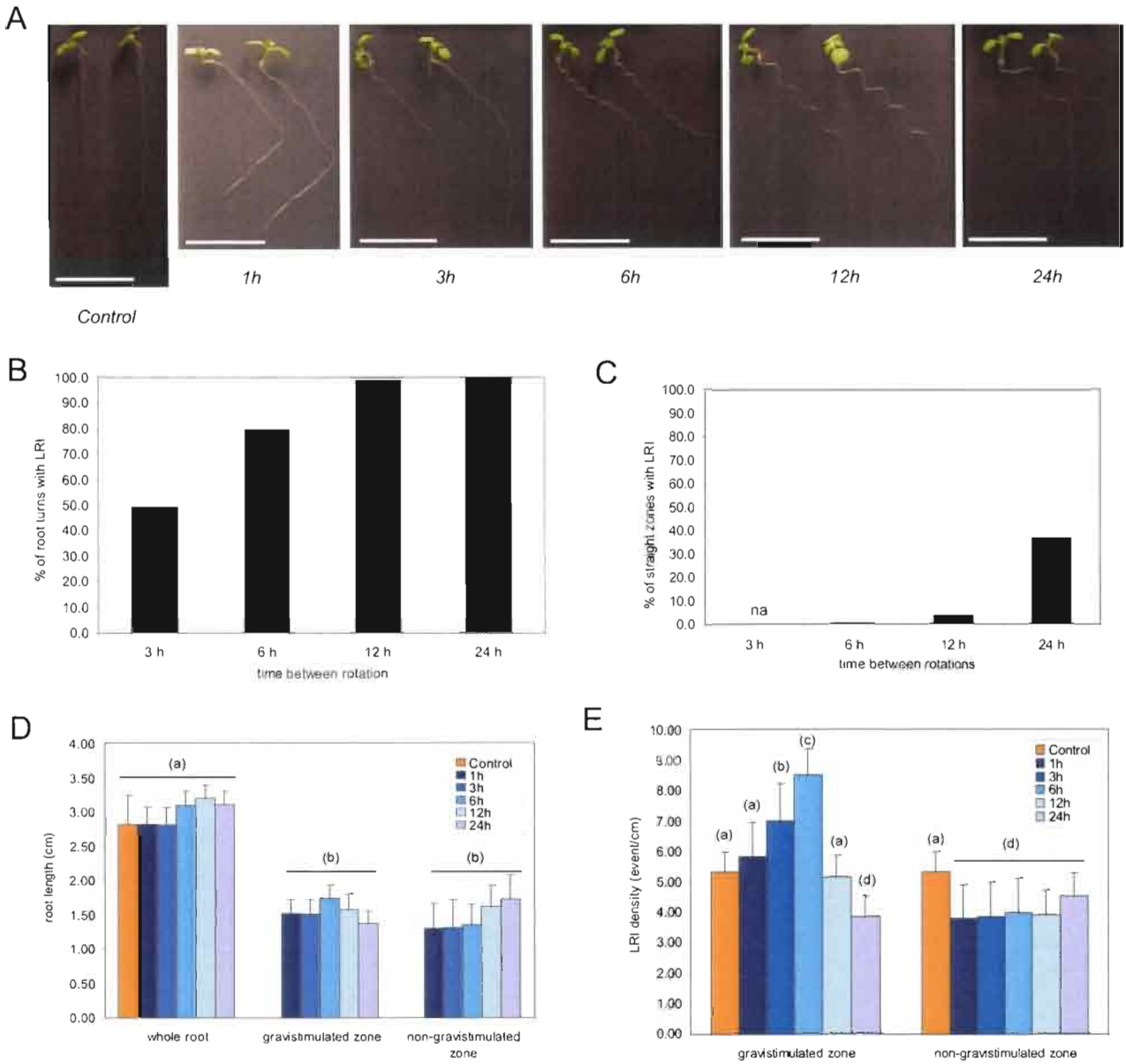

Figure 2. Influence of the gravistimulation interval on lateral root initiation density. (A) Vertically grown *Pro*$_{CYCB1}$*:GUS* seedlings were left to grow (control; n=20) or were subjected to gravistimulation at intervals of 1 h (n = 24), 3 h (n = 20), 6 h (n = 21), 12 h (n = 21) or 24 h (n= 24) over a period of 3.5 days (1), then left to grow for 2.5 days without stimulation (2). Bars = 1 cm. (B) Occurrence of lateral root initiation in root turns. (C) Occurrence of lateral root initiation between root turns. Due to the particular configuration of roots subjected to gravistimulation at intervals of 1 h and 3 h (respectively presenting no visible turns and only turns), some values were not determined (na = not applicable). (D) Effect of gravistimulation on root growth. The length of the gravistimulated root segments (first 5 days of growth) and non-gravistimulated root segments (last 2.5 days of growth) was also determined. (E) Lateral root initiation densities were determined in the gravistimulated and non-gravistimulated root segments. Different letters indicate significantly different results as tested by a Student T-test ($P < 0.01$).

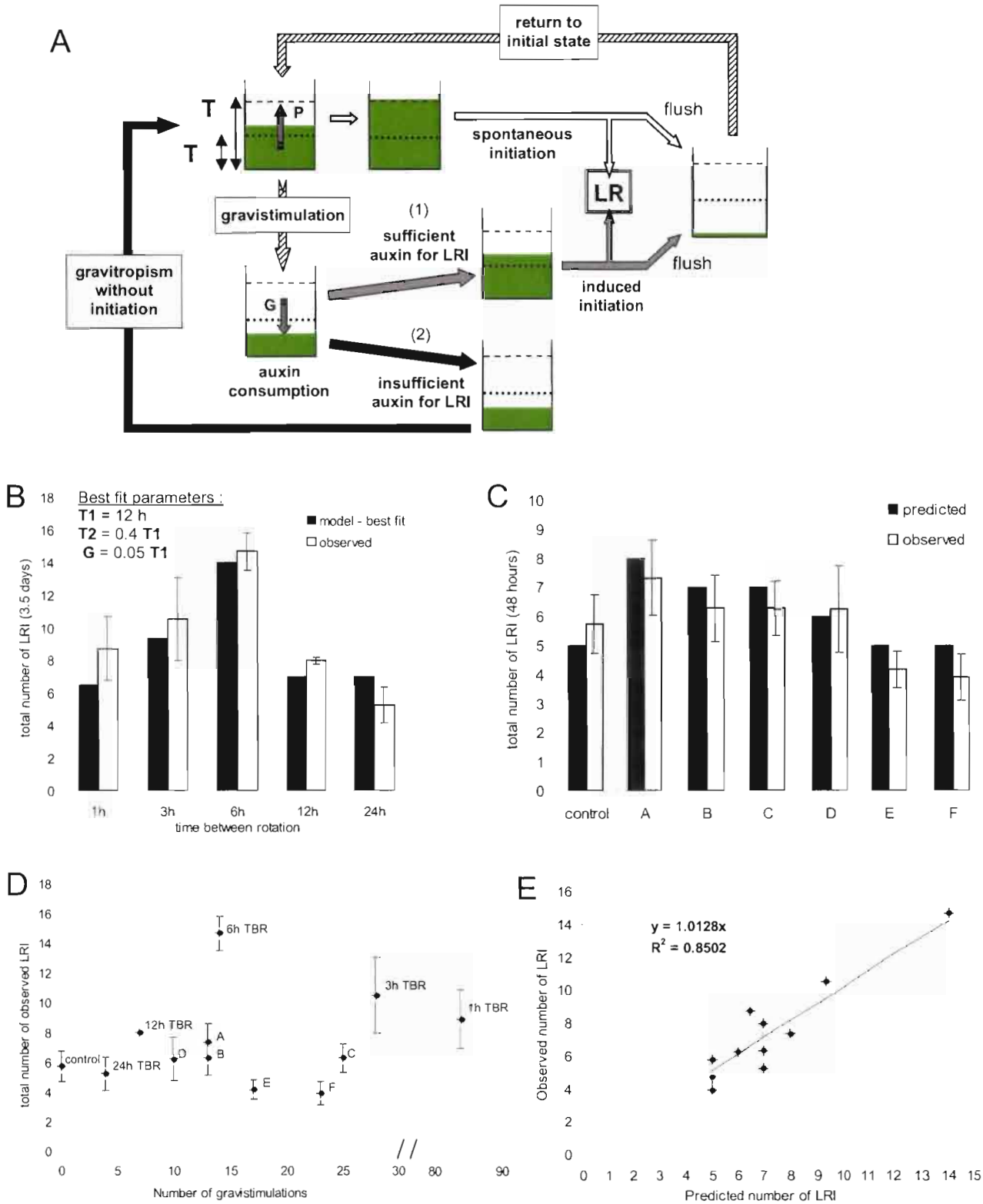

Figure 3. Model of lateral root initiation regulation. (A) Logical circuit of the model. Auxin accumulates with a production rate P, and when its level is above the threshold T1 a lateral rot initiation (LRI) occurs. Initiations cause a flush of the auxin pool. Gravistimulations induce an auxin consumption (G) and an initiation if the remaining auxin level is higher than a second threshold T2. (B) Comparison of observed LRI densities and of the best fit output of the logical model. The parameters corresponding to the best fit were determined by extensive automated parameters space exploration. (C) Evaluation of the predictive power of the logical model. The predicted LRI densities and the LRI densities observed for each gravistimulation treatment were compared (n = 20, see figure S4 for additional details on the treatments). The control is a non-gravistimulated seedlings lot grown in the same condition as the gravistimulated seedlings (n = 20). (D) There is no relation between the number of gravistimulations and the number of LRI. Each point corresponds to one of the treatments presented in (B) or (C), as identified by the corresponding tag. TBR: time between rotations. E) Number of observed LRI as a function of the predicted number of LRI. Each point corresponds to one of the treatments presented in (B) or (C). This graph shows that the values observed match closely the predicted value.

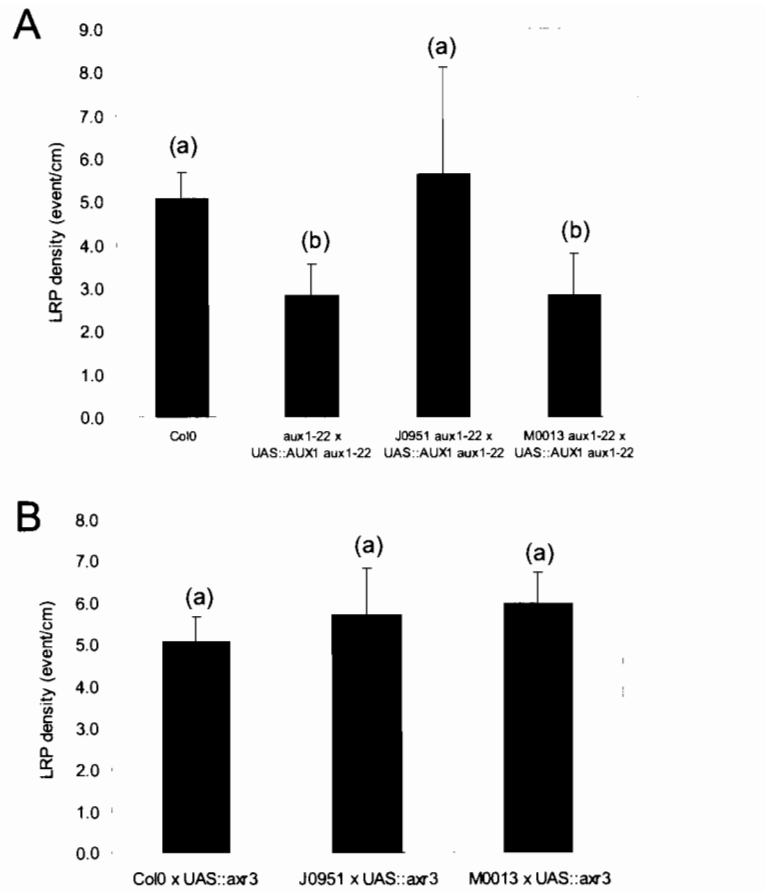

Figure 4. Effect of *AUX1* and *axr3* transactivation on lateral root initiation. LRP densities were determined for the AUX1 complementation crosses (A) and the axr3 transactivation (B). Different letters indicate significantly different results as tested by a Student T-test ($P < 0.01$).

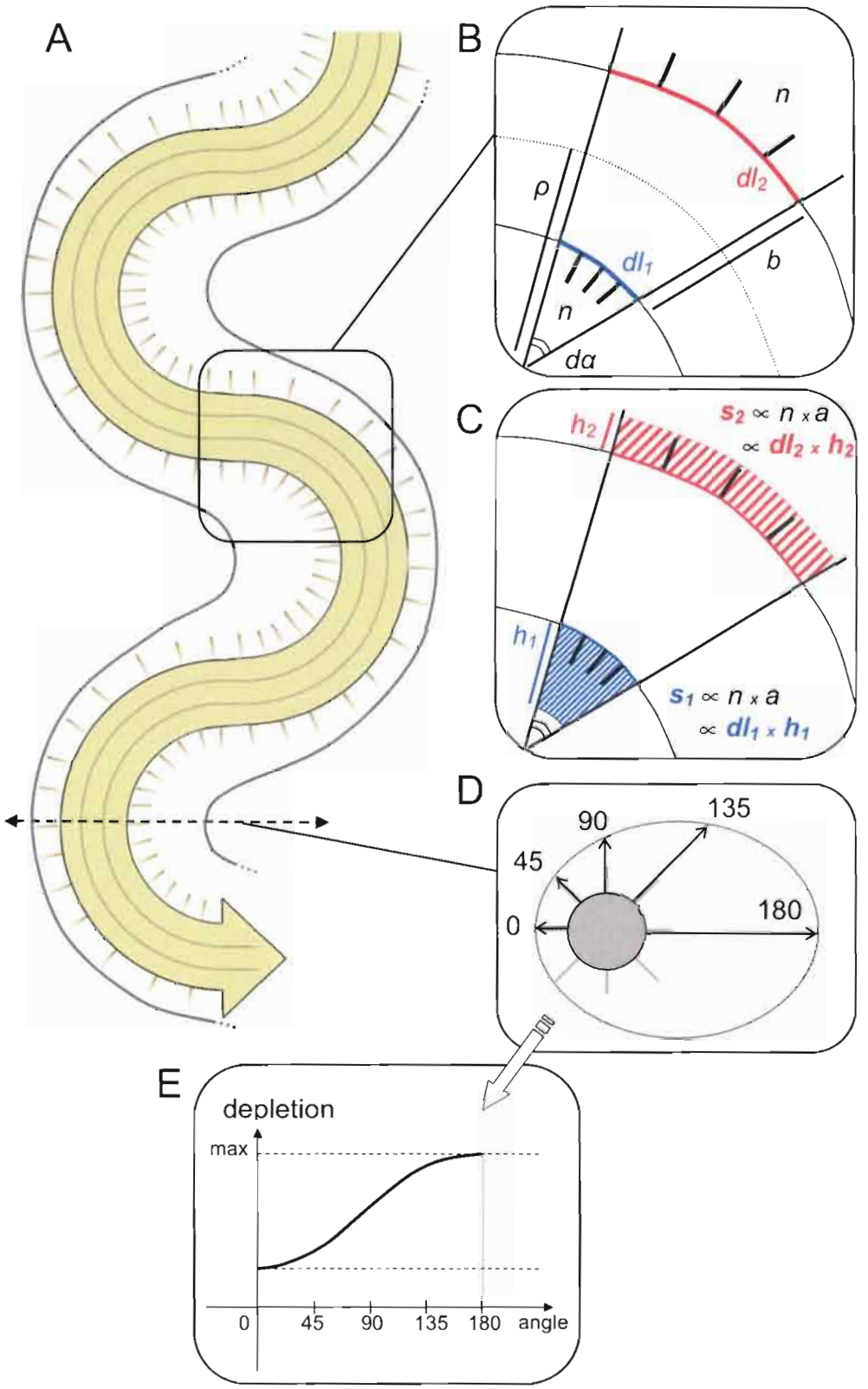

Figure 5. Influence of root bending on resource exploitation. (A) Exploitation of soil resources by a bent root (grey zone). (B) Infinitesimal portion of root turn. Parameters are (n), number of root hairs; (ρ), curve radius of selected zone; (b), thickness of the root; ($d\alpha$), angle made by selected zone; (dl_1) and (dl_2), length of curved zone on each side of the root turn. (C) Area of soil exploited. Parameters are (s_1) and ($s2$), area of soil exploited each side of the root turn; (a), absorption strength of a single root hair ; (h_1) and (h_2), depth of soil exploited on each side of the root turn. (D) Transversal profile of soil exploitation at a root turn. (E) Corresponding depletion of resources.

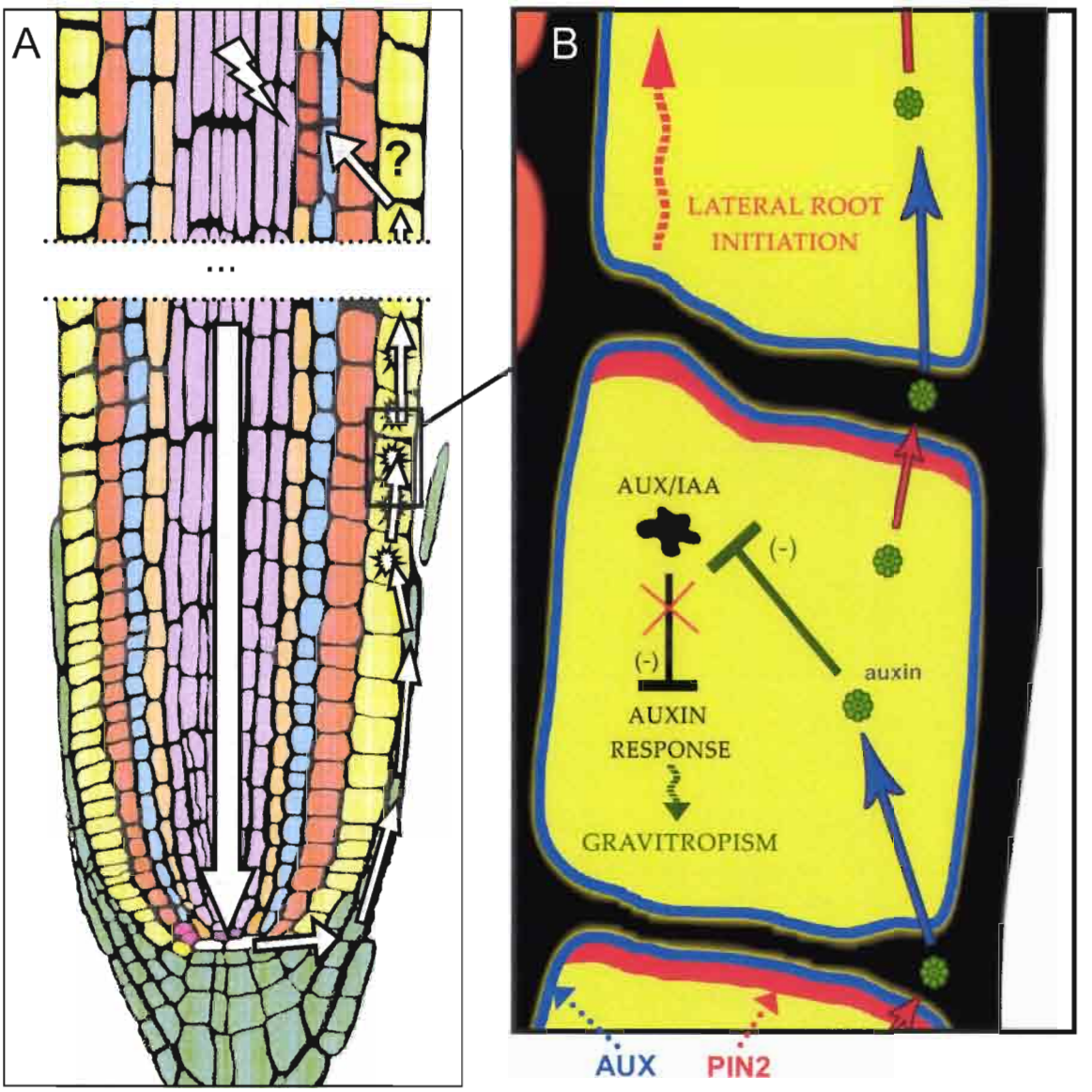

Figure 6. Model of gravitropism and lateral root initiation signaling pathways. Auxin fluxes responsible for gravitropism (A) pass through the lateral root cap and are perceived in the epidermal cells via the AUX/IAA molecular pathway, eliciting auxin response (B). Auxin fluxes responsible for lateral root initiation pass through the lateral root cap and the epidermis, but do not require interaction with the AUX/IAA molecular pathway, suggesting a more direct influence on internal tissues further along the root.

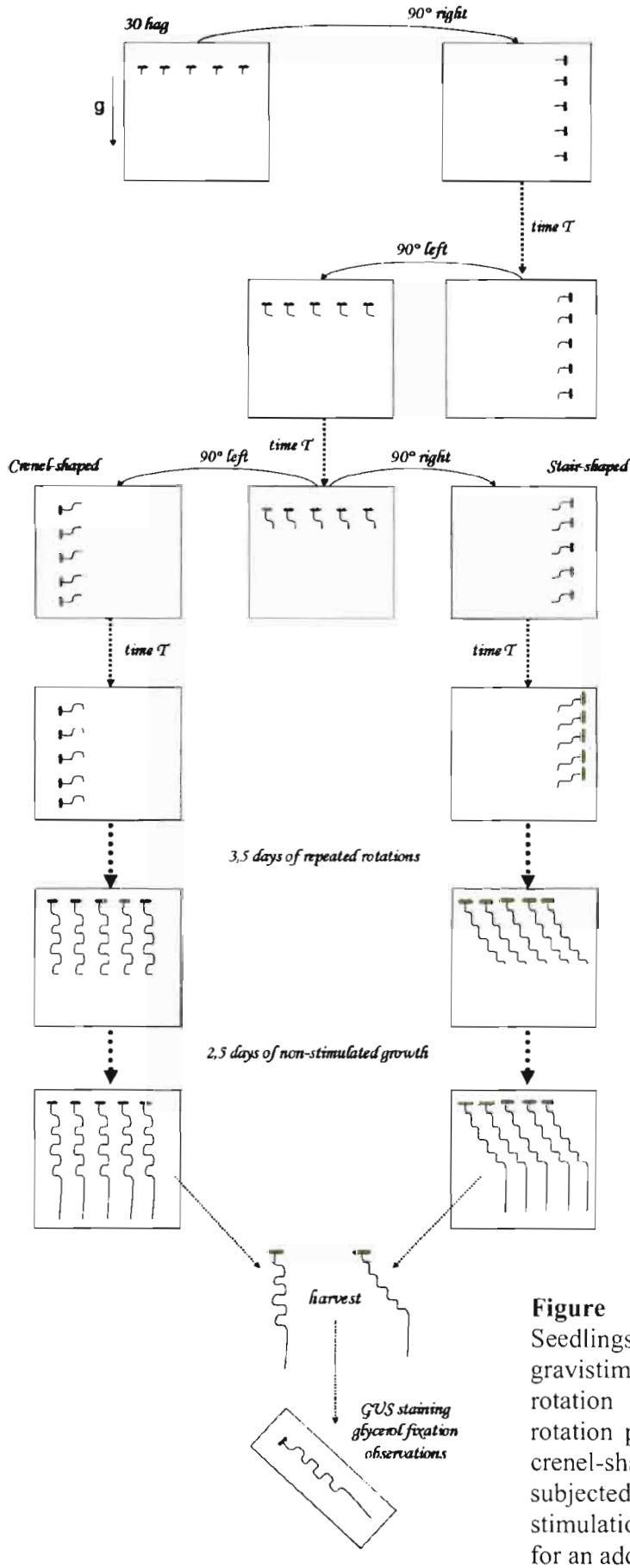

Figure S1. Gravistimulation protocols. Seedlings were grown on vertical plates and gravistimulated by a periodic (period T) 90° rotation of the growth plates. Two different rotation protocols were used to generate either crenel-shaped or stair-shaped roots. Roots subjected to these protocols were grown under stimulation for 3.5 days and with no stimulation for an additional 2.5 days before harvesting.

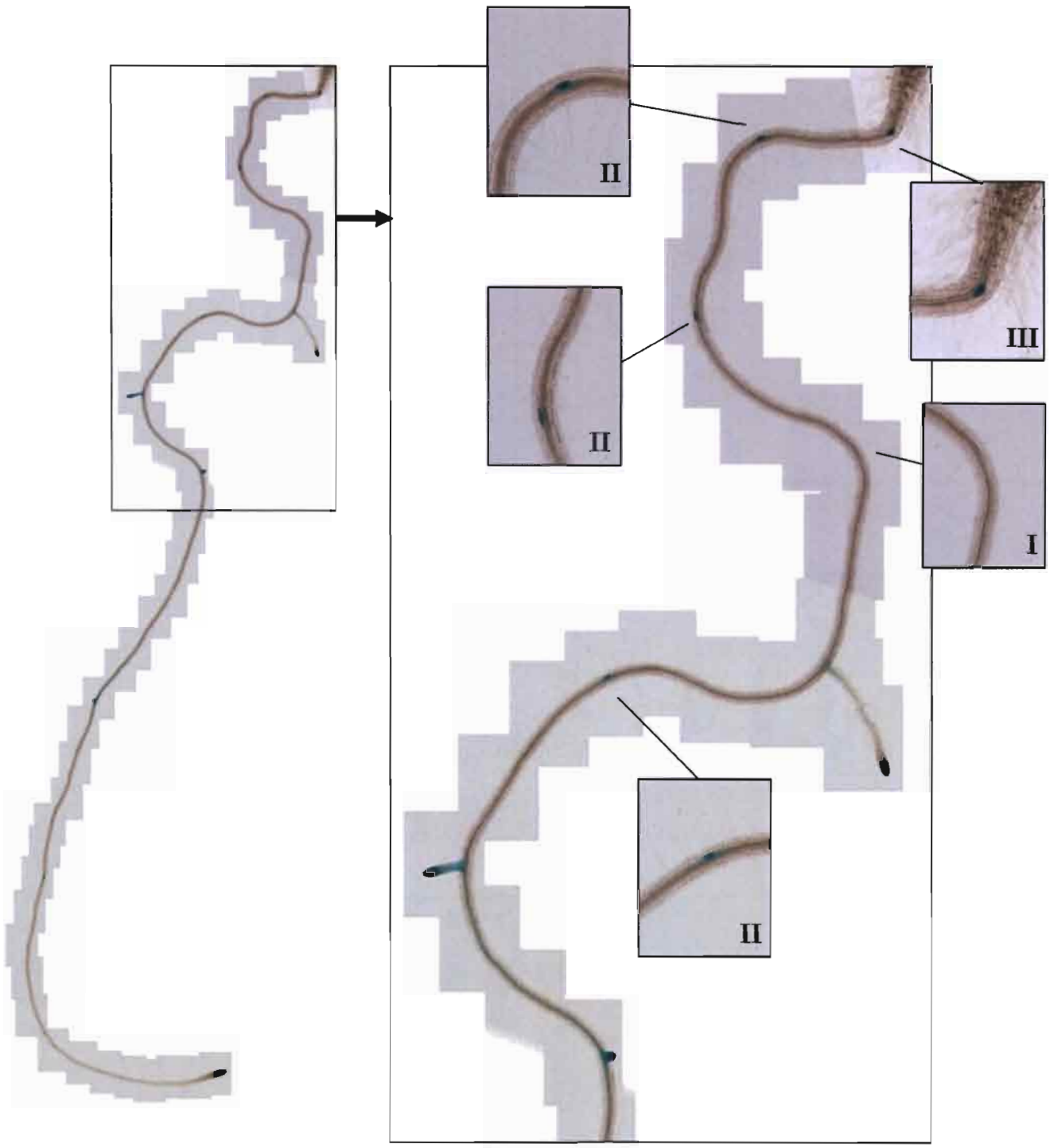

Figure S2. Localisation of lateral root initiation in a gravistimulated root. A Pro_{CYCB1}::GUS seedling was subjected to crenel gravistimulation at 12-h intervals. Lateral root initiations were localised and their development scored.

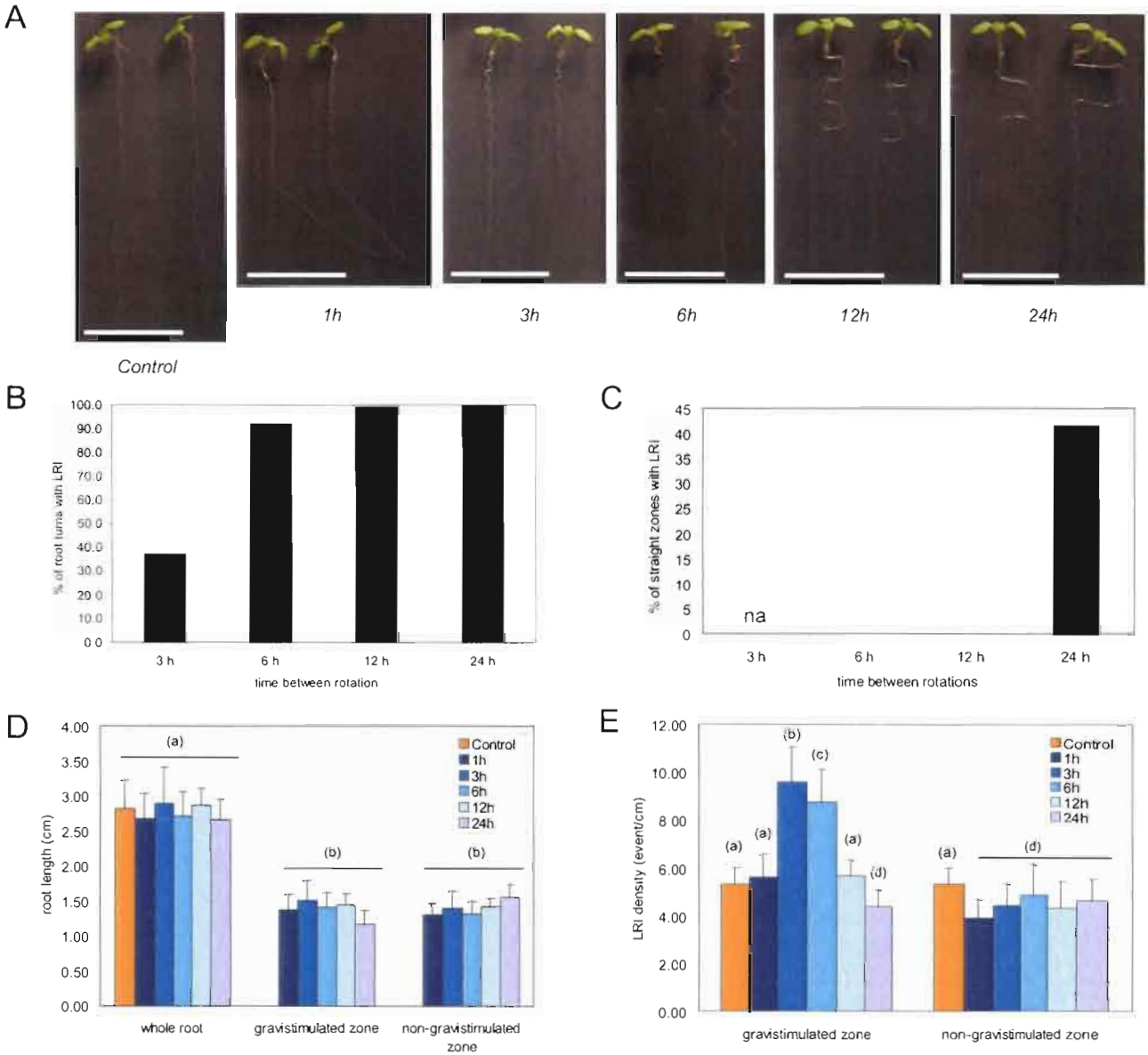

Figure S3. Influence of varying gravistimulation on lateral root initiation density (crenel-shaped roots). (A) Vertically grown Pro_{CYCB1}::GUS seedlings were left to grow (control; n=20) or were subjected to gravistimulation at intervals of 1 h (n = 24), 3 h (n = 20), 6 h (n = 21), 12 h (n = 21) or 24 h (n= 24) over a period of 3.5 days (1), then left to grow for 2.5 days without stimulation (2). Bars = 1 cm. (B) Occurrence of LRI in root turns. (C) Occurrence of lateral root initiation between root turns. Due to the particular configuration of roots subjected to gravistimulation at 1-h and 3-h intervals (respectively presenting no visible turns and only turns), some values were not determined (na = not applicable). (D) Effect of gravistimulation on root growth. Length of the gravistimulated root segments (first 5 days of growth) and non-gravistimulated root segments (last 2.5 days of growth) were also determined. (E) Lateral root initiation densities were determined in gravistimulated and non-gravistimulated root segments. Different letters indicate significantly different results as tested by a Student T-test ($P < 0.01$).

The RootInit algorithm

INPUT

- *time_length* = observation duration
- *initial_pool* = starting auxin reserve
- *production_per_hour* = amount of auxin produced during 1 hour
- *T1* = spontaneous initiation threshold
- *T2* = induced initiation threshold
- *G* = auxin consumption following gravistimulation
- *grav_signal[t]* = array of boolean representing the gravistimulation signal, set to true if there is a gravistimulation at time t, set to false otherwise

OUTPUT

- *initiation[t]* = array of booleans representing the initiation process, set to true if an LRI occurs at time t, set to false otherwise

RootInit Algorithm

```
auxin_pool = initial_pool
for  t = 0 to time_length :
    if  auxin_pool < T1 :
        auxin_pool = auxin_pool + production_per_hour
    if  grav_signal[t] = true :
        auxin_pool = auxin_pool - G
        if auxin_pool  < 0 :
            auxin_pool = 0
    if auxin_pool >= T1 or grav_signal[t] = true :
        initiation_signal = true
    else initiation_signal = false
    if initiation_signal = true and auxin_pool > T2 :
        initiation[t] = true
    else initiation[t] = false
    if initiation[t] = true :
        auxin_pool = 0
```

Figure S4. The RootInit algorithm corresponding to the mechanistic model. The pseudo-code is expressing the mechanisms described in Fig. 3A in discrete time.

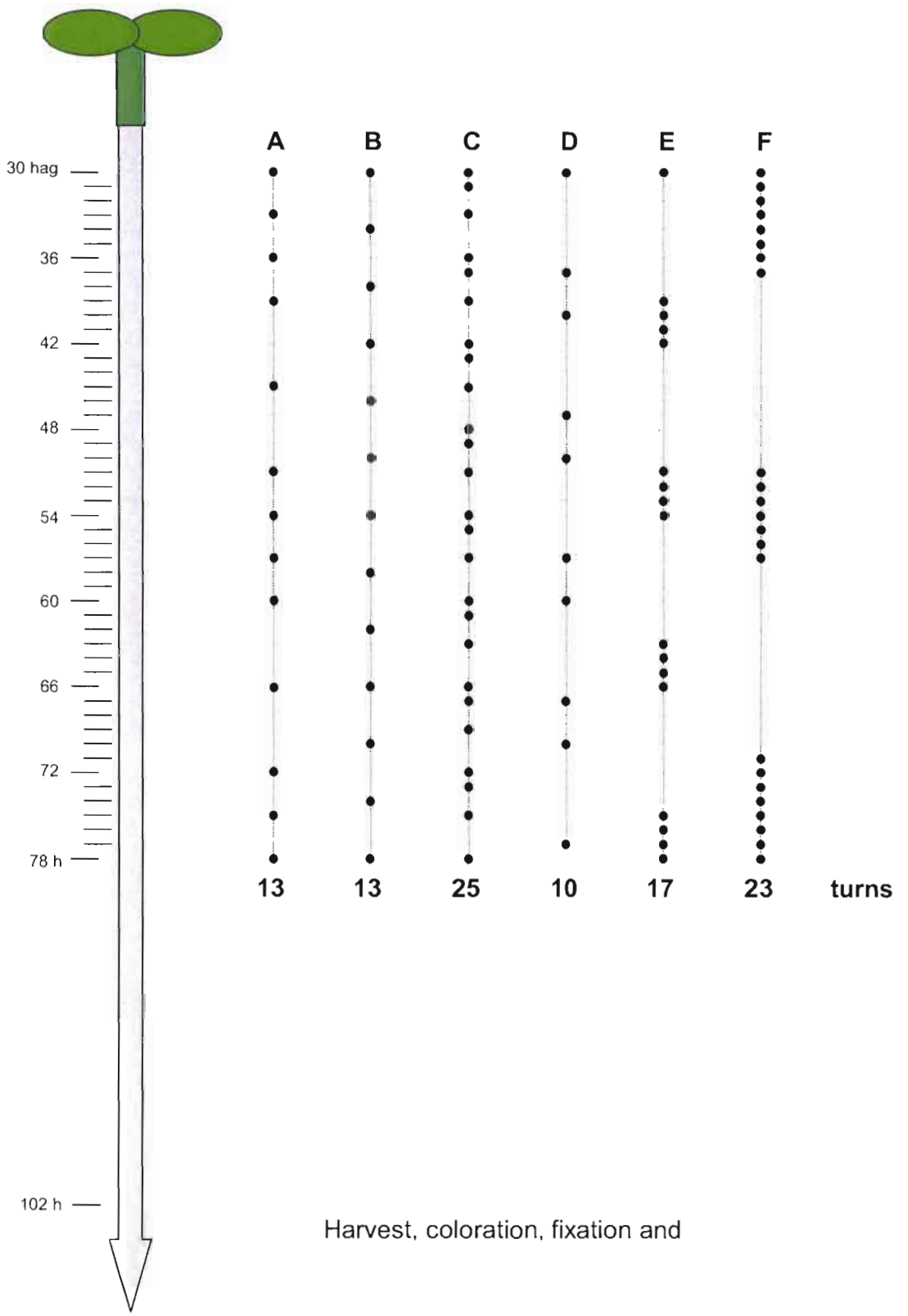

Fig. S5. Gravistimulation patterns used for the evaluation of our model. Six previously non-tested gravistimulation patterns were applied to seedlings over a 48h period starting 30 hours after germination. Gravistimulation are indicated by black dots. The total number of gravistimulation for each pattern varies between 10 and 25. After the last gravistimulus, seedlings were left to grow undisturbed for 24h before harvest and observation.

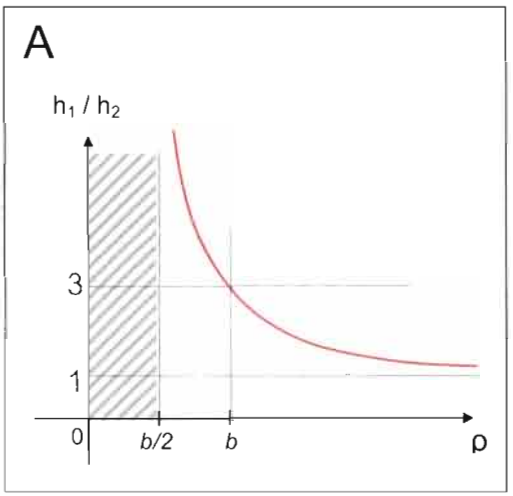

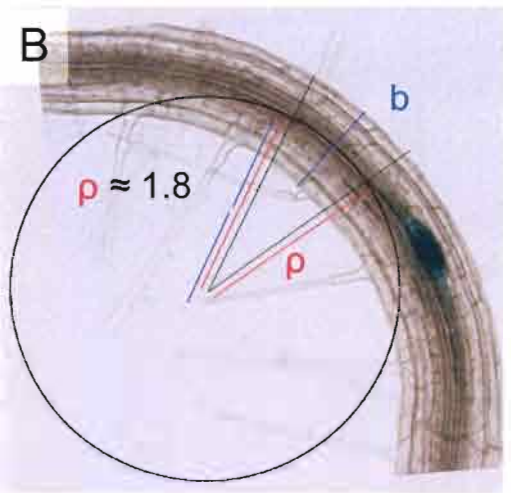

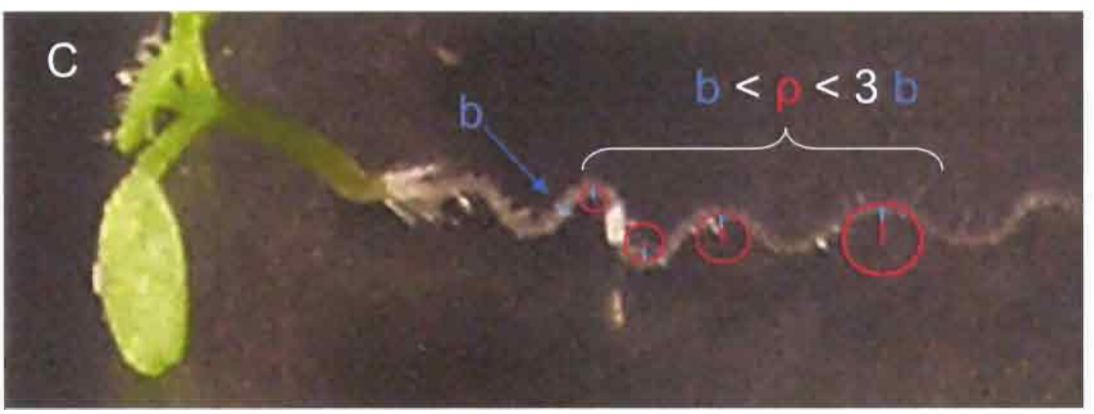

D

ρ value	b/2	b	1.2 b	1.8 b	2 b	3 b	∞
h_1 / h_2	∞	3	2.42	1.7	1.6	1.4	1

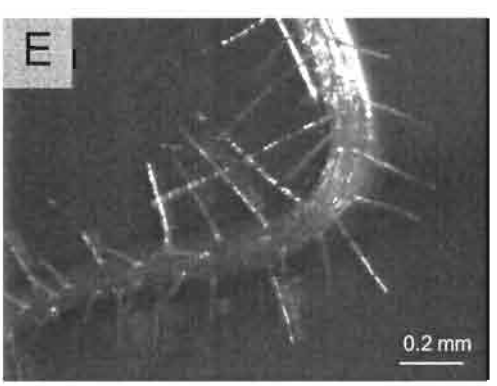

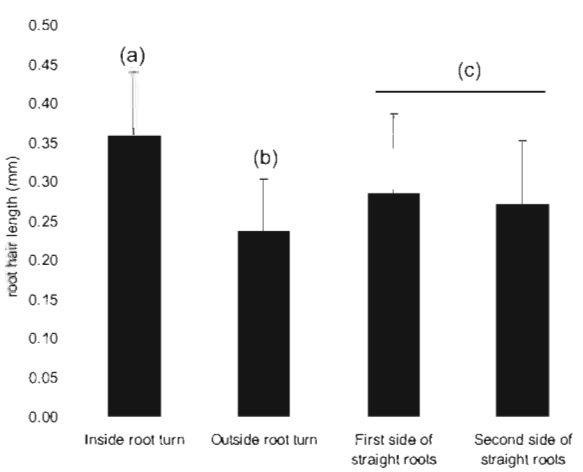

Fig. S6. Curve radius, depth of exploration and root hair length. (A) Curve of the function $h_1 / h_2 = (\rho + b / 2) / (\rho - b / 2)$. (see figure 4 for additional details on the parameters) (B) Curve radius estimated for a portion of a gravistimulated root (90° re-orientation). b and ρ are the thickness and the curve radius of the chosen root portion respectively. (C) Curve radius estimated for various root turns of a waving root. (D) Ratio of exploration depths (h_1 / h_2) for various values of (ρ). (E) Direct visualisation of root hair on both sides of a root turn. (F) Root hair length was measured on both sides of root turns (n=20) and straight roots. Different letters indicate significantly different results as tested by a Student T-test ($P < 0.01$).

- PART III -

Lateral inhibition during root branching in *Arabidopsis thaliana* revealed by a systems biology approach

I) Introduction

As discussed in Chapter I, plant development is essentially post-embryonic. Meristems create new organs and develop branching structures under the influence of intrinsic and extrinsic factors. The resulting shoot architecture appears highly modular, while the root architecture seems devoid of such regular structure. While auxin is a key factor controlling both roots and shoots branching, no global mechanism was ever proposed to unify those two phenomena.

As recent studies tended to support the hypothesis that lateral root initiation was in fact more regular than initially thought (J G Dubrovsky et al. 2006; De Smet et al. 2007), we investigated here the mechanisms regulating initiation and emergence of lateral root primordia at the macroscopic scale. As initiation and emergence both depend on auxin, we also studied the potential interaction between these two phenomena.

II) Results summary

We used a combination of biological, mathematical and *in silico* modelling approaches to understand the mechanisms regulating root branching in *Arabidopsis*. We found macroscopic regularities both in initiation and emergence levels. These macroscopic regularities in initiation and emergence were found to be stable as the root develops and to be identical at each ramification level of the root system. Using stochastic modelling, we extracted rules followed by

initiation and emergence patterns at the microscopic level. Among those rules, we observed similar mechanisms to the auxin-based inhibitory fields regulating phyllotaxis in the aerial part of the plant. We were also able to show that lateral root initiation and development/emergence interact in a feedback system based on auxin fluxes. Based on our results and previous studies, we designed a mechanistic model of root ramification integrating auxin-based inhibitory field control of lateral root initiation and emergence. This mechanistic model accurately predicted the phenotypes of mutant plants altered in initiation or emergence. Lastly, we used gravistimulated plants to further study the balance between initiation and emergence. We confirmed the existence of a balance between initiation and emergence, and found that gravistimulation also enhances emergence. We were able to use the mechanistic model to reproduce the observed effect of gravistimulation on emergence.

The results we obtained will be submitted for publication to Plos Biology in June 2008.

Research Article

Lateral inhibition during root branching in *Arabidopsis thaliana* revealed by a systems biology approach

Running head: The auxin economy of root branching

Lucas, M.[1,2,3], Guédon, Y.[2], Jay-Allemand, C.[3], Godin, C.[2], and Laplaze L.[1,*]

[1] IRD, UMR DIAPC (INRA/IRD/Montpellier SupAgro/UM2), Equipe Rhizogenèse, Montpellier, France

[2] INRIA, UMR DAP (CIRAD/INRIA/INRA/Montpellier SupAgro/UM2), Virtual Plants, Montpellier, France

[3] Université Montpellier II, UMR DIAPC (INRA/IRD/Montpellier SupAgro/UM2), Equipe Rhizogenèse, Montpellier, France

Corresponding author: Laurent Laplaze, IRD, UMR DIAPC, Equipe Rhizogenèse, 911 avenue Agropolis, 34394 Montpellier cedex 5, France, Tel: +33 (0)4 67 41 62 02, Fax: +33 (0)4 67 41 62 22, E-mail: laurent.laplaze@ird.fr

Date of submission: July 2nd, 2008

10 figures

2 tables

3 supplementary figures

Submitted to Plos Biology

Author Summary

In order to develop and grow successfully, plants essentially need air, light, water and nutrients. Air and light are freely exploited in the open by the leaves of the shoot system, while water and nutrients must be searched for underground by the root system. As the soil is a highly heterogeneous medium, the harvesting of resources by roots is strongly dependant on the architecture of the root system as a whole. This architecture arises from the combination of two process, lateral root initiation, and lateral root emergence. Lateral root initiation positions potential future roots (a.k.a. primordia) along existing ones, and lateral root emergence determine which of those potential roots will effectively become full fledge roots. These two processes are repeated each time a new root is formed, progressively building the adult root system. Hence, the comprehension of each of those two processes is essential to understand how roots adapt themselves to different environmental conditions. Here, we studied the interactions existing between those two processes, and showed that they appears to be more closely linked than previously thought. We proposed a mechanistic model of root ramification integrating these findings, and showed that the model could be use to accurately predict the phenotype of various mutants of initiation and emergence. Investigating the balance between initiation and emergence, we uncovered an unforeseen effect of gravistimulation (the act of suddenly changing a root orientation) on primordia development and emergence.

Blurb

Root branching mechanisms are often perceived as completely distinct from stem ramification mechanisms, but is it really the case?

Summary

Root architecture is a crucial part of plant adaptation to soil heterogeneity and is mainly controlled by root branching. The process of root system development can be divided into two successive steps: lateral root initiation and lateral root development/emergence which are controlled by different fluxes of the plant hormone auxin. While shoot architecture appears to be highly regular, following rules such as the phyllotactic spiral, root architecture appears more chaotic. We used stochastic modeling to extract hidden rules regulating root branching in *Arabidopsis thaliana*. These rules were used to build an integrative mechanistic model of root ramification based on auxin. This model was experimentally tested using plants with modified rhythm of lateral root initiation or mutants perturbed in auxin transport. Our analysis revealed that lateral root initiation and lateral root development/emergence are interacting with each other to create a global balance between the respective ratio of initiation and emergence. A mechanistic model based on auxin fluxes successfully predicted this property and the phenotype alteration of auxin transport mutants or plants with modified rythms of lateral root initiation. This indicates that root branching is controlled by mechanisms of lateral inhibition and a competition between initiation and development/emergence for auxin.

Keywords: auxin transport, gravitropism, lateral root initiation, lateral root emergence, Markovian model, computer model

Introduction

Unlike animal development, plant development is essentially occurring post-embryonically. New organs are constantly derived from the activity of groups of undifferentiated cells called meristems that integrate both intrinsic developmental instructions and environmental constraints to give rise to an adapted architecture. Both the shoot and the root system depend on the functioning of meristems to develop branching structures. While the shoot architecture appears to be highly regular, following rules such as the phyllotactic spiral [1], the root architecture appears more chaotic and seems to be almost exclusively dependent on the environment. This might be the evolutionary consequence of the higher heterogeneity of the subterranean environment, compared to the above-ground conditions [2,3] and suggests that shoot and root branching may be controlled by different mechanisms.

The plant hormone auxin is a key factor controlling lateral root formation from pericycle cells [4,5]. Auxin controls both lateral root initiation [6,7] and the development and emergence of lateral root primordia [8,9,10] but while the initiation of lateral root primordia depends on auxin coming from the root tip (acropetal transport) [4,9], their development and emergence depend on auxin flowing from the aerial part toward the root tip (basipetal transport) [8,9,11]. As lateral root primordia arise from an inner root tissue (the pericycle), and are invisible until they eventually emerge [12,13], the outward appearance of the root system does not reflect its internal structure. Recent studies tend to support the hypothesis that lateral root initiation is in fact more regular than initially thought [7,14,15].

In this study we used a combination of biological, stochastic and *in silico* modeling approaches to understand the mechanisms regulating root branching in the model plant *Arabidopsis thaliana*. We found that root branching shows macroscopic regularities at all times and at each structural level of the root system. We used stochastic modeling to extract rules followed by lateral root patterns. Among those, we observed the existence of feedback regulation between lateral root initiation and development/emergence. We designed a mechanistic model of root ramification integrating lateral inhibition due to competition for auxin. The predictions of the mechanistic model were confirmed by analyses of mutant plants altered in initiation or emergence. Lastly, we used gravistimulated plants to further study the balance between initiation and emergence and showed that gravistimulation enhances emergence. We were able to use the mechanistic model to reproduce the observed effect of gravistimulation on emergence.

Results

Arabidopsis root development exhibits scale-free, persistent macroscopic regularities

In order to analyze the regulation of root architecture, we built and analyzed an extensive database of root developmental sequences of Arabidopsis seedlings. 400 *Col-0* seedlings aged from 3 to 12 days were observed and their developmental profiles were encoded as presented in Figure 1. It has been reported previously that mature Arabidopsis roots exhibit a stable mean number

of lateral root primordia under controlled growth conditions [13,14,15]. The chronological analysis of root developmental profiles revealed a strong regularity in lateral root initiation rhythm expressed as a function of root length (expressed as a number of cells, Figure 2A). This initiation rhythm was stable for root aged from 3 to 12 days. Moreover, this regularity was observed for primary roots as well as for secondary and tertiary roots of the 10 and 12-days old seedling (Figure2A, orange and red data points for root length less than 150 cells long). While initiation appears to be highly regular from on the first stages of growth, emergence only appears stable after sufficient growth (Figure 2B). In our growth conditions, lateral root emergence stabilized at around 50 % after one week of growth (Figure 2C).

As such, these macroscopic observations show that initiation of new primordia follows a stable rhythm at each developmental stage and each branching order of the root system, whereas emergence reaches equilibrium after one week.

Stochastic modeling of root development

While it was possible to exhibit strong regularities when observing large sets of roots at the macroscopic level, individual roots showed a high variability in developmental profiles at the microscopic level, as illustrated by the sample in Figure 3. We thus used a stochastic approach to rapidly and thoroughly explore such an extensive database of root profiles. This made it possible to identify developmental patterns and regularities that were not directly apparent, due to the diversity of the root architectures.

For the following database analysis, we defined a "root segment" as the developmental unit formed by two successive lateral organs (primordia or lateral root) and the distance between them, recorded as the observed number of epidermal (trichoblast) cells between the two lateral organs. From the developmental profiles composed by the succession of root segments, we extracted 3 types of developmental data for further analysis (Figure 3):

- sequences of developmental stages, considering only the developmental stages of the successive lateral organs,
- sequences of root segment lengths, considering only the distances between successive lateral organs,
- cell strings, resulting from the encoding of the full developmental profiles, with the following convention: 1 codes for non-emerged primordia, 2 codes for emerged lateral root and 0s indicate the segment length between two primordia.

The cell string transcription of the database was used as a basis to build a stochastic model based on Markov chains (see Materials and Methods for additional details). Such a model can be seen as an abstraction of the root developmental sequence (Figure 4) that efficiently summarizes all the observed root developmental profiles in a single unified model. The parameters were obtained by a classical likelihood maximization procedure [16,17]. The estimated model is composed of 6 states (numbered 0-5). States 0, 2, 4 and 5 represent the segments (expressed as a sequence of cells) between lateral organs. The length of each segment is defined by a distribution associated with each of these states

(Figure 4, top row). States 1 and 3 represent the production of lateral organs. An additional terminal state was introduced to indicate the end of the sequence. In each state, outgoing arrows indicate the possible transitions from this state to the others. Each arrow is associated with a probability that reflects the frequency of the corresponding transition in the cell string.

The model makes it possible to identify 4 main zones in roots from the collet to the root tip. The first zone (model state 0) corresponds to the short developmental period following germination and preceding the first lateral root initiation (collet zone). The second macroscopic zone (proximal zone) is composed of state 1 (presence of an emerged lateral root or of a blocked primordia) and state 2 (root segment without initiation) and corresponds biologically to the mature zone of the root. The third zone ("distal zone") is composed of state 3 (presence of a primodium), and state 4 (root segment without initiation) and corresponds to the zone of primordia development. The fourth zone (state 5) corresponds to the developing root apex, where the next primordia will appear (apical zone).

Several theoretical distributions were computed from the estimated stochastic model and were compared to the corresponding empirical distributions. The predicted distributions of the number of lateral organs per root fitted well the corresponding empirical distributions extracted from the observed data (P-value of 0.08 for primordia and 0.62 for emerged lateral roots with the Chi-square goodness of fit test) (Figure 5). This indicates that the stochastic model adequately captures the structure of the developmental sequences in the database.

Stochastic model reveals interaction between primordia initiation and development

Along the complete root, lateral organs can be of three different types: developing LRP, blocked LRP and emerged lateral roots. In order to study the relationship between the distance and types of successive lateral organs, we had to restrict our analysis to regions where the fate of lateral organs was known (i.e. containing no developing LRP). Since lateral root initiation was shown not to occur between existing primordia [14], the analysis was made on proximal zones, where LRPs could be considered blocked in their development. The stochastic model was used to identify the proximal zone on each root by computing the most probable state sequence corresponding to the cell string. As a result, each cell string was optimally segmented into collet, proximal, distal and apical zones. We then analyzed the distribution of root segment lengths between lateral organs in the proximal zones (Figure 6). If the initiations were made at random and independently with respect to one another, one would expect geometric segment length distributions (the shorter the segment, the higher its frequency). However, in the observed distributions the most frequent segments have intermediate lengths and the shortest segments have low frequencies. This shows that the initiations are not independent of one another and suggests the existence of a lateral inhibition mechanism that prevents successive initiations at short distances.

We then considered whether particular rules were governing the emergence of lateral organs. We first wanted to know whether lateral root emergence events were interacting with each other and over which distance. For this, we built a

variable-order Markov chain to model the succession of lateral organ types (blocked LRP or emerged LR denoted respectively by P, E) in the proximal zones. Such a model makes it possible to automatically detect frequent patterns in the analyzed sequences while keeping a minimal number of parameters in the model. In our case, the observed sequences were best fitted by a variable-order Markov model of maximum order 2 (Figure 7). Frequent patterns were identified (Table 1):

i) at order 1 as P → E (0.52) i.e. a blocked primordium was followed by an emerged lateral root in 52% of the cases.

ii) at order 2 as: P,E → E (0.55), i.e. an emerged root following a blocked primordium was followed by an emerged root in 55% of the cases; E,E → E (0.75) i.e. two successive emerged roots were followed by an emerged root in 75% of the cases.

While primordia appear to have a 50% chance of emerging if they are directly preceded by a non-emerged primodium, the probability of emergence rises to 0.75 if the two previous primordia both emerged. Thus, the variable-order Markov chain analysis strongly supports the idea that successive lateral root emergence are not independent.

Then, to test whether the distance between successive lateral organs had an influence on the development of those organs, we studied the distribution of segment length before and after each organ depending on their type within the proximal zone. We found that the segments before and after a blocked primordium were significantly shorter than the segments before and after an

emerged root according to the Student *t* test (Table 2). As primordia positioning is sequential at the root apex, this correlation between organ development and position can be interpreted as the consequence of an inhibitory effect between primordia on lateral organ development. This effect tends to decrease as adjacent primordia are initiated farther away from each other.

Design of a mechanistic model of lateral root initiation and development

Our statistical analysis revealed an unexpected feedback between lateral root initiation and development suggesting a competition for auxin. To test this hypothesis, we designed a mechanistic model of root ramification based on auxin fluxes (Figure 8A). For this, we used a set of hypotheses which attempts to combine various knowledge sources coming from literature with our analysis in an integrated framework:

1 – Acropetal auxin fluxes come from the aerial parts, and increase after one week of growth [18]. The increase in auxin production after one week coincides with the acceleration of initiation rhythm we observed at the macroscopic level (Figure 2A – almost twice as much primordia appeared during the last 5 days than during the first 7).

2 – Developing primordia consume a fraction of the acropetal auxin flux according to an age-based hierarchy (older primordia have precedence on younger ones) [19].

3 – Primordia which have consumed enough auxin emerge (emergence threshold – ET) and stop consuming auxin [18].

4 – After a given time (developmental window – DW), primordia which have not emerged are blocked and stop consuming auxin [14].

5 – The remaining auxin flux arrives at the root apex, where it takes part in a reflux system [7,15,20]. The mathematical properties of the reflux system (Figure 8B) lead to a stable point in flux intensity, which depends on the efficiency of the reflux at the apex and within the initiation zone, on the flux coming from the development zone, and on the auxin degradation rate (Figure 8C). For strong effective reflux values, the stable point flux in the initiation zone become increasingly responsive to small variation of parameters.

6 – Some of the auxin coming from the reflux flow through the lateral root cap and the epidermis accumulates in the initiation zone (IZ) where initiation can take place. Initiation occurs when the level of auxin in this zone, considered as a pool of auxin, reaches a predefined initiation threshold (IT). The initiation of a new primordium empties the pool [7,15,19].

7 – To account for the biological variability observed in the data, both the initiation and emergence thresholds (IT and ET) were submitted to random (Gaussian) fluctuations.

In a previous study, we showed that initiation patterns can be significantly altered by controlled gravistimulation during root growth [15]. Such perturbations can be used to test the predictive power of the model. We therefore used the following hypotheses already tested by Lucas et al. 2008 to take into account the effect of gravistimulation in the model:

8 – Gravistimulation induces the initiation of new primordia by reducing the initiation threshold (IT).

9 – Gravistimulation consumes a fraction of the auxin available for initiation (quick repetitions of gravistimulations inhibit initiation).

10 – Gravistimuli disappear over 4 hours, and as a consequence both the drop of IT and consumption of auxin in the IZ induced by a gravistimulus decrease regularly (linearly) over a 4 hour period.

The corresponding computer algorithm is presented in supplementary Figure S2. The parameters of the model were either directly extracted from observation (e.g. observed initiation rate, percentage of emergence, number of simultaneously developing primordia), or estimated through extensive parameter space exploration and comparison between model outputs and observation (see Supplementary Figure S3 for a detailed outlook of the reference used for parameters calibration). Due to the stochastic variation of IT and ET, each parameter set was tested by a run of simulations whose output were used for statistical comparison between observation and prediction. Figure 9 A & B shows the distribution of initiation and emergence obtained through calibration of the mechanistic model.

We were able to generate a set of parameters for which the model's output closely followed the observed number of lateral root initiation for normal root growth as well as for various gravistimulation patterns (Figure 9 A, B & C; Supplementary Figure S3).

Mechanistic model predicts a balance between initiation and development

We used the mechanistic model to explore the potential interactions between primordia initiation and development. We first studied the effect of varying the

reflux efficiency parameter from 20% to 99% and proceeded to the analysis of the resulting initiation and emergence levels. The model predicted that a drop of reflux efficiency leads to a decrease of the initiation level and a concomitant increase of the emergence rate. For instance, if the reflux efficiency changes from 95% to 50%, the model predicts a 4-fold reduction of the initiation level and a 2-fold increase of the emergence rate (Figure 9D). In order to validate this prediction, we used *Arabidopsis* mutants in which the auxin reflux mechanism is altered. Changes in the auxin reflux can be found in *pin2* and *aux1-22* mutants, in which the auxin reflux in the lateral root cap is reduced (with a stronger reduction in *aux1-22* than in *pin2*). We compared the initiation and emergence densities of the *aux1-22* and *pin2* mutants to wild-type Col-0 seedlings. We found that mutants exhibited a rise in emergence level compared to the wild type, with a mean 2.5-fold increase in emergence for the most severe reflux reduction of *aux1-22* (Figure 9F).

We then studied the consequences of a premature arrest of primordia development on the initiation system in our model. Newly-formed primordia were artificially arrested in their development (stopping auxin consumption from the central flux) when they reached a predefined development level. This analysis was done for decreasing development levels, ranging from full development to no development at all. The model predicted a roughly 2.5-fold increase of initiation level when primordia development was arrested as soon as new primordia appeared (Figure 9E). Premature arrest of primordia development can be found in another mutant of active auxin transporter, the *lax3* mutant [10]. This mutant exhibited a mean 2.5-fold increase in initiation levels compared to wild-type plants [10; Figure 9F].

Balance between initiation and development is enhanced by gravistimulation

The consistency of our model predictions with different mutant phenotypes provides a first validation of the model's assumptions. In order to further test the concept of balance between initiation and development, we decided to artificially perturb the primordium initiation process and study the consequences on the development process.

We used a system of gravistimuli-induced initiation previously described [15]. This system allows for a wide range of controlled alteration of initiation level. We applied regular gravistimulation patterns with a time between rotations ranging from 1 to 24 hours. As a result, the initiation and emergence densities observed in the gravistimulated zones were negatively correlated (Figure 10A). This confirmed the existence of a balance between initiation and emergence that was predicted by the model and observed in the mutant analysis. In addition, gravistimulated roots presented a homogeneous rise in emergence rate (Figure 10A). To elaborate on this, we compared the development of lateral root primordia for different gravistimulation rhythms (Figure 10B). We observed that, independently from the gravistimulation pattern applied, seedlings which were stimulated with low level of gravistimulation (12h and 24h between gravistimulation) presented a four-fold increase in percentage of emerging lateral organs. As the seedlings gravistimulated every 24h presented primordia initiation in-between root gravistimulations, we were able to directly compare the development of primordia occurring during or outside of gravistimulus (Figure 10C). The observed distribution of developmental stages showed a clear distinction between those two primordia populations. Primordia initiated by

gravistimulations at root bends developed faster (and/or more strongly) than primordia occurring outside bends.

We integrated this new effect due to gravistimulation in the mechanistic model by assuming that gravistimulation facilitates the emergence of lateral roots. This was translated in the model as a drop of ET for primordia formed during gravistimulation. This single hypothesis was sufficient to reproduce the negative linear correlation between the initiation and emergence densities due to gravistimulation, with comparable variation amplitudes (Figure 10D).

Discussion

In this study, we used a combination of stochastic analyses, *in silico* modeling and biological observations to study the mechanisms regulating root branching in the model plant *Arabidopsis thaliana*. A large number of roots (400) from plants aged from 3 to 12 days were analyzed and encoded to generate a database of developmental profiles. The study of this dataset indicated that while lateral root initiation and development shows strong macroscopic regularities, there was a large variability between individual roots. We therefore used a stochastic model to extract a succinct set of probabilistic rules that capture this diversity. This stochastic model demonstrated that root branching is strongly structured and follow some developmental rules. Moreover it revealed a feedback regulation between lateral root primordia initiation and development/emergence. This was an unexpected finding as those two phenomena occur in distinct parts of the root. Moreover, while auxin is the main regulator of both lateral root initiation [6] and development/emergence [9,10], these two processes were shown to depend on

different auxin fluxes. [4,7,10,21]. Lateral root initiation is regulated by auxin coming form the root tip (acropetal transport) [6,7,15] while lateral root development/emergence depends on auxin coming from the shoot (basipetal transport).

We generated a novel mechanistic model of root branching based on auxin fluxes that was able to reproduce the observed competition between primordia initiation and development. This model was also found to accurately predict the phenotype of mutants perturbed in root acropetal auxin transport (*pin2*, *aux1-22*) and lateral root emergence (*lax3*). The feedback between lateral root initiation and development/emergence was further confirmed by analyzing plants with modified rates of initiation using gravistimulations [15], with the added observation that emergence was enhanced by gravistimulation. We showed that a simple extension of the mechanistic model was sufficient to predict the effect of gravistimulation on lateral root initiation and development/emergence.

Additional studies will need to investigate the enhancement of lateral root development by gravistimulation. The higher emergence rate observed in root turns may be linked with the mechanical constraints existing within the outer tissue layer. It has been shown that emergence is linked with a remodeling of the cell walls in the endoderm, cortex and epidermis, allowing the emerging primordia to push through the outer tissue layer without tearing up the surrounding cells [10]. Differential cell elongation occurring during root bending would theoretically induce longitudinal strains on the tissue, facilitating dissociation of cell walls in the same zone where the primordia appears and will potentially emerge. Potential experiments to investigate this hypothesis include

physical measurements of the strains existing within root turns and study of the emergence level in root turns for emergence mutants such as *lax3*.

Taken together, our findings indicate that even if lateral root initiation and development/emergence are dependent on different auxin fluxes in the root, they use the same limited pool of auxin thus creating feedback mechanisms. These mechanisms are akin to inhibitory fields as defined by Hofmeister [22]. Inhibitory fields were historically proposed as a theoretical explanation for the phyllotaxis arising from the shoot apical meristem [23]. It has been shown in the last few years that the inhibitory fields regulating phyllotaxis, and subsequently shoot branching, were related to auxin and auxin transport [24,25,26]. Root branching however was known to be regulated by auxin since the discovery of the hormone itself, but no regular mechanism was ever proposed to explain how auxin directs root branching. Our findings suggests that regulation of root and shoot branching by auxin share common theoretical bases, pointing to potentially unified molecular mechanisms of plant development.

Mechanistic modeling proved to be a powerful tool to integrate and test biological concepts that would be too complex to comprehend otherwise. As our knowledge of auxin flux regulation grows, the opportunities to use mechanistic modeling to study auxin transport occurring at the cellular level during lateral root initiation multiply. We are currently developing an *in silico* cellular model of auxin fluxes to understand how the redistribution of auxin in the root apex may control the fine positioning of lateral root initiation.

Materials and methods

Plant material and growth conditions. Wild type (Col-0), *pin2* and *aux1-22* mutants (Col-0 background) seeds were obtained from the NASC. *Pro$_{CYCB1}$:GUS* (Col-0 background) seeds were provided by Dr P. Doerner (University of Edinburgh, UK). Plants were grown on vertical plates as previously described [27]. When applied, gravistimulations consisted of 90° successive rotations of the plates. For additional details on the periodical gravistimulation, see [15].

Microscopy. Seedlings were collected and incubated in a solution containing 50 mM sodium phosphate buffer, pH 7.0, 0.5 mM $K_3Fe(CN)_6$ and $K_4Fe(CN)_6$, 0.05% (v/v) Triton X-100, 0.05% (v/v) DMF, 0.02% (v/v) EDTA, and 1 mM 5-bromo-4-chloro-3-indolyl-□-glucuronic acid and incubated at 37°C for several hours. Seedlings were then cleared in 70% (v/v) ethanol for 24 h, before being immersed for 2 h in 10% (v/v) glycerol 50% (v/v) ethanol; 2h in 30% (v/v) glycerol 30% (v/v) ethanol; 2h in 50% (v/v) glycerol. Seedlings were mounted in 50% (v/v) glycerol and visualized using a DMRB microscope (Leica). Pictures of the plants were obtained using a MZFLIII (Leica) dissecting microscope equipped with a digital camera.

Observation. Development stages of successive lateral organs (as defined by [12]) and the distances between them (i.e. number of epidermal hair cells) were scored using the previously mentioned optical microscope. Special care was taken to follow continuous epidermal cell file in scoring the distance between successive lateral organs. When root spiraling became too important to allow the

observation of a single continuous epidermal cell file, observation was resumed on a visible cell file in phase with the previous one. Cell counting always started at the collet, and cell counting ended when protoxylem ladder-structure was no longer visible.

Basic statistical analyses were made using the Excel statistical package.

Stochastic model. We chose to model the cellular string structure by a specific hidden Markovian model. Our model incorporates four semi-Markovian states with attached occupancy distributions to model the four types of segments of non-differentiated cells and two Markovian states to model the occurrence of either primordia or emerged roots in the two median zones. In this study, we assumed that the end of an observed sequence systematically coincides with the transition from the last segment state to an extra absorbing "end" state. The estimated hidden hybrid Markov/semi-Markov chain is shown in Figure 4. The model is "hidden" since non-differentiated cells (output 0) can be observed in the four semi-Markovian states while both primordia (output 1) and emerged roots (output 2) can be observed in Markovian state 1 (hence, the observed cell differentiation stage does not enable to determine the state in the model). The resulting hidden hybrid Markov/semi-Markov chain is thus defined by four subsets of parameters:

- Initial probabilities to model which is the first state occurring in the primary root,
- Transition probabilities to model the succession of states along the primary root,

- Occupancy distributions attached to semi-Markovian states to represent the segment length in number of non-differentiated cells,
- Observation distributions to model the composition properties within a state. All the observation distributions are degenerated i.e. a single output can be observed in a state except the observation distribution for the Markovian state 1 with a mixture of primordia an emerged roots.

The maximum likelihood estimation of the parameters of a hidden hybrid Markov/semi-Markov chain requires an iterative optimization technique, which is an application of the expectation-maximization (EM) algorithm [16,17]. The hidden hybrid Markov/semi-Markov chain was estimated on the basis of 185 sequences of cumulated length 14,065. The 20 parameters consist of 3 independent initial probabilities, 4 independent transition probabilities, 12 parameters for the occupancy distributions attached to the four semi-Markovian states (all these occupancy distributions are negative binomial distributions defined by three parameters, including an additional shift parameter), and 1 independent observation probability (Markovian state 1). Once the hidden hybrid Markov/semi-Markov chain had been estimated, the most probable state sequence was computed with the Viterbi algorithm [17] for each observed sequence. On the basis of this global stochastic model of cell string structure, various sub-samples and data characteristics were extracted and analyzed.

All the statistical analyses were made using the VPlant statistical package (successor of AMAPmod [28]) integrated in the OpenAlea platform [29], available at http://openalea.gforge.inria.fr/wiki/doku.php?id=openalea.

Variable order Markov chain modeling. The succession of primordia and emerged roots was analyzed within the proximal zone using variable-order Markov chains. In variable-order Markov chains, the order (or memory length) is variable and depends on the context within the sequence instead of being fixed. We applied the algorithm proposed by [30] for estimating variable-order Markov chains. This algorithm both selects the optimal set of memories and estimates the transition probabilities attached to each memory (for instance the transition probabilities attached to the second-order memory "primordium, emerged root"). Variable-order Markov chains of maximum order 3 were compared on the basis of 43 proximal zones of long roots sequences (cumulated length 445). The variable-order Markov chain with memories "primordium" (order 1), "primordium, emerged root" and "emerged root, emerged root" (order 2) was selected; see Table 2 for the estimated transition probabilities with associated confidence intervals. Compared with a fixed first-order Markov chain, the fit of the runs length of emerged roots was greatly improved (Figure 7).

Mechanistic modeling. The root branching process was formalized as a mechanistic model (Figure 8A). Let Φ_D and Φ_I be respectively the flux entering the apex from the development zone and the reflux returning to the apex from the initiation zone (Figure 8B). Let α (respectively β) be the fraction of the auxin flux leaving the apex (respectively the initiation zone) toward the initiation zone (respectively the apex), with $\alpha, \beta \in]0;1[$. Hence the accumulation of auxin within the meristem ($\frac{dc}{dt}$) and within the initiation zone ($\frac{dc'}{dt}$) can be written as:

$$\frac{dc}{dt} = (1-\alpha)(\Phi_D + \Phi_I) - \delta c \ , \qquad (1)$$

$$\frac{dc'}{dt} = \alpha(1-\beta)(\Phi_D + \Phi_I) - \delta c' , \qquad (2)$$

where δ is the degradation rate of auxin.

The conservation of fluxes at the IZ node leads to:

$$\Phi_I = \alpha\beta(\Phi_D + \Phi_I), \qquad (3)$$

Isolating Φ_I in the left-hand term yields:

$$\Phi_I = \frac{\alpha\beta}{1-\alpha\beta}\Phi_D \ . \qquad (4)$$

From (1), (2) and (4) we can express the accumulation of auxin within the meristem and initiation zone as:

$$\frac{dc}{dt} = \frac{1-\alpha}{1-\alpha\beta}\Phi_D - \delta c \ , \qquad (5)$$

$$\frac{dc'}{dt} = \frac{\alpha(1-\beta)}{1-\alpha\beta}\Phi_D - \delta c' \ . \qquad (6)$$

We can thus express the auxin concentration within the meristem and initiation zone at equilibrium:

$$c_{eq} = \frac{1-\alpha}{\delta(1-\alpha\beta)}\Phi_D \ , \qquad (7)$$

$$c'_{eq} = \frac{\alpha(1-\beta)}{\delta(1-\alpha\beta)}\Phi_D \ , \qquad (8)$$

and integrate (5) and (6) as:

$$\begin{cases} \text{if } \dfrac{(1-\alpha)\Phi_D}{(1-\alpha\beta)} > 0, & C = \dfrac{(1-\alpha)\Phi_D}{\delta(1-\alpha\beta)}(1-e^{-\delta t}) \ , \\ \text{otherwise} & C = C_0 e^{-\delta t} \end{cases} \qquad (9)$$

$$\begin{cases} \text{if } \dfrac{\alpha(1-\beta)\Phi_D}{(1-\alpha\beta)} > 0, & C' = \dfrac{\alpha(1-\beta)\Phi_D}{\delta(1-\alpha\beta)}(1-e^{-\delta t}), \\ \text{otherwise} & C' = C'_0\, e^{-\delta t} \end{cases} \qquad (10)$$

where C_0 and C'_0 are the initial auxin concentrations within the meristem and initiation zone. As $\alpha, \beta \in]0;1[$, equations (9) and (10) are true as long as $\Phi_D > 0$.

Supplementary Figure S1 compares the values of C and C' for different values of δ and Φ_D.

The equation (4) shows that Φ_I is particularly sensitive to values of $\alpha\beta$ that are close to 1. For such values, the system shows large variations in Φ_I even for small changes in either $\alpha\beta$ or Φ_D (Figure 8C).

A discrete version of this model written in the Python programming language is given in Supplementary Figure S2.

The different model parameters were either estimated directly from observed data (e.g. mean time between successive initiations, mean percentage of emergence, simultaneous number of developing primordia) or inferred from observed data through automated parameters' space exploration. Over 1000 parameter combinations were tested. Due to the stochastic distribution of IT and ET, each parameter combination was tested for run of 20 simulations, and outputs were used for statistical evaluation of the parameter set. The parameter combination corresponding to the best fit of lateral root initiation and emergence densities to the observed values was selected for subsequent model prediction. The Python stand-alone module is available from the authors.

References

1. Douady S, Couder Y (1992) Phyllotaxis as a physical self-organized growth process. Phys. Rev. Lett. 68: 2098-2101

2. Malamy JE (2005) Intrinsic and environmental response pathways that regulate root system architecture. Plant Cell & Env. 28: 67-77

3. Hodge A (2006) Plastic plants and patchy soils. J. Exp. Bot. 57: 401-411

4. Casimiro I, Beeckman T, Graham N, Bhalerao R, Zhang H, Casero P, Sandberg G, Bennett MJ (2003) Dissecting Arabidopsis lateral root development. Trends Plant Sci. 8: 165-171

5. De Smet I, Vanneste S, Inzé D, Beeckman T (2006) Lateral root initiation or the birth of a new meristem. Plant Mol. Biol. 60: 871-887

6. Casimiro I, Alan M, Rishikesh PB, et al (2001) Auxin transport promotes Arabidopsis lateral root initiation. Plant cell 13: 843-52

7. De Smet I, Tetsumura T, De Rybel B, Frei Dit Frey N, Laplaze L, Casimiro I, Swarup R, Naudts M, Vanneste S, et al (2007) Auxin-dependent regulation of lateral root positioning in the basal meristem of Arabidopsis. Development 134: 681-690

8. Bhalerao R, Eklöf J, Ljung K, Marchant A, Bennett M, Sandberg G, et al (2002) Shoot-derived auxin is essential for early lateral root emergence in Arabidopsis seedlings. Plant J. 29: 325-32

9. Benková E, Michniewicz M, Sauer M, Teichmann T, Seifertová D, Jürgens G, Friml J (2003) Local, efflux-dependent auxin gradients as a common module for plant organ formation. Cell 115: 591-602

10. Swarup K, Benková E, Swarup R, et al. (2008) The auxin influx carrier LAX3 promotes lateral root emergence. Nat. Cell Biol., in press.

11. Laskowski M, Biller S, Stanley K, Kajstura T, Prusty R (2006) Expression Profiling of Auxin-Treated Arabidopsis Roots: Toward a Molecular Analysis of Lateral Root Emergence. Plant Cell Physiol. 47: 788-792

12. Malamy JE, Benfey PN (1997) Organization and cell differentiation in lateral roots of Arabidopsis thaliana. Development 124: 33-44

13. Dubrovsky JG, Doerner PW, Colón-Carmona A, Rost TL (2000) Pericycle cell proliferation and lateral root initiation in Arabidopsis. Plant Physiol. 124: 1648-1657

14. Dubrovsky JG, Gambetta GA, Hernández-Barrera A, Shishkova S, González I (2006) Lateral root initiation in Arabidopsis: developmental window, spatial patterning, density and predictability. Ann. Bot. 97: 903-15

15. Lucas M, Godin C, Jay-Allemand C, Laplaze L (2008) Auxin fluxes in the root apex co-regulate gravitropism and lateral root initiation. J. Exp. Bot. 59: 55-66

16. Guédon, Y (2003) Estimating hidden semi-Markov chains from discrete sequences. J. Comp. Graph. Stat. 12: 604-639

17. Guédon, Y (2005) Hidden hybrid Markov/semi-Markov chains. Comp. Stat. & Data Anal. 49: 663-688

18. Ljung, K, Anna KH, John C et al (2005) Sites and regulation of auxin biosynthesis in Arabidopsis roots. Plant cell 17: 1090-104

19. Celenza J, Grisafi P, Gerald RF (1995) A pathway for lateral root formation in Arabidopsis thaliana. Genes Dev. 9: 2131-42

20. Swarup R, Kramer EM, Perry P, Knox K, Leyser HM, Haseloff J, Beemster GT, Bhalerao R, Bennett MJ (2005) Root gravitropism requires lateral root cap

and epidermal cells for transport and response to a mobile auxin signal. Nat. Cell Biol. 7: 1057-1065

21. Reed RC, Brady SR, Muday GK (1998) Inhibition of auxin movement from the shoot into the root inhibits lateral root development in Arabidopsis. Plant Physiol. 118: 9847111

22. Hofmeiester W (1868) Allgemeine morphologie der gewachse. In *Handbuch der Physiologischen botanik*, 2. W. hofmeister. Leipzig: W. Engelmann

23. Snow M, Snow R (1962) A Theory of the regulation of phyllotaxis based on Lupinus albus. Phil. Trans. Roy. Soc. Lond. 244: 483-513

24. Jönsson, Henrik, Marcus G Heisler, Bruce E Shapiro, Elliot M Meyerowitz, and Eric Mjolsness. 2006. An auxin-driven polarized transport model for phyllotaxis. Proc. Natl. Acad. Sci. U. S. A. 103, no. 5 (January 31): 1633-8.

25. de Reuille, Pierre Barbier, Isabelle Bohn-Courseau, Karin Ljung, et al. 2006. Computer simulations reveal properties of the cell-cell signaling network at the shoot apex in Arabidopsis. Proc. Natl. Acad. Sci. U. S. A. 103, no. 5 (January 31): 1627-32.

26. Smith, Richard S, Soazig Guyomarc'h, Therese Mandel, et al. 2006. A plausible model of phyllotaxis. Proc. Natl. Acad. Sci. U. S. A. 103, no. 5 (January 31): 1301-6.

27. Laplaze L, Parizot B, Baker A, Ricaud L, Martinière A, Auguy F, Franche C, Nussaume L, Bogusz D, Haseloff J (2005) GAL4-GFP enhancer trap lines for genetic manipulation of lateral root development in Arabidopsis thaliana. J. Exp. Bot. 56: 2433-2442

28. Godin C, Guédon Y & Costes E (1999) Exploration of plant architecture databases with the AMAPmod software illustrated on an apple-tree hybrid family. Agron. 19: 163-184

29. Pradal C, Dufour-Kowalski S, Boudon F, Fournier C, Godin C (2008) OpenAlea: A visual programming and component-based software platform for plant modelling. Funct. Plant Biol., in press.

30. Csiszár I, Talata Z (2006) Context tree estimation for not necessarily finite memory processes, via BIC and MDL. IEEE Transactions on Information Theory 52: 1007-1016.

Aknowledgements

We thank P. Doumas (INRA, Equipe Rhizogenèse, Montpellier, France) for helpful discussion and critical reading of the manuscript.

Funding

This work was supported by IRD, INRIA (Virtual Plants project) and CIRAD. M.L. is the recipient of a PhD grant from the French *Ministère de l'Enseignement Supérieur, de la Recherche et de la Technologie*.

Author contributions. ML, CG, CJA and LL conceived and designed the experiments, performed the experiments and analyzed the data. YG designed the Markovian models and performed the Markovian statistical analysis. ML

designed and evaluated the mechanistic model of initiation. ML, CG, LL and YG wrote the paper.

Tables

Table 1: Transition probabilities (with confidence intervals) of the estimated variable-order Markov chain.

Previous state(s) \ Next state	primordium (P.)	emerged root (E.)	count
Primordium (P.)	0.48 (0.41, 0.55)	0.52 (0.45, 0.59)	197
primordium - emerged root (P. E.)	0.45 (0.34, 0.57)	0.55 (0.43, 0.62)	73
emerged root - emerged root (E. E.)	0.24 (0.17, 0.32)	0.76 (0.68, 0.83)	127

Table 2: Empirical distributions of the segment length between two lateral organs

μ, σ (sample size)	segment before	segment after
primordium	7.66, 5.6 (159)	8.74, 6.19 (191)
emerged root	10.4, 5.39 (243)	10.1, 5.91 (244)

Figures legends

Figure 1. Determination of root developmental profile

Transgenic seedlings (n=397) aged 3 to 12 day and expressing the *Pro$_{CYCB1}$:GUS* marker were observed using a Leica DMRB microscope. The developmental stage of each primordium and the distance (i.e. number of root hair cells) between them were scored along the primary root and emerged laterals. Each root was then assigned a unique identification code and developmental profile as illustrated here.

Figure 2. Macroscopic regularities of root development

Each data point corresponds to a single primary or secondary root (n = 397). The color of the point indicates the age of the root when observation took place (3 to 12 days after germination).

(A) The global number of lateral root primordia initiation is proportional to the total root length (measured in number of root hair cells).

(B) The global emergence rate of lateral roots stabilizes around 50%.

(C) Stabilization of emergence rate occurs after the first week of growth. Data point size indicates the relative number of similar observed values.

Figure 3. Encoding the root structure

We defined three kinds of sequences based on full blown developmental profiles. The sequence of developmental stages considers only the developmental stages of the successive lateral organs.

The sequence of root segment length (root segment being defined as the unit formed by two successive organs and the distance between them) considers only the distances between the successive lateral organs.

The cellular string sequence were obtained by transcoding and expanding the developmental profile. The transcoding of the developmental stages is shown below the cellular string: observed un-differentiated cells were coded as 0, non-emerged primordia were coded as 1, and emerged lateral roots were coded as 2.

Figure 4. Stochastic model of root development

This model traduces all observed developmental profiles.

Each state is represented by a vertex which is numbered in red in its lower right corner (except the final end state). The possible transitions between states are represented by arcs with the attached probabilities noted nearby. Dotted arcs entering in states indicate initial states. The attached initial probabilities are noted nearby. Only arcs with attached initial or transition probabilities > 0.03 are figured. The occupancy distributions of the semi-Markovian states 0, 2, 4, and 5 are figured above the corresponding vertex. The possible outputs in a state are noted in the corresponding vertex with the attached observation probabilities when < 1. States 1-2 (respectively 3-4) define the proximal (respectively distal) functional zones.

The lower part of the panel present the most probable state sequence predicted for the given cellular string.

Figure 5. Primordia and lateral root distributions in the stochastic model

The observed distributions (number of lateral organs of a given type per root) are extracted from the data while the theoretical distributions are computed from the estimated stochastic model.

Figure 6. Empirical distribution of root segment length in the proximal zone (state 2 in the stochastic model)

Figure 7. Distribution of the run length of emerged roots

The observed distribution (i.e. number of successive emerged roots) is extracted from the data while the theoretical distributions are computed from an estimated first-order or variable-order Markov chain.

Figure 8. Mechanistic model of lateral root initiation and development

(A) Structure of the model. Auxin reflux takes place though the initiation zone (IZ). A fraction of the reflux accumulates until the initiation threshold (IT) is reached. A new primordium then appears and depletes auxin in the IZ. Primordia going through the development zone (DZ) drain a percentage of the central auxin flux. Primordia will emerge if their auxin content is higher than the emergence threshold (ET). Emerged laterals cease consuming auxin. Primordia which have not yet emerged when they leave the DZ for the emergence zone (EZ) will stop developing. Gravistimulation is considered to induce a drop of IT and to consume a fraction of the auxin in the IZ. IT and ET both vary dynamically according to Gaussian distributions. Auxin production augments after one week.

(B) Mathematical representation of the reflux system. Fluxes coming from the development and initiation zone are denoted as Φ_D and Φ_I. The reflux efficiencies are denoted α and β, while δ expresses auxin degradation in the meristem and in the IZ.

(C) Auxin fluxes passing through the IZ at equilibrium. As the reflux is considered to be imperfect, the flux going through the IZ will reach a stable point depending on the efficiencies of the refluxes α and β and on the central flux entering the IZ from the DZ (value in arbitrary units of production per minute). For high values of reflux efficiency, a small variation in reflux efficiency or entering fluxes will lead to a strong change of stable point (black arrows).

Figure 9. Mechanistic model calibration and predictions

(A & B) Initiation and emergence in the model were calibrated according to the observed mean initiation and emergence level (see figure 2). Runs of 20 simulations were done for each condition. Data point size indicates the relative number of simulations giving the same output.

(C) Fit between model prediction and observation for various gravistimulation patterns (see Supplementary Figure S3 for additional details on the gravistimulation patterns). Runs of 20 simulations were done for each condition.

(D) Predicted emergence rate and initiation level as a function of apical reflux. Runs of 20 simulations were done for each condition (reflux efficiency ranging from 20% to 99%).

(E) Predicted initiation level as a function of development level of primordia. Development of primordia in the model was either full or arrested at various level ranging from 4/5th of full development to no development at all. Runs of 20 simulations were done for each condition. Data point size indicates the relative number of simulations giving the same output.

(F) Observed initiation and emergence densities in mutants and wild-type Col-0. Initiation and emergence densities were scored for the mutants *pin2* and *aux1*, and normalized in regard to the emergence density of wild-type Col-0 plants. Data for the *lax3* mutant were provided by Pr. Malcolm Bennett. Each data point corresponds to a set of more than 20 seedlings.

Figure 10. Gravistimulation enhanced balance between initiation and development

(A) Initiation density and emerged lateral root density were scored for plants gravistimulated according to the gravistimulation protocol presented in [15]. The results are given for primordia located in gravistimulated zones. Measurements were normalized in regard to the emergence density of non-gravistimulated plants. Each data point corresponds to a set of more than 20 seedlings. Non-gravistimulated Col-0 seedlings were used as a control group.

(B) Emergence of lateral roots in gravistimulated roots. White bar: emerged lateral root percentage. Gray bar: non-emerged primordia percentage. Non gravistimulated Col-0 seedling were used as a control.

(C) Distribution of primordia developmental stages for the 24h time between gravistimulation treatment. White bar: primordia appearing and developing between gravistimulation (n = 72). Black bar: primordia appearing and developing in root turns (n = 373).

(D) Initiation and emergence densities predicted by the mechanistic model with the added hypothesis of a drop of ET under gravistimulation.

Supporting Information

Figure S1. Auxin accumulation in the meristem and initiation zone

(Top row) Auxin accumulation during time within the meristem (C) and initiation zone (C') as a function of auxin fluxes coming from the differentiation zone, computed according to the reflux system presented in Figure 8B. $\alpha = 0.9$; $\beta = 0.9$; $\delta = 0.01$. Auxin level is expressed in arbitrary units.

(Bottom row) Auxin accumulation during time within the meristem (C) and initiation zone (C') as a function of auxin degradation, computed according to the reflux system presented in Figure 8B. $\alpha = 0.9$; $\beta = 0.9$; $\Phi_D = 10$. Auxin level is expressed in arbitrary units.

Figure S2. The RootFeedback algorithm corresponding to the mechanistic model
The pseudo-code is expressing the mechanisms described in Fig. 8A in discrete time.

Figure S3. Gravistimulation patterns used for the calibration and evaluation of the model

Seedlings were grown in vertical plates and gravistimulated by a 90° rotation (black dot) of the growth plates.

Treatments labeled 1 to 24 were applied for 3.5 days using either crenel-shape-generating or stair-shape-generating protocols (see [15] for additional details). The results obtained following those treatments were use to calibrate the model presented in figure 8.

Treatment labeled A to I were applied for 48 hours after germination using stair-shape-generating protocols. The results obtained following those treatments were directly compared to model output using the parameters previously defined.

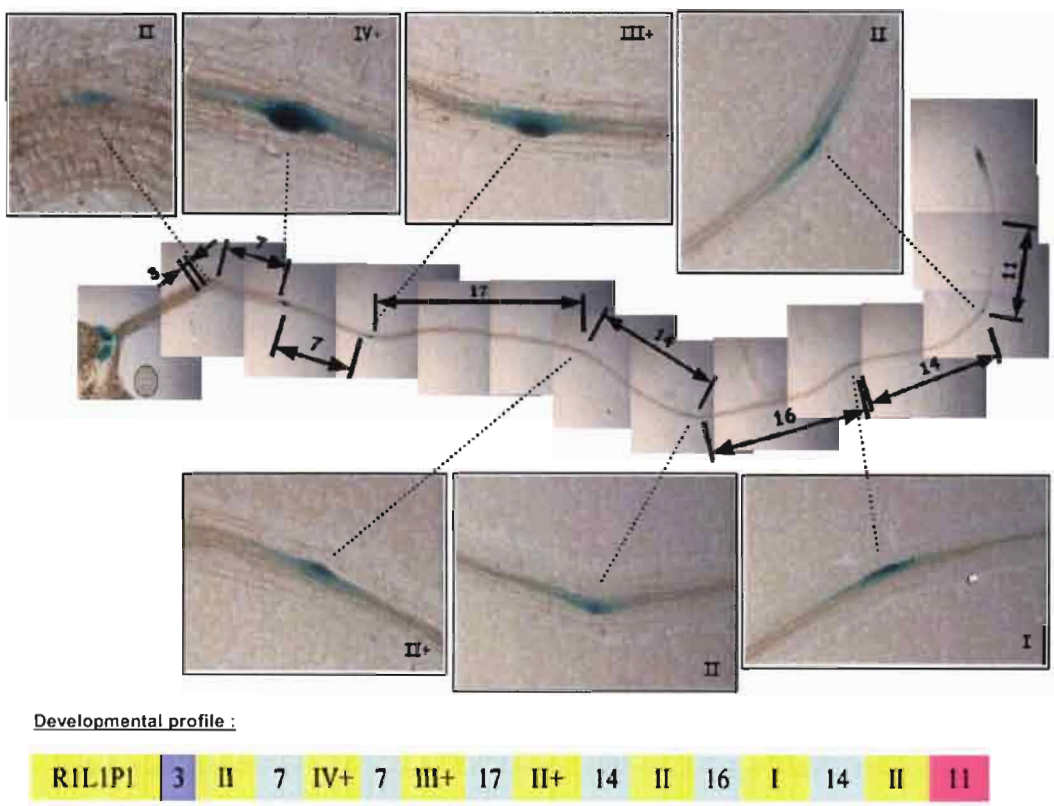

Figure 1. Determination of root developmental profiles
Transgenic seedlings (n=397) aged 3 to 12 day and expressing the *Pro*$_{CYCB1}$*:GUS* marker were observed using a Leica DMRB microscope. The developmental stage of each primordium and the distance (i.e. number of root hair cells) between them were scored along the primary root and emerged laterals. Each root was then assigned a unique identification code and developmental profile as illustrated here.

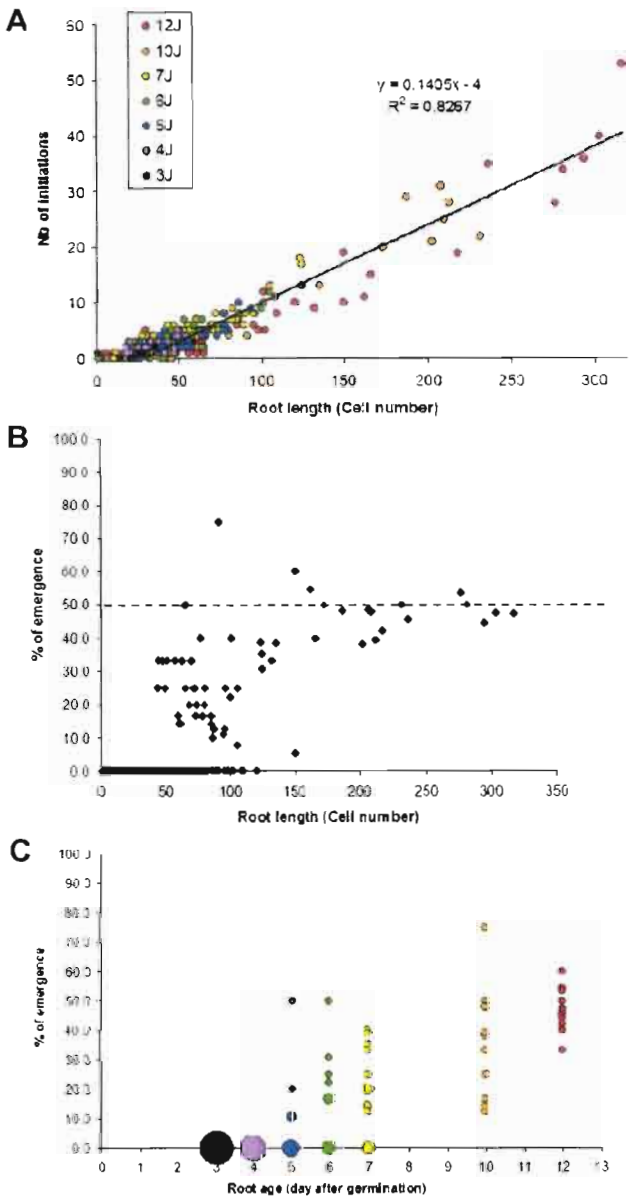

Figure 2. Macroscopic regularities of root development

Each data point corresponds to a single primary or secondary root (n = 397). The color of the point indicates the age of the root when observation took place (3 to 12 days after germination).

(A) The global number of lateral root primordia initiation is proportional to the total root length (measured in number of root hair cells).

(B) The global emergence rate of lateral roots stabilizes around 50%.

(C) Stabilization of emergence rate occurs after the first week of growth. Data point size indicates the relative number of similar observed values.

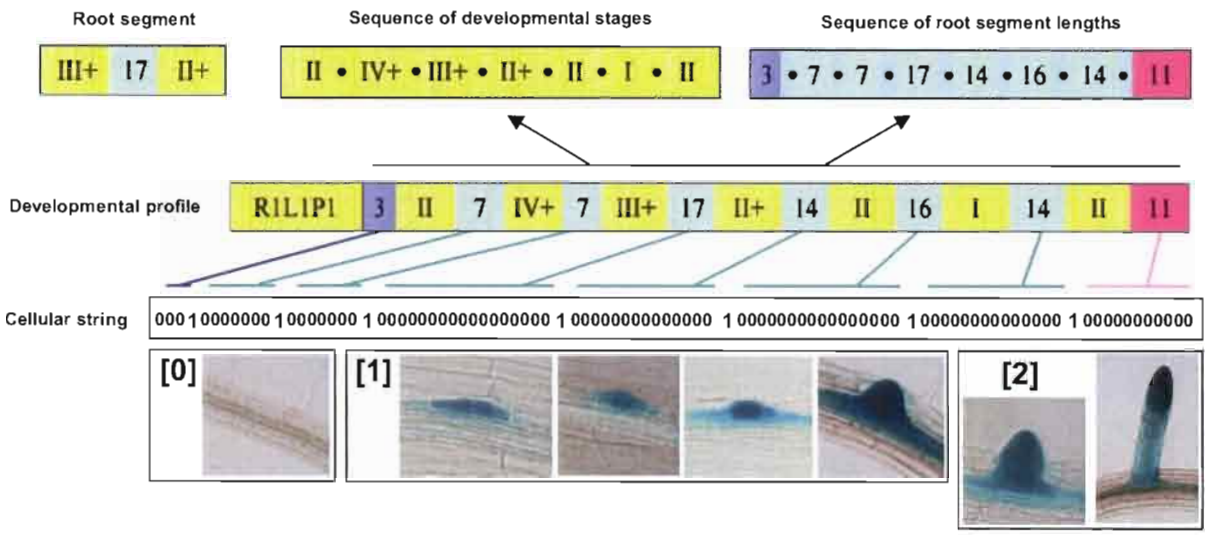

Figure 3. Encoding of the root structure
We defined three kinds of sequences based on full blown developmental profiles.
The sequence of developmental stages considers only the developmental stages of the successive lateral organs.
The sequence of root segment length (root segment being defined as the unit formed by two successive organs and the distance between them) considers only the distances between the successive lateral organs.
The cellular string sequence were obtained by transcoding and expanding the developmental profile. The transcoding of the developmental stages is shown below the cellular string: observed un-differentiated cells were coded as 0, non-emerged primordia were coded as 1, and emerged lateral roots were coded as 2.

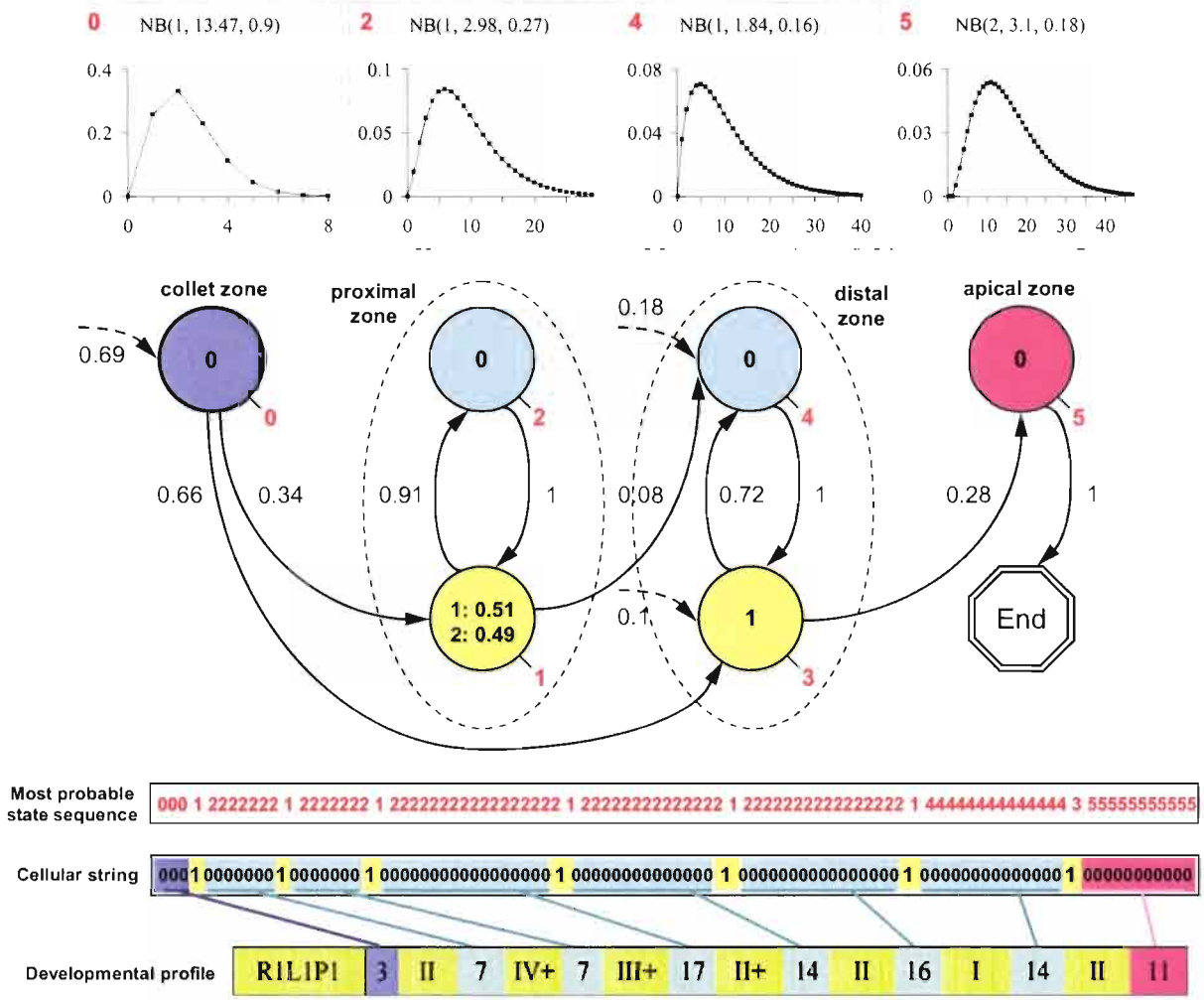

Figure 4. Stochastic model of root development
This model traduces all observed developmental profiles.
Each state is represented by a vertex which is numbered in red in its lower right corner (except the final end state). The possible transitions between states are represented by arcs with the attached probabilities noted nearby. Dotted arcs entering in states indicate initial states. The attached initial probabilities are noted nearby. Only arcs with attached initial or transition probabilities > 0.03 are figured. The occupancy distributions of the semi-Markovian states 0, 2, 4, and 5 are figured above the corresponding vertex. The possible outputs in a state are noted in the corresponding vertex with the attached observation probabilities when < 1. States 1-2 (respectively 3-4) define the proximal (respectively distal) functional zones.
The lower part of the panel present the most probable state sequence predicted for the given cellular string.

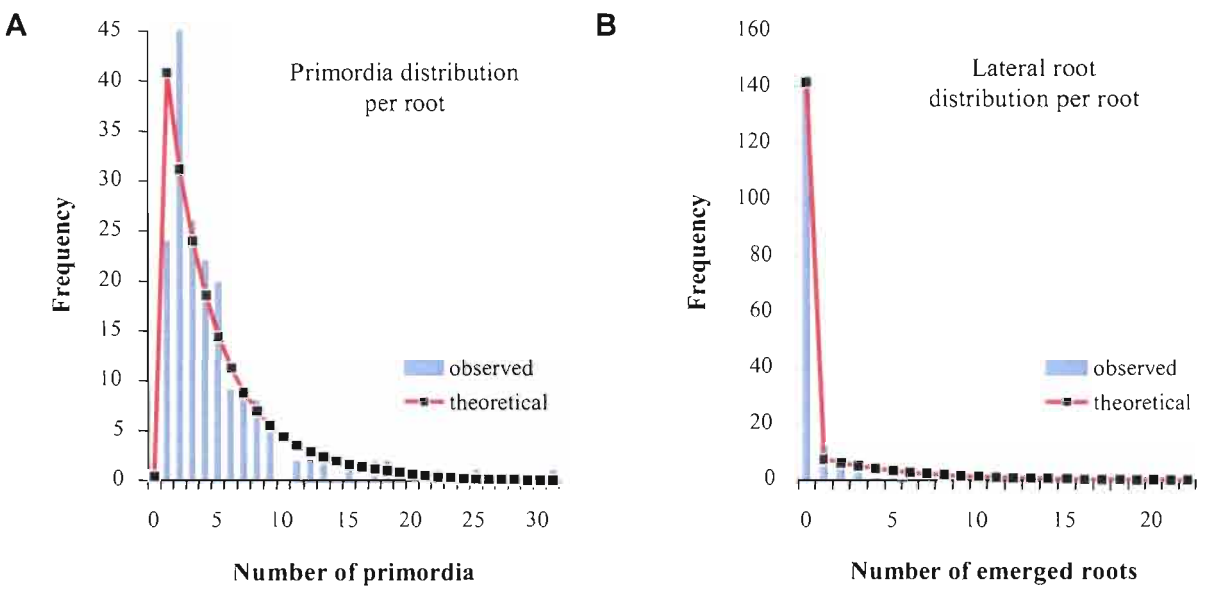

Figure 5. Primordia and lateral root distributions in the stochastic model
The observed distributions (number of lateral organs of a given type per root) are extracted from the data while the theoretical distributions are computed from the estimated stochastic model.

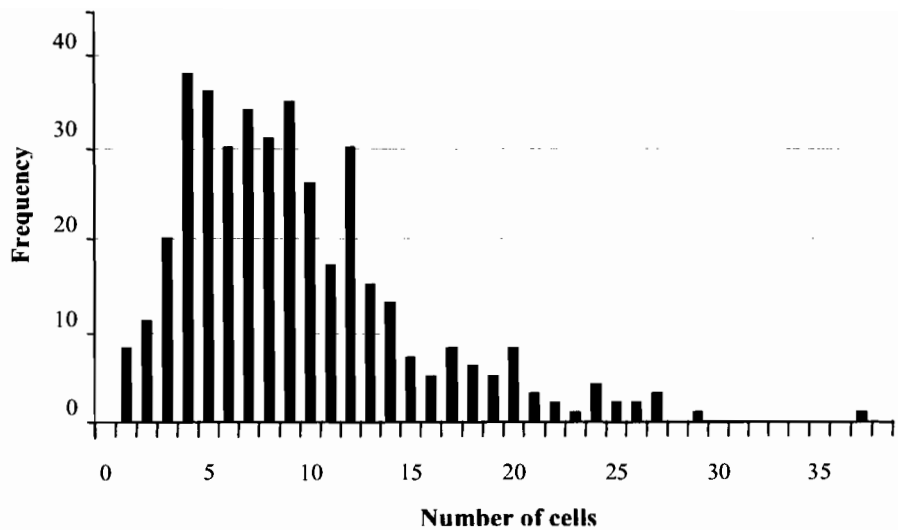

Figure 6. Empirical distribution of root segment length in the proximal zone (state 2 in the stochastic model)

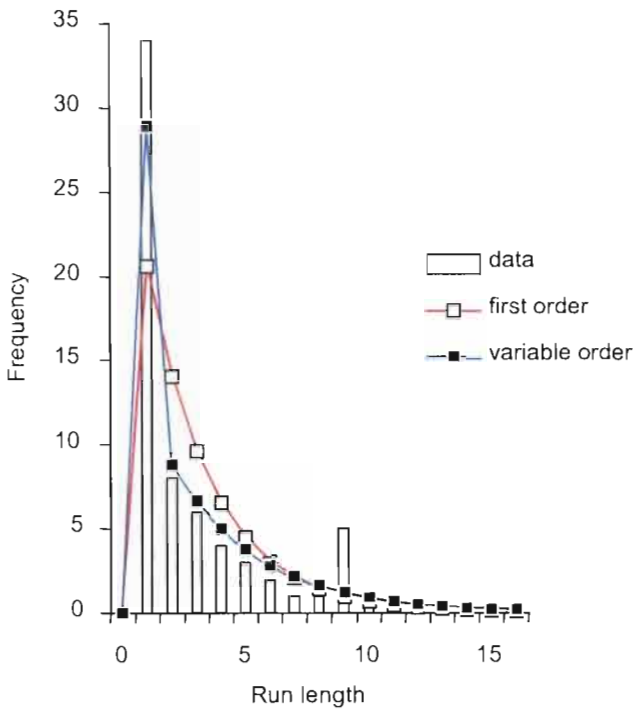

Figure 7. Distribution of the run length of emerged roots
The observed distribution (i.e. number of successive emerged roots) is extracted from the data while the theoretical distributions are computed from an estimated first-order or variable-order Markov chain.

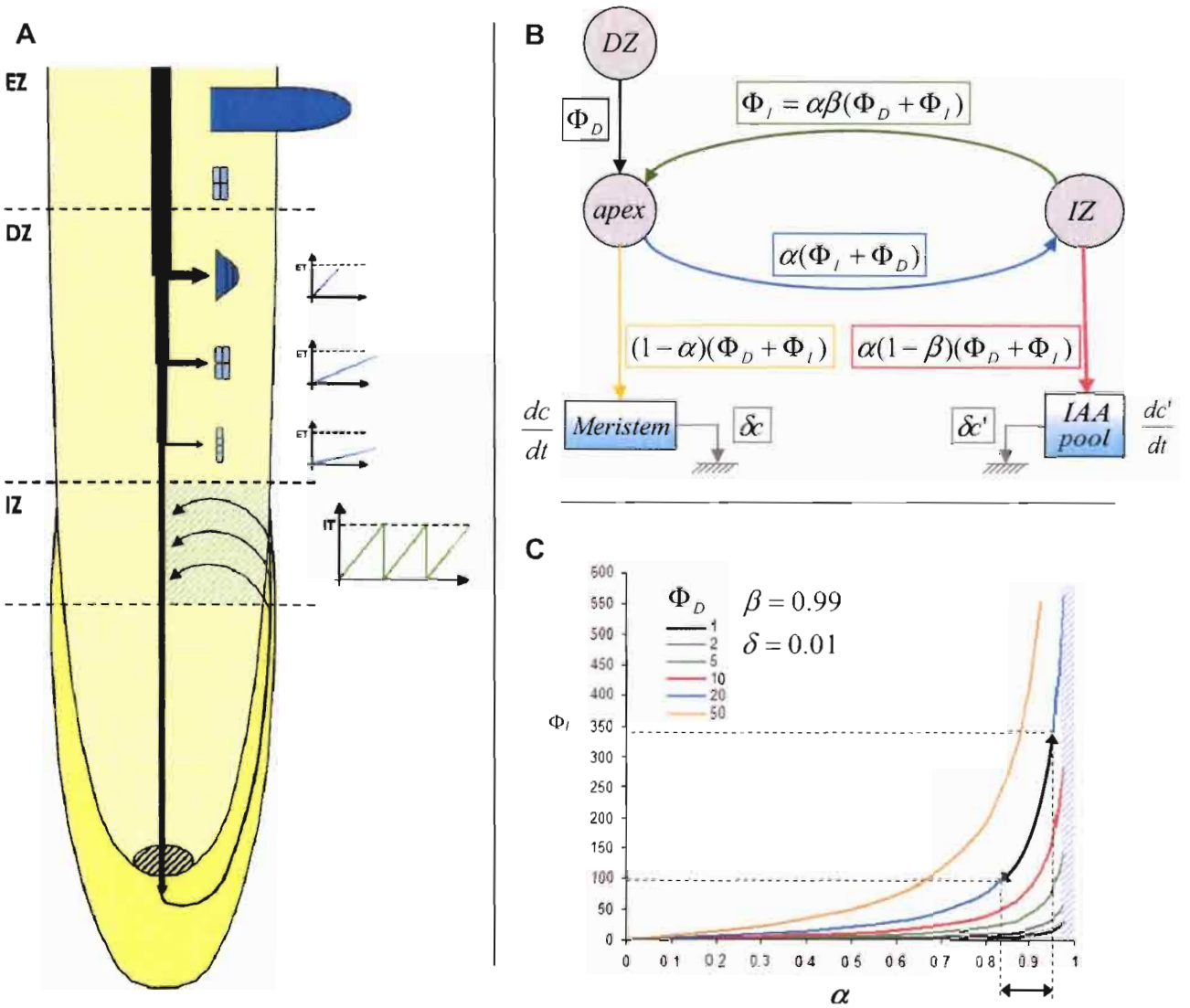

Figure 8. Mechanistic model of lateral root initiation and development

(A) Structure of the model. Auxin reflux takes place though the initiation zone (IZ). A fraction of the reflux accumulates until the initiation threshold (IT) is reached. A new primordium then appears and depletes auxin in the IZ. Primordia going through the development zone (DZ) drain a percentage of the central auxin flux. Primordia will emerge if their auxin content is higher than the emergence threshold (ET). Emerged laterals cease consuming auxin. Primordia which have not yet emerged when they leave the DZ for the emergence zone (EZ) will stop developing. Gravistimulation is considered to induce a drop of IT and to consume a fraction of the auxin in the IZ. IT and ET both vary dynamically according to Gaussian distributions. Auxin production augments after one week.

(B) Mathematical representation of the reflux system. Fluxes coming from the development and initiation zone are denoted as Φ_D and Φ_I. The reflux efficiencies are denoted α and β, while δ expresses auxin degradation in the meristem and in the IZ.

(C) Auxin fluxes passing through the IZ at equilibrium. As the reflux is considered to be imperfect, the flux going through the IZ will reach a stable point depending on the efficiencies of the refluxes α and β and on the central flux entering the IZ from the DZ (value in arbitrary units of production per minute). For high values of reflux efficiency, a small variation in reflux efficiency or entering fluxes will lead to a strong change of stable point (black arrows).

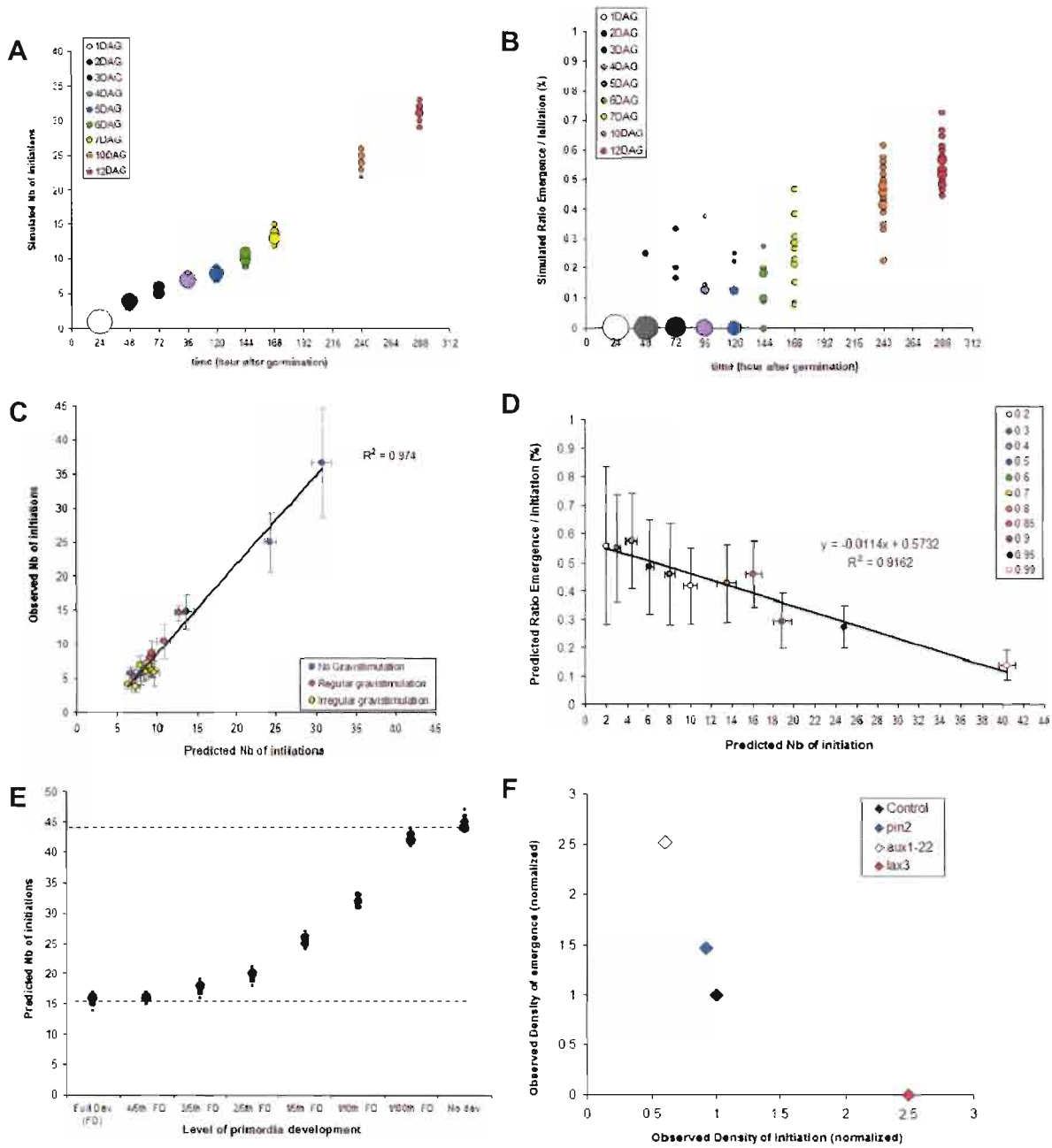

Figure 9. Mechanistic model calibration and predictions

(A & B) Initiation and emergence in the model were calibrated according to the observed mean initiation and emergence level (see figure 2). Runs of 20 simulations were done for each condition. Data point size indicates the relative number of simulations giving the same output.

(C) Fit between model prediction and observation for various gravistimulation patterns (see Supplementary Figure S3 for additional details on the gravistimulation patterns). Runs of 20 simulations were done for each condition.

(D) Predicted emergence rate and initiation level as a function of apical reflux. Runs of 20 simulations were done for each condition (reflux efficiency ranging from 20% to 99%).

(E) Predicted initiation level as a function of development level of primordia. Development of primordia in the model was either full or arrested at various level ranging from 4/5th of full development to no development at all. Runs of 20 simulations were done for each condition. Data point size indicates the relative number of simulations giving the same output.

(F) Observed initiation and emergence densities in mutants and wild-type Col-0. Initiation and emergence densities were scored for the mutants *pin2* and *aux1*, and normalized in regard to the emergence density of wild-type Col-0 plants. Data for the *lax3* mutant were provided by Pr. Malcolm Bennett. Each data point corresponds to a set of more than 20 seedlings.

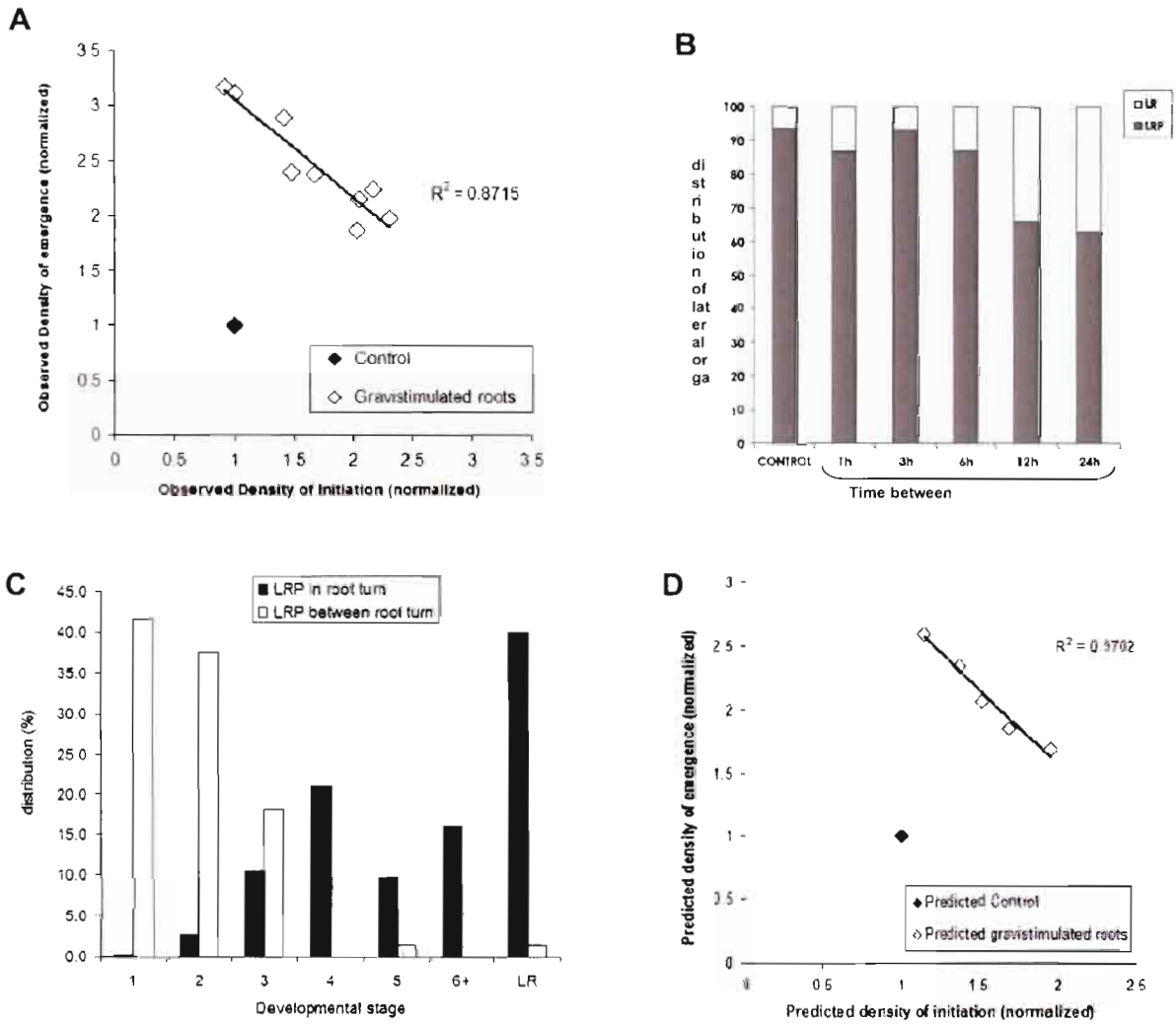

Figure 10. Gravistimulation enhanced balance between initiation and development
(A) Initiation density and emerged lateral root density were scored for plants gravistimulated according to the gravistimulation protocol presented in [15]. The results are given for primordia located in gravistimulated zones. Measurements were normalized in regard to the emergence density of non-gravistimulated plants. Each data point corresponds to a set of more than 20 seedlings. Non-gravistimulated Col-0 seedlings were used as a control group.
(B) Emergence of lateral roots in gravistimulated roots. White bar: emerged lateral root percentage. Gray bar: non-emerged primordia percentage. Non gravistimulated Col-0 seedling were used as a control.
(C) Distribution of primordia developmental stages for the 24h time between gravistimulation treatment. White bar: primordia appearing and developing between gravistimulation (n = 72). Black bar: primordia appearing and developing in root turns (n = 373).
(D) Initiation and emergence densities predicted by the mechanistic model with the added hypothesis of a drop of ET under gravistimulation.

Supplementary figure S1

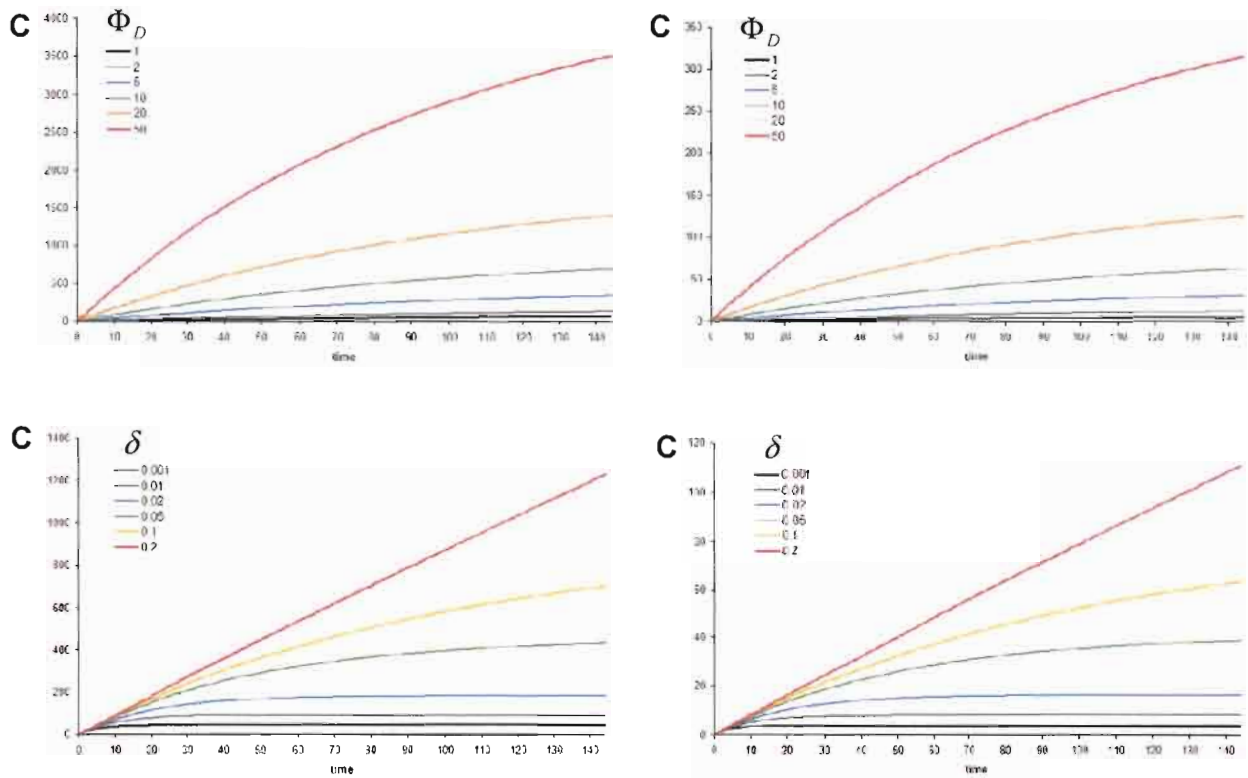

Figure S1. Auxin accumulation in the meristem and initiation zone
(Top row) Auxin accumulation during time within the meristem (C) and initiation zone (C') as a function of auxin fluxes coming from the differentiation zone, computed according to the reflux system presented in Figure 8B. $\alpha = 0.9$; $\beta = 0.9$; $\delta = 0.01$. Auxin level is expressed in arbitrary units.
(Bottom row) Auxin accumulation during time within the meristem (C) and initiation zone (C') as a function of auxin degradation, computed according to the reflux system presented in Figure 8B. $\alpha = 0.9$; $\beta = 0.9$; $\Phi_D = 10$. Auxin level is expressed in arbitrary units.

Supplementary figure S2

The RootFeedback algorithm

INPUT

- *time_length* = observation duration in minutes
- *base_flux(t)* = amount of auxin produced during 1 minute ; augment after 1 week of growth
- α = root apex reflux efficiency
- *IT* = mean initiation threshold ; σ_I standard deviation from IT
- *I_conso* = accumulation factor in the initiation zone
- *LRP_conso* = primordia consumption
- *ET* = mean emergence threshold ; σ_E standard deviation from ET
- *developmental_window* = period of primordia development
- *return_time* = time needed to return to normal after gravistimulation
- *gravitropic_effect_max* = maximum reduction factor of IT under gravistimulation
- *G_max* = maximum auxin consumption following gravistimulation
- *grav_signal[t]* = array of boolean representing the gravistimulation signal, set to true if there is a gravistimulation at time t, set to false otherwise

OUTPUT

- *LRP_index* = array indexing the id (time of initiation) of initiated LRP
- *LR_index* = array indexing the id (time of initiation) of emerged LR
- *LRP[t]* = array of real representing the amount of auxin in the primordia formed at time t, equal to -1 if the primodia has not been initiated (initial condition for every potential primordia)

RootFeedback Algorithm

[gauss(μ,σ) return a random value from the distribution of $\mathcal{N}(\mu,\sigma^2)$]

```
auxin_pool[0] = 0 ; IZ_flux[0] = 0 ; DZ_flux[0] = 0 ; LRP_index = [] ; LR_index = []
for  t = 1 to time_length :
    DZ_flux[t] = base_flux(t)
    if grav_signal[t] :
        G[t] = G_max
        gravitropic_effect[t] = gravitropic_effect_max
    else :
        G[t] = G[t-1] - (G_max / return_time)
        gravitropic_effect[t] = gravitropic_effect[t-1]-(gravitropic_effect_max / return_time)
    for id in LRP_index :
        if ( id > (t - developmental_window) ) :
            LRP[id] = LRP[id] + DZ_flux[t]*LRP_conso
            DZ_flux[t] = DZ_flux[t] * (1-LRP_conso)
            if (LRP[id] > gauss(ET, σ_E)):
                LR_index.append(id)
                LRP_index.remove(id)
    IZ_flux[t] = ( DZ_flux[t] + IZ_flux[t-1] ) * α
    auxin_pool[t] = auxin_pool[t-1] + IZ_flux[t] * I_conso - G[t]
    IZ_flux[t] = IZ_flux[t] * (1-I_conso)
    if ( auxin_pool[t] > gauss(IT*(1-gravitropic_effect[t]),σ_I*(1-gravitropic_effect[t])) ) :
        LRP[t] = 0
        LRP_index.append(t)
        auxin_pool[t] = 0
```

Supplementary figure S3

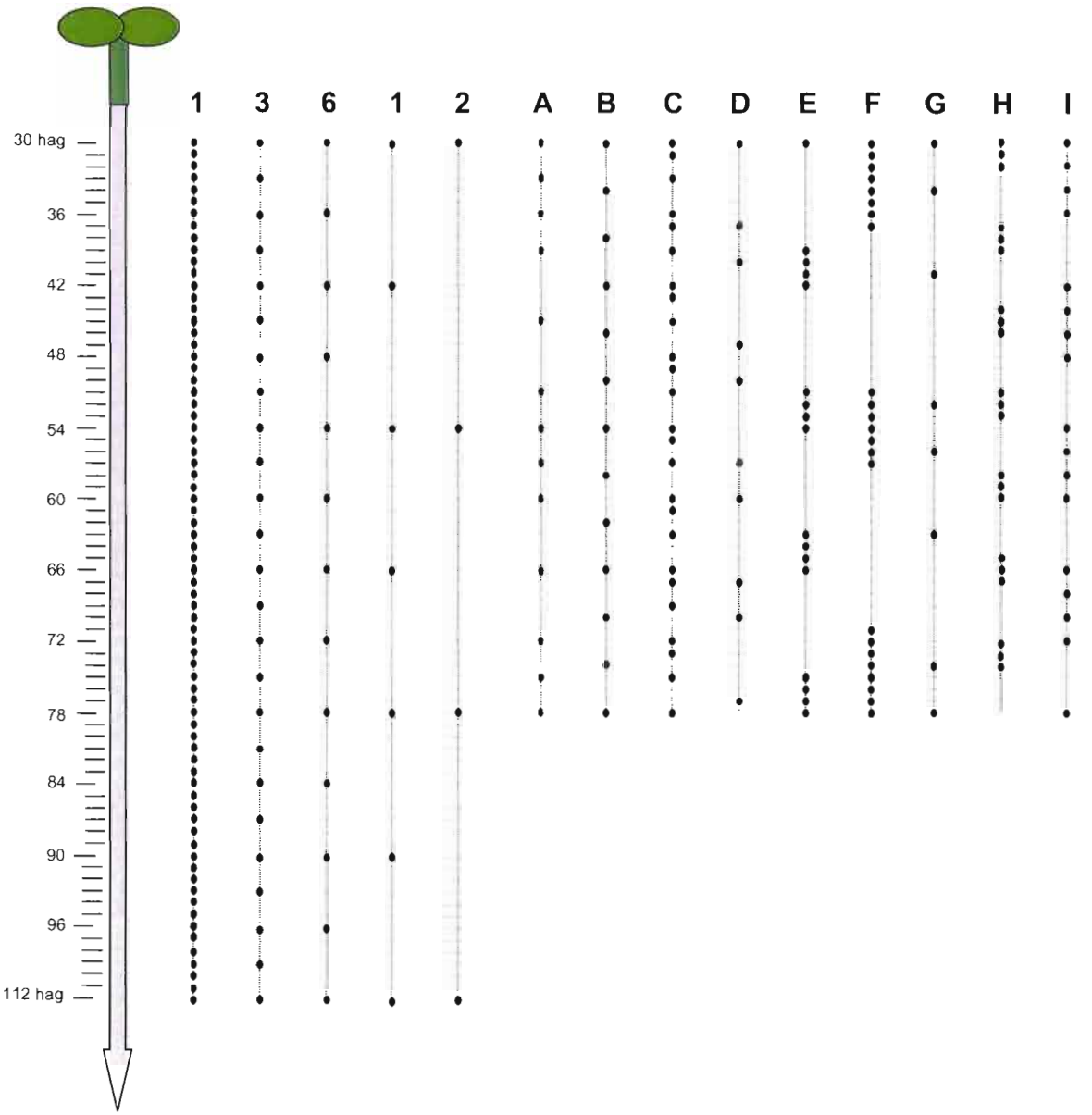

Figure S3. Gravistimulation patterns used for the calibration and evaluation of the model
Seedlings were grown in vertical plates and gravistimulated by a 90° rotation (black dot) of the growth plates.
Treatments labeled 1 to 24 were applied for 3.5 days using either crenel-shape-generating or stair-shape-generating protocols (see [15] for additional details). The results obtained following those treatments were use to calibrate the model presented in figure 8.
Treatment labeled A to I were applied for 48 hours after germination using stair-shape-generating protocols. The results obtained following those treatments were directly compared to model output using the parameters previously defined.

- PART IV -

Macroscopic and microscopic models of auxin fluxes within the root system.

I) Macroscopic model of auxin fluxes

Root growth and development both depend on auxin fluxes which have been well described at the macroscopic level. Auxin flows from the aerial parts through the phloem, and reaches the root apex where its flux is directed by active auxin transporters in a complex reflux circulation. It is possible to use the data available in the literature to draw a map of the potential auxin fluxes within the root apex (Swarup et al. 2001; Marchant et al. 2002; Jirí Friml et al. 2002; Benková et al. 2003; Blilou et al. 2005; Sauer et al. 2006; Tanaka et al. 2006; Wisniewska et al. 2006) (Figure 29).

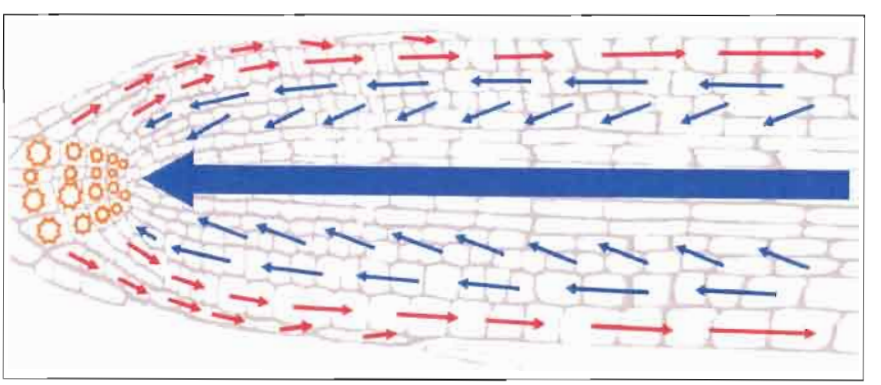

Figure 29. Cellular auxin fluxes within the root apex
Available data on auxin carriers distributions can be used to propose a synthetic view of auxin fluxes expected within the root apex. Blue arrows, acropetal auxin fluxes; red arrows, basipetal auxin fluxes; orange stars, non directed auxin fluxes and sites of auxin accumulation.

The root itself is a constantly evolving structure, new cells appearing through cellular division, existing cells growing and changing their shape through differential elongation, mechanical properties altered by tissue differentiation... And still auxin flows through the tissues, directing their evolution and simultaneously submitted to it as the pathway it follows is progressively altered by the structural changes. This feedback between the information propagating in a system and the structural evolution of this system is

characteristic of a class of systems called "Dynamical System in a Dynamical Structure", or DS^2 (Giavitto and Michel 2003; Giavitto 2003). The complexity of this kind of systems makes it particularly challenging to understand and predict their behavior.

One way to solve this problem however is to use conceptual, mathematical or dynamical models to abstract these complex processes. Here, we designed a macroscopic model of fluxes within a virtual root based on L-systems, in the hope of deciphering the interactions between auxin fluxes and root development.

I.A) L-systems modelling

Lindenmayer systems (or L-systems) are a mathematical formalism introduced by Aristid Lindenmayer in 1968 to model multi-cellular organisms (Lindenmayer 1968; Prusinkiewicz and Lindenmayer 1990). As a biologist, Lindenmayer worked with yeast and filamentous fungi and studied the growth patterns of various types of algae, such as the blue/green bacteria Anabaena catenula. Originally the L-systems were devised to provide a formal description of the development of such simple multicellular organisms, and to illustrate the neighborhood relationships between plant cells. Later on, this system was extended to describe higher plants and complex branching structures.

Rewriting

L-systems are based on the central concept of rewriting. Rewriting is a process allowing the generation of complex objects by iterative replacement of

elemental parts of an original simple object, according to a set of predefined rules or productions.

This iterative process is similar to the one used to generate fractal patterns such as the snowflake curve, defined in 1905 by Koch (von Koch 1905). Mandelbrot proposed the following snowflake construction method (Mandelbrot 1982):

"One begins with two shapes, an initiator and a generator. The latter is an oriented broken line made up of N equal sides of length r. Thus each stage of the construction begins with a broken line and consists in replacing each straight interval with a copy of the generator, reduced and displaced so as to have the same end points as those of the interval being replaced."

The Figure 30 illustrates this iterative building process.

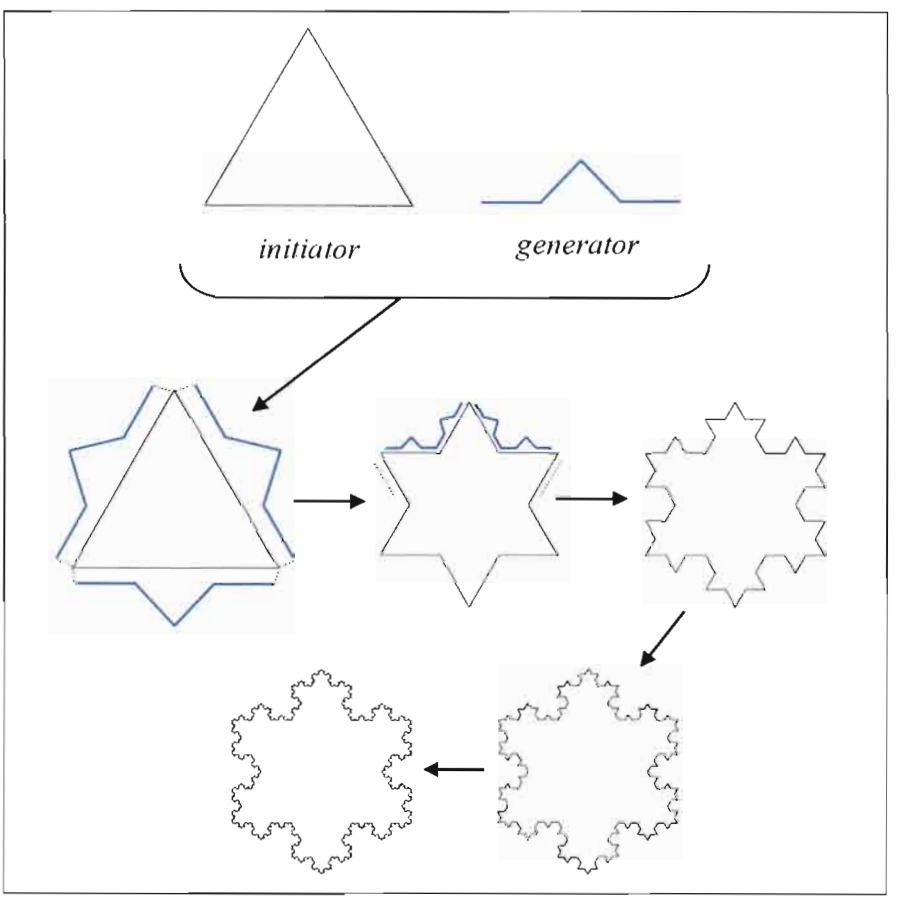

Figure 30. Construction of Koch snowflake curve by geometrical rewriting
At each iteration, all straight segments of the figure are simultaneously replaced by a scaled copy of the iterator.

While the Koch construction recursively replaces open polygons, rewriting systems are not limited to these simple geometrical operations. For example, Wolfram studied patterns generated by rewriting arrays of rectangular elements (Wolfram 1984; Wolfram 1985). The game of life invented by Conway is also based on similar array-rewriting principles (Gardner 1970; Gardner 1971).

The most extensively studied and the best understood rewriting systems are not geometrical, but rather operate on character strings and are called Grammars. String rewriting came into the spotlight in the late 1950s, following Noam Chomsky's work on formal grammars (Chomsky 1956), where he applied the concept of rewriting to describe the syntactic features of natural languages.

L-system formalisms: D0L-systems

In 1968 the biologist Aristid Lindenmayer introduced a new type of string-rewriting mechanism, subsequently termed L-systems (Lindenmayer 1968). The principal difference between grammars defined by Chomsky and L-systems lies in the method of applying productions. In Chomsky grammars productions are applied sequentially, replacing one element at a time, whereas in L-systems productions are applied in parallel and simultaneously, replacing all letters in a given word at the same time. Indeed, productions in L-systems are intended to represent cell divisions in multicellular organisms, where division processes may occur simultaneously. Parallel production application has an essential impact on the formal properties of L-system. For example, it exist some languages which can be generated by L-systems but not by Chomsky grammars (Salomaa 1973; Herman and Rozenberg 1975).

The simplest type of L-systems is the D0L-system: Deterministic, context-free (0), L-system (Rozenberg and Salomaa 1980). They can be formally defined as follows:

• An alphabet is a finite set of letters denoted as V. The letters are also called modules.

• A word is a sequence of letters over an alphabet. The set of all words over alphabet V is denoted as V^*.

• A production is a pair (a, u) denoted as $a \rightarrow u$, where a is a letter and u is a word. a is called predccessor and u is called successor.

• A D0L-system is a triplet $G = \langle V, \omega, P \rangle$, where V is an alphabet, $\omega \in V^*$ is a word called the axiom, and P is a set of productions such that $\forall a \in V : \exists^{1} p_a \in P$, where p_a denotes a production that has module a as its predecessor.

By convention it is assumed that if no production is explicitly specified for a module a, then the identity production $(a \rightarrow a)$ is added implicitly to P. Note that the term production does not imply that the current module will always be replaced by another, as production can specify the removal of a module from the string. This is expressed by specifying an asterisk (*) or ε (empty production in formal notation) as the successor.

Note also that as L-systems have been defined as a way to model biological entities, the modeler usually needs to visually judge the adequacy of the L-system representation to its biological counterpart. Thus the character string is often interpreted and represented geometrically using a pre-defined set of interpretation rules. In the most usual interpretation, each symbol of the string will be replaced by a series of instruction for a LOGO-style turtle (Abelson and

diSessa 1982; Prusinkiewicz et al. 1996). The turtle will then proceed to draw the visual interpretation of the string according these interpretation rules.

D0L-systems have been classically used to describe the growth of linear tissues or organs such as the vegetative segment of the Anabaena catenula bacteria (Lindenmayer 1971; De Koster and Lindenmayer 1987). To represent branching structures using a string of letters (linear structures by definition), two specific modules were introduced as a part of the original definition of L-systems (Lindenmayer 1968). These modules are the left and right brackets [and]. They respectively specify the beginning and the end of a branch. The following L-system is an example of simple branching process (Figure 31).

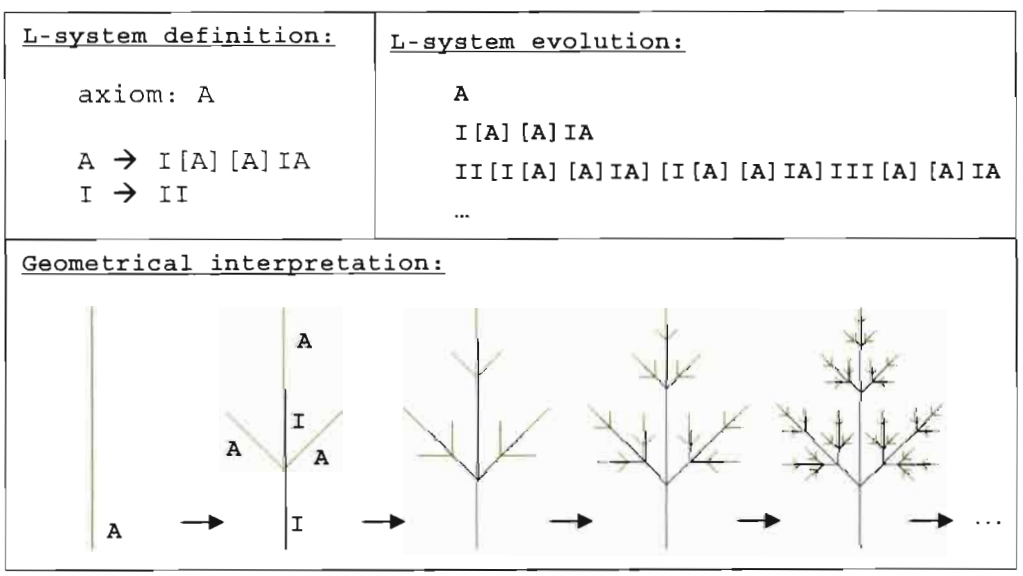

Figure 31. Definition and visualization of a branched L-system
This system does not present any terminal symbols (symbols which map onto themselves), and will continue to evolve until stopped or a predefined depth of decomposition is reached. The visual interpretation of the string is based on a turtle interpreter.

L-systems formalisms: parametric and context sensitive L-systems

D0L-systems, as presented in the previous section, can convey qualitative information as each type of module in the model represents a different type of biological components, such as cells or organs.

However modelers often need to consider dynamic and/or continuous quantitative information associated with these components, such as varying concentration of hormones in cells, or organ size changes. Parametric L-systems were formalized to answer this need (Hanan 1992). In parametric L-systems each symbol of the alphabet can be associated with numerical parameters, which are referred to using formal parameters when computing the production of the L-system. Additionally, formal parameters can be used in arithmetic expressions to calculate new values of parameters in the productions successors.

The formal definition of parametric D0L-systems can be written as follows (Prusinkiewicz and Lindenmayer 1990):

- V is the alphabet.
- Σ is the set of formal parameters.
- $C(\Sigma)$ is the set of all logical expressions with parameters from Σ.
- $E(\Sigma)$ is the set of all arithmetic expressions with parameters from Σ.
- $\omega \in (V \times \Re^*)^+$ is a nonempty parametric word called the axiom.
- P is a finite set of ordered productions of the form $pred$: $cond_{opt} \rightarrow succ$,

such that $pred \in V \times \Sigma^*$, $cond \in C(\Sigma)$ and $succ \in (V \times E(\Sigma)^*)^*$. These components of the production expression are respectively called predecessor, condition and successor. The condition *cond* can be omitted, in which case it is assumed to evaluate to true. Due to the existence of the conditions, the process of string rewriting is slightly more complex than for D0L-systems. For a production to match a module in the string, the following conditions must be met:

1) The module's letter must match the letter in the predecessor,

2) The number of actual parameters associated with the module and the number of formal parameters in the predecessor must be the same,

3) The condition *cond* must evaluate to true.

Parametric D0L systems associate quantitative information with the qualitative representation of the character string. However they do not take into account the interactions between neighboring modules. In biological objects, neighbor cells or organs are rarely completely independent, and often influence each other state and fate, for example by transmitting hormonal fluxes. Context-sensitive L-systems were thus introduced and made it possible to specify what modules must be in the neighborhood of the modules being replaced for the production to be applied (Lindenmayer 1968).

Coupled with conditions evaluation of the parametric L-systems, the context-sensitive L-systems are sufficient to model complex processes such as information flow circulating within the modeled structure and directing its evolution. The formal expression of context-sensitive production takes the form:

$$lc < pred > rc : cond \rightarrow successor$$

The symbols < and > separate the left context (*lc*), the strict predecessor (*pred*) and the right context (*rc*). Note that context-sensitive production rules take precedence on context-free production rules applying on the same strict predecessor. The process of matching a production rule with a strict predecessor within a branched context-sensitive parametric L-system can be highly complex, and won't be detailed here. The problems associated with this process have been extensively reviewed in (Radoslaw 2002).

Figure 32 illustrates a simple signal propagation process within a context-sensitive L-system.

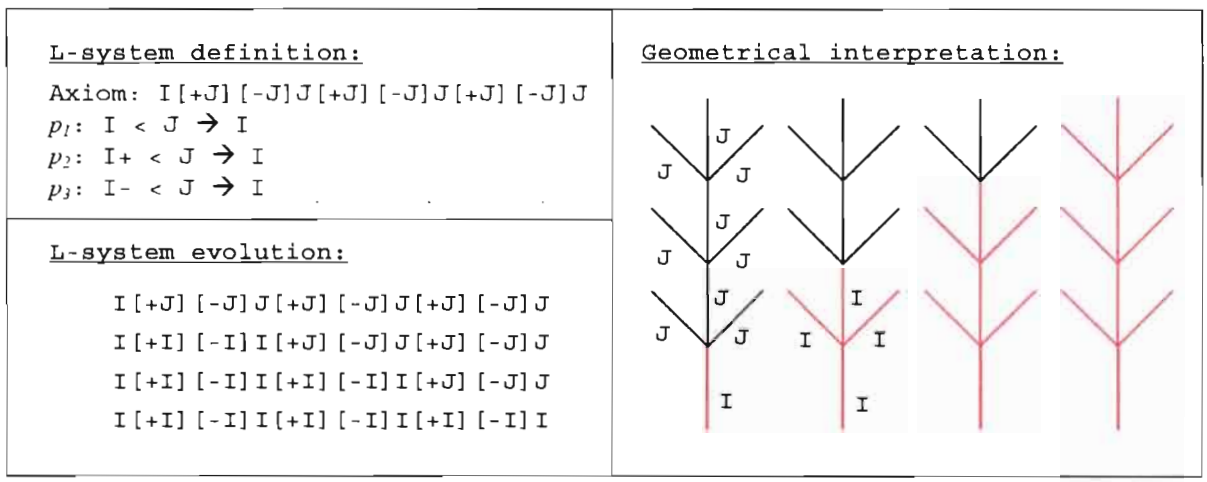

Figure 32. Information propagation within a context-sensitive L-system
All production rules defined here are only sensitive to left context, and allow simulation of information propagation from the base to the tip of the system. The + and – modules are special modules interpreted as geometric orientation of the branches by the turtle.

L-system formalisms: L+C

L+C is a language based on the previously described formalism of parametric L-systems. It has been created to address the need for a formalism that would allow the expression of complex plant models (Radoslaw 2002). In previous L-system formalisms, the parameters which can be associated with components of the model are inherently limited to numerical arguments. L+C was developed to allow inclusion of parameters of any type to describe the state of detailed plant models. In L+C, user-defined structures can be used as parameters for the modules, and user-defined functions can be called upon while processing the character string. Definition of elements known from general-purpose programming, such as functions and user-defined data types (structures), is done according to the C++ syntax, hence the name L+C of this particular formalism.

L+C notably extends the formalism of L-systems by introducing the concepts of derivation direction and new context. These two concepts are the foundation for the fast information transfer method, a way to propagate signals instantaneously in linear and branching structures represented by L-system strings. This feature is specifically targeted at the modelling of processes on fairly different timescale, such as the propagation of forces and torques in biomechanical models which appears instantaneous compared to the speed of cellular division and growth.

I.B) Root macroscopical modelling

To adequately capture the various feature of the developing root system, we designed a macroscopic model based on the L+C formalism.

The general principles behind this model are presented in Figure 33. We considered the root system as a stack of slices, each of them formed by a set of concentric cylindrical tissues.

Each of those slices was associated with a L-system module, taking the inner structure of concentric cylinders as a user-defined parameter. To model auxin diffusion and transport, each of those cylinders was subdivided in a central "cell" compartment and four surrounding independent "walls" compartments. Auxin was assumed to be able to diffuse between adjacent walls, and to be transported from and to the walls by active carriers present in cells (as discussed in Part I of this manuscript). Efflux carriers were assumed to be polarized, while influx carriers were assumed to be evenly distributed around cell membranes.

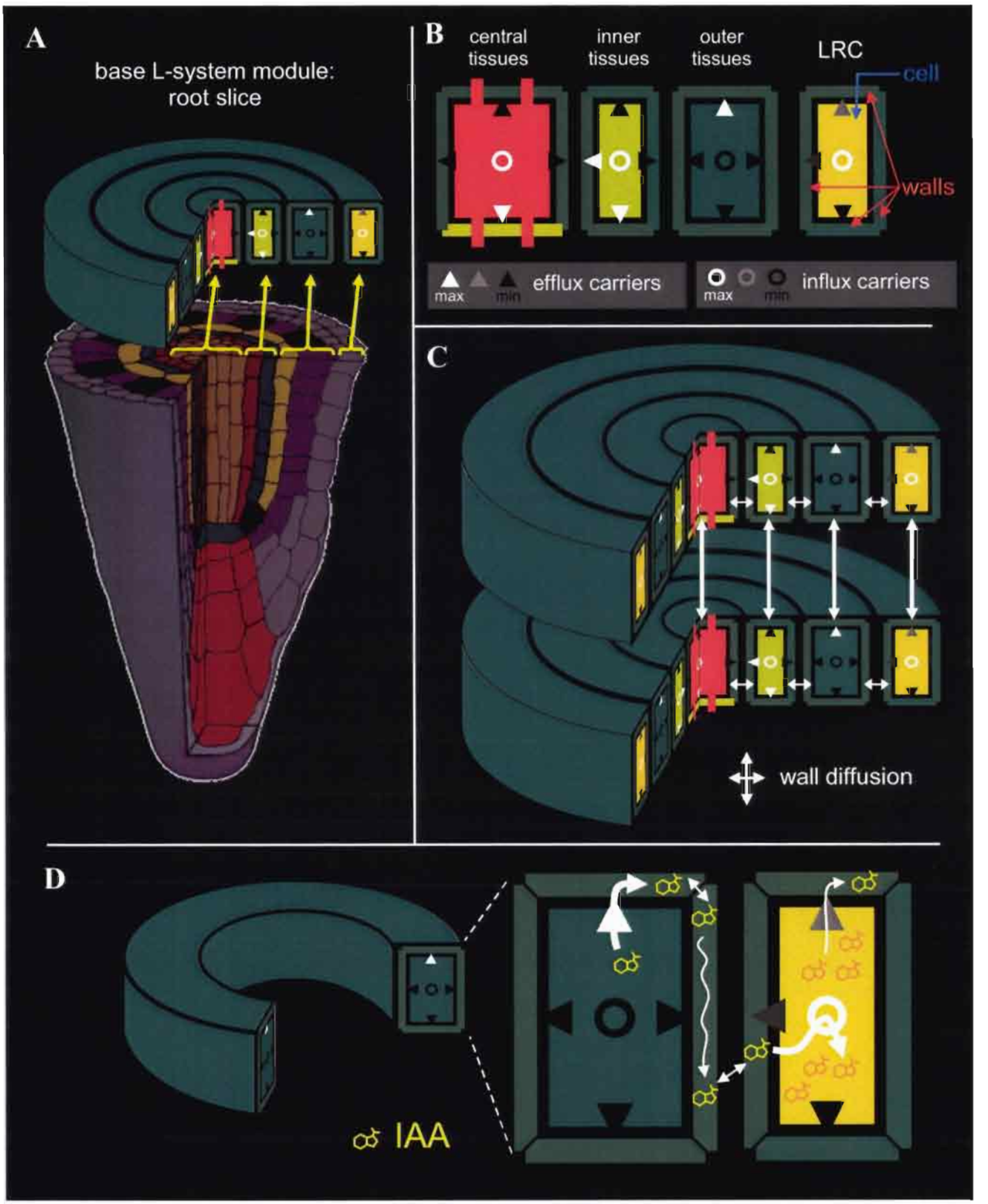

Figure 33. Definition of a root macroscopical L-system model

A – The base module of our system represents a root slice, and takes the various sub-compartment of this slice as user-defined parameters. The tissue layers are simplified as concentric cylinder slices. Each of these is itself separated in a central compartment ("cell") and four adjacent compartments ("walls").

B – For simplicity sake, we define the following layers in our model (from outer to inner): lateral root cap (LRC), outer tissues (equivalent to epidermis & cortex), inner tissues (equivalent to endodermis & pericycle) and central tissues (corresponding to the vasculature). Each of those layers is considered to express polarized efflux carriers and non-polar influx carriers with varying intensity (white – strong expression, black – no expression).

C & D – Auxin within the walls compartment is considered to diffuse between neighbour wall layers and adjacent layers of successive root slices. Auxin will flow through the structure, actively transported from cell to wall, diffusing from wall to wall, and actively transported back from wall to cells. Compartment colour expresses its auxin concentration.

Our system also took into account root growth with re-writing rules stating that the slices corresponding to the initials (as defined in Part I) should be re-written as two slices at regular time intervals, one of them retaining the initials identity, the other being a "normal" root slice (Figure 34). We also integrated various biological considerations such as the limited life-length of lateral root cap cells, elongation of root slice leaving the root apex, the production of auxin in the aerial part and its transport by the vascular system up to the root tip.

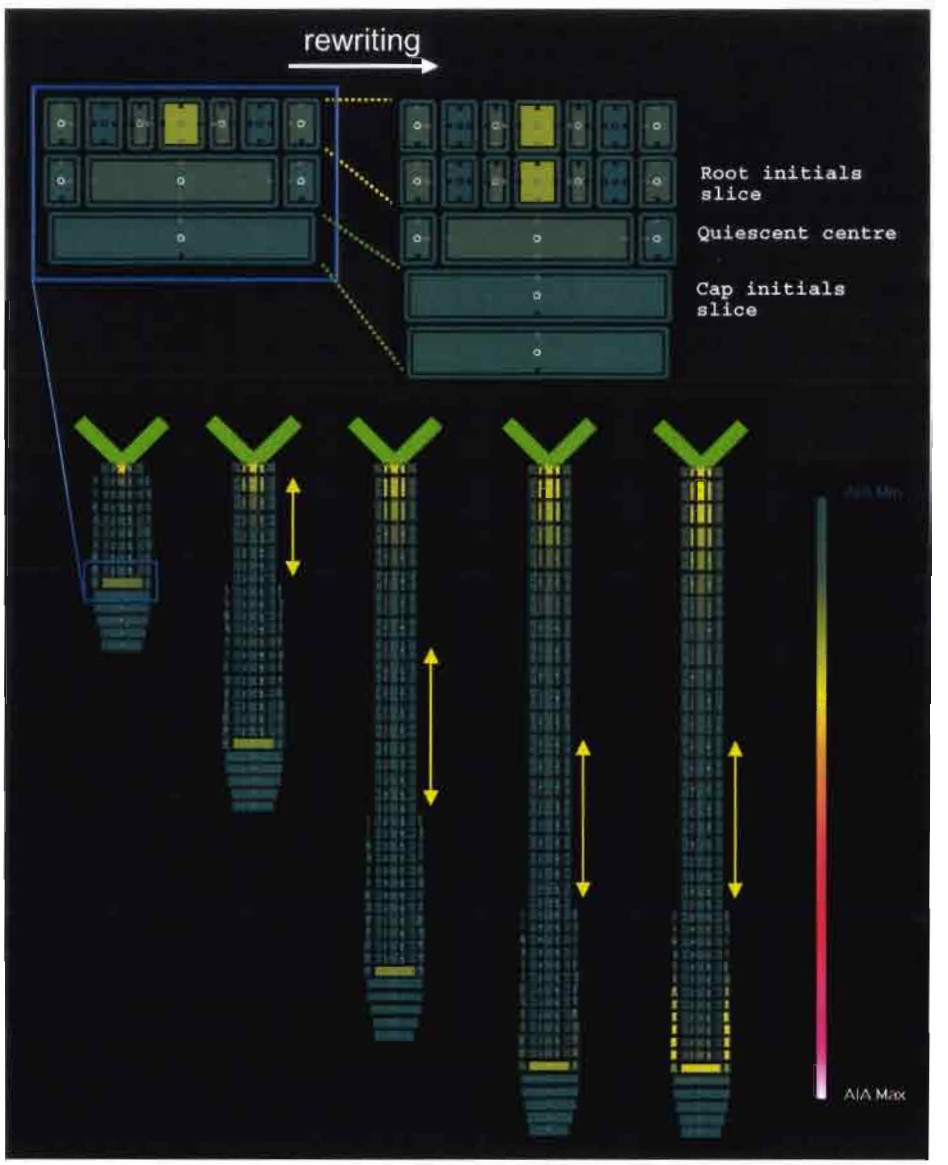

Figure 34. Growth of the root L-system
To comply with biological reality, new root slices are only added by re-writing of the root slices corresponding to the initials of the root apical meristem (top). Older root slices also loose the cylindrical layer corresponding to the lateral root cap (bottom). Those slices then undergo longitudinal elongation for a limited time after leaving the root apex (yellow arrow).

The philosophy of this modelling approach was to create a model of root development that would serve as food for thought to devise and direct further biological investigations. We thus implemented our model in the *lpfg* programming environment to take advantage of the interactivity toolbox available (Radoslaw 2002) (Figure 35).

Initial parameterization of auxin carriers distribution within the root L-system was done accordingly to biological observations (Swarup et al. 2001; Marchant et al. 2002; Jirí Friml et al. 2002; Benková et al. 2003; Blilou et al. 2005; Sauer et al. 2006; Tanaka et al. 2006; Wisniewska et al. 2006) (Figure 36), allowing preliminary simulations of auxin fluxes (Figure 37).

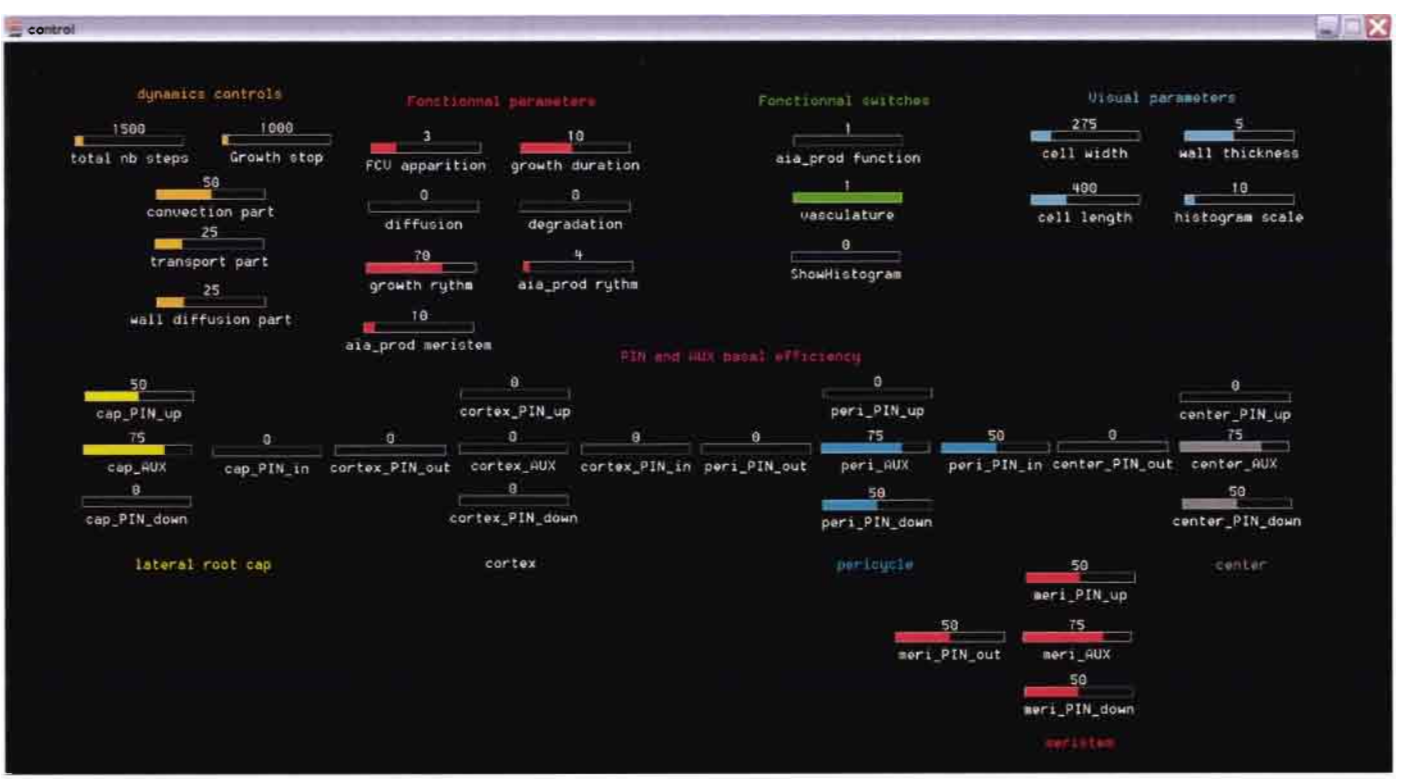

Figure 35. Control panel of the root L-system
The *lpfg* environment offers the possibility to access and modify model parameters on the fly. We thus designed the root L-system to allow the user to change the following system parameters directly from the control panel while the simulation is running: depth of the L-system derivation (number of derivation steps), number of steps of growth (during subsequent steps only auxin fluxes are updated), relative importance of each flux mechanism (convection, active transport, wall diffusion), membrane diffusion and degradation of auxin, vasculature maturation delay... We also offered the possibility to choose from different auxin production curve for the aerial part (such as constant or cyclic auxin production). The main feature of the parameter access by control panel is the possibility to change the efficiency of each auxin carrier type independently and rapidly evaluate the impact of each modification on the whole system.

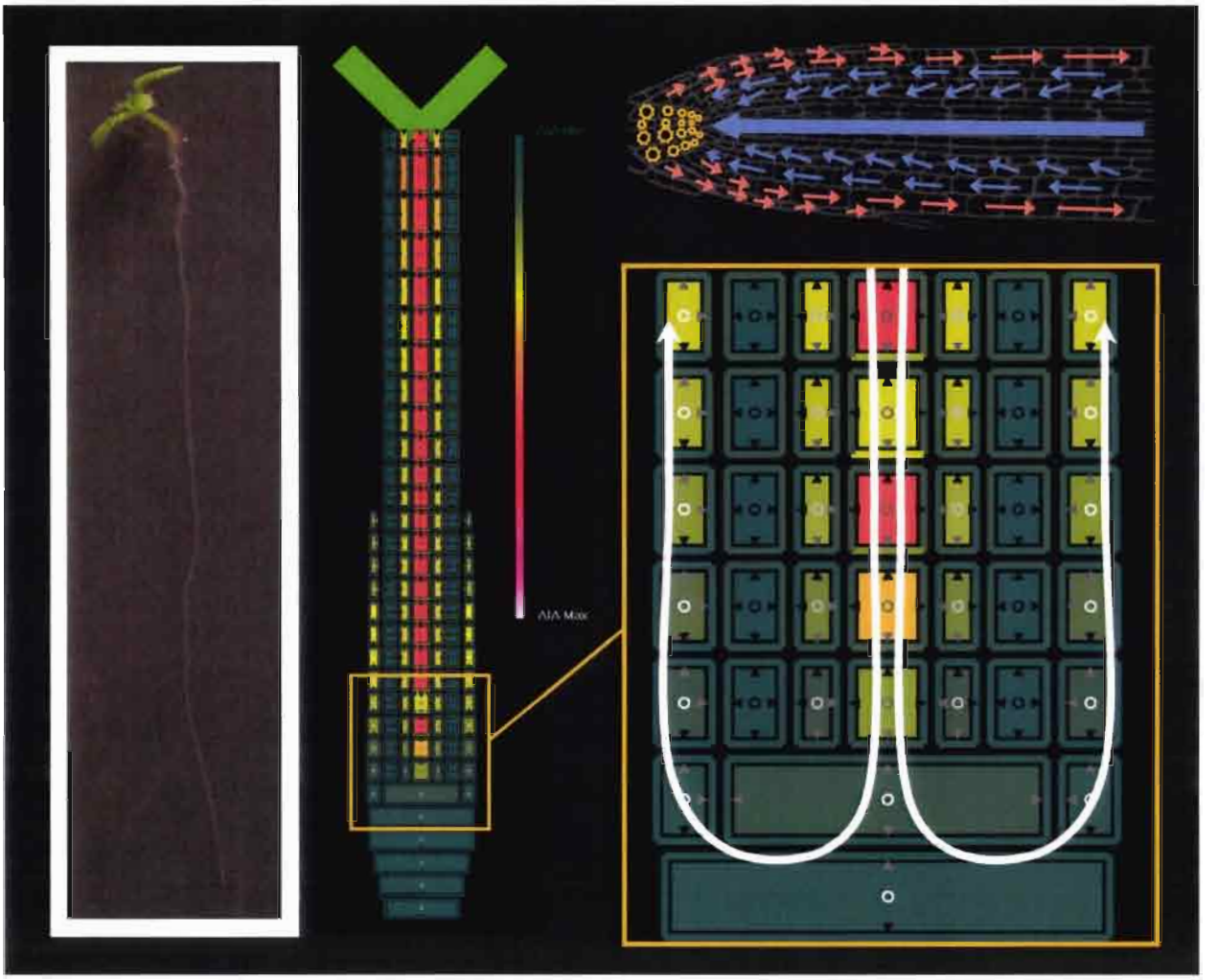

Figure 36. Parameterization of the root L-system
The auxin carriers patterns were determined based on transporters map available in the literature. The global distribution of those carriers created an apical reflux system. The main auxin source was considered to be the aerial parts, and we took vascular auxin transport into account in this system as a strong convective transport system propagating the auxin flux along the root more rapidly than the active transporters could do it.

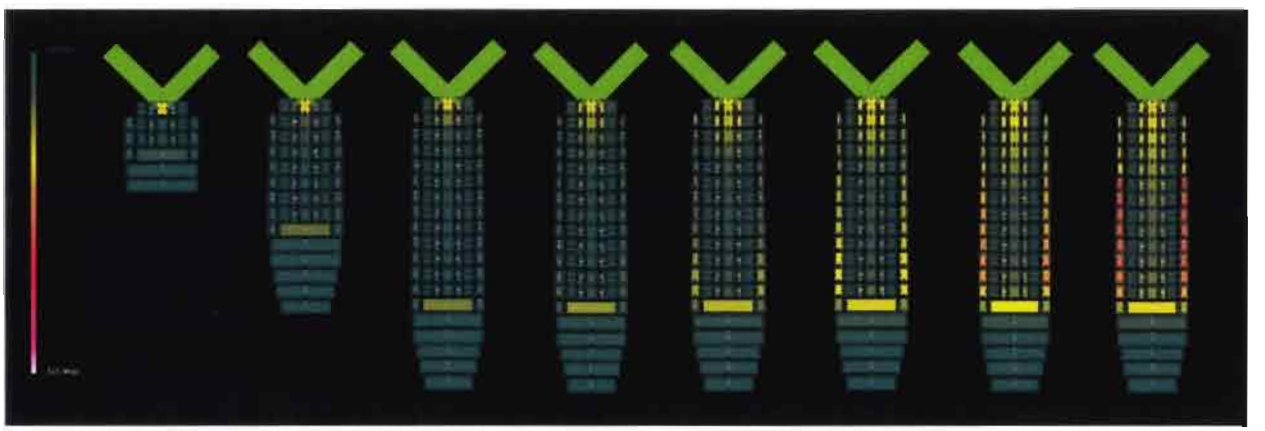

Figure 37. Example of fluxes dynamics in the root L-system
The root L-system was allowed to grow for a limited period of time, and then only auxin transport was allowed to take place. In this system, auxin accumulates within the quiescent centre during root growth, and upon root growth arrest will quickly saturate the lateral root cap. A movie for a similar simulation is available on the DVD, in the /Media/movies/ directory.

The current implementation of the root L-system is available in the DVD joined to this manuscript, under the /Programming/Lsystem_root/ directory. A movie of dynamical simulation is also available in the /Media/movies directory.

This macroscopic model offered us a first opportunity to ponder on the interaction between auxin fluxes and the growing root structure. It notably drove us to reflect on the control of lateral root primordia initiation and positioning. As at the time of this model conception, no hypothesis existed to explain how auxin fluxes determined the positioning of lateral root primordia, integrating ramification in our model proved to be rather problematic.

We thus initiated a series of biological studies in order to gather sufficient data to answer this question. A first study aimed at elucidating which auxin fluxes controlled lateral root primordia initiation, and how to perturb it. The story behind this study has been presented in Part II. In a second study, we searched for the rules of root ramification regulation existing at the macroscopical scale. This study and its results have been extensively presented in Part III.

By the time these two studies were concluded, we had a clearer view of how root branching may be regulated by auxin fluxes, but the first macroscopical model we developed and presented here lacked the precision necessary to further investigate on the topic primordia initiation. Indeed, the fluxes of auxin responsible for initiation were discovered to be confined to a fairly specific region of the root apex, at the level of the elongation zone (De Smet et al. 2007). To be able to predict primordia initiation precisely, we needed to consider the auxin fluxes at a smaller scale, and thus decided to model them at the cellular level, with the intention of slowly bridging the gap between the microscopic and macroscopical models.

II) Microscopic model of auxin fluxes

One biological observation in particular specifically required us to consider the fluxes at a cellular scale. During gravistimulation, auxin fluxes are globally redirected toward the lower side of the root, and auxin accumulates on what will be the inner side of the future root bend (Hangarter 1997; Moore 2002; Ottenschläger et al. 2003; Perrin et al. 2005). As it has been shown that auxin promote lateral root primordia initiation, one would expect a primordia to appear at the site of auxin accumulation (Casimiro et al. 2001; Casimiro et al. 2003; Celenza, Grisafi, and Fink 1995). However primordia induced by gravistimulation always appeared on the outside of root bend, where an auxin minimum would be expected (Fortin, Pierce, and Poff 1989; De Smet et al. 2007; Lucas et al. 2008) (Figure 38).

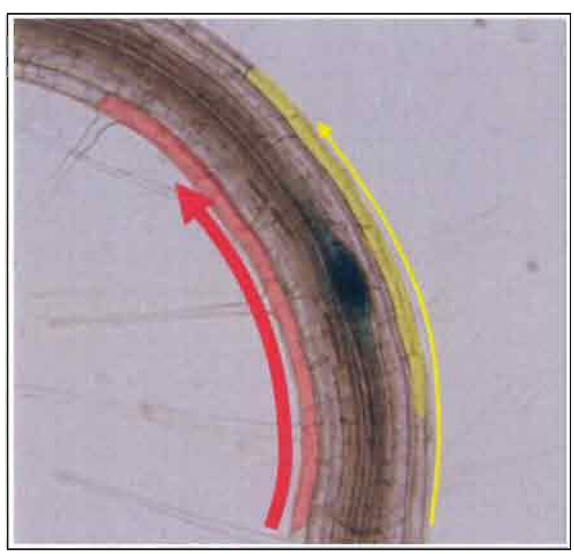

Figure 38. The paradox of initiation upon gravistimulation
The auxin fluxes driving root gravitropism lead to an auxin maximum on the inner side of the root bend (red), and an auxin minimum on the outer side of the bend (yellow). While primordia are considered to depend on high auxin level to be initiated, they always appear on the outer side of the bend (blue).

Trying to solve this paradox required the capacity to follow and quantify auxin fluxes with gravitropism simultaneously causing differential cell elongation, mechanical constraints, and changes in fluxes orientation. One sensible way to predict the behavior of this dynamical equilibrium of competition

and exchange was to consider a fine-scale model of the system, based at the cellular level.

Our study of auxin fluxes at the cellular scale was built upon similar studies of cellular auxin fluxes developed on other plant organs and developmental processes, such as:

- leaf venation (Mitchison 1980; Mitchison 1981; Francois G Feugier, Mochizuki, and Iwasa 2005; François G Feugier and Iwasa 2006),
- trunk vascular patterning (Kramer 2001; Kramer 2002),
- shoot apical meristem phyllotaxis (de Reuille et al. 2006; Jönsson et al. 2006; Smith et al. 2006),
- root gravitropism (Swarup et al. 2005),
- auxin accumulation at the root apex (Grieneisen et al. 2007).

This work was done within the "virtual meristem" subgroup of the VirtualPlants team, in close interaction with Szymon STOMA, responsible for the study of similar flux models in the shoot apical meristem, and Jérome CHOPARD, who works on auxin fluxes and mechanical properties of the floral meristem development. We will present here how the cellular model was designed and implemented, and some of the preliminary results it yielded.

II.A) Building a virtual root

As described earlier, lateral root primordia initiation occurs within the root apex, at the level of the elongation zone (De Smet et al. 2007). From observations of PIN patterns, the root apex itself has been defined as a "fountain system", where auxin flows acropetally within the central tissues and then basipetally back along the outer tissue layers (Swarup et al. 2001; Marchant et al.

2002; Jirí Friml et al. 2002; Benková et al. 2003; Blilou et al. 2005; Sauer et al. 2006; Tanaka et al. 2006; Wisniewska et al. 2006). This reflux system has been proved to play an important role in initiation of new primordia (Casimiro et al. 2001; De Smet et al. 2007; Lucas et al. 2008). We thus chose to model the entire zone of reflux, from the root tip to the elongation zone onward.

Fluxes within a given network of elements strongly depend on the specific topology and geometry of the considered system. The root apex cells exhibit a wide range of forms and size (Figure 5), so we chose to build an *in silico* root apex on the basis of real root images. The process of digitizing we used is semi-automatic. With vectorial imagery software, we annotated manually the root apex images to locate cell corners and walls. The vectorial image could then be processed automatically to generate the graph corresponding to the annotated tissue, with a geometry and topology truthful to those existing *in vivo*.

In addition, we captured specific annotations adding physiological information to the virtual tissue. This process was used notably to specify the identity of the different root cell layers within the virtual tissue and to initialize the localization of the PINs proteins for each of the graph cells. The whole process of digitizing was applied to a range of root apex microscopy images, allowing generation of several virtual tissues with distinct geometry and topology (Figure 39).

The virtual tissue itself can be defined as a two-dimensional graph whose nodes represent the different elements composing the biological tissue (cell, cell walls) and edges represent the physical connection existing between those elements *in vivo*. We choose to implement a discretization in which each cell in the initial tissue corresponds to exactly one auxin compartment (one graph node)

in the virtual tissue. This choice was made under the assumption that gradient of auxin within cells can be considered as irrelevant for the study of primordia initiation. This assumption can be challenged for some of the longer cell existing in the elongation zone, but is reasonable for the vast majority of the root apex tissues where cells are relatively small (see (Kramer 2007) for discussion on intracellular auxin gradients).

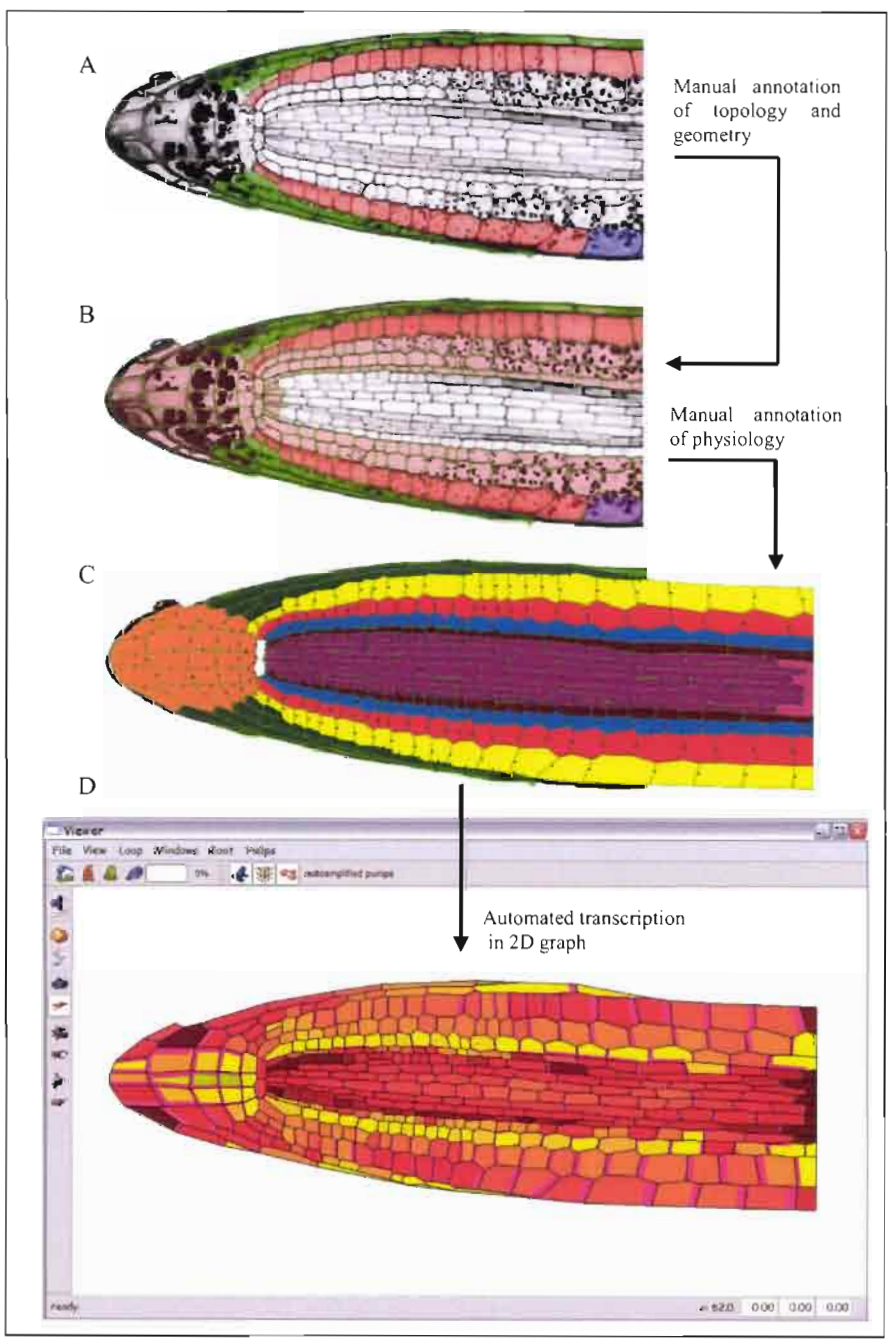

Figure 39. Root apex digitization process
Steps B & C were performed with vectorial digital imagery software. The resulting vectorial image was automatically transcribed in a 2D graph including the provided physiological information. The virtual tissue can then be directly manipulated through the adequate user interface.

II.B) Virtual tissue implementation

We adopted the recursive simplicial complex implementation as defined in the PlantGL environment (Pradal et al. 2008). In simpler terms, we considered our tissue as a two-dimensional structure composed of polygonal cells. The intersections between adjacent cells define cell walls, and the intersections between cell walls define the cell corners (Figure 40).

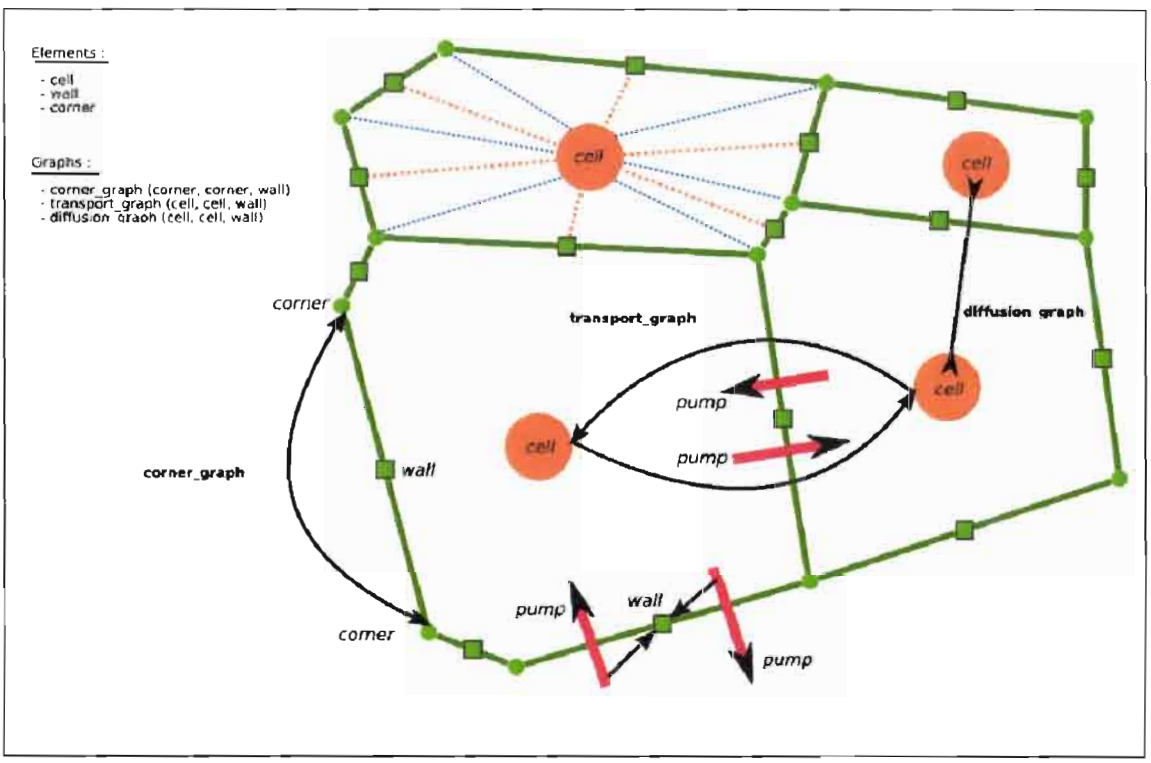

Figure 40. Implementation of the virtual tissue structure
The tissue is composed of three types of elements (cell, wall, cell corners). Adjacent cells share wall and cell corners, and each cell element maintains an index of its associated wall and cell corners. The information on pump localization and orientation digitized from the source tissue is associated with wall elements. The corner graph is used to represent the tissue spatial organisation. The transport graph is directed according to the information on pump localization and orientation. The diffusion graph expresses the relation of adjacency between cells.

As such, the virtual root tissue can be defined by a set of interconnected graphs. To describe those graphs, we will adopt the following conventions:

- a non-directed graph G_I composed by the vertices of set V linked by edges from the set E will be denominated as $G_I(V, E)$.

- a directed graph G_2 composed by the vertices from the set V linked by oriented arcs from the set U will be denominated $G_2(V, U)$. Elements from U can be written as (v_1, v_2) where v_1 and v_2 are elements from V.

The elements composing the virtual tissue are associated with information coming from the source tissue and used in the flux simulations. Each element belongs to one of the following three sets:

- C is the set of cells. Each element of C corresponds to a single unique cell in the biological source tissue. Each element in this set is associated with a physical compartment that can contain, produce, degrade, and transport auxin.

- W is the set of walls. Cells are digitized as polygon and each intersection between two of those polygons is added to W as a unique element. As such, a single element of W can be associated with at most two cells in the tissue. In the current implementation, W is used to maintain the information concerning auxin transporters localization and orientation.

- A is the set of cell corners. Element of A are defined as the intersection between elements of W. Adjacent cells are considered as sharing corners in direct contact, and as such a single element of A can be associated with multiple cells in the tissue. A only maintains the information of tissue geometry and topology.

Depending on the biological connection we want to represent, each element of those three sets may be used to identify either a node or an edge of the considered graph. Based on these three sets, we defined the following graphs:

- the graph of corners G_C (A, W). This graph represents the physical 2D structure (shape and position of cells) of the source tissue.

- The graph of transport G_T (C, P), with P defined as $\{ (c_s, c_t) \mid c_s, c_t \in C \}$. This graph expresses the existence of an organized auxin transporter network, and its directed edges are associated with information on transporter localization and polarization stored within the corresponding element of W (common wall between cell c_s and c_t).

- the graph of diffusion G_D (C, W). This graph represents the physical link existing between adjacent cells in the source tissue.

In addition, each element of C maintains a formal index of the associated elements from A and W, as defined by the cell structure digitized from the source tissue.

II.C) Auxin dynamics

The notations we will use here were taken from previous studies of auxin fluxes at the cellular level (Mitchison 1980; Smith et al. 2006; Jönsson et al. 2006; de Reuille et al. 2006).

As mentioned earlier, each element of C is associated with a physical compartment which can contain a certain concentration of auxin. Based on

biological knowledge of auxin physiology (cf. Part I), we consider that three main dynamical processes regulate this concentration: production/degradation, passive diffusion and active transport. Each of these processes is governed in our model by a specific equation.

Auxin Production and Degradation

Auxin is synthesized with a certain rate of production α_a $(mol.m^{-3}.s^{-1})$ and existing auxin is simultaneously decayed with a rate of degradation β_a (s^{-1}). Hence the rate of change in auxin concentration $\frac{\partial a_i}{\partial t}$ in compartment c_i during in infinitesimal timestep can be written as:

$$\frac{\partial a_i}{\partial t} = \alpha_a - \beta_a a_i . \qquad (1)$$

Auxin production and degradation takes place within each compartment associated with elements of *C*.

Passive Auxin Diffusion

A flux of molecules is defined as the number of molecules passing through a given surface within a given timeframe. Here the flux $J^D_{i\to n}$ due to diffusion between two adjacent compartments c_i and c_n containing the respective auxin concentrations a_i and a_n is modeled according to Fick's first law:

$$J^D_{i\to n} = \gamma_D (a_i - a_n), \qquad (2)$$

where γ_D $(m.s^{-1})$ is the constant of permeability reflecting how easily auxin can cross the barrier separating the two compartments. In our implementation, auxin

is considered to diffuse directly from cell to cell, and the apoplastic compartment between cells (cell wall) is neglected. The respective cell volume and interface surface between adjacent cells is however taken into account to compute the flux, and from (2) we can express the rate of change in auxin concentration $\frac{\partial a_i}{\partial t}$ in a compartment c_i by diffusion between c_i and the ensemble of neighbouring compartments N_i:

$$\frac{\partial a_i}{\partial t} = -\frac{1}{V_i} \sum_{n \in N_i} S_{i.n} J^D_{i \to n}, \qquad (3)$$

where V_i is the volume of compartment c_i and $S_{i,n}$ the area of the interface between compartment c_i and c_n. By convention, all out-coming fluxes are considered positive. Diffusion fluxes are computed for each edges connected to each element of the diffusion graph G_D.

Active Auxin Transport

We also neglected the apoplastic compartment when considering active transport. As a consequence, we did not differentiate between auxin influx and efflux carriers in our model, and used a generalized transporter representation in which auxin is pumped directly from one cell to another. The flux $J^A_{i \to n}$ due to active transport between two compartments c_i and c_n containing the respective auxin concentrations a_i and a_n and auxin transporters of respective concentration $p_{i,n}$ (transporters oriented from c_i to c_n) and $p_{n,i}$ (transporters oriented from c_n to c_i) has been formalized according to Mitchison equation (Mitchison 1980; Mitchison 1981):

$$J^A_{i \to n} = \gamma_A \left(a_i p_{i,n} - a_n p_{n,i} \right), \qquad (4)$$

where $\gamma_A (m^3.mol^{-1}.s^{-1})$ characterizes the transport efficiency of the transporters.

From (4) we can derive the rate of change in auxin concentration $\frac{\partial a_i}{\partial t}$ in a compartment c_i by active transport between c_i and the ensemble of neighboring compartments N_i:

$$\frac{\partial a_i}{\partial t} = -\frac{1}{V_i} \sum_{n \in N_i} S_{i,n} J^A_{i \to n}, \qquad (5)$$

where V_i is the volume of compartment c_i, and $S_{i,n}$ the area of the interface between compartment c_i and c_n. Transport fluxes are computed for each directed edges connected to each element of the transport graph G_T.

Global Auxin flux

From equations (1) to (5), we can derive the global expression governing the rate of change in auxin concentration $\frac{\partial a_i}{\partial t}$ in a compartment c_i:

$$\begin{aligned} \frac{\partial a_i}{\partial t} &= \alpha_a - \beta_a a_i + \\ &\quad -\frac{1}{V_i} \sum_{n \in N_i} S_{i.n} \gamma_D (a_i - a_n) + \\ &\quad -\frac{1}{V_i} \sum_{n \in N_i} S_{i.n} \gamma_A (a_i p_{i,n} - a_n p_{n,i}). \end{aligned} \qquad (6)$$

II.D) Transporter dynamics

As illustrated in equations (4) and (6), the flux of auxin in a cell depends on the relative concentrations of active transporters pumping auxin from and into

the considered cell. In our model, we considered pump concentration to be a dynamic parameter, and expressed its dynamics according to the following hypotheses.

Transporter synthesis and degradation

As discussed in Chapter I, auxin transporters are submitted to a constant recycling *in vivo* (Jirí Friml et al. 2002; Paponov et al. 2005; Blilou et al. 2005). To take this recycling into account in the model, we considered the following equation expressing the rate of change in transporter concentration $\frac{\partial p_{i,n}}{\partial t}$ accumulating at the membrane of c_i and directed from compartment c_i to c_n:

$$\frac{\partial p_{i,n}}{\partial t} = \alpha_p - \beta_p p_{i,n}, \qquad (7)$$

where α_p ($mol.m^{-3}.s^{-1}$) is the rate of transporter production and β_p (s^{-1}) is the rate of decay of existing transporters.

Transporter reallocation and auxin feedback

Auxin transporters have been shown to be able to react to external stimuli and to auxin signaling in specific tissues either by re-allocation along the membranes or by modification of their recycling rates (Jirí Friml et al. 2002; Sauer et al. 2006; Abas et al. 2006). We thus defined a specific function Φ as a way to integrate these phenomena in the virtual tissue. Φ alters the dynamic of auxin transporters as follows:

$$\frac{\partial p_{i,n}}{\partial t} = \alpha_p - \beta_p p_{i,n} + \Phi(i,n). \qquad (8)$$

Depending on its form, the Φ function can take various arguments such as the value of the local auxin gradient or the effective auxin flux exchanged between two compartments. We have tested in our model some of the forms which have been canonically used in cellular models of auxin fluxes.

We will now present the model implementation and some preliminary results obtained with Φ functions.

II.E) Model implementation

The root apex is represented by a set of polygonal cell forming a 2-D surface. This surface corresponds to the tissular organization observed for a longitudinal section passing through the centre of the root tissue. Each edge of the polygonal cells represents a cell wall as defined earlier. We defined specific subset of cells as pertaining to the distinct root cell layers, so as to be able to manipulate each of theses subsets separately. This also allowed the specification of distinct auxin reaction rules for each of the subsets, in accordance to biological observations of the behavior of root tissues (Sauer et al. 2006). The tissue was considered to be fixed from a structural and geometrical point of view, and neither cell growth nor cell divisions were implemented here. The non-linear system of equations describing the auxin fluxes is integrated over pre-defined time-steps using the Scipy package designed for ODE solving.

The code of the model itself has been designed as a module for the OpenAlea software platform for plant modelling, integrated within the Virtual Meristem framework developed by Jérome CHOPARD & Szymon STOMA.

The visualization of tissue simulations was carried out with PlantGL, an open-source graphic toolkit for the creation, simulation and analysis of 3D virtual plants available in OpenAlea (Pradal et al. 2008). In all figures representing the virtual root apex, we adopted the following graphical conventions (Figure 41):

- auxin concentration in cells is represented as a gradient of green (lowest concentration as black, highest concentration as bright green). Intermediate concentrations are represented by linear interpolation between these two extremes.

- Polar active transporters from cell c_i to cell c_n are represented as red bars on the c_i side of the interface between c_i and c_n. The thickness of the red bar expresses the concentration of these specific transporters.

For each figure presenting a simulation result, we provide a corresponding movie showing the system dynamics. The movies are available in the DVD joined to this manuscript, inside the media/movies/ folder, and are named after the figures. We also provided additional movies showing the behavior of the cellular model under a simulated gravistimulation and a virtual root cut for two types of pumps dynamics (fixed pumps or semi-fixed pumps, where 50% of the pumps total concentrations are subjected to the "against the gradient" regulation rules we describe in the following chapter).

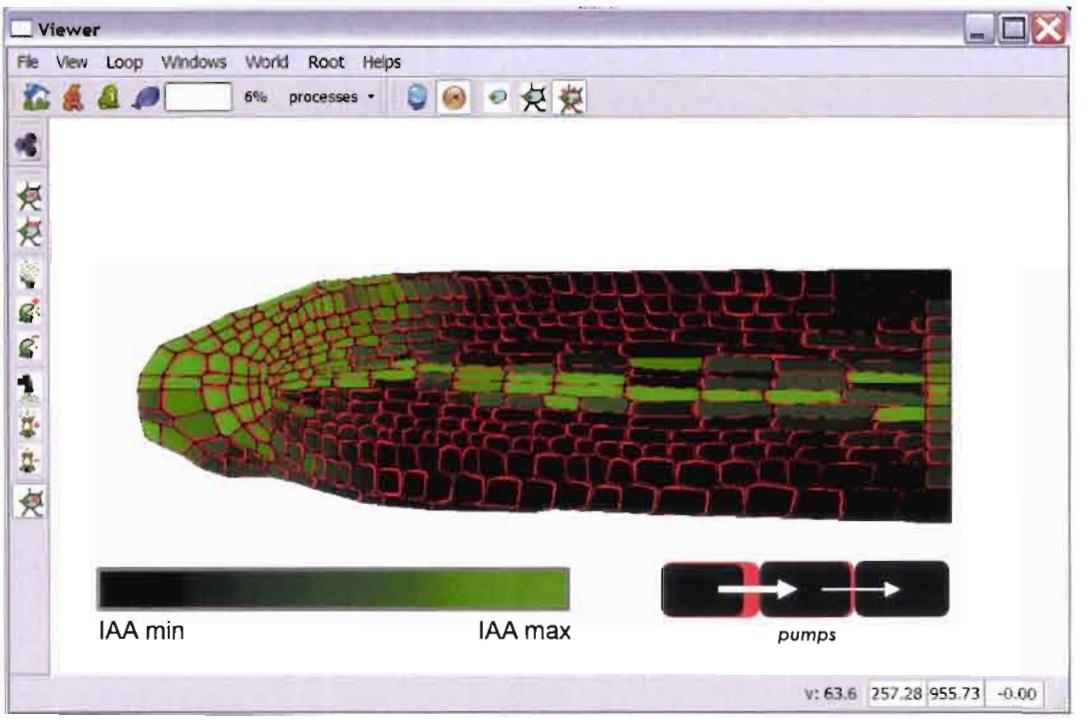

Figure 41. Graphical user interface and representation of the virtual root apex
The horizontal toolbar is used for control of the simulation and visualization.
The vertical toolbar is used for direct interaction with the virtual tissue. From top to bottom, the available tools are: cell selection, wall selection, creation of permanent auxin sink (auxin contempt disappear at each time-step), augmentation of auxin degradation, diminution of auxin degradation, creation of permanent auxin source (fixed maximal auxin concentration), augmentation of auxin production, diminution of auxin production, return auxin production/degradation to normal.

III) Comparative study of transporters dynamics

III.A) Different types of transporter dynamics

Auxin carriers distribution can be altered *in vivo* through perception of a physical or hormonal stimulus (Swarup et al. 2005; Francois G Feugier, Mochizuki, and Iwasa 2005; Sauer et al. 2006). We aimed here to test potential regulation rules for this perception and response in our system. We compared three of the major classical options:

- fixed pumps (no dynamics) were tested for two reasons – the first one being the strong stability of pump patterns observed at the root apex which might be simply due to limited pump reaction in the root tissues – and the second reason being the possibility to use this fixed system as a reference for the other tested dynamics.

- "Pumping against the gradient" hypothesis. In this hypothesis, the Φ function takes the form $\Phi(i,n) = \eta(a_n - a_i)$, where η is a constant and a_i, a_n the respective auxin concentrations inside the considered cell and its neighbor. In this case, Φ depends on the local auxin gradient between adjacent cells, and induces higher production of pumps oriented against this gradient. In the case of negative flux (net flux corresponding to an auxin entry), the Φ function is truncated to 0. This type of Φ function has been used to explain the mechanisms driving phyllotaxis in the shoot apical meristem (Jönsson et al. 2006; Smith et al. 2006). This hypothesis implies the existence of cellular sensor of auxin gradient *in vivo*, whose potential existence and identity is still unknown (Merks et al. 2007).

- "Pumping with the flux", also known as "canalization" hypothesis. According to Sachs' original concept (Sachs 1969; Sachs 1984), canalization relies on a feedback mechanism from the auxin fluxes on its transporters. More precisely, we assume that the value of the Φ function for production of transporters oriented from cell c_i to cell c_n will depend on the effective flux $J_{i\to n}$ passing through the interface between c_i and c_n.

The effective flux is defined as the total amount of auxin leaving cell c_i through the considered interface by mean of diffusion and active transport. Canalization has been widely used to model veination patterning (Sachs 1969; Mitchison 1980; Francois G Feugier, Mochizuki, and Iwasa 2005; Rolland-Lagan and Prusinkiewicz 2005; François G Feugier and Iwasa 2006), and more recently for phyllotaxis modelling (Merks et al. 2007).

We tested two types of Φ function for canalization:

- linear Φ function $\Phi_L(J_{i\to n}) = \kappa(J_{i\to n}/J_{ref})$, (9)

- quadratic Φ function $\Phi_Q(J_{i\to n}) = \kappa(J_{i\to n}/J_{ref})^2$, (10)

with κ $(mol.m^{-2}.s^{-1})$ is a constant parameter and J_{ref} $(mol.m^{-2}.s^{-1})$ and arbitrary reference flux to keep constant units in the equations. For negative flux (net flux corresponding to an auxin entry), both Φ functions were truncated to 0.

The boundary conditions were the same for each simulation: the tissue was considered to be isolated from its environment, and boundary cells do not present any specific interaction outside of those existing with inner cells of the tissue. Initial conditions varied, and will be detailed in each case.

Simulation needed to be validated against biological observation to be considered relevant. Tissular modelling studies of auxin flows have used various biological observations as validation criterion, such as:

- localization and polarization of auxin carriers (de Reuille et al. 2006),

- pattern of auxin accumulation (de Reuille et al. 2006; Grieneisen et al. 2007),

- prediction of mutants phenotypes (Grieneisen et al. 2007; Prusinkiewicz et al. 2007).

In our case, we restricted our validation analyses of simulation to the observed patterns of transporters and auxin distributions (see Figure 20 & Figure 24 for reference). We namely expected the apparition and maintenance of a stable auxin accumulation at the root apex, centered on the columella and apical meristem. We compared the three regulations of pump transporters dynamic presented earlier. We used the following setting:

- auxin production and degradation was reduced to 0 for each cell.

- Each cell in the tissue contains a non-null initial auxin concentration. This implies that the total initial amount of auxin in the tissue is known beforehand.

- Two sinks (cells with a fixed null auxin concentration) where added on the basal boundary of the tissue, to comply with the biological assumption that auxin may be evacuated from the root apex through the epidermis (Swarup et al. 2005).

- Initial transporters distributions were fixed according to auxin carriers distributions observed in confocal microscopy (Swarup et al. 2001; Marchant et al. 2002; Jirí Friml et al. 2002; Benková et al. 2003; Blilou et al. 2005; Sauer et al. 2006; Tanaka et al. 2006; Wisniewska et al. 2006). Transporters concentrations were initially fixed as either 0 (no

transporters) or 1 (maximum concentration of transporters along the considered interface), and subsequently evolved during simulation according to the chosen transporter dynamic.

III.B) Preliminary results

Fixed pumps

Fixed pump distribution allowed for the rapid apparition of the apical auxin maximum within the quiescent centre and columella. However this maximum was not maintained and auxin was evacuated from the tissue through the epidermis and the sink cells (Figure 42.A).

It appeared that pure apical and basal polarizations of the pumps within the epidermis and cortex were insufficient to induce the reflux needed to establish an auxin circulation within the root apex. This raises an interesting question as these pumps distributions were based on biological observations. It could be possible that auxin actually diffuses more strongly than expected between cells of the different layers, or that it exists strong direct cell-to-cell connections such as plasmodesmata (cytoplasmic bridges between adjacent cells) driving fluxes unaccounted for in our model.

Pumping against the gradient

The "pumping against the gradient" mechanism did not allow for apical auxin accumulation, rather inducing the apparition of multiple auxin maxima whose position and size depended on the specific topology and geometry of the tissue, as well as on the initial transporters distribution (Figure 42.B).

Canalization

The canalization hypothesis proved to be sufficient to create and maintain a stable auxin maximum at the apex (Figure 42.C). To complement this finding, we then studied the canalization processes in a setting comparable to the situation existing *in vivo*. In this case, cells were initially devoid of auxin, and an auxin source (cell with a fixed maximal auxin concentration) was added at the basal boundary of tissue, at the level of vascular tissue from which auxin is expected to flow into the root *in vivo*. We showed that canalization rapidly induced the apparition of a linear auxin maximum within the vascular tissue in addition to the apical auxin accumulation. Upon disappearance of the auxin source, the auxin maximum in the vascular tissue quickly fades away, while the apical auxin accumulation stays stable (Figure 43). This behavior was observed with both linear and quadratic Φ functions. Canalization was also found to slightly alter the initial pattern of pump distribution, organizing a strong reflux component from outer to inner cell layers.

The results concerning the canalization dynamics came as a support for an article by Szymon STOMA et al. In this article, canalization is discussed as a potential unification mechanism for auxin fluxes within the shoot apical meristem, leaf veination and the root apex. This article was submitted to Plos Computational Biology. The submitted manuscript is presented in at the end of this Part.

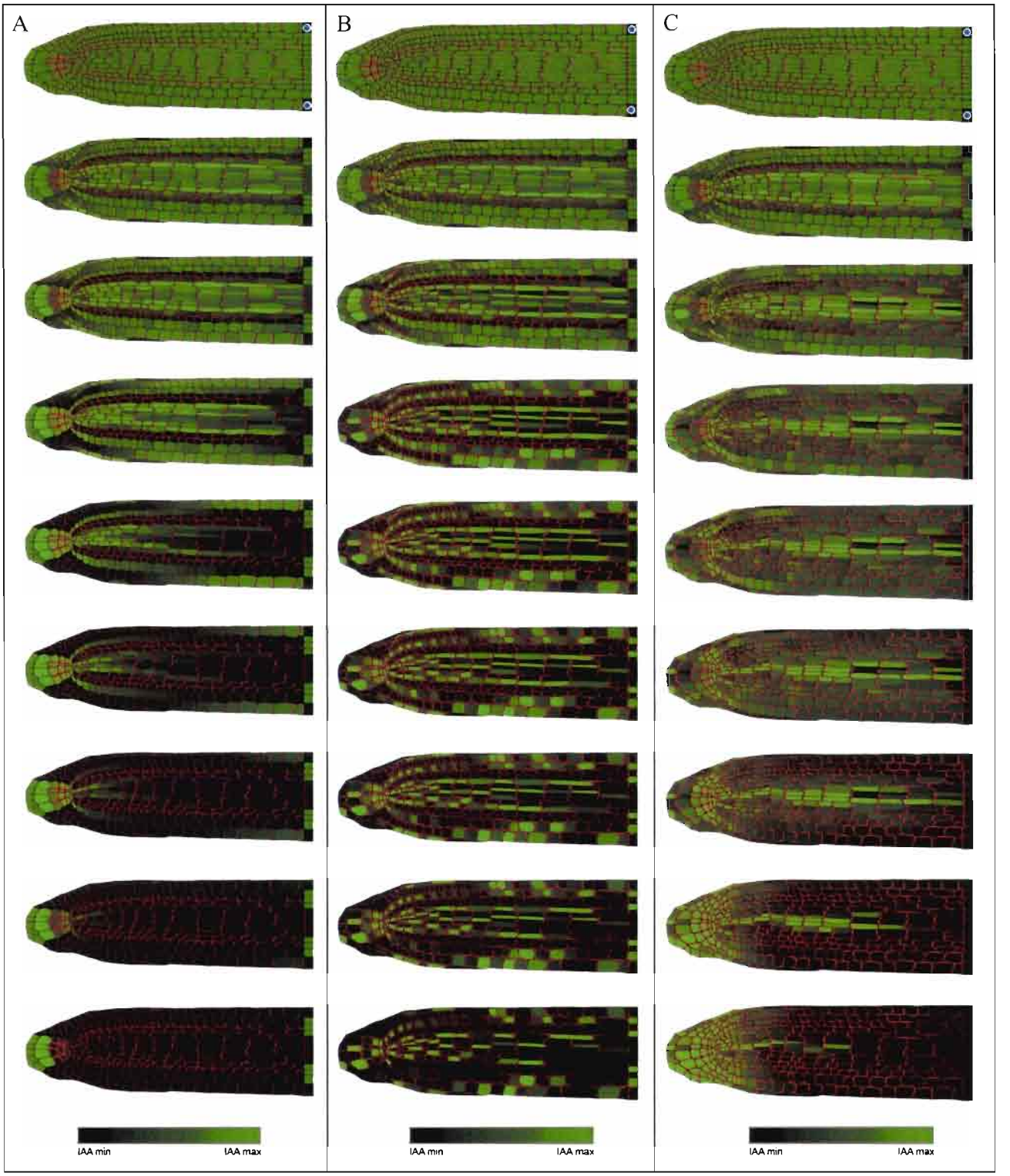

Figure 42. Comparative study of auxin transporters dynamics

All simulation runs are done with the same initial conditions, and same physiological parameters (pump efficiency, diffusion coefficient). There is no auxin synthesis or degradation in the cells, and each cell contains an initial non-null auxin concentration. Two sinks are added at the boundary (blue dotted cells in top most image) to represent evacuation of auxin from the root apex. The only difference between simulation is the type of Φ function used (A – no dynamic, B – pumping against the gradient, C – canalization, quadratic).

Each row of images corresponds to simulation snapshots taken at equivalent simulation time. The bottom row corresponds to the quasi-stable state of the system (evolution of auxin distribution negligible over one hundred timesteps).

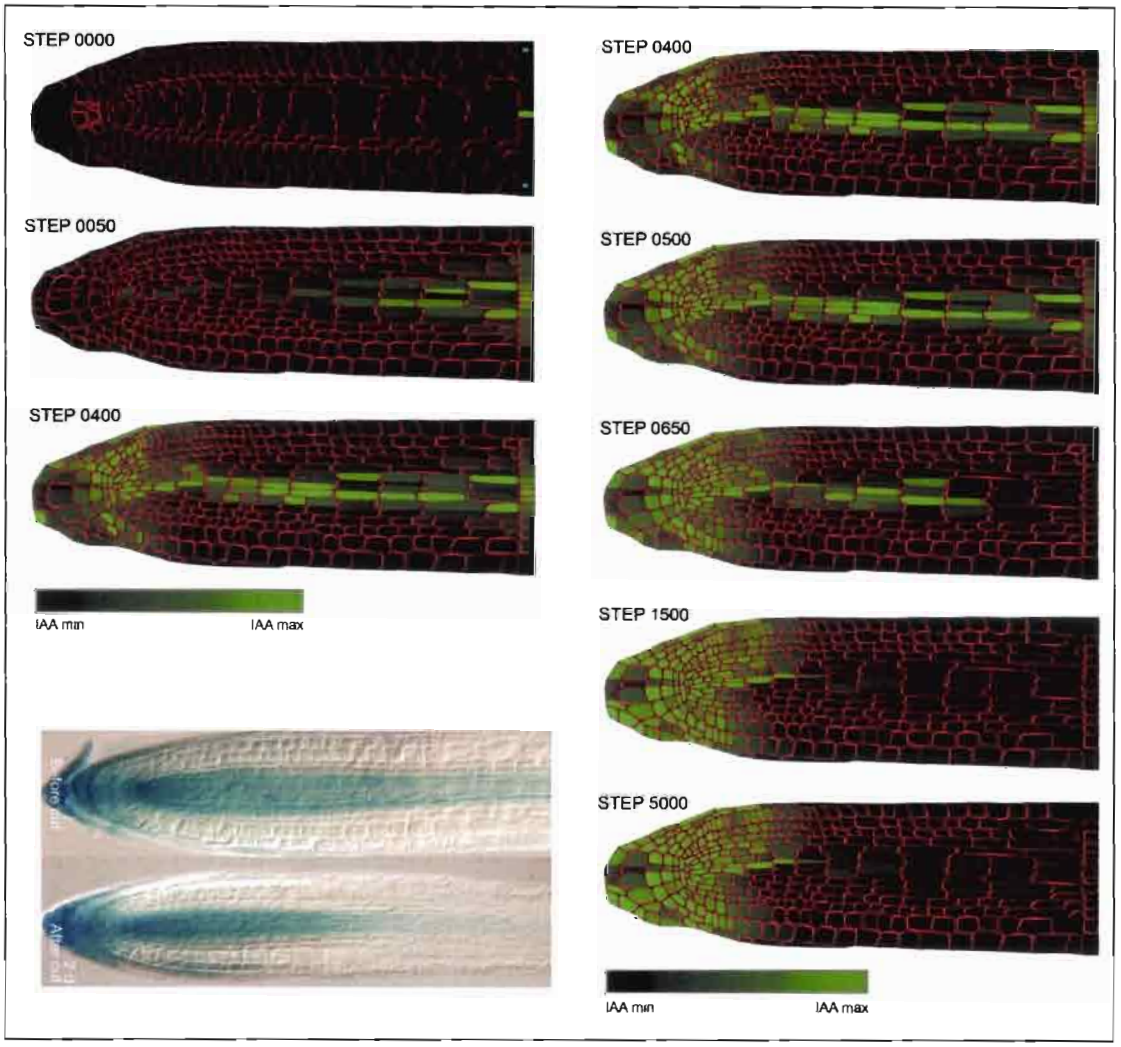

Figure 43. Canalization in physiological settings
Cells initially contained no auxin concentration, and an auxin source was added at the basal boundary (step 0000, bright green cell). At time step 400, the auxin source was removed. Auxin circulating within the whole tissue subsequently accumulated stably at the apex.
Bottom-left insert: visualisation of auxin accumulation (blue) in root using a GUS marker, before (top) and 2 day after root cut (bottom). From Grieneisen et al. 2007.

IV) Limits and evolution of the cellular model

The current implementation of the virtual tissue presents several limits that we wish to overcome in future evolutions of the model. We will here briefly evoke each of those limits and we plan to deal with them.

Distinction between efflux and influx auxin carriers

As mentioned in Chapter I, auxin transport *in vivo* does not occur directly from cell cytoplasm to cell cytoplasm. Auxin is imported from cells wall by the AUX1/LAXs proteins, and exported from the cell cytoplasm to the cell wall by PINs protein. This dual transport can be approximated as a direct transport from one cell to another if the following conditions are met:

- the considered cells must express both influx and efflux carriers
- the diffusion of auxin within cell walls must be slower than its uptake by auxin influx carrier, so that auxin exported from cells do not "escape" the wall before being imported into the next cell.

Diffusion within cell walls has been extensively characterized by E. Kramer (Kramer 2006; Kramer, Frazer, and Baskin 2007; Kramer 2008). He showed that for a cell wall 0,1 µm thick bordered by cells that do not express an auxin carrier, an auxin molecule may travel up to ~5 µm. Depending on the size of the considered cells, this may imply that auxin can leave the wall where it was exported. Within the root apex, cell size varies strongly, with small cubic cells toward the apex (cell size around 10 µm), thin elongated cells in the vascular

tissue (cell length between 10 and 50 µm, cell width around 5-10 µm), and longer cells in the elongation zone (cell length up to 100 µm) (Figure 5). This implies that depending on the considered part of the root apex, it may be necessary to consider auxin diffusion within the apoplast (cell wall). Moreover, the auxin influx carrier AUX1 is not express in all root apex cells (Figure 20). It is specifically present within the protophloem, the apical meristem, the lateral root cap and epidermis.

It should be necessary to investigate in detail the role of the apoplast, and take it into account into future model version, as illustrated in Figure 44. Processes of auxin diffusion and transport shall be adapted accordingly to the new tissular structure, and a process of physical diffusion between cell wall will need to be added to the system.

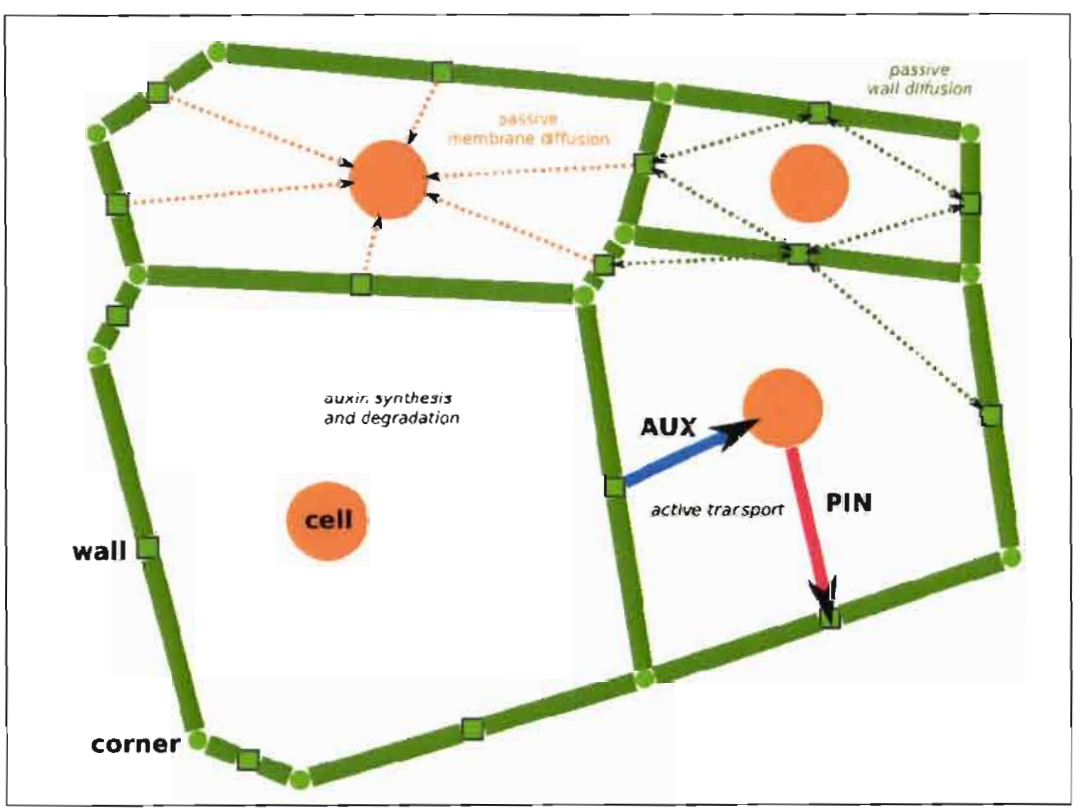

Figure 44. Future implementation of the virtual tissue
Cell wall will eventually need to be considered as potential auxin reservoir. Processes of diffusion and active transport shall then take place between a cell and its cell walls, with possible diffusion occurring between adjacent cell walls.

Cell-to-cell direct connectivity

Until now, we have described each cell as an individual entity, separated from its neighbors by its membrane and cell wall. This is not totally true, as plant cells exhibit specific structures called plasmodesmata (Oparka 2005). These structures are microscopic channels traversing the cell walls and directly connecting adjacent cells cytoplasm. Plasmodesmata allow for direct, regulated, symplastic intercellular transport of substances between cells. The connected cells form what is called a syncytium. The existence of syncytium territories has been demonstrated at the root apex by microscopy and use of fluorescent diffusive markers (Sack and Kiss 1989; Imlau, Truernit, and N. Sauer 1999).

From a modelling point of view, future implementation of the virtual tissue may take the existence of plasmodesmata into account with a simple cell-to-cell diffusion, much like the diffusion of auxin is considered to take place in the current implementation of the virtual tissue. Additional biological information will be needed however to distinguish each syncytium territory existing within the root apex.

Model Parameterization

Two strategies are possible for parameterization of the model. First, we can choose (invent) parameters with few to no experimental reference, considering that the model parameters are validated *a posteriori*, from comparison between model output and biological observations. Such parameters are often subjected to robustness analyses to show that model outputs are stable in given range around the chosen parameters values. This approach was the one used in the study presented previously.

Another approach is to capture the biological mechanisms by using parameters derived from biological observation. Here, this implies the need to choose realistic parameters for production, degradation, diffusion or transport of each molecule type in the model (be it auxin or a transporter). Whenever possible, those parameters should be extracted from known biological observations or directly measured. Missing parameters may be estimated on the same basis that is used for the first parameterization approach. As biologically relevant parameters become more and more easily available, this second approach will be preferably used in future simulations studies on the virtual root tissue.

2D vs. 3D root

The current virtual tissue implementation does not take into account the potential radial auxin fluxes and cell interactions. While the root tissue layers form continuous 3D cylinders *in vivo*, tissues layers appear disjointed in the 2D model (Figure 45). We plan to use two strategies to resolve this issue.

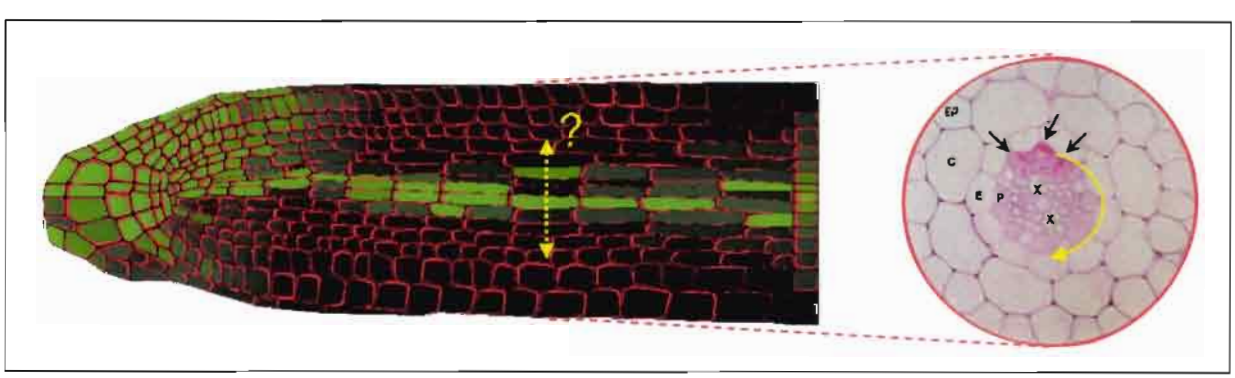

Figure 45. Longitudinal and transversal root view
The current virtual root tissue does not take into account potential interactions occurring between cells of the same cell cylinder (yellow arrows).

First, we can use the digitizing approach for transversal views of the root tissue, and evaluate the fluxes distribution within virtual transversal sections of the root at different levels (cap, meristem, sub-meristematic, elongation zone ...).

Second, we may eventually consider a full three-dimensional approach. A research program of 3D-digitization of root apex is currently under development by Romain Fernandez, PhD student in the VirtualPlants team. Once the technique of 3D digitization will be complete, we envisage using the tools developed by Jérome Chopard for 3D modelling of the floral meristem and build a 3D-model of auxin fluxes in the root apex.

Tissue mechanics

The current implementation of the virtual tissue was considered entirely fixed from a structural point of view. However, the root apex is a zone of intense cellular division and growth *in vivo*. It might prove to be necessary to take these processes into account to predict the site of lateral root primordia initiation. As the root tissue structure has been defined from the start to be compatible with tools of mechanical simulations developed by Jérome Chopard for the study of the floral meristem, we have the possibility use those tools for future mechanical simulation of the root apex.

Research Article

Canalization as a Plausible Unifying Mechanism for Auxin Transport in Meristem Development.

Szymon Stoma[1,2], Mikael Lucas[1], Jérôme Chopard[1], Marianne Schaedel[2], Jan Traas[2,*], Christophe Godin[1,*]

[1] INRIA, Virtual Plants Project-Team, UMR DAP, TA A96/02, 34398 Montpellier, France.

[2] RDP Team, Laboratoire de Reproduction et Développement des Plantes, ENS-Lyon, 46 allée d'Italie 69364 Lyon Cedex 7, France.

Corresponding authors:

christophe.godin@inria.fr, jan.traas@ens-lyon.fr

Date of submission: May 2008

9 figures

1 supplementary material documentation

Submitted to Plos Computational Biology

Canalization as a Plausible Unifying Mechanism for Auxin Transport in Meristem Development

Szymon Stoma[1,2], *Mikael Lucas*[1], *Jérôme Chopard*[1], *Marianne Schaedel*[2], *Jan Traas*[2,*], *Christophe Godin*[1,*]

[1] INRIA, Virtual Plants Project-Team, UMR DAP, TA A96/02, 34398 Montpellier, France.

[2] RDP Team, Laboratoire de Reproduction et Développement des Plantes, ENS-Lyon, 46 allée d'Italie 69364 Lyon Cedex 7, France.

*Corresponding authors:
christophe.godin@inria.fr, jan.traas@ens-lyon.fr

Summary (250-300 words) Plants continuously generate new organs through the activity of small populations of stem cells called meristems. The shoot apical meristem initiates leaves, flowers and lateral meristems in highly ordered spiralled or whorled patterns via a process called *phyllotaxis*. It is commonly accepted that the active transport of the plant hormone auxin plays a major role in this process. Current hypotheses propose that cellular hormone transporters of the PIN family create local auxin maxima at precise positions, which in turn lead to the initiation of organ primordia. To explain how auxin transporters could create hormone fluxes to distinct regions within the plant, different concepts have been proposed. A widely accepted hypothesis, *canalization*, proposes that the auxin transporters act by amplifying and stabilizing existing fluxes, which could be initiated by local diffusion. This hypothesis very convincingly explains the organised auxin fluxes in internal tissues during vein formation. For the shoot apical meristem, however, a distinct mechanism was proposed, where the hormone would be systematically transported towards the areas with the highest concentrations. This implies the co-existence of two radically different mechanisms for auxin transport, one flux based, the other based on local concentration sensing. Here, using a dedicated computer simulation tool, we show that canalization is able to explain auxin transport at the shoot meristem as well, thus providing a unifying concept for the control of auxin distribution in the plant. Therefore, canalization could provide a unifying concept for the control of auxin distribution in the plant. In addition, we propose an experimental predictive framework that should be able to distinguish between canalization and other hypotheses that explain the direction of auxin fluxes.

Author's summary (150-200 words) Shoot apical meristems continuously create new stems, leaves and flowers in highly precise positions. It is widely accepted, that the plant hormone auxin plays an important role in this process. This hormone is actively transported throughout the plant by proteins located at the plasma membranes of many cells. These transporters, so-called PIN-proteins, create fluxes of hormone in the plant that lead to the formation of local hormone maxima and minima which are subsequently interpreted in terms of differential cell behaviour. Two hypotheses have been used to explain the formation of the organised hormone fluxes. The first hypothesis proposes that auxin is transported against existing gradients. This concept can account for the observed auxin fluxes at the shoot apex and probably also for those in other tissues. The second hypothesis, called canalization, proposes that the transporters act by amplifying and stabilising small existing fluxes. This concept is most widely used to explain the pattern of fluxes in internal tissues, but so far it was unclear whether it could also ac-

count for fluxes at the shoot apex. Here we show, using computational simulations of virtual tissues that the canalization hypothesis can be used to explain all observed auxin fluxes in the plant. Based on these simulations, we propose an experimental framework that should allow us to test the validity of both proposed mechanisms.

Introduction

During plant development, organs are continuously created by small populations of stem cells called *apical meristems*. The so-called shoot apical meristem (SAM) generates all the aerial parts of the plant. The SAM is a highly organized structure, composed of a central zone required to maintain the meristem surrounded by a peripheral zone, which is competent to initiate new organ primordia [1]. The young organs are usually initiated in highly ordered spiralled or whorled patterns. This remarkable arrangement of organs is called "phyllotaxy" and varies according to particular plant species and growth conditions. Over the last two centuries, phyllotaxy has been extensively studied and different models for this patterning process have been proposed. From a mechanistic point of view, it is now widely accepted that phyllotaxy emerges from a process of local lateral inhibition: each primordium creates an inhibitory field in its vicinity where no other primordium can develop. This basic "inhibitory field" hypothesis (see [2] for a review), is potentially able to generate a wide range of phyllotactic patterns [3, 2 , 4 , 5 , 6].

Hypotheses concerning the physiological nature of these inhibitory fields were proposed only recently [7]. They rely on the signalling role of a key hormone called *auxin* , that plays a crucial role in primordium formation [1]. Auxin is actively transported throughout the plant from cell to cell by carriers that are located at the cell plasma membranes [8]. First cell-influx carriers of the AUX/LAX family, facilitate auxin transport into the cells. This is in contrast to the family of efflux carriers, also called PIN-FORMED (PIN) proteins, which are facilitating efflux [9]. Interestingly, PIN proteins are often accumulated on a particular side of the cell, thus suggesting that auxin is evacuated preferentially via that side. Importantly, PIN carriers often show locally coherent orientations between groups of neighbouring cells, indicating that PIN orientation is coordinated at the level of tissues [7, 10]. It is therefore easy to imagine how cells could transport auxin from cell to cell throughout the plant, thereby creating fluxes that lead to local hormone maxima and minima [11, 12]. These differences in concentration would subsequently be interpreted in terms of differential gene expression and growth rates.

At the SAM, auxin importers and exporters are mainly expressed at the meristem surface. When auxin transport is inhibited, organ initiation is severely affected or even totally absent [13]. In addition, the cells at the SAM orient their PIN proteins towards the young primordia and it is now currently thought that organs are initiated at auxin accumulation points, while the hormone is depleted in their neighbourhoods [7]. The young primordia would thus create drainage basins in their vicinity which would be equivalent to the inhibitory fields proposed previously. While the coherent behaviour of PIN proteins in cell populations is well established, the actual mechanism behind this phenomenon is still not well understood. So far two basic concepts have been proposed in this context.

A first hypothesis is based on the pioneering work of Sachs (1969) on vascular tissue differentiation in plants [14]. Sachs proposed that the auxin transport is facilitated during the process of vascular tissue induction. He suggested that the positive feedback between flux and transport is able to amplify small fluxes and can potentially create *canals* of auxin between auxin sources and sinks that subsequently differentiate into vein tissues. This *canalization* hypothesis was then formalized by Mitchison [15, 16] who developed a mathematical model of this process that increases membrane permeability of cell plasma membrane on the sides where the net flux of auxin is positive. This model was then further studied in the context of leaf venation pattern by several authors [17, 18 , 19 , 20] who interpreted the canalization hypothesis as a feedback mechanism between auxin fluxes and PIN transporters and studied the properties of such a coupling both on a fixed shape and during leaf development. From the biological point of view, recent experiments tend to support the canalization hypothesis, at least in the inner tissues of the plant

[21, 22 , 23]. However, whether it could also account for the behaviour of auxin transporters in other parts of the plant such as the shoot and root apical meristem or leaf margins remains an open question.

More recently, a second concept for auxin transport was proposed to explain auxin transport at the SAM surface [24, 25]. Based on the observation that PIN carriers point to primordia initiation sites in the SAM which supposedly correspond to auxin maxima, it was hypothesized that every cell orients its transporters toward the neighbour, if any, with higher auxin concentration. They would thus tend to export auxin against the auxin concentration gradient (i.e. "pump against the gradient"), thus amplifying local concentrations of auxin when they appear and creating *local maxima or spots* of auxin [22]. Using computational modelling, several authors were able to show that this hypothesis can produce spiralled and whorled phyllotactic patterns. In a recent article, Merks et al. proposed a modified *"against the gradient"* hypothesis [26]. Interestingly although it still requires further development, it is potentially able to explain the formation of veins in internal tissues. Could it, therefore, represent a unifying mechanism for the control of auxin fluxes throughout the plant? A major argument against this idea is that the model does not seem to be compatible with the presence of stable auxin maxima in certain tissues [27]. This is typically the case at the root meristem, where a continuous, stable auxin maximum is maintained with incoming and outgoing fluxes, which cannot be explained by this model.

Since "*pumping against the gradient*" cannot provide on its own a unifying mechanism for the control of auxin fluxes in the plant, we investigated whether *"canalization"*, as the other major concept in the field could provide a realistic alternative.

In this paper, we show that a computational model based on the canalization concept is able to i) generate spiral phyllotactic patterns observed in the SAM ii) produce pro-vascular strands below primordia in the sub-epidermal meristem layers and iii) reproduce stable auxin maxima as observed in root meristems. We therefore conclude that canalization could provide a unifying principle for the guidance of auxin fluxes in the plant. In addition, our model leads to a set of testable predictions, that should be able to distinguish between the *"canalization"* and "*against the gradient*" hypotheses.

Models

Biological assumptions

To model auxin transport in a tissue we used a set of hypotheses derived from biological observations taken from the literature (see also introduction). In the text we refer to them as Auxin Hypotheses (AH):

1. **Auxin concentration in a cell changes as a result of transport processes between cells and local creation/degradation** [25, 10, 24].

2. **Auxin is created locally in every cell** (suggested by Reinhard et al. [28], used also in other models [17, 25 , 24]). Tissues such as growing leaves and developing flowers produce auxin [29], but we do not know at which stage of primordium development auxin biosynthesis is triggered. Small apical explants that retain only the meristem and one primordium with submeristematic tissues are capable of organ formation, suggesting that the sources of auxin are close to the meristem [28]. When PIN shaped meristems kept under influence of NPA (a transport inhibitor) are relieved from transport inhibition, they resume leaf formation despite the absence of pre-existing leaves [1]. This suggests that stem tissues are capable of sufficient auxin production to promote organ formation. However, the relative contributions of the different tissues in the apex (i.e. primordia, stem and meristem) to auxin biosynthesis remain largely unknown.

3. **Auxin is degradated locally in every cell.** e.g. see [30].

4. We assume that auxin is transported from the cell into the inter-cellular space according the chemiosmotic model [Rubery&Sheldrake, 1974]. Briefly, it supposes that it is very difficult for auxin to leave the cell by diffusion because of the neutral pH of the cytoplasm, while

it can enter it more freely from the acidic intercellular space. Therefore, the plant has developed a system of transporters that facilitates the transport from cell to cell [31, 8]. At the meristem, only PIN transporters seem to be polarised, while the AUX/LAX influx carriers are homogeneously distributed over the membrane. We model this overall transport process using a simplified system. First, we assume direct flux of auxin from cell to cell with omission of wall compartment. Second, due to the symmetry of influx carriers, only PIN is simulated explicitly. Therefore **we model auxin redistribution in the meristem as a result of passive diffusion between cells and polar transport which is governed by PIN.** A similar approach was also used in other transport models [17, 25 , 24 , 10 , 26].

5. **PIN concentration in a cell wall is upregulated by auxin flux through this wall** [14]. This hypothesis is explained in detail in the Mathematical Formalization section.

To design the model of phyllotaxis, we extended the AH with a set of hypotheses related to phyllotaxis. In the text we refer to them as Phyllotaxis Hypotheses (PH):

1. The shoot apical meristem is a dome shaped structure, containing up to thousands of cells. **We distinguish the epidermal layer, called L1, that is one cell thick from the sub-epidermal cells that makes up the rest of the dome.**

2. **The L1 layer is itself composed of a central zone surrounded by a peripheral zone (also called competence zone).** These zones exhibit different properties [32].

3. **Primordia can appear only in the peripheral zone of the meristem [1].** Once a primordium is initiated, it moves away from the meristem summit following a radial trajectory, due to cell growth throughout L1 [2, 33].

4. **In the L1, primordium cells act as sinks by removing auxin from the L1 layer downwards.** This hypothesis is justified by the presence of vascular strands below each primordium which seem to transport auxin downwards. We assume that a primordium can easily remove any amount of auxin (the saturation level is much higher than the amount of auxin available in meristem).

5. Longitudinal sections show that pro-vascular strands are approximately three cells wide (data not shown). Therefore we assume that **a primordium is constructed from a central cell and all its direct neighbours.**

6. **A new primorium is formed as a response to high auxin accumulation in a cell** [1].

7. **Auxin and PIN reallocation are faster than growth and cell differentiation.** Therefore, as a simplification, we consider auxin concentrations and PIN localisation to be in equilibrium at the time scale used to model growth.

8. **Auxin is concentrated in the L1 and accesses the inner layers via primordia.** Because of the presence of **AUX/LAX** importers, it has been proposed that auxin is concentrated in the L1 layer. It is mainly transported to the inner tissues via the pro-vascular strands in the primordia.

Canalization model

Our model is essentially based on the canalization concept, introduced by Sachs [14] who suggested that auxin transport is increased during the vascular induction by the auxin flux itself, leading to the *canalization* of the flux (for earlier mathematical formalizations see also [15, 16 , 17 , 18 , 34].

Conservation law for the transport of auxin. Let us denote a_i $(mol.m^{-3})$ the concentration of auxin in a cell i and $p_{i,n}$ $(mol.m^{-2})$ the concentration of PIN proteins in the membrane facilitating transport from cell i to cell n. V_i (m^3) denotes cell volume and N_i denotes the set of neighbouring cells

of cell i. If i and n are two neighbouring cells, then $S_{i,n}$ (m^2) denotes the exchange surface between these two cells. We assume that the auxin variation rate results from the combination of three processes *i)* diffusion *ii)* active transport of auxin by PIN *iii)* local cell auxin synthesis and decay (based on AH 1-4).

$$\frac{\partial a_i}{\partial t} = -\frac{1}{V_i}\sum_{n\in N_i} S_{i,n}J^D_{i\to n} + -\frac{1}{V_i}\sum_{n\in N_i} S_{i,n}J^A_{i\to n} + \alpha_a - \beta_a a_i, \quad (1)$$

where $J^D_{i\to n}$, $J^A_{i\to n}$ are the fluxes of auxin $(mol.m^{-2}.s^{-1})$ due todiffusion from cell i to its neighbouring cell n, active transport from cell i to n respectively (by convention, out-coming fluxes are positive). α_a $(mol.m^{-3}.s^{-1})$ is a constant that describes the rate at which auxin is produced in cells and β_a (s^{-1}) is a rate of auxin decay. Diffusion is modelled using Fick's first law, $J^D_{i\to n} = \gamma_D\,(a_i - a_n)$ where γ_D is the constant of permeability reflecting how easy it is for auxin to move across the membrane $(m.s^{-1})$. In his original paper from 1981, Mitchison proposed to model the flux due to active transport across a wall between cells i and n as $J^A_{i\to n} = \gamma_A\,(a_i p_{i,n} - a_n p_{n,i})$ where γ_A $(m^3.mol^{-1}.s^{-1})$ characterizes the transport efficiency of the PIN pumps. Hence the auxin variation rate in a cell i can be expressed as:

$$\frac{\partial a_i}{\partial t} = -\frac{1}{V_i}\sum_{n\in N_i} S_{i.n}\gamma_D\,(a_i - a_n) + -\frac{1}{V_i}\sum_{n\in N,} S_{i.n}\gamma_A\,(a_i p_{i,n} - a_n p_{n,i}) + +\alpha_a - \beta_a a_i. \quad (2)$$

Canalization hypothesis According to Sachs' original concept, canalization relies on a feedback mechanism from the auxin fluxes on its transporters. More precisely, we assume that the concentration of PIN proteins $p_{i,n}$ in cell i transporting auxin to cell n changes due to *i)* synthesis induced by the flux *ii)* internal reaction mechanisms (local synthesis and decay of PIN). The net flux of auxin that crosses wall from cell i to cell n is $J_{i\to n} = J^D_{i\to n} + J^A_{i\to n}$.

$$\frac{\partial p_{i,n}}{\partial t} = \Phi(J_{i\to n}) + \alpha_p - \beta_p p_{i,j}, \quad (3)$$

where Φ defines the intensity of PIN production due to the feedback of the auxin flux, α_p $(mol.m^{-2}.s^{-1})$ describes the rate of PIN synthesis in the cell, and β_p (s^{-1}) the decay rate at the cell membrane. Depending on the nature of the Φ function, different types of canalization regimes can be obtained, [17] (and see below). In this paper we use two types of functions: a linear function $\Phi_L\,(J_{i\to n}) = \kappa(J_{i\to n}/J_{ref})$ and a quadratic function $\Phi_Q\,(J_{i\to n}) = \kappa\,(J_{i\to n}/J_{ref})^2$, where κ $(mol.m^{-2}.s^{-1})$ is a constant parameter and J_{ref} $(mol.m^{-2}.s^{-1})$ is an arbitrary reference flux that makes it possible to keep constant units in the equation. For negative flux the functions are trunctated to 0.

SAM model

As mentioned above we suppose that auxin flows essentially in two separated conduits: the L1 layer and the sub-epidermal layers (PH 8). The two systems meet at the primordia cells. This very localized coupling between epidermal and sub-epidermal domains makes it possible to model the transport in each pathway independently and to account for their interaction at the sites of primordia only.

Epidermal model We represent the L1 layer by a set of polygonal cells forming a 2D surface, representig the outer walls of the epidermis. Each edge of a polygon represents a cell wall. Similarly to other models of auxin transport at the SAM [25, 24], the inter-cellular space was not represented as a compartment of its own (however see [35]) and the contact between cells was abstracted as a single "wall" allowing auxin molecules to flow between adjacent cells and PIN molecules to accumulate on either side. To model phyllotaxis we included certain topological and geometrical assumptions. We identify a particular point z as the meristem centre. Different zones of the meristem are defined relatively to this centre z. The centroid of each cell

i is denoted by o_i. The central zone, $\mathcal{Z}$, is the set of cells whose centroids have a euclidian distance to the meristem centre z less than or equal to the constant radius $R_{\mathcal{Z}}$. Similarly, a cell i belongs to the peripheral (or competence) zone $\mathcal{C}$ when the distance between its centroid o_i and the meristem centre z is less than or equal to $R_{\mathcal{C}}$ and greater than $R_{\mathcal{Z}}$. Cells i in the peripheral zone can be promoted to primordia cells (which is denoted by $i \in \mathcal{P}$).

Sub-epidermal model Second, to model the vascular pathways below the primordia, we designed a 2D model of a longitudinal section of the SAM where the connection between the epidermal and sub-epidermal layers could be explicitly represented. In the sub-epidermal layer, the definition of the zones $\mathcal{Z}$, $\mathcal{C}$, and of primordia cells $\mathcal{P}$ is analogous to that of the epidermal model. Cells are also represented as 2D planar polygons whose edges represent cell walls. In addition, a new set of cells is identified which represent the outset of the internal organ vasculature $\mathcal{V}$.

Growth of the SAM To simulate the meristem dynamics throughout time, we used a purely kinetic description of meristem growth [25]. We explicitly defined the velocity v of every point at the meristem surface in a reference frame attached to the meristem centre z. The velocity $v(x)$ of a point x at the meristem surface is assumed to be proportional to its distance to the meristem centre: $v(x) = \rho\,|x - z|$, thus simulating isotropic radial growth [2]. The constant ρ defines the growth intensity. Due to this global kinetic process, the vertices of each cell move toward the meristem periphery with a velocity growing exponentially. This movement makes the cells grow smoothly as they go away from the meristem centre. As soon as a cell surface exceeds a prescribed threshold S_{max}, the cell divides by creating a new wall inside. The position of this wall is computed using a modification of the optimization criterion introduced by Nakielski [36], *i.e.* finding a wall that both minimizes the distance between two opposite walls of the cell and that divides the cell into two polygons with the same surface. Then, similarly to [25], the cell vertices of newly created walls are slightly moved toward each other to provide a more realistic aspect. After a cell division, auxin and PIN concentrations are inherited by the daughter cells from their parent.Primordium identity is inherited by randomly choosing one daughter of the primordium cell as the new primordium cell. The new wall is initialized with basic amount of PIN α_p/β_p on both sides. Finally, to keep a constant size of the overall simulation, a cell i that gets too far away from the meristem centre z (its centroid o_i is at a distance greater than R_{sim}) is removed from the simulation.

In order to integrate in a single model the different processes involved in the system, *i.e.* auxin transport, cell growth, division, PIN allocation, and cell differentiation, we assume that these processes take place at different paces. Auxin transport is supposed to be much faster than growth and cell differentiation so that in the growing meristem, auxin concentrations are always at equilibrium.

Practical aspects of simulation

Numerical solving The non-linear system of equations describing the canalization process is integrated using the Scipy package designed for ODE solving [37]. The integration algorithm uses the Adams predictor-corrector method in the non-stiff case and the Backward Differentiation Formula (BDF) methods in the stiff case [38]. Solver iterations are performed until a stable state is obtained, i.e. until change in auxin concentration becomes less than a predefined threshold value ϵ_{min} in every cell.

Boundary and initial conditions The boundary conditions for every simulation are specified in the supplementary material. In most simulations boundary cells do not receive any auxin flux from the outside and we assume fixed, null concentration in sinks. In all simulations we assume that the initial auxin concentrations are null and PIN concentration in the wall is initiated is with basic amount of PIN α_p/β_p.

Visualisation and simulation environment The visualization of tissue simulations was carried out with PlantGL, an open-source graphic toolkit for the creation, simulation and analysis of 3D virtual

plants [39] available in the OpenAlea software platform for plant modelling.

General convention for figures In all figures representing 1-D or 2-D tissues, we adopted the following graphical conventions: an absence of auxin in a cell is represented by black color while high concentration is shown in green. Intermediate concentrations are represented by interpolations between these two extremes (see supplementary materials). Polar active transporter concentrations are represented in red, with a thickness proportional to the concentration of transporter on the wall. In simulations, sink cells are tagged with blue dots. In "top view" simulations central zone cells are marked with white dots and primordia with blue dots. In "transversal" simulations **L1** was tagged with black dots, vasculature and old primordia with white dots and newly created primordium with blue dot.

Supplementary materials For every figure showing a dynamic system, we provide a corresponding movie to capture system dynamics. Movies are available as supplementary materials and named after the figures. Also supplementary text is available, specifying equations, parameters, boundary and initial conditions and display specific conventions.

Results

The study of systems controlled by canalization is not straightforward as the process relies on a feedback loop between auxin concentrations and auxin fluxes in tissues. To address this problem, we first defined different remarkable properties of the canalization process that are essential in the generation of patterns. These properties are illustrated on simplified 1D or 2D "virtual tissues". Based on this analysis, we then investigate the ability of canalization to produce phyllotactic patterns at the SAM in a way that is consistent with the current biological knowledge and observations.

Canalization amplifies fluxes In the canalization paradigm, any small flux appearing locally in the system is immediately reinforced by a positive feedback due to the increase of active transporters generated by this flux. Initial fluxes may typically be generated by diffusion between zones with different concentrations. We illustrated this phenomenon on a 1-dimensional tissue with two perfect auxin sinks at both extremities (Figure 1A). The auxin is produced in every cell except of the sink cells. Initially, the highest flux appears close to the sink cells, due to diffusion. According to the canalization principle, this small initial flux is reinforced by a polar allocation of *PIN* transporters in each cell that favours the evacuation of auxin in the direction initiated by the original flux. If the auxin sink is maintained, the auxin flux reaches a stable state with maximum concentration of auxin appearing at the maximal distance from both sinks (Figure 1A). Figure 1A shows that the concentration of *PIN* in each cell wall linearly increases from the location of the auxin maximum up to the sinks. This is because each cell is producing auxin at a constant rate α_a and in the stationary state this amount of auxin must be evacuated to the neighbouring cells (if we neglect auxin degradation). It implies that the auxin flux should grow linearly in the direction of the closest sink. If the feedback function Φ is linear, this results in a linearly increasing allocation of PINs to the cell walls in the direction of the closest sink.

Canalization allows auxin to flow with or against auxin gradients Although the molecular mechanism underlying PIN polarization is still unknown, PIN proteins can polarize either *with* or *against* the gradient of auxin [40, 22 , 8]. If a unique transport mechanism is operating in the plant it should thus be able to reproduce this property. In the previous example, auxin fluxes were amplified from regions of high concentration of auxin to regions of low concentration (Figure 1A). Auxin thus flowed *with* the auxin gradient.

To show that canalization can also lead to flow against the gradient, we modified the above 1-dimensional model by weakening the sinks in such a way that they were only able to degrade auxin at a finite constant rate. This simple modification produces a drastic change in the system's behaviour.

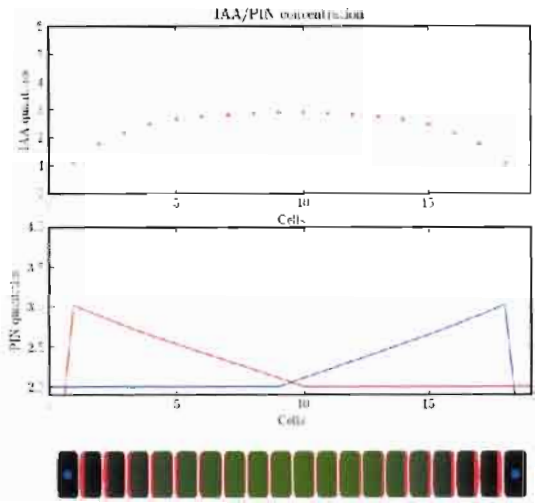

A Canalization with the gradient.

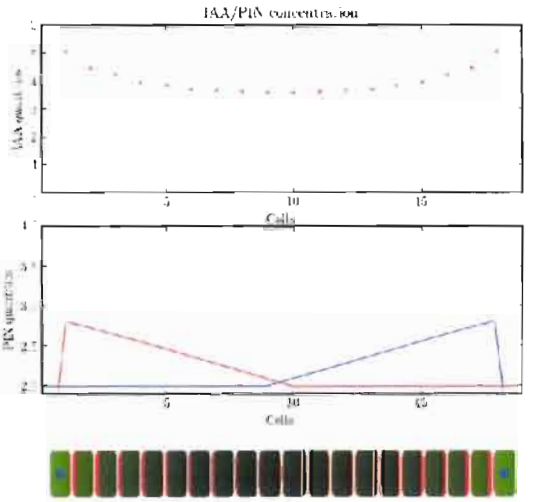

B Canalization against the gradient.

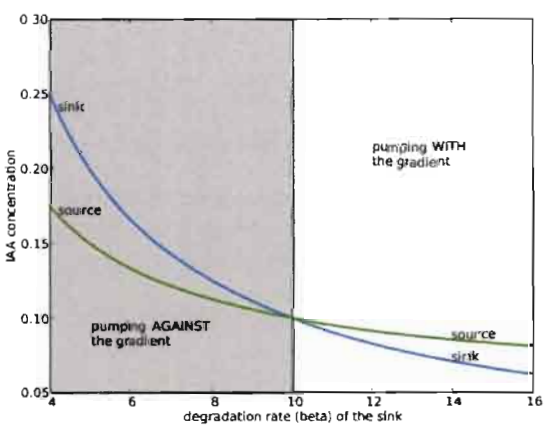

C

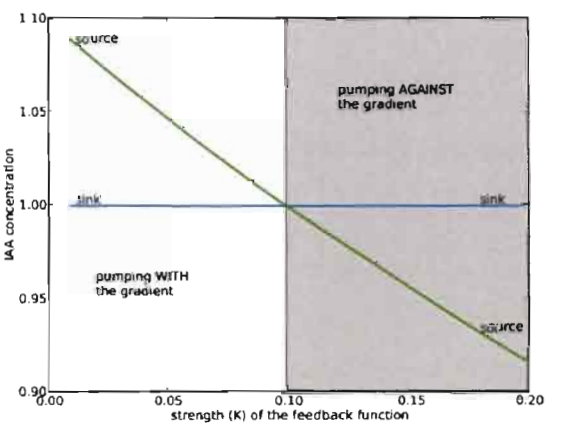

D

Fig. 1: **Canalization in a 1-dimensional cellular system.** The system consists of a file of 20 cells. Boundary cells are acting as sinks, hence they evacuate or destroy auxin. The simulation starts by imposing initial conditions on the system with null auxin concentration in all cells. Then the simulation runs until a stable state emerges. On two first plots blue and red line correspond to PIN concentration in the right and left wall respectively. The two systems differ only by the way auxin is removed: in 1A we assume that the removal in the sink cells is very efficient whereas in 1B the removal efficiency is limited. This difference leads us to two different stationary patterns in which the auxin gradients are opposite and the sink cells are minima of auxin 1A or maxima 1B. In Figure 1C concentrations of auxin in the two cells in the stable state as a function of the degradation rate β of the sink. The green (resp. blue) curve corresponds the source (resp. the sink). In the grey region, pumping is carried out against the auxin gradient, while in the white region, pumping follows the gradient; In Figure 1D similar curves for the variation of the feedback strength κ of flux on PIN synthesis.

The auxin gradient is now reversed in the stable state, with highest concentrations at the sink locations and lowest in the places maximizing the distance to all sinks. Figure 1B shows the corresponding stationary state of this system. The transition between both regimes, pumping "with" or "against" the gradient, can be obtained by varying different parameters of the model (Figure 1).

To study the conditions for either pumping "with" or "against" the gradient, we considered a system of two cells sharing a wall. One cell is a source of auxin while the other acts as a sink destroying auxin at a constant rate. Once this system reaches a stable state, the net flux across the wall separating the two cells is exactly equal to the rate at which the source creates auxin and leads to a polarization of PIN from the source to the sink. Depending on the model parameters, the system can reach different levels of concentration in both cells. Two regimes may be obtained as shown by the following graphs. The transition between both regimes, pumping "with" or "against" the gradient, can be obtained by varying different parameters of the model (Figure 1).

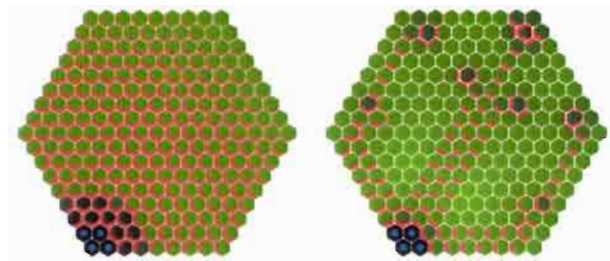

A Linear Φ B Quadratic Φ

Fig. 2: **Weak and strong canalization.** In Figure 2A stable state in case of weak canalization. The 2D lattice of hexagonal cells is initialized with empty cells (i.e. cells that do not contain auxin). The sink cells are tagged with blue dots. Auxin concentration is progressively increasing from the sink towards the periphery. PIN, marked in red, is present in all cells leading to a laminar flow over the entire surface. In Figure 2B strong canalization with one sink leading to the formation of canals (where PIN is present) and patches of cells without transporter.

Canalization has two different regimes ("weak" and "strong") Initially, the concept of canalization was introduced to model the formation of vascular canals in stem and leaf tissues [15, 16 , 17 19, 34]. This may seem in contradiction with the absence of canals at the meristem surface. Feugier et al. [17] demonstrated that a canalization regime where the feedback function Φ was linear did not result in the formation of canals in a tissue. We further confirmed this by comparing the behaviour of auxin transporters in a 2D sheet of cells showing weak or strong feedback. When the feedback function Φ is "non-accelerating" (increasing linearly or less rapidly than linearly) the process creates laminar flows transported by homogeneous arrangement of PINs and converging to the sink (Figure 2A). We will call such a system "weak" canalization. Conversely, when the feedback function Φ is "accelerating" (increasing more rapidly than linearly), canals appear, creating branching structures in the 2D tissue (Figure 2B). We will call such a system "strong" canalization. In both cases, fluxes may be oriented with or against the gradient, depending on the model parameters and initial conditions.

"Weak" canalization may produce fields of lateral inhibition of varying intensities. As explained earlier, the most widely accepted theory of phyllotaxy relies on the formation of inhibitory fields around each primordium. Recent models propose that these fields are in fact zones where auxin is depleted [3, 2 , 6]. To show that canalization can indeed be considered as a plausible hypothesis, we demonstrated that it can generate such inhibitory fields with varying intensities.

Weak canalization as shown in Figure 2A leads to the formation of a zone around the sink where auxin is depleted. The intensity of the auxin depletion fields around sinks can be changed by tuning parameter κ that controls the feedback level of auxin fluxes on the synthesis of PIN proteins in walls. Figure 3 shows the extent of inhibitory fields (in black) around the blue sinks for increasing values of parameter κ. It can be observed that PIN is regularly distributed throughout the tissue, with a polarity that is determined by the relative distance of the cell to the different sinks. Weak canalization

thus makes it possible to continuously vary the intensity of auxin depletion level around sinks. It is therefore a potential candidate physiological mechanism to explain the formation of inhibitory fields during organ initiation at the SAM.

Canalization as a source of patterning in a growing structure The mechanism that controls PIN orientation in cells takes place in a growing structure. Therefore we constructed a dynamic model with dividing and growing cells. Like previously, we assume that all cells create auxin except for a limited number of cells marked as sinks in which auxin concentration is fixed to 0. To produce phyllotactic patterns, the combination of canalization and tissue growth should therefore show a recurrent, temporal patterning property. We show this property in a simplified 1D model by introducing a sink creation threshold, i.e. an auxin concentration at which a new auxin sink is created. In a growing system, neighboring auxin sinks are pushed apart. Due to the weakening of the sink influence and the constant local hormone production the level of auxin increases in the zone between these two sinks. At a particular auxin threshold (the sink initiation threshold ω), the amount of hormone is sufficient to initiate a new sink at the location which is the farthest from the two sinks, Figures 4A-4B. As a result of sink creation, some of the PIN pumps reverse toward the new sink, with PIN and auxin patterns similar to that of the previous sinks. By changing the sink initiation threshold ω, it is possible to augment or to decrease the initiation frequency, Figures 4C-4D and 4E-4F.

Canalization can reproduce observed PIN maps and realistic influence zones In Barbier et al. 06, we showed that the distribution of PIN at the SAM (called "PIN map") is very specific in Figures 5A-5B . In particular PIN labelled membranes are pointing to nearest primordia (blue dots in Figures 5B-5C) and in addition a significant number of cells appear to transport auxin to the meristem summit. A plausible model of phyllotaxy should be able to reproduce similar distributions of PIN.

To determine to what extent canalization could reproduce realistic PIN maps, we digitized the cell walls on the images of real immunolabelled meristems. We recorded the PIN orientation in each cell as described in [10]. This defined "real PIN maps", Figure 5C. The position of each primordium could be clearly identified as indicated by the convergence of PIN toward particular cells and the presence of vascular strands below these primordia seen on other sections of the same meristem (blue dots in Figure 5B, longitudinal images data not shown). We also identified a central zone of about 6 cells in diameter at the meristem summit. This zone is usually free of primordia in the wild type *Arabidopsis* SAM.

We then simulated the emerging arrangement of PIN distributions according to the canalization hypothesis on the digitized maps. Primordia were considered as perfect sinks while all other cells in the meristem were assumed to produce auxin at a fixed rate according to Equation 2 . The resulting PIN distributions are shown in Figure 6 . Close to the primordia, the simulated PIN arrangements are converging toward the sink cell and look similar to the PIN arrangements on the real PIN maps (Figure 5A). Besides, auxin accumulates at the position where one would expect the next initium in a spiral phyllotaxy (Figure 6A). However, contrary to real PIN maps, virtual PIN patterns did not show any significant converging tendency towards the centre of the meristem. To alleviate this discrepancy, we made a second simulation, where the cells in the meristem centre were assumed to degrade auxin at a higher rate. Results are shown in Figure 6C. While the convergence of PIN toward the primordia cells is preserved, a convergence of PIN toward the centre is now observed, reflecting more faithfully the observed distributions of PIN in the immunolabelling images.

To go beyond a simple visual inspection for similarity, we computed the influence zone of the primordia and of the central zone in the real meristem and compared them to those in the simulated meristems. The influence zone of a region (i.e. a cluster of cells) is the set of meristem cells that are connected to a cell of the considered region through a path of PIN arcs oriented in the direction of this

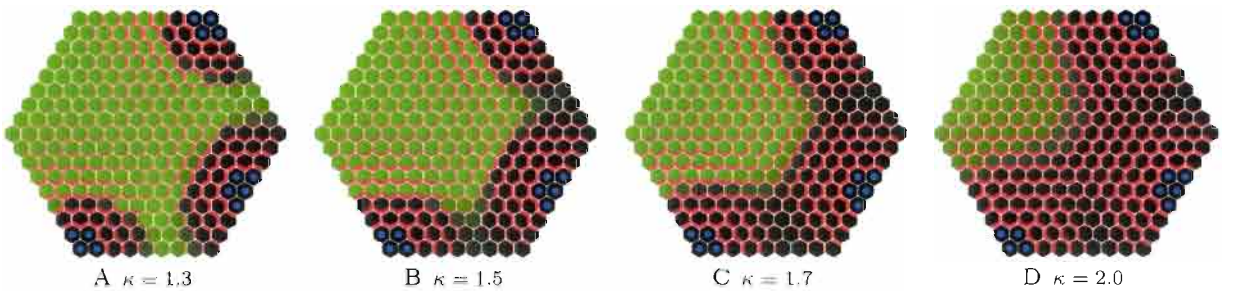

Fig. 3: **Inhibitory fields induced by a canalization system.** The size of the field changes according to the value of parameter κ which regulates the feedback of fluxes on PIN pumps synthesis.

region. Figure 7 shows the influence zones of different regions (centre and primordia) on real (Figures 7A-7D) and simulated (Figures 7E-7L) PIN maps. In real maps, pumps are distributed in such a way that auxin can reach the central zone from all the directions between each pair of primordia (with a small auxin pathway between P_0 and P_2, a larger one between P_0 and P_1 and the largest pathway between P_1 and P_2). Influence zones of the primordia are restricted to the neighbourhood of each primordia and do not overlap with the cells of the central zone. In comparison, the influence zones computed in the first simulation (where the central zone cells are not sinks) did not give satisfactory matching both for the central and the P_0 zones. For the central zone (Figure 7E), only two auxin pathways of equivalent width can be observed. The pathway between P_0 and P_2 that is observed on the real data has disappeared. The influence zone of P_0 in the real map is restricted to the direct neighbourhood of P_0, while the same influence zone largely crosses the meristem centre in 7F of the first simulation. By contrast, the influence zones of the simulations with auxin depletion in the centre (Figures 7I-7L) showed better agreement with the influence zones computed from real PIN maps: with three auxin pathways of gradually increasing width going to the meristem centre and the influence zones of primordia being almost not overlapping with cells in the central zone.

Formation of phyllotactic patterns and provascular strands Based on the previous results, we designed a dynamic model of phyllotaxy using the canalization hypothesis. The epidermal and sub-epidermal layers were assumed to be relatively independent, except at the primordia locations were the two systems interact by exchanging auxin. In particular, we assumed that auxin could not leak from the L1 layer due to the presence of influx carriers of the AUX/LAX family on the cell walls. This made it possible to simulate the two processes separately and to summarize their interactions as boundary conditions. Since in the L1 layer no canals of auxin transport are observed, we supposed that weak canalization prevailed at the surface. For vein formation in inner tissues, we supposed strong canalization.

The simulations using the model characteristics described above resulted in a dynamic pattern of auxin distribution and primordium formation. The following general scenario was observed. In the L1 layer, each primordium evacuates auxin by its provascular system to the inner parts of the meristem. In L1, the primordium can thus be considered as a sink depleting auxin in its immediate neighbourhood. This in turn inhibits the formation of new primordia close to the existing ones, Figure 8A. Due to cell growth, primordia progressively move away from each other, which allows sufficiently distant cells to accumulate auxin. A maximum of auxin concentration gradually appears in the place maximising the distance between all primordia, thus defining the location of the next initium (Figure 8G). As soon as the auxin concentration exceeds a predefined threshold in a cell, the identity of this cell changes and becomes that of a primordium (Figures 8B, 8G). This implies

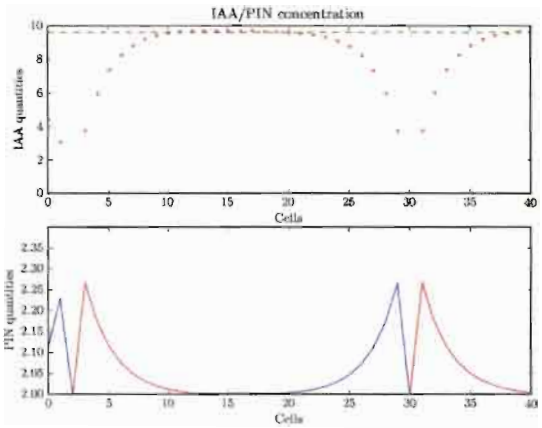

A $\omega = 9.6$

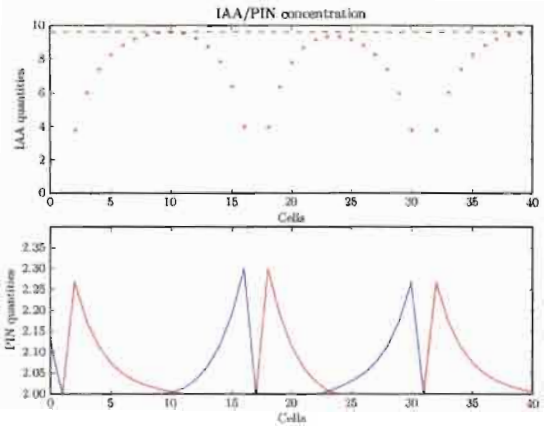

B $\omega = 9.6$

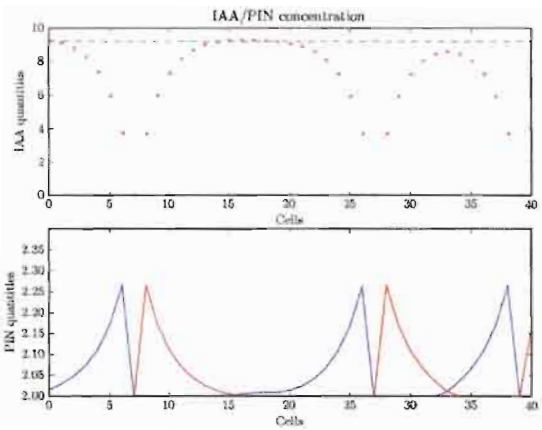

C $\omega = 9.2$

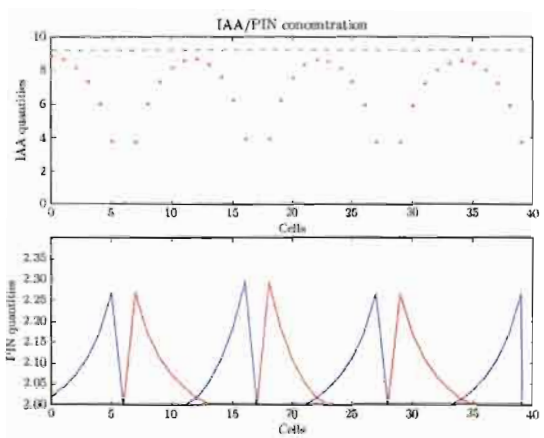

D $\omega = 9.2$

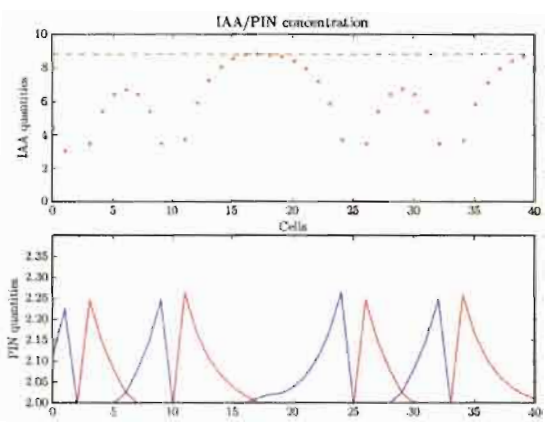

E $\omega = 8.8$

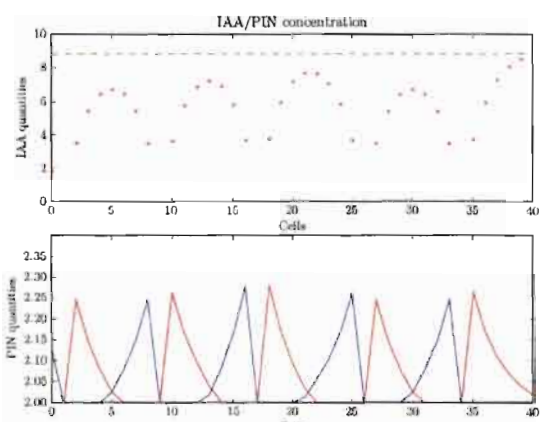

F $\omega = 8.8$

Fig. 4: **Dynamic patterning with canalization.** Figures 4A-4B, 4C-4D, 4E-4F present three simulations respectively with different thresholds ω for primordium initiation. Figures 4A,4C,4E present the step just before primordium initiation for different models and Figures 4B,4D,4F present the step just after primordium initiation. The frequency of primordium initiation increases with a decrease of the initiation threshold ω.

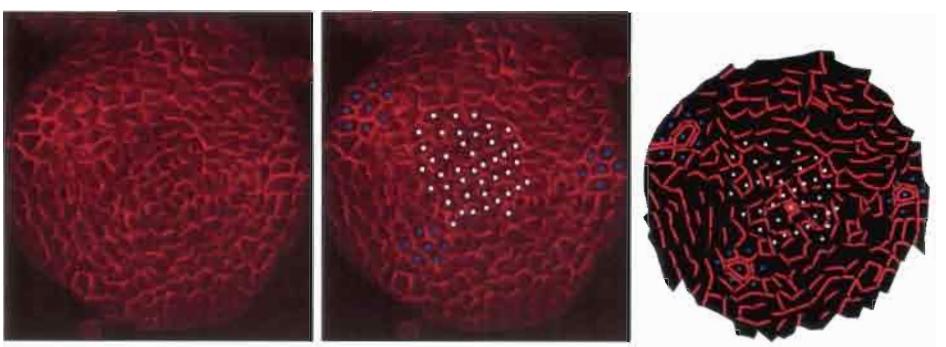

A B C

Fig. 5: **SAM digitalization.** In Figure 5A PIN distribution in the meristem obtained from immunolabelling. In Figure 5B same image showing primordia cells (blue dots), and central cells (white dots). In Figure 5C reproduction of PIN distribution and polarity in a digitized meristem.

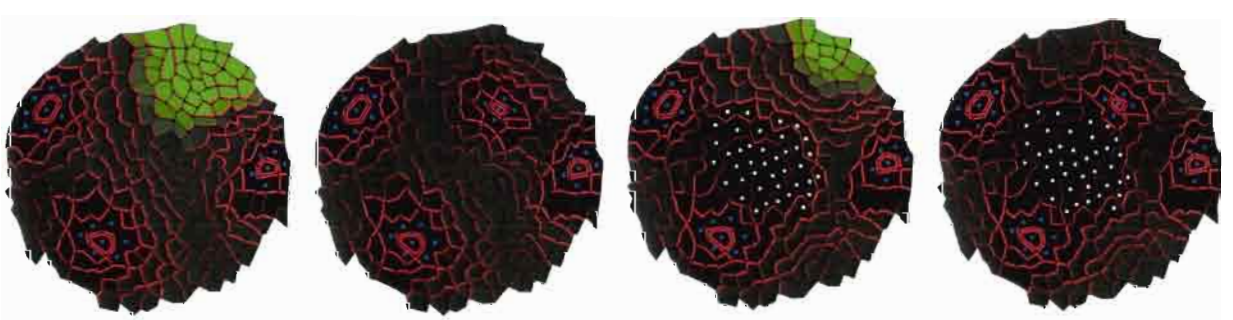

A B C D

Fig. 6: **Simulation of auxin transport in a digitized meristem based on the canalization hypothesis.** The cells and primordia of the real meristem shown in Figure 5 were used to initialize the system, and the virtual PIN maps were then calculated based on the canalization hypothesis. Green depicts virtual auxin concentration. In Figure 6A simulation with centre playing no special role in the auxin flux. In Figure 6B generation of the initium at the highest auxin concentration point at the junction between the central zone and the peripheral zone. In Figure 6C simulation with centre destroying auxin. In Figure 6D initium creation in case of a centre destroying auxin.

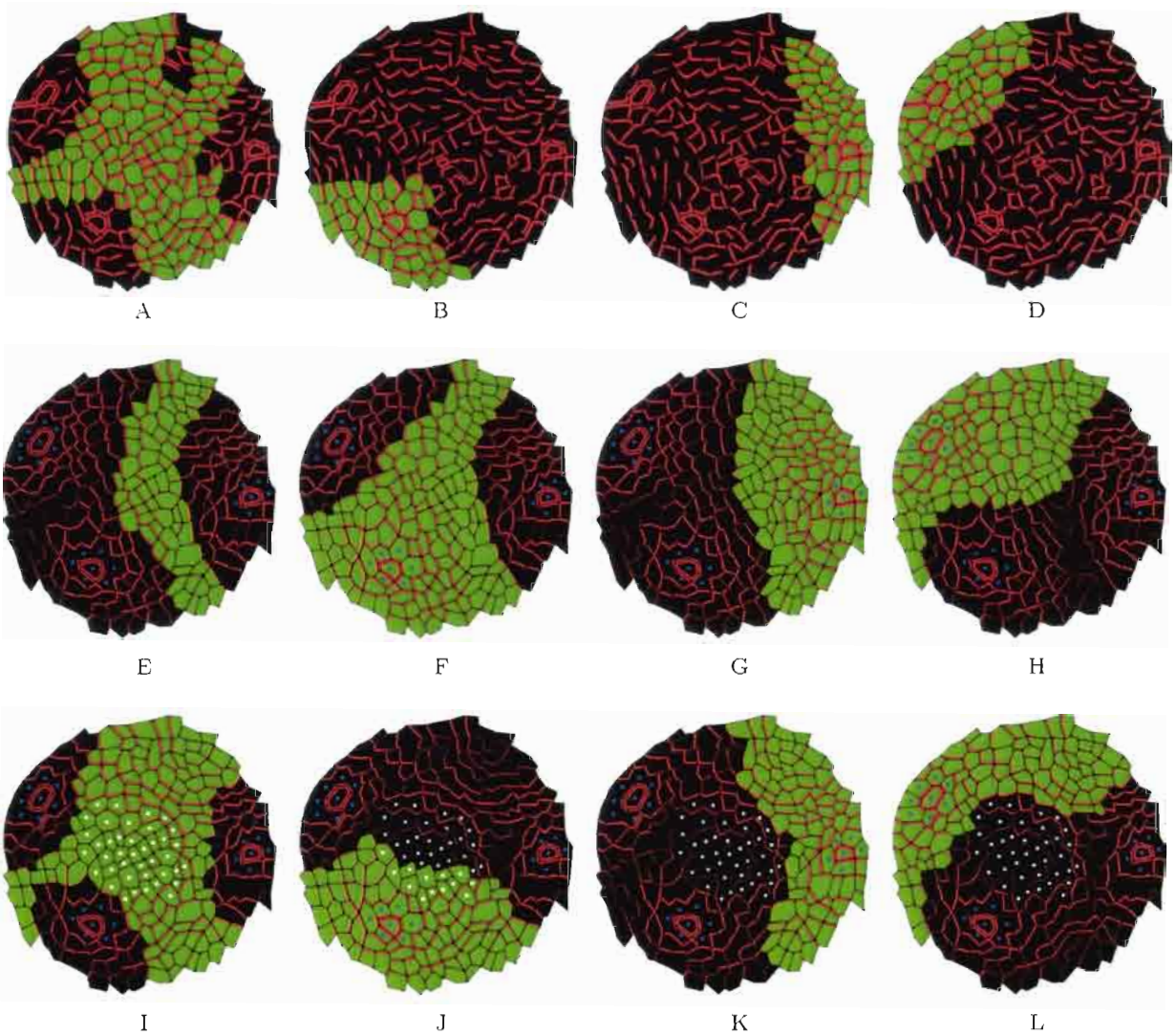

Fig. 7: **Influence zone analysis.** The influence zones are calculated for the central zone (first column), P_0 (second column), P_1 (third column), P_2 (fourth column) respectively in Figures 7A-7D real maps with actual digitized pumps. In Figures 7E-7H digitized maps with simulated pumps. Cells in the central zone are identical to other cells. Primordia (blue cells) are perfect sinks 7I-7L digitized maps with simulated pumps. Both primordia and cells in the central zone (white cells) are removing auxin.

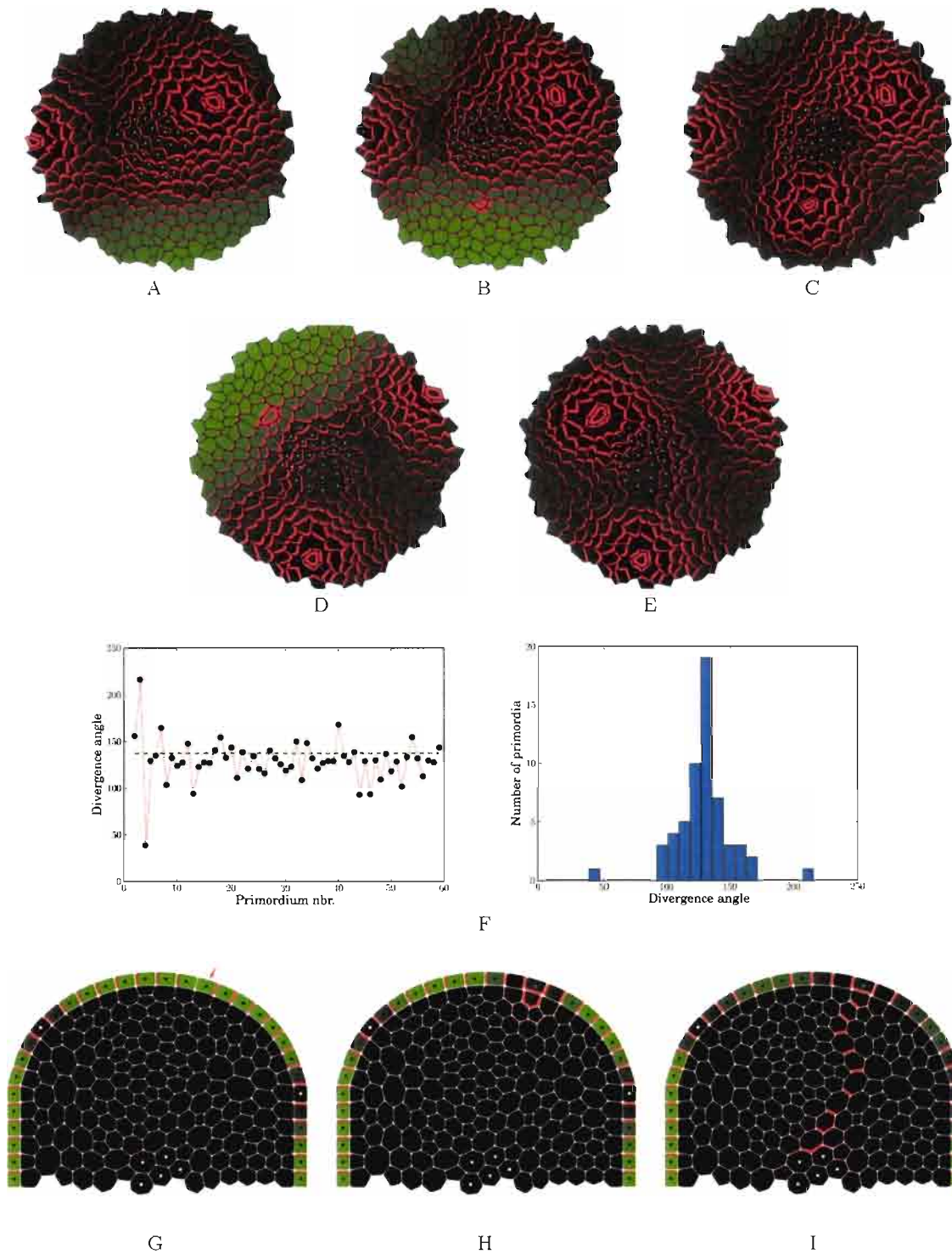

Fig. 8: **Formation of phyllotactic pattern.** In a stationary regime, primordia close to the centre deplete auxin from the meristem (Figure 8A). While primordia get apart from each other due to growth, auxin progressively invades the meristem centre across the widest pathway left by primordia. After the level of auxin has reached a critical threshold in a particular cell (Figure 8G under the red arrow), this cell gets the identity of a primordium (Figure 8B). Auxin then leaks from the L1 layer into the sub-epidermal layers (Figures 8H,8C) and forms a vascular strand via the canalization process in the inner layers (Figure 8I). Phyllotaxy then proceeds and further primordia are created similarly (Figures 8D-8E). In Figure 8F the position of 65 primordia were recorded. Time variation of the divergence angle at cell scale during a simulation . The mean value is close to the golden angle (137°5).

that auxin can leak at the initium location into the inner layers, which triggers the creation of the primordium vascular strand (Figure 8H). The vein being formed below the initium drains the auxin out from the L1 layer and converts the initium into an auxin minimum (Figures 8C, 8H). The flux induced by this process reverses pump polarisations in the direction of the initium in the L1 (Figures 8C, 8I). Then, due to tissue growth, the primordia get further apart from each other and the process reiterates the formation of an initium at a position rotated by a phyllotactic angle with respect to the previous one (Figures 8D-8E). This system is able to produce a stable phyllotactic pattern, with a mean angle close to the golden angle, 137°5 (Figure 8F).

Discussion

Canalization as a unifying concept So far two different concepts have been proposed to explain the patterned distribution of auxin during plant development. First, the "up the gradient" hypothesis provides a satisfactory explanation for phyllotaxis [24, 25]. It was also recently suggested that this hypothesis may account for venation patterns as well [26]. However, the ability of this hypothesis to generate a range of vascular patterns (loops, branching systems of different types, reaction to wounds, etc.) remains to be thoroughly studied. In addition, it cannot explain the maintenance of stable peaks of auxin as observed in the root meristem [27], implying that at least one other mechanism must operate in the plant. In a recent study, Sauer et al. suggested that cell-type specific factors could decide whether one or the other mechanism would be used [23], but this remains to be proven. An alternative is canalization, which proposes a gradual reinforcement of auxin transport by the hormone flow itself. Previous work has shown that canalization can account for major developmental patterning processes in plants, including vein formation or embryo axis formation. We show here, that it can also explain phyllotaxis, predicting patterns of PIN distribution that are very similar to the observed ones. In addition, since canalization allows for transport with and against gradients, it also provides a plausible explanation for the stable auxin maxima observed at the root tip. Indeed, our simulations show that this model can reproduce realistic patterns of PIN and auxin distribution in the root as well, Figure 9 . We therefore conclude that canalization clearly provides a unifying concept for auxin transport throughout the plant. It is important to note, that canalization, like the "up the gradient" model is an obvious abstraction of reality. They both do not take into account the intercellular space for instance, nor do they indicate how auxin fluxes or auxin concentration gradients are sensed. A process like canalization could, therefore, be much more complex than just PIN proteins sensing auxin particles flowing through the cell. What is important here is that the overall behaviour of the system can be described accurately by canalization with predicted, testable properties.

Some implications of the model for phyllotaxis The model proposes a patterning process that mainly occurs in the L1 layer at the meristem surface. This is based on the hypothesis that auxin is concentrated there by auxin importers (AUX1 and LAX proteins) which are strongly expressed in the L1 [42]. The model leads to a classical inhibitory field scenario where the very young primordia pump auxin towards the inner tissues, draining the hormone away from their immediate vincinity. As long as these sinks are close to the competence zone, no new primordia can be formed. However, as growth drives the sinks away, auxin concentration can locally build up again because of local synthesis and transport, creating a new auxin maximum. The model proposes that the import capacity of AUX1/LAX proteins at the surface is overridden when a certain auxin concentration threshold is reached after which the hormone starts to leak away to inner tissues. This initial diffusion-driven flux will be reinforced by canalization. This in turn will rapidly create an auxin transport channel connecting the local surface maximum to the inner vasculature and transforming it into a sink. The main requirement here is that canalization should be relatively weak at the surface, switching to a higher regime in inwards directed fluxes .

An intriguing aspect of the model concerns the Central Zone cells. Like for the other models [24, 25], canalization does not require any particular property of this zone, other than a lack of competence to generate a primordium. We could, however, only

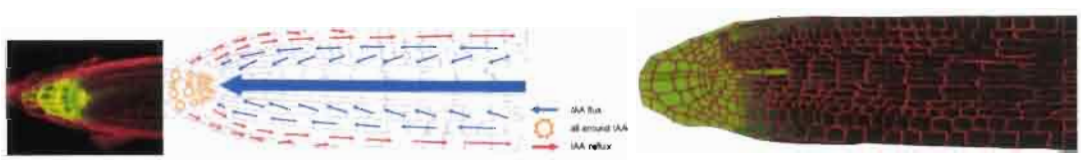

A B C

Fig. 9: **Canalization in the root system.** Canalization is compatible with the maintenance of an auxin maximum and with the general organization of PIN at the root tip. The existence of a stable auxin maximum at the root tip was demonstrated experimentally [13] (Figure 9A). At the shoot apex, the general organization of the different PIN transporters in the different tissues may be summarized from the literature as a "fountain model" (Figure 9B). In the simulation we performed, a root apex was digitized from *Arabidopsis* root optical and confocal microscopy pictures. Similarly to PIN maps at the shoot apex, the polarity of PIN was recorded in each cell. This PIN maps were used as an initial condition for the simulation. The cellular system was provided with a fixed global quantity of auxin initially divided equally between each cells. In addition, two border cells of the epidermis were chosen as auxin sinks, to comply with the biological assumption that a fraction of auxin is evacuated from the root tip along the epidermis [41]. Auxin arriving in these sink cells is completely depleted at each simulation step. The apical auxin maximum and transporters patterns were maintained by the circulation of auxin and showed a strong resilience while transitory auxin maxima present in the central tissues progressively disappeared. This was also the case when cells contained almost no initial auxin and a permanent auxin source was added on the border of the cellular system and provided auxin in a constant fashion, in accordance to biological auxin source localization in the vascular bundle (data not shown). Simulations revealed that transporter dynamics based on canalization are sufficient to enable and maintain auxin accumulation in the collumella and quiescent centre Figure 9C, as observed in Figure 9A. Additionally, transporter distribution profile were maintained by the canalization process, while new pumps appeared directed toward inner tissues, reinforcing the reflux system.

obtain realistic patterns of PIN distribution when we attributed a sink function to this zone. This is in line with earlier observations by Barbier et al. (2006) who provided evidence that the CZ does accumulate auxin [10]. Interestingly, auxin sensors like the DR5 promoter remaine insensitive to auxin in the Central Zone, suggesting that auxin perception there is quite different. A possible explanation for this could be that the CZ requires auxin for its proper function.

An experimental framework to compare and test the models Having established two potential mechanisms for patterning at the meristem surface, it now becomes essential to compare and test the models as rigorously as possible. We have made a first step towards this procedure by comparing the predicted PIN protein patterns with the observed ones. This test, which in principle should be very stringent, must now also be performed on the *up the gradient'* model. This might not be sufficient to discriminate between the two. However, we can already indicate some major differences between the two mechanisms. One of the main implications of the *up the gradient model'* is that auxin maxima must be maintained at the summit of the young initiating primordium to guarantee correct patterning. Canalization, by contrast, requires that this maximum should be transformed rapidly into a minimum. In principle this should be testable. For instance, auxin sensors such as the DR5 promoter could be used in this context [10]. Alternatively, modifying the amount of auxin in the young primordia should have different effects depending on the proposed mechanism. Typically, we would expect that increasing auxin in the primordium using transgenic plants locally overproducing hormone synthesizing enzymes would have more dramatic effects in the case of canalization than in the case of the *up the gradient'* hypothesis. The interpretation of these results, however, might not be that straightforward. We do not know, for example, whether the DR5 auxin sensor reacts to absolute auxin concentration or not. Indeed, since high amounts of auxin transit through a cell when the flux is high, it might also be possible that auxin response sensors are sensitive to both flux and concentration. By any means, the testing of the hypotheses will imply the development of new tools. In view of the very precise predictions with cellular resolution, these tools should typically involve live imaging technology, quantitative microscopy and the possibility to manipulate cell behaviour in a very localised manner.

References

[1] Reinhardt D, Mandel T, Kuhlemeier C (2000) Auxin regulates the initiation and radial position of plant lateral organs. Plant Cell 12:507–518. URL http://www.plantcell.org/cgi/content/abstract/12/4/507.

[2] Douady S, Couder Y (1996) Phyllotaxis as a dynamical self organizing process part ii: The spontaneous formation of a periodicity and the coexistence of spiral and whorled patterns. Journal of Theoretical Biology 178:275–294. doi:10.1006/jtbi.1996.0025. URL http://dx.doi.org/10.1006/jtbi.1996.0025.

[3] Snow M, Snow R (1962) A theory of the regulation of phyllotaxis based on lupinus albus. Philosophical Transactions of the Royal Society of London Series B, Biological Sciences 244:483–513. URL http://links.jstor.org/sici?sici=0080-4622%2819620228%29244%3A717%3C483%3AATOTRO%3E2.0.CO%3B2-0.

[4] Atela P, Golé C, Hotton S (2002) A dynamical system for plant pattern formation: A rigorous analysis. Journal of Nonlinear Science V12:641–676. doi:10.1007/s00332-002-0513-1. URL http://dx.doi.org/10.1007/s00332-002-0513-1.

[5] Shipman PD, Newell AC (2004) Phyllotactic patterns on plants. Physical Review Letters 92:168102+. doi:10.1103/PhysRevLett.92.168102. URL http://dx.doi.org/10.1103/PhysRevLett.92.168102.

[6] Smith R, Kuhlemeier C, Prusinkiewicz P (2006) Inhibition fields for phyllotactic pattern formation: a simulation study. Canadian Journal of Botany 84(11):1635–1649. URL http://rparticle.web-p.cisti.nrc.ca/

rparticle/AbstractTemplateServlet?journal=cjb\&volume=84\&year=\&issue=\&msno=b06-133\&calyLang=eng.

[7] Reinhardt D, Pesce ER, Stieger P, Mandel T, Baltensperger K, et al. (2003) Regulation of phyllotaxis by polar auxin transport. Nature 426:255–260. doi:10.1038/nature02081. URL http://dx.doi.org/10.1038/nature02081.

[8] Vieten A, Sauer M, Brewer PB, Friml J (2007) Molecular and cellular aspects of auxin-transport-mediated development. Trends in Plant Science 12:160–168. doi:10.1016/j.tplants.2007.03.006. URL http://dx.doi.org/10.1016/j.tplants.2007.03.006.

[9] Petrasek J, Mravec J, Bouchard R, Blakeslee JJ, Abas M, et al. (2006) Pin proteins perform a rate-limiting function in cellular auxin efflux. Science 312:914–918. doi:10.1126/science.1123542. URL http://dx.doi.org/10.1126/science.1123542.

[10] Barbier de Reuille P, Courseau BI, Ljung K, Morin H, Carraro N, et al. (2006) Computer simulations reveal novel properties of the cell-cell signaling network at the shoot apex in arabidopsis. PNAS 103:1627–1632. URL http://www-sop.inria.fr/virtualplants/Publications/2006/BBLMCGT06.

[11] Reinhardt D, Kuhlemeier C (2002) Plant architecture. EMBO Rep 3:846–851. doi:10.1093/embo-reports/kvf177. URL http://dx.doi.org/10.1093/embo-reports/kvf177.

[12] Kuhlemeier C (2007) Phyllotaxis. Trends in Plant Science 12:143–150. URL http://www.sciencedirect.com/science/article/B6TD1-4NBY8XG-1/2/dbb9b1ddfe04a1d82e7b4b8e24b34936.

[13] Okada K, Ueda J, Komaki MKK, Bell CJJ, Shimura Y (1991) Requirement of the auxin polar transport system in early stages of arabidopsis floral bud formation. The Plant cell 3:677–684. doi:10.1105/tpc.3.7.677. URL http://dx.doi.org/10.1105/tpc.3.7.677.

[14] Sachs T (1969) Polarity and the induction of organized vascular tissues. Ann Bot 33:263–275. URL http://aob.oxfordjournals.org/cgi/content/abstract/33/2/263.

[15] Mitchison GJ (1980) A model for vein formation in higher plants 207:79–109.

[16] Mitchison GJ (1981) The polar transport of auxin and vein pattern in plants 295:461–471.

[17] Feugier FG, Mochizuki A, Iwasa Y (2005) Self-organization of the vascular system in plant leaves: Inter-dependent dynamics of auxin flux and carrier proteins. Journal of Theoretical Biology 236:366–375. doi:10.1016/j.jtbi.2005.03.017. URL http://dx.doi.org/10.1016/j.jtbi.2005.03.017.

[18] Rolland-Lagan AG, Prusinkiewicz P (2005) Reviewing models of auxin canalization in the context of leaf vein pattern formation in arabidopsis. The Plant Journal 44:854–865. doi:10.1111/j.1365-313X.2005.02581.x. URL http://www.blackwell-synergy.com/doi/abs/10.1111/j.1365-313X.2005.02581.x.

[19] Runions A, Fuhrer M, Lane B, Federl P, Rolland-Lagan AG, et al. (2005) Modeling and visualization of leaf venation patterns. ACM Trans Graph 24:702–711. doi:10.1145/1073204.1073251. URL http://portal.acm.org/citation.cfm?id=1073204.1073251.

[20] Dimitrov P, Zucker SW (2006) A constant production hypothesis guides leaf venation patterning. PNAS 103:9363–9368. doi:10.1073/pnas.0603559103. URL http://dx.doi.org/10.1073/pnas.0603559103.

[21] Scarpella E, Francis P, Berleth T (2004) Stage-specific markers define early steps of procambium development in arabidopsis leaves and correlate termination of vein formation with mesophyll differentiation. Development 131:3445–3455. doi:10.1242/10.1242/dev.01182. URL http://dx.doi.org/10.1242/10.1242/dev.01182.

[22] Scarpella E, Marcos D, Friml J, Berleth T (2006) Control of leaf vascular patterning by

polar auxin transport. Genes Dev 20:1015–1027. doi:10.1101/gad.1402406. URL http://dx.doi.org/10.1101/gad.1402406.

[23] Sauer M, Balla J, Luschnig C, Wisniewska J, Reinohl V, et al. (2006) Canalization of auxin flow by aux/iaa-arf-dependent feedback regulation of pin polarity. Genes Dev 20:2902–2911. doi:10.1101/gad.390806. URL http://dx.doi.org/10.1101/gad.390806.

[24] Jönsson H, Heisler MG, Shapiro BE, Meyerowitz EM, Mjolsness E (2006) An auxin-driven polarized transport model for phyllotaxis. Proc Natl Acad Sci U S A 103:1633–1638. doi:10.1073/pnas.0509839103. URL http://dx.doi.org/10.1073/pnas.0509839103.

[25] Smith RS, Guyomarc'h S, Mandel T, Reinhardt D, Kuhlemeier C, et al. (2006) A plausible model of phyllotaxis. PNAS 103:1301–1306. URL http://www.pnas.org/cgi/content/abstract/103/5/1301.

[26] Merks RM, Van de Peer Y, Inze D, Beemster GT (2007) Canalization without flux sensors: a traveling-wave hypothesis. Trends in Plant Science 12:384–390. doi:10.1016/j.tplants.2007.08.004. URL http://dx.doi.org/10.1016/j.tplants.2007.08.004.

[27] Grieneisen VA, Xu J, Maree AF, Hogeweg P, Scheres B (2007) Auxin transport is sufficient to generate a maximum and gradient guiding root growth. Nature 449:1008–1013. doi:10.1038/nature06215. URL http://dx.doi.org/10.1038/nature06215.

[28] Reinhardt D, Frenz M, Mandel T, Kuhlemeier C (2005) Microsurgical and laser ablation analysis of leaf positioning and dorsoventral patterning in tomato. Development 132:15–26. doi:10.1242/dev.01544. URL http://dx.doi.org/10.1242/dev.01544.

[29] Ljung K, Bhalerao RP, Sandberg G (2001) Sites and homeostatic control of auxin biosynthesis in arabidopsis during vegetative growth. The Plant Journal 28:465–474. doi:10.1046/j.1365-313X.2001.01173.x. URL http://www.blackwell-synergy.com/doi/abs/10.1046/j.1365-313X.2001.01173.x.

[30] Ljung K, Hull AK, Kowalczyk M, Marchant A, Celenza J, et al. (2002) Biosynthesis, conjugation, catabolism and homeostasis of indole-3-acetic acid in arabidopsis thaliana. Plant Molecular Biology 49:249–272. doi:10.1023/A:1015298812300. URL http://dx.doi.org/10.1023/A:1015298812300.

[31] Geldner N, Friml J, Stierhof YD, Jurgens G, Palme K (2001) Auxin transport inhibitors block pin1 cycling and vesicle trafficking. Nature 413:425–428. doi:10.1038/35096571. URL http://dx.doi.org/10.1038/35096571.

[32] Steeves T, Sussex I (1972) Patterns in Plant Development. Englewood Cliffs, New Jersey: Prentice Hall, Inc.

[33] Reddy VG, Heisler MG, Ehrhardt DW, Meyerowitz EM (2004) Real-time lineage analysis reveals oriented cell divisions associated with morphogenesis at the shoot apex of arabidopsis thaliana. Development 131:4225–4237. doi:10.1242/dev.01261. URL http://dx.doi.org/10.1242/dev.01261.

[34] Fujita H, Mochizuki A (2006) Pattern formation of leaf veins by the positive feedback regulation between auxin flow and auxin efflux carrier. J Theor Biol 241:541–551. doi:10.1016/j.jtbi.2005.12.016. URL http://dx.doi.org/10.1016/j.jtbi.2005.12.016.

[35] Kramer EM, Bennett MJ (2006) Auxin transport: a field in flux. Trends in Plant Science 11:382–386. doi:10.1016/j.tplants.2006.06.002. URL http://dx.doi.org/10.1016/j.tplants.2006.06.002.

[36] Nakielski J (2000) Tensorial model for growth and cell division in the shoot apex. In: Carbone A, Gromov M, Prusinkiewicz P, editors, Pattern Formation in Biology, Vision and Dynamics, Signapore: World Scientific Publishing Co. Pte. Ltd. pp. 252–267.

[37] Jones E, Oliphant T, Peterson P (2001). Scipy: Open source scientific tools for python. URL http://www.scipy.org/Citing_SciPy.

[38] Curtiss CF, Hirschfelder JO (1952) Integration of stiff equations. Proceedings of the National Academy of Sciences of the United

States of America 38:235–243. URL http://view.ncbi.nlm.nih.gov/pubmed/16589085.

[39] Pradal C, Boudon F, Nouguier C, Chopard J, Godin C (2007) Plantgl : a python-based geometric library for 3d plant modelling at different scales. Technical report, INRIA.

[40] Heisler, M, Jonsson, H (2006) Modeling auxin transport and plant development. Journal of Plant Growth Regulation 25:302–312. doi: 10.1007/s00344-006-0066-x. URL http://dx.doi.org/10.1007/s00344-006-0066-x.

[41] Swarup R, Kramer EM, Perry P, Knox K, Leyser OHM, et al. (2005) Root gravitropism requires lateral root cap and epidermal cells for transport and response to a mobile auxin signal. Nature Cell Biology 7:1057–1065. doi: 10.1038/ncb1316. URL http://dx.doi.org/10.1038/ncb1316.

[42] Bainbridge K, Guyomarc'h S, Bayer E, Swarup R, Bennett M, et al. (2008) Auxin influx carriers stabilize phyllotactic patterning. Genes Dev 22:810–823. doi:10.1101/gad.462608. URL http://dx.doi.org/10.1101/gad.462608.

Supplementary materials

1 Simulation overview

1.1 Conventions

Notations: In the equations describing changes in PIN and auxin concentrations we use the Iverson notation [1, 2]: if ψ denotes a logic statement then,

$$[\psi] = \begin{cases} 1 & \text{if } \psi \text{ is True} \\ 0 & \text{otherwise} \end{cases}$$

Supplementary movies: For each figure demonstrating a system changing in time, a movie showing the process dynamics is provided. These movies are named after the Figures with supplementary letter "S" at the beginning (eg. the movie corresponding to Figure 2B is called "`SMovie2B.avi`").

PIN display conventions: The thickness of the line representing the PIN accumulation in cell membranes is proportional to the computed PIN concentration in this membrane. However, high values are truncated to allow better inspection of visual results. The minimal displayed value of PIN concentration is always equal to α_p/β_p, whereas the higher value corresponds to the maximum displayed concentration of PIN, which is $2\alpha_p/\beta_p$. All values of PIN exceeding this value are capped to $2\alpha_p/\beta_p$, allowing a ratio of 200% between extreme values.

Auxin display conventions: Auxin concentrations below minimal (resp. above maximal) threshold a_{min} (resp. a_{max}) are depicted in black $RGB(0,0,0)$ (resp. in green $RGB(0,255,0)$). Intermediate values of auxin concentrations are depicted with a double linear interpolation function: a percentage p_{mid} of the visible auxin range $[a_{max}, a_{min}]$ defines the auxin concentration $a_m$for which the colour should be intermediate $RGB(0,127,0)$. Colours are then linearly interpolated between a_{min} and a_m and a_m and a_{max} respectively to render the colour of any auxin concentration within the interval $[a_{max}, a_{min}]$. Values for parameters p_{mid}, a_{max}, a_{min} are defined for each simulation in table 1.

Integration: The number of snapshots was specified for each simulation. For each simulation a number of steps is also given. This number is used to integrate the system with given, fixed step h between taking a snapshot. For some simulations the number of steps may vary if we target in having a quasi stable state between the snapshots (eg. phyllotaxy simulation). A stable state is reached when the change in IAA concentrations in every cell becomes less than

a predefined threshold value ϵ_{min} (using L_∞ norm). In such a case the time interval between each snapshot may be different. If it is the case it is specified in the simulation details.

At each step a non-linear system of equations describing the canalization process is integrated using the SciPy package designed for ODE solving [3]. This package wraps ODE PACK, which is a collection of Fortran solvers for the initial value problem for ordinary differential equation systems [4]. The collection is suitable for both stiff and non-stiff systems of the form $dy/dt = f(t, y)$ where y is a vector. For solving the equation system, the LSODE (Livermore Solver for Ordinary Differential Equations) solver is used. It uses Adams methods (predictor-corrector) in the non-stiff case, and Backward Differentiation Formula (BDF) methods in the stiff case [5]. All linear systems that arise are solved by direct methods (LU factor/solve). As mentioned before, solver iterations are performed i) until a stable state is obtained ii) for fixed number of steps. The precision values for the algorithm LSODE are set to be 10 times smaller than ϵ_{min} ($rtol = atol = 0.1\epsilon_{min}$), which determines the number of sub-steps taken by solver.

2 Simulations

2.1 The basic system of equations

The basic system of equations equations, which we use in the simulations are defined as in the article:

$$\frac{\partial a_i}{\partial t} = -\sum_{n \in N,} \frac{S_{i \to n}}{V_i} J_{i \to n} + \alpha_a - \beta_a a_i \tag{1}$$

$$\frac{\partial p_{i,n}}{\partial t} = \Phi\left(J_{i \to n}\right) + \alpha_p - \beta_p p_{i,n} \tag{2}$$

$$J_{i \to n} = \gamma_a \left(a_i p_{i,n} - a_n p_{n,i}\right) + \gamma_d \left(a_i - a_n\right) \tag{3}$$

$$\Phi_L(x) = \begin{cases} \kappa x & x \geq 0 \\ 0 & x < 0 \end{cases} \tag{4}$$

$$\Phi_C(x) = \begin{cases} \kappa x^2 & x \geq 0 \\ 0 & x < 0 \end{cases} \tag{5}$$

In the forthcoming sections we report which basic equation is used and which is modified for a particular simulation. The parameters for the system can be found in the supplementary Table 1 .

2.2 Figure 1A

Specification: The cells which belong to Si were selected as described in the main article. The simulation was run for fixed amount of steps. The system reached the stability before the last step.

Model: We use equations 2 , 4 , we redefine 1 , 3 :

$$\frac{\partial a_i}{\partial t} = \left(- \sum_{n \in N_i} J_{i \to n} + \alpha_a - \beta_a a_i \right) [i \notin Si]$$

$$J_{i \to n} = \gamma_a \left(a_i p_{i,n} - a_n p_{n,i} \right),$$

where $\Phi = \Phi_L$.

2.3 Figure 1B

Model: The simulation differs from 2.2 only by modifying equation 1 in the following way:

$$\frac{\partial c_i}{\partial t} = - \sum_{n \in N_i} J_{i \to n} + \alpha_a - \left(\beta_a + \beta'_a [i \notin Si] \right) c_i$$

All the parameters are exactly the same and can be found in the Table 1 .

2.4 Figure 2A

Specification: The cells which belong to Si were selected and the simulation was run for fixed amount of steps. The system reached the stability before the last step.

Model: We use equations 2 , 3 , 4 , we redefine 1 :

$$\frac{\partial a_i}{\partial t} = \left(- \sum_{n \in N_i} J_{i \to n} + \alpha_a - \beta_a a_i \right) [i \notin Si]$$

And we assume that $\Phi = \Phi_L$

2.5 Figure 2B

Specification: The cells which belong to Si were selected and the simulation was run for fixed amount of steps. The system was stable after the last step. The figure presented in the text is not the last step of the simulation. The system still develops and creates more complex vein pattern (with loops). This evolution can be observed on the supporting movie.

Model: We use equations 2 , 3 , 5 , we redefine 1 :

$$\frac{\partial a_i}{\partial t} = \left(- \sum_{n \in N_i} J_{i \to n} + \alpha_a - \beta_a a_i \right) [i \notin Si]$$

And we assume that $\Phi = \Phi_C$.

2.6 Figure 3A-3D

Model: We use equations 2 , 3 , 4 , we redefine 1 :

$$\frac{\partial a_i}{\partial t} = \left(- \sum_{n \in N_i} J_{i \to n} + \alpha_a - \beta_a a_i \right) [i \notin Si]$$

And we assume that $\Phi = \Phi_L$.

2.7 Figure 4A-4F

Model: We use equations 2 , 3 , 4 , we redefine 1 :

$$\frac{\partial a_i}{\partial t} = \left(- \sum_{n \in N_i} J_{i \to n} + \alpha_a - \beta_a a_i \right) [i \notin Pr]$$

And we assume that $\Phi = \Phi_L$.

2.8 Figure 6A-D

Specification: The simulation was run in two variants: with and without a centre. In case of "with centre" simulation a subset of cells which belong to Cz was chosen. These cells were destroying the auxin. The initial geometry of cells was acquired from con-focal images. The simulation was run for 60 steps. It reached a stable state with a visible maximum of auxin formed in the place of the future initium. Then the initium was inserted and the simulation was run for additional 60 steps.

Model: We use equations 2 , 3 , 4 , we redefine 1 :

$$\frac{\partial a_i}{\partial t} = \left(- \sum_{n \in N_i} \frac{S_{i \to n}}{V_i} J_{i \to n} + \alpha_a - \left(\beta_a + \beta'_a \left[i \notin Cz \right] \right) a_i \right) \left[i \notin Pr \right]$$

And we assume that $\Phi = \Phi_L$.

2.9 Figure 8A-8E

Specification: To simulate the influence of old primordia, each removed primordium was tagging a closest neighbour cell with a special cell identity, "annealing primordium". This property was propagated over a given time. The cells tagged with "annealing primordium" identity were acting as sinks but the sink strength was gradually decreasing with time. These cells are tagged with yellow dots.

Model: We use equations 2 , 3 , 4 , we redefine 1 :

$$\frac{\partial a_i}{\partial t} = \left(- \sum_{n \in N_i} \frac{S_{i \to n}}{V_i} J_{i \to n} + \alpha_a - \left(\beta_a + \beta'_a \left[i \notin Cz \right] \right) a_i \right) \left[i \notin Pr \right]$$

And we assume that $\Phi = \Phi_L$.

2.10 Figure 8G-8I

Specification: Cells with white dots are simulating sinks and they belong to Si, cells with black dots are L1 cells and they belong to $L1$, the cell with blue dot is a new primordium and it belongs to Pr set (and $L1$ as well). We assume that the L1 cells are separated from the inside cells except for the primordium cell. This cell is allowed to exchange the auxin with both L1 and inner cells. The feedback from flux on PIN polarisation in L1 and and inner cells is different and it is modelled with a change in Φ function. Also, the cells in L1 layer produce much more auxin auxin than inner layer cells.

Model: We use equations 3 , 4 , 5 we redefine 1 , 2 :

For cells i such as $i \in L1$:

$$\frac{\partial a_i}{\partial t} = \left(- \sum_{n \in N_i} \frac{S_{i \to n}}{V_i} J_{i \to n} \left[n \in L1 \vee i \in Pr \right] + (\alpha_a + \alpha_{L1}) - \beta_a a_i \right) \left[i \notin Si \right]$$

$$\frac{\partial p_{i,j}}{\partial t} = \Phi_L \left(J_{i \to j} \right) \left[j \in L1 \right] + \Phi_L \left(J_{i \to j} \right) \left[j \notin L1 \right] + \alpha_p - \beta_p p_{i,j}$$

For cells i such as $i \notin L1$:

$$\frac{\partial a_i}{\partial t} = \left(- \sum_{n \in N_i} \frac{S_{i \to n}}{V_i} J_{i \to n} \left[n \notin L1 \vee i \in Pr \right] + \alpha_a - \beta_a a_i \right) \left[i \notin Si \right]$$

$$\frac{\partial p_{i,j}}{\partial t} = \Phi_C \left(J_{i \to j} \right) + \alpha_p - \beta_p p_{i,j}$$

Parameters: $\alpha_{L1} = 0.3$

2.11 Figure 9C

Specification: The simulation was run until the system reached a stable state. In this state an auxin maximum was established in the root apex. The fact that some parameters strongly differ from those used in previous simulations is due

to specific structural choices of the root model (eg. PIN and auxin constrained to a $[0, 1]$ range).

We use equations 3 , 2 , 5 we redefine 1 :

$$\frac{\partial a_i}{\partial t} = \left(- \sum_{n \in N_i} \frac{S_{i \to n}}{V_i} J_{i \to n} + \alpha_a - \beta_a a_i \right) [i \notin Si]$$

And we assume that $\Phi = \Phi_C$.

Initial conditions: $\forall i \notin Si.a_i = 0.3; \forall i \in Si.a_i = 0.0; p_{i.j} = 1.0 if\ PIN\ exists in\ vivo\ else\ 0$

References

[1] Iverson KE (1962) A Programming Language.1. John Wiley & Sons. URL `http://www.amazon.ca/exec/obidos/redirect?tag=citeulike09-20%&path=ASIN/0471430145`.

[2] Knuth DE (1992) Two notes on notation. Am Math Monthly 99:403–422. doi:10.2307/2325085. URL `http://portal.acm.org/citation.cfm?id=151009`.

[3] Jones E, Oliphant T, Peterson P (2001). Scipy: Open source scientific tools for python. URL `http://www.scipy.org/Citing_SciPy`.

[4] Hindmarsh AC (1983) ODEPACK, A Systematized Collection of ODE Solvers , R. S. Stepleman et al. (eds.), North-Holland, Amsterdam, (vol. 1 of), pp. 55-64., volume 1 of *IMACS Transactions on Scientific Computation*. North-Holland Amsterdam, 55–64 pp.

[5] Curtiss CF, Hirschfelder JO (1952) Integration of stiff equations. Proceedings of the National Academy of Sciences of the United States of America 38:235–243. URL `http://view.ncbi.nlm.nih.gov/pubmed/16589085`.

Parameter	1A	1B	2A	2B	3A-D	4A-F	6A-D	8A-E	8G-I	9C
α_a	0.1	0.1	0.1	0.1	0.1	0.1	0.1	0.3	0.01*	0.0
β_a	0.01	0.01	0.01	0.01	0 01	0 01	0.01	0.03	0.01	0.0
β'_a	-	0.1	-	-	-	-	-/0.08	0.06	-	-
α_p	0.1	0.1	0.1	0.1	0.1	0.1	0.1	0.1	0.1	0.0
β_p	0 05	0 05	0.01	0.01	0.01	0.05	0.01	0.01	0.01	0.5
γ_a	0.1	0 1	0.1	0.1	0.1	0.1	0.1	0.125	0.1	100.0
γ_d	-	-	0.03	0.03	0.03	0.001	0.03	0 03	0.03	0.001
Φ	L	L	L	C	L	L	L	L	L+C	C
κ_L	0.15	0.15	0.2	-	1.3/1 5/1.7/2.0	0.15	0 18	0.11	0.09	-
κ_C	-	-	-	1.3	-	-	-	-	1.1	0.2
h	2 2	2.2	1 0	0.025	1.0	1.0	0.25	1.0	1.0	0.1
ϵ_0	-	-	-	-	-	0.01	-	0.01	-	-
init a_i	0 0	0.0	0.0	0.0	0.0	0 0	0.0	0.0	0.0	0.3
init $p_{i,j}$	$\frac{\alpha_p}{\beta_p}$	$\frac{\alpha_p}{\beta_p}$	$\frac{\alpha_p}{\beta_p}$	$\frac{\alpha_p}{\beta_p}$	$\frac{\alpha_p}{\beta_p}$	$\frac{\alpha_p}{\beta_p}$	$\frac{\alpha_p}{\beta_p}$	$\frac{\alpha_p}{\beta_p}$	$\frac{\alpha_p}{\beta_p}$	*
PIN max	-	-	2.0	1.0	2.0	-	2.0	2.0	2.0	1.0
snapshots	100	100	60	240	120	400	60 + 60*	*	30 + 80*	2500
steps	100	100	10	400	10	-	10	-	10	10
$[a_{min}, a_{max}]$	-	-	[0, 5]	[0, 5]	[0, 5]	-	[0. 4.8]	[0. 6.8]	[0, 12]	[0. 1]
p_{mid}	-	-	0.94	0.94	0 94	-	0.9	0.7	0 6	0.5

Tab. 1: The simulation parameters. The "*" is used when the parameter is changed in complex way (which is explained in details in the text), the "/" means alternative values used in simulation and "-" means that the value is not included in the experiment equations. The units for the parameters were specified in the main article.

- PART V –
Conclusions & Perspectives

" *root: the all powerful administrative user, bearing absolute system control.* "

The Linux Information Project

It is of interesting note that roots, the most hidden part of plants, have become a symbol of uttermost importance in the world of computer science.

Roots have played a capital role in the conquest of emerged lands by plants, offering them support and anchorage. In our society, roots have since become synonymous of strong attachment to place, time or people.

Here we have tried to shed some light on these organs growing in darkness using the model plant *Arabidopsis*. We were able to show that the ramification of the root system is intimately linked with the perception of gravity. Both initiation and emergence of new lateral roots are enhanced by changes in gravity, and we found that auxin plays an important role in this link.

We also demonstrated that initiation and emergence of new lateral roots are not random processes, and obey intrinsic developmental rules. By mean of observation and statistics, we isolated some of the specific properties arising from these rules. We postulated that these rules could be auxin-based, and proposed an integrative model of ramification based on inhibitory field concepts, drawing a parallel between root ramification and shoot phyllotaxis (Figure 46). Where the phyllotaxis of the stem depends on the ratio between the size of the competence zone and the size of inhibitory fields, the global architecture of the root will depend on the inhibitory effect of developing primordia in regard to the cost of initiation of new primordia. While allowing for a high level of variability, this process may well merit the name "rhizotaxis", for it apparently depends on the same mechanisms as phyllotaxis.

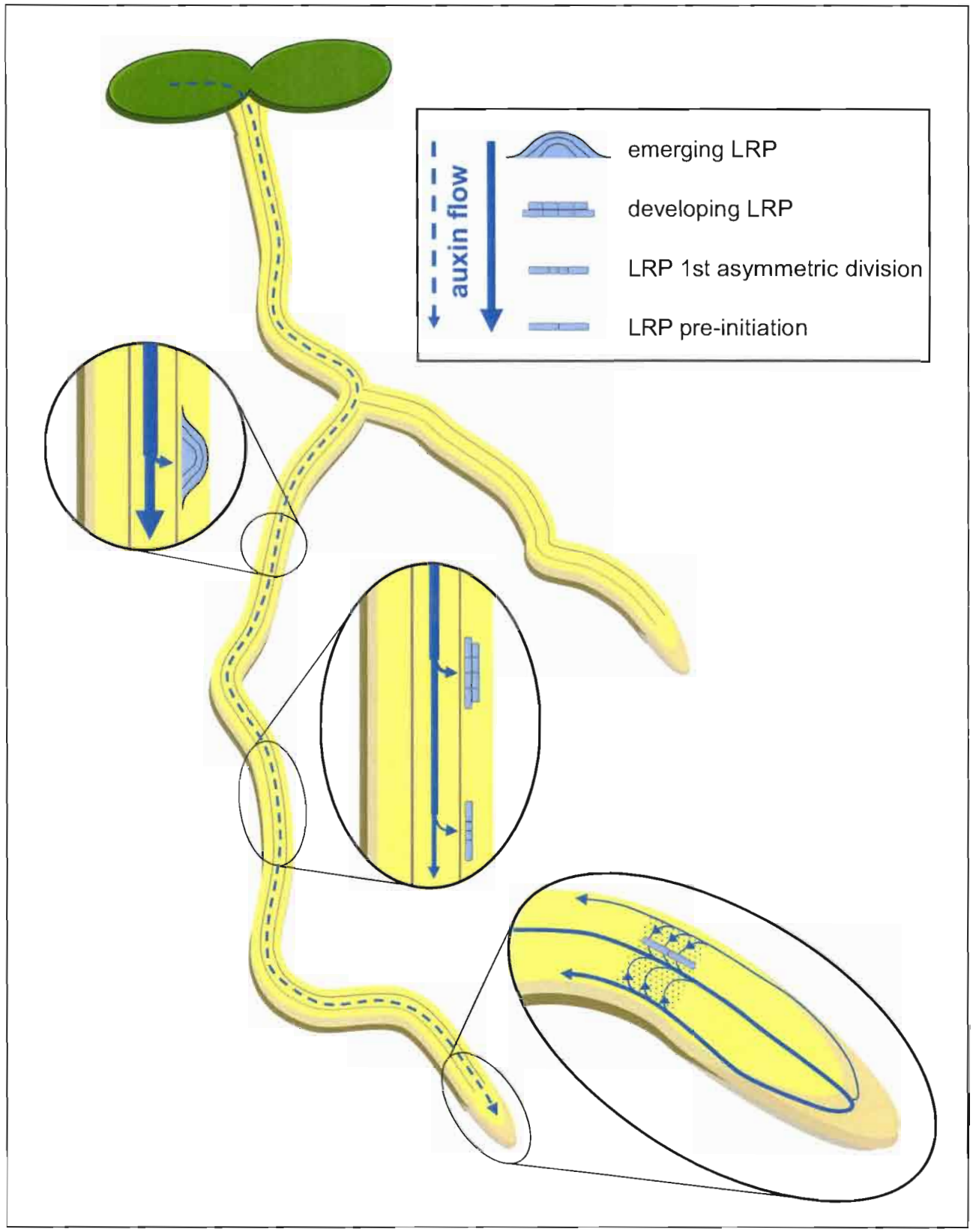

Figure 46. An integrated view of root ramification

We propose that auxin coming from the aerial parts regulates the development and emergence of primordia along the roots, and that the remaining auxin take part in a reflux at the root apex, where it will regulate the initiation of new primordia. The competition for resources between developing primordia and the initiation system at the root apex will determine the final architecture of the whole system.

The precise nature of initiation control by the reflux system and its interaction with graviperception are still unclear.

We initiated a multiscale modelling approach, considering the development of the root system either at a macroscopic or cellular level. The models we designed were invaluable tools to ponder on biological issues that were left in the dark at the time. There are still a lot of black-boxes left however, such as the mechanisms of transition from vascular auxin transport in the phloem to active auxin transport into the root tip, or the precise extent of symplastic territories allowing auxin to diffuse directly from cell to cell.

The subject of root ramification regulation itself is far from being a closed topic too, as auxin is not the only player on this specific field. Others hormones such as cytokinins (Nordström et al. 2004; Laplaze et al. 2007; Kuderová et al. 2008; Zhao 2008) or ethylene (Ivanchenko, Gloria K Muday, and Joseph G Dubrovsky 2008; Negi, Ivanchenko, and Gloria K Muday 2008) and molecules such as flavonoids (Murphy, Peer, and Taiz 2000; Brown et al. 2001; Besseau et al. 2007) also play a role in root development, if only by interacting with auxin fluxes and auxin signaling.

Circadian rhythm also appears to affect the regulation of auxin fluxes and auxin response (Salisbury et al. 2007; Covington and Harmer 2007). More generally speaking, variation in auxin sensitivity and response has not yet been fully investigated at the cellular level, and may prove to be a critical factor in the mechanisms controlling lateral root primordia initiation.

Another factor we have not taken into consideration here is the existence of long-distance exchanges and synchronisms between the shoot and root systems (Costes et al. 2006). Indeed, the aerial part of the plant is the main source of auxin and photoassimilates essential for root development, while the root system is the source of water and nutrient essential for shoot development.

Hence both parts of the plant need to develop in a closely coordinated fashion. Further biological investigation will be needed to elucidate the details of shoot/root interactions and synchronisms.

"There are two lasting bequests we can give our children. One is roots. The other is wings."

Hodding Carter Jr.

We wish here to propose a possible pursuit for our work.

We have the intimate conviction that the next step in understanding plant development will come from the unification of shoot and root studies, for the plant organism should be considered as a whole. As it would appear inadequate for a zoologist to study half a dog, so should studying half a plant appear inadequate for a botanist.

On the basis of what has been presented here, we consider it important to direct future studies toward the interaction existing between the aerial and underground organs of plants. Experimental strategies should be designed to evaluate the synchronism between leaf and root emergence, using the available quantification tools to establish the timeline of auxin fluxes and exchanges between these organs. Perturbation of these exchanges might be considered as a hypotheses validation process, be it from the use of mutants, chemical compounds altering hormones fluxes, or any others means. Multiscale computer models would be an asset for this investigation; provided that they incorporate dynamics of sources and sinks interaction to account for observed mechanisms.

Only through such dual approach combining biological experimentation and modelling can we eventually hope to one day create the seeds and blooms of true virtual plants. And shall we be always wary of the inevitable thorns.

APPENDIXES

APPENDIX 1

Parts of our work were presented as oral communications and as a poster during international congresses. The corresponding abstracts are gathered in this appendix and presented as they were submitted and accepted.

The first abstract was submitted and accepted for the 5th Functional Structural Plant Model Congress (FSPM07), held in Napier, New Zealand, from the 4th to the 10th of November, 2007. In this communication, we presented our macroscopic and microscopic models of root development. The file used for the presentation and the complete proceedings are available are available in the DVD joined to this manuscript, under the /communication/oral_communication/ FSPM07 directory.

The second abstract was submitted and accepted for the 1st Advanced Workshop on the Understanding and Modelling of Auxin Transport in Plants, held in Nottingham, United Kingdom, from the 14th to the 16th of May, 2008. In this communication, we presented the principles governing cellular model of auxin fluxes and the results we obtained on the topic of auxin transporter dynamics. The file used for the presentation is available in the DVD, under the /communication/oral_communication/Nottingham08 directory.

The poster was submitted and accepted for the Agronomics Workshop on Growth Phenotyping and Imaging in Plants, held in Montpellier, France, from the 17th to the 19th of July, 2007. In this poster, we presented the results we obtained concerning gravistimulation and lateral root initiation (Part II of this manuscript). The poster .tiff image is also available in the DVD, under the /communication/poster/ directory.

Modelling auxin fluxes and *Arabidopsis* root ramification at different scales

Mikaël LUCAS[1,2], Laurent LAPLAZE[1], Christian JAY-ALLEMAND[1], Christophe GODIN[2]

[1] Equipe Rhizogènese, UMR DIA-PC (Agro.M/INRA/IRD/UMII), Institut de Recherche pour le Développement (IRD), 911 Avenue Agropolis, 34394 Montpellier Cedex 5, France

[2] Equipe VirtualPlants (INRIA/CIRAD/INRA), UMR DAP - Développement et Amélioration des Plantes, TA40/02, Cirad, Avenue Agropolis, 34398 MONTPELLIER CEDEX 5, France

Keywords: *Arabidopsis*, auxin transport, root development, lateral root initiation

Introduction

Plant primary growth occurs in two opposite directions, stems and roots both generating branched patterns during their development. However, where stem development appears extremely regular, based on phyllotactic patterns, root architecture appears somewhat random, controlled essentially by external clues such as nutrients concentration (Malamy et al. 2005).

The regularity of stem development has been ground to a large panel of pure mathematical and physical modelling (Adler et al. 1997). By contrast, the apparent chaos of root development has essentially directed the modelling effort toward ecophysiological and environmentally constrained models (Doussan et al. 2003).

Yet, as the biological knowledge of development and the available microscopy tools evolves, mathematicians and computer scientists are now able to glimpse at the cellular level of development. They can create new models taking into account previously ignored mechanisms and giving rise to new perception on ancient problems, as described by Barbier de Reuille et al. (2006), Jönsson et al. (2006), and Smith et al. (2006) on the topic of phyllotaxis.

Until recently, root systems development was considered too chaotic to be modeled on the same basis as shoot development. However, recent biological results suggest that lateral root initiation (LRI), main determinant of root architecture, may itself be more regular than first supposed (Dubrovsky et al. 2000; Dubrovsky et al. 2006; De Smet et al. 2007; Lucas et al. 2007). Global root architecture now appears as the superposition of regular LRI and irregular emergence, the latter phenomenon being more strongly subjected to environmental conditions.

As LRI and root development both depend on complex auxin fluxes and genetic interactions, we used a modelling approach to integrate the large biological knowledge available on root development and the complexity of flux dynamics. The models we choose to develop address the control of LRI by auxin fluxes. Our aim was to test various hypotheses concerning LRI regularity and the positioning of root primordia.

Modeling root development and auxin fluxes

Auxin fluxes occurring during root development can be considered at the macroscopic (tissue level) or microscopic (cellular level) scales. We will here distinguish between two kinds of models we developed, each aiming to reproduce the fluxes at one of those two levels.

The first kind of model is centered on the whole root. It is geared toward a representation of the whole developmental sequence, and well adapted to treat the problem of the regularity and distribution of LRI. The spatial representation of the root

in this model can be considered as almost linear. The main computational topic of this model is one of competition and transport within a dynamic system based upon a dynamic structure, also known as $(DS)^2$. The principal advantage of this model is the ultimate possibility to generate LRI distribution to be compared with LRI distribution observed *in vivo*. We addressed the inherent lack of precision on the positioning of LRI at the microscopic scale by developing our second model.

Based on the cellular structure of a single root slice, the second model is geared towards the simulation of cellular auxin fluxes dynamics. This approach is similar to the one currently applied to stem apical meristem modelling (Barbier de Reuille et al. 2006). The cellular structure of the root slice is here represented as a static graph taking into account each cell and its cell wall. The main computational topic associated with this kind of model is the complex flux dynamics and the study of its stability. This model has the advantage to allow us to test various hypotheses concerning the precise positioning of root primordia, and to experiment *in silico* on the consequences of auxin fluxes perturbation on initiation. It is however static, and as such can only be used to simulate a snapshot of the auxin accumulation points during root development.

Results

The large scale model was developed based on L-System. Biological studies indicates that LRI is caused by basipetal auxin fluxes, flowing back from the apical root meristem along the lateral root cap, and that primordia development and lateral root emergence are caused by acropetal auxin fluxes coming from the aerial parts (Casimiro et al. 2001; Bhalerao et al. 2002). We introduced those two fluxes in our model as well as auxin production in the aerial parts and at the apex. We were able to generate auxin accumulation at the root apex under certain conditions, and to test which parameters influence this accumulation, as well as other characteristics of the fluxes (fig. 1).

Introducing LRI in the model proved to be problematic, as little was known of the precise dynamic of auxin fluxes which take place above the root apical meristem and are responsible for initiation. We proceeded to a thorough structural analysis of LRI. We showed that LRI appears tightly co-regulated with gravitropism in *Arabidopsis*, as the mechanisms controlling those two phenomena involve a common auxin transport route (Lucas et al. 2007). We suggested that observed LRI regularities may in fact be linked to the periodical nature of gravitropic and thigmotropic responses.

We integrated those results in the fine scale model, as well as known dynamics of auxin fluxes in root tissue whenever such data was available (Friml et al. 2002; Blilou et al. 2005; Swarup et al. 2005; Sauer et al. 2006; Fukaki et al. 2007) (see fig. 2 for an example of flux dynamics). To palliate for the lack or imprecision of data concerning some tissues, we implemented in our model rules for PIN dynamics such as those described in Feugier et al. (2005, 2006), Jönsson et al. (2006) and Smith et al. (2006).

We will insist in our talk on the cellular modeling approach and on the associated problems. One of the main topics we will address is how to account for the observed inconsistency between the positions of the gravitropic responsive tissues and the lateral root primodium. Indeed, the auxin maximum causing the gravitropic response in the epidermis appears on the inside of root turns, whereas LRI always takes place on the outside of root turns, where one would expect the lowest auxin level. We will present one hypothesis to explain this paradox and the results of its implementation in our model. We will also discuss of the potential evolution of the cellular model toward a $(DS)^2$ model.

References

Adler I, Barabe D, Jean RV. 1997. A History of the Study of Phyllotaxis. *Annals of Botany* **80**, 231-244

Bhalerao RP, Eklöf J, Ljung K, Marchant A, Bennett MJ, Sandberg G. 2002. Shoot-derived auxin is essential for early lateral root emergence in Arabidopsis seedlings. *The Plant Journal* **29**, 325-332

Blilou I, Xu J, Wildwater M, Willemsen V, Paponov I, Friml J, Heidstra R, Aida M, Palme K, Scheres B. 2005. The PIN auxin efflux facilitator network controls growth and patterning in Arabidopsis roots. *Nature* **433**, 39-44

Casimiro I, Marchant A, Bhalerao RP, Beeckman T, Dhooge S, Swarup R, Graham N, Inzé D, Sandberg G, et al.. 2001. Auxin transport promotes Arabidopsis lateral root initiation. *The Plant Cell* **13**, 843-852

Barbier de Reuille P, Bohn-Courseau I, Ljung K, Morin H, Carraro N, Godin C, Traas J. 2006. Computer simulations reveal novel properties of the cell-cell signaling network at the shoot apex in *Arabidopsis*. *PNAS* **103**, 1627-1632.

De Smet I, Tetsumura T, De Rybel B, Frei Dit Frey N, Laplaze L, Casimiro I, Swarup R, Naudts M, Vanneste S, et al.. 2007. Auxin-dependent regulation of lateral root positioning in the basal meristem of Arabidopsis. *Development* **134**, 681-690

Dubrovsky JG, Doerner PW, Colón-Carmona A, Rost TL. 2000. Pericycle cell proliferation and lateral root initiation in Arabidopsis. *Plant Physiology* **124**, 1648-1657

Dubrovsky JG, Gambetta GA, Hernández-Barrera A, Shishkova S, González I. 2006. Lateral Root Initiation in Arabidopsis: Developmental Window, Spatial Patterning, Density and Predictability. *Annals of Botany (Lond)* **97**, 903-915

Feugier FG, Mochizuki A, Iwasa Y. 2005. Self-organization of the vascular system in plant leaves: inter-dependent dynamics of auxin flux and carrier proteins. *J Theor Biol.* **236**, 366-75

Feugier FG, Iwasa Y. 2006. How canalization can make loops: A new model of reticulated leaf vascular pattern formation. *J Theor Biol.* **243**, 235-244

Friml J, Wiśniewska J, Benková E, Mendgen K, Palme K. 2002. Lateral relocation of auxin efflux regulator PIN3 mediates tropism in Arabidopsis. *Nature* **415**, 806-809

Fukaki H, Okushima Y, and Tasaka M. 2007. Auxin-Mediated Lateral Root Formation in Higher Plants. *International Review of Cytology* **256**, 113-137

Jönsson H, Heisler MG, Shapiro BE, Meyerowitz EM, Mjolsness E. 2006. An auxin-driven polarized transport model for phyllotaxis. *PNAS* **103**, 1633-1638

Lucas M, Godin C, Jay-Allemand C, Laplaze L. 2007. Auxin fluxes in the root apex co-regulate gravitropism and lateral root initiation. Submitted to Journal of Experimental botany.

Malamy JE. 2005. Intrinsic and environmental response pathways that regulate root system architecture. *Plant Cell Environment* **28,** 67-77

Doussan C, Pages L, Pierret A. 2003. Soil exploration and resource acquisition by plant roots: an architectural and modelling point of view. *Agronomie* **23,** 419-431

Sauer M, Balla J, Luschnig C, Wisniewska J, Reinöhl V, Friml J, Benková E. 2006. Canalization of auxin flow by Aux/IAA-ARF-dependent feedback regulation of PIN polarity. *Genes & Develpment* **20,** 2902-2911

Smith RS, Guyomarc'h S, Mandel T, Reinhardt D, Kuhlemeier C, Prusinkiewicz P. 2006. A plausible model of phyllotaxis. *PNAS* **103,** 1301-1306

Swarup R, Kramer EM, Perry P, Knox K, Leyser HM, Haseloff J, Beemster GT, Bhalerao R, Bennett MJ. 2005. Root gravitropism requires lateral root cap and epidermal cells for transport and response to a mobile auxin signal. *Nature Cell Biology* **7,** 1057-1065

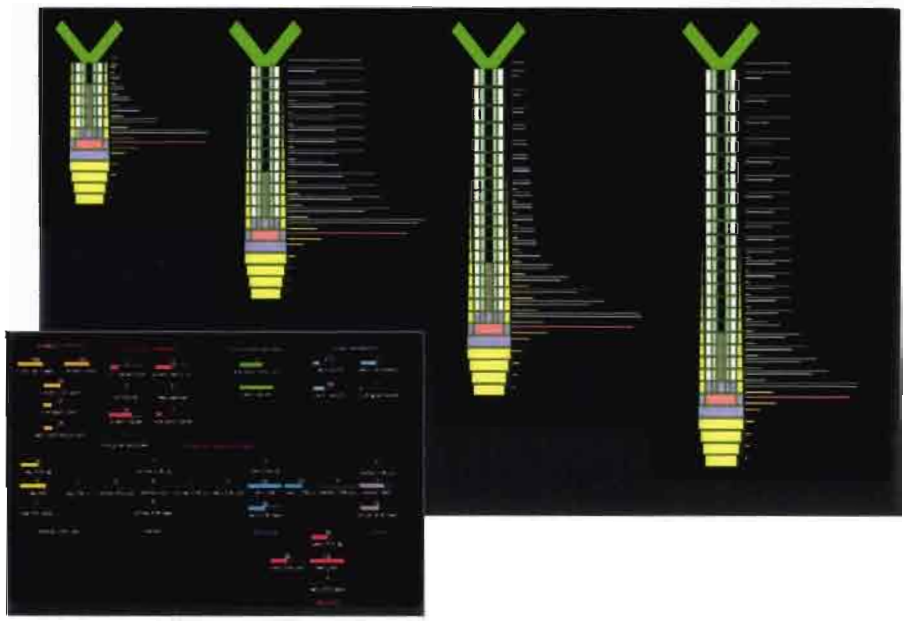

Figure 1.
L-System based model of auxin fluxes in a growing root

Global auxin fluxes are the synthesis between cell wall diffusion, cell/cell diffusion, active transport and convection of auxin.

Auxin production takes place in the aerial part and at the root apex.

The control panel on the bottom left show the various parameters that can be changed to challenge the stability of the model.

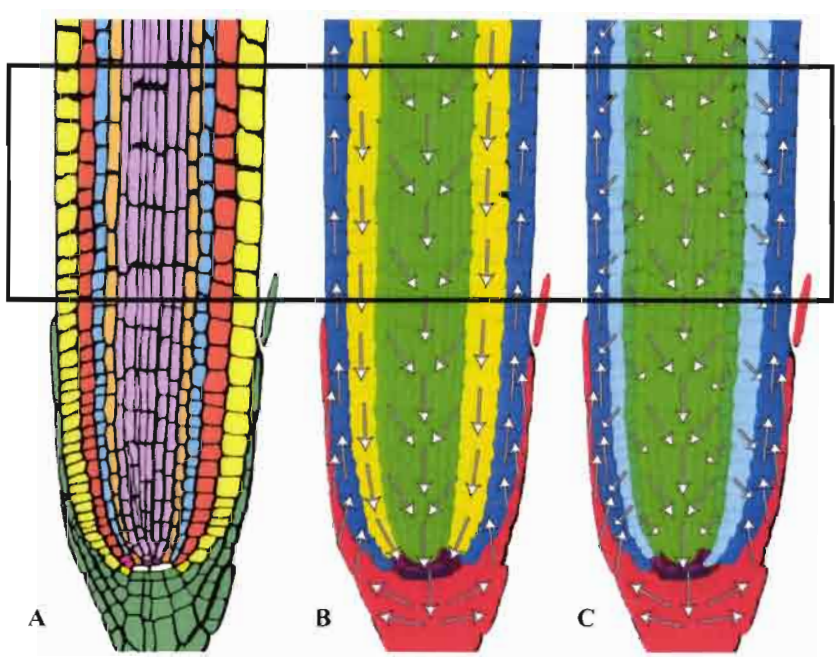

Figure 2.
Dynamic of auxin fluxes in root tissues

A. Root superstructure. Each colour identifies a specific tissue.

B. Global auxin fluxes. Tissues are grouped under a new common colour when they direct the flux along a common path.

C. Changes in auxin fluxes patterns during an exogenous auxin application. Tissues react according different rules, creating divergent auxin paths and isolating inner tissues from auxin present in outer tissues.

The black border define the size and position of the root slice considered in the fine scale model.

Cellular Model of Auxin Fluxes and Lateral Root Initiation in *Arabidopsis*

- session 1 : Root Growth and Development -

Mikaël LUCAS[1,2], Jérome CHOPARD[2], Laurent LAPLAZE[1], Christian JAY-ALLEMAND[1], Christophe GODIN[2]

[1] Equipe Rhizogènese, UMR DIA-PC (Agro.M/INRA/IRD/UMII), Institut de Recherche pour le Développement (IRD), 911 Avenue Agropolis, 34394 Montpellier Cedex 5, France

[2] Equipe VirtualPlants (INRIA/CIRAD/INRA), UMR DAP - Développement et Amélioration des Plantes, TA40/02, Cirad, Avenue Agropolis, 34398 MONTPELLIER CEDEX 5, France

Keywords: *Arabidopsis*, auxin flux, root development, lateral root initiation

Study of plant development and growth is a fructuous field. In order to integrate biological data, a numbers of high-level conceptual models have been formulated through time, such as the ABC-model of floral development or inhibitory-field driven phyllotaxis[(1)]. However, as biological knowledge is refined and experimental data accumulate to the point of being sometime inextricable, more mechanistic models are becoming both a possibility, and a need.

Computer models of auxin fluxes are prime examples of such a mechanistic modelling approach, seeking to integrate and explain mechanisms behind complex phenomena such as phyllotaxis[(2,3,4)], vein patterning[(5,6,7)], or gravitropic root reorientation[(8)].

We propose here to explain through modelling the role of auxin fluxes in root ramification. Our model is geared towards the simulation of cellular auxin fluxes within

the root tip of *Arabidopsis thaliana*. The cellular structure of the root apex is represented as a digitized static graph taking into account each cell, its cell wall and auxin transporters. The dynamic of the transporters themselves is also taken into account.

We will present the advantages and issues associated with this cellular modelling approach and the results it yielded. We will show how far this type of model explains lateral root primordia positioning, how it allows to experiment *in silico* on the consequences of auxin fluxes perturbation, and which auxin transporters dynamics allow simulation to fit with observations. As a perspective, we will discuss the various computational and biological obstacles which will need to be addressed in order to develop fully dynamic cellular models.

References

1 - Adler I, Barabe D, Jean RV. 1997. A History of the Study of Phyllotaxis. *Annals of Botany* **80**, 231-244

2 - Barbier de Reuille P, Bohn-Courseau I, Ljung K, Morin H, Carraro N, Godin C, Traas J. 2006. Computer simulations reveal novel properties of the cell-cell signaling network at the shoot apex in *Arabidopsis*. *PNAS* **103**, 1627-1632.

3 - Jönsson H, Heisler MG, Shapiro BE, Meyerowitz EM, Mjolsness E. 2006. An auxin-driven polarized transport model for phyllotaxis. *PNAS* **103**, 1633-1638

4 - Smith RS, Guyomarc'h S, Mandel T, Reinhardt D, Kuhlemeier C, Prusinkiewicz P. 2006. A plausible model of phyllotaxis. *PNAS* **103**, 1301-1306

5 - Feugier FG, Mochizuki A, Iwasa Y. 2005. Self-organization of the vascular system in plant leaves: inter-dependent dynamics of auxin flux and carrier proteins. *J Theor Biol.* **236**, 366-75

6 - Feugier FG, Iwasa Y. 2006. How canalization can make loops: A new model of reticulated leaf vascular pattern formation. *J Theor Biol.* **243**, 235-244

7 - Merks R.M.H., Van de Peer Y., Inze D., Beemster G.T.S. 2007. Canalization without flux sensors: a traveling-wave hypothesis. *T.I.P.S.*. **12**, 384-390

8 – Swarup R., Kramer E.M., Perry P., Knox K., Ottoline Leyser H.M., Haseloff J., Beemster G.T.S., Bhalerao R., Bennett M.J.. 2005. Root gravitropism requires lateral root cap and epidermal cells for transport and response to a mobile auxin signal. *Nat. Cell Biol.* **7**, 1057-1065

APPENDIX 2

We will present here some specific achievements which were left aside from the main discussion for the sake of clarity.

Virtual Plants team visual identity

As an independent project, we designed the characteristic logo of the newly created Virtual Plants team, as well as the website iconography (Figure 47). The chosen logo represents the focus of the team on plants and their meristems. The various graphic files of this project are available on the DVD joined to this manuscript, under the /Media/VP_website directory. The website itself is accessible at the following internet address:

http://www-sop.inria.fr/virtualplants/wiki/doku.php

Growing roots iconography

We chose to focus part of our effort on the development of a set of high quality / high resolution pictures of roots growing *in vitro* (Figure 48). This iconography is to be made freely available with the release of our work, as an ongoing effort to promote exchanges of scientific illustration material. Samples from the picture set are available on the DVD joined to this manuscript, under the /Media/pictures/whole_root/ directory.

Radiophonic Interview

Our studies were presented during a short radiophonic interview for the radiophonic show "Surpris par la nuit". This interview was part of the "root episode" of a special series of emission themed on the underground, and was aired on the 15th of May 2008 on Radio France Culture.

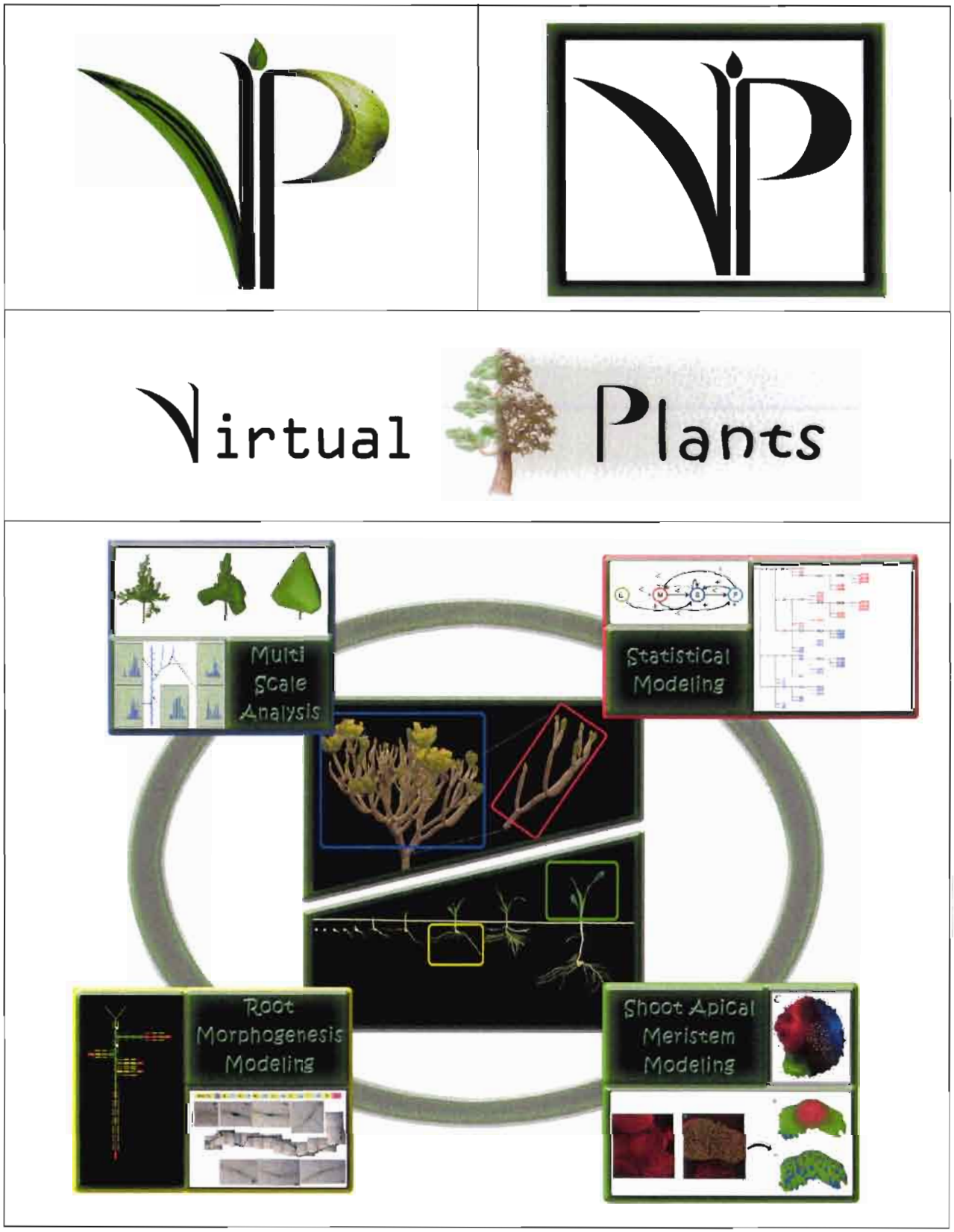

Figure 47. Virtual Plants iconography
The logo, its alternate version, the banner and the website iconography were all designed and created by yours truly.

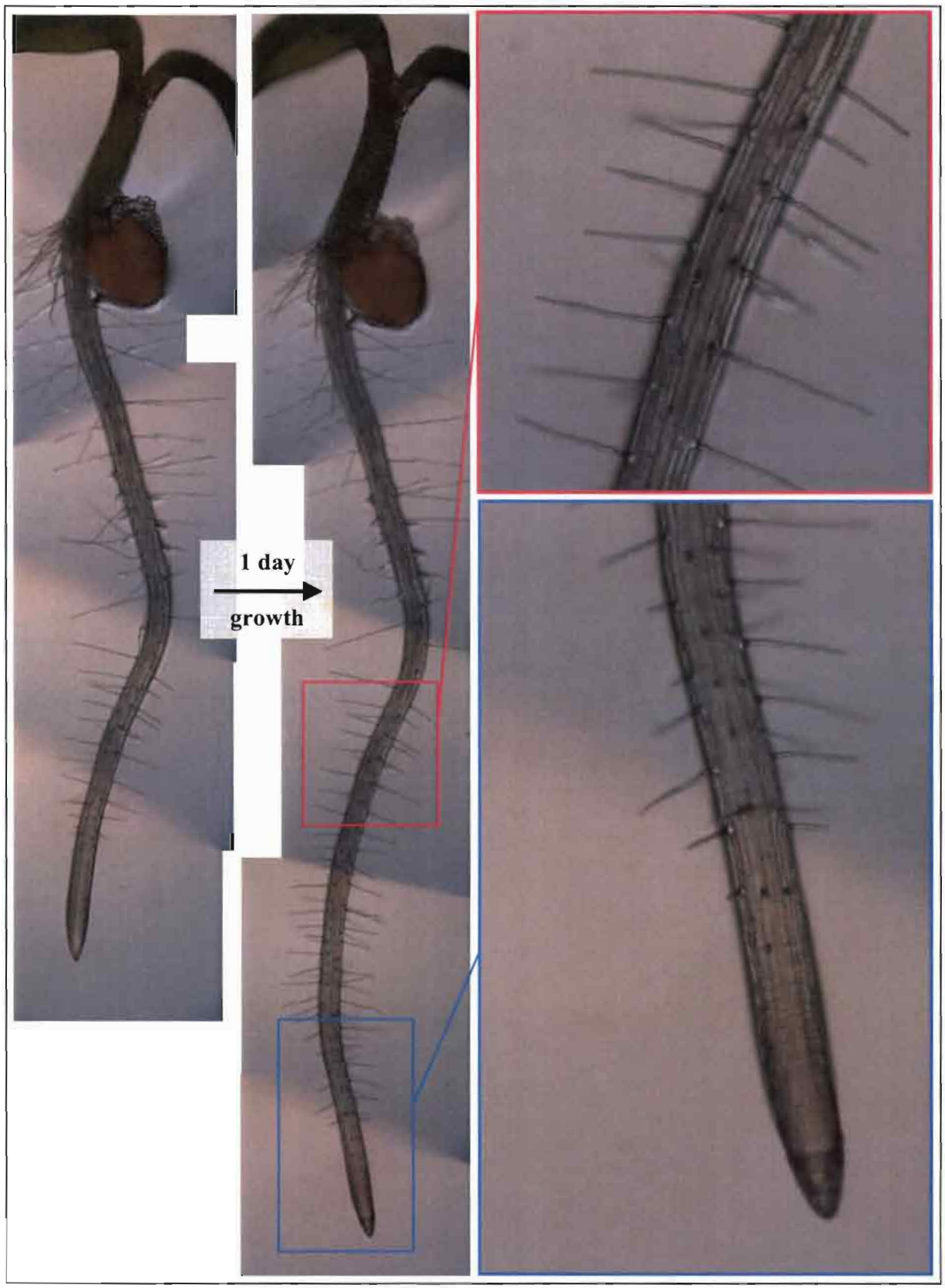

Figure 48. Sample of the high resolution root images database
Pictures were taken in optical microscopy, and fused using image processing software.

BIBLIOGRAPHIE

Abas, Lindy, René Benjamins, Nenad Malenica, et al. 2006. Intracellular trafficking and proteolysis of the Arabidopsis auxin-efflux facilitator PIN2 are involved in root gravitropism. *Nature cell biology* 8, no. 3 (March): 249-56.

Abelson, H, and A A diSessa. 1982. *Turtle geometry*. Cambridge, UK: MIT Press.

Bartel, Bonnie. 1997. AUXIN BIOSYNTHESIS. *Annual review of plant physiology and plant molecular biology* 48 (June): 51-66. doi:15012256.

Benfey, Philip, and Ben Scheres. 2000. Root development. *Current biology : CB* 10, no. 22 (November 16): R813-5.

Benková, Eva, Marta Michniewicz, Michael Sauer, et al. 2003. Local, efflux-dependent auxin gradients as a common module for plant organ formation. *Cell* 115, no. 5 (November 26): 591-602.

Bennett, Malcolm J, Alan Marchant, H G Green, et al. 1996. Arabidopsis AUX1 gene: a permease-like regulator of root gravitropism. *Science (New York, N.Y.)* 273, no. 5277 (August 16): 948-50.

van den Berg, Claudia, Peter Weisbeek, and Ben Scheres. 1998. Cell fate and cell differentiation status in the Arabidopsis root. *Planta* 205, no. 4 (August): 483-91. doi:9684353.

van den Berg, Claudia, Viola Willemsen, Willem Hage, Peter Weisbeek, and Ben Scheres. 1995. Cell fate in the Arabidopsis root meristem determined by directional signalling. *Nature* 378, no. 6552 (November 2): 62-65. doi:10.1038/378062a0.

van den Berg, Claudia, Viola Willemsen, Giel Hendriks, Peter Weisbeek, and Ben Scheres. 1997. Short-range control of cell differentiation in the Arabidopsis root meristem. *Nature* 390, no. 6657 (November 20): 287-289. doi:10.1038/36856.

Berger, Fred, Jim Haseloff, John Schiefelbein, and Liam Dolan. 1998. Positional information in root epidermis is defined during embryogenesis and acts in

domains with strict boundaries. *Current Biology* 8, no. 8 (April 9): 421-430. doi:10.1016/S0960-9822(98)70176-9.

Besseau, Sébastien, Laurent Hoffmann, Pierrette Geoffroy, et al. 2007. Flavonoid accumulation in Arabidopsis repressed in lignin synthesis affects auxin transport and plant growth. *The Plant cell* 19, no. 1 (January): 148-62. doi:tpc.106.044495.

Bhalerao, Rishikesh P, Jan Eklöf, Karin Ljung, et al. 2002. Shoot-derived auxin is essential for early lateral root emergence in Arabidopsis seedlings. *The Plant journal : for cell and molecular biology* 29, no. 3 (February): 325-32. doi:11844109.

Blilou, Ikram, Jian Xu, Marjolein Wildwater, et al. 2005. The PIN auxin efflux facilitator network controls growth and patterning in Arabidopsis roots. *Nature* 433, no. 7021 (January 6): 39-44.

Brown, D E, A M Rashotte, A S Murphy, et al. 2001. Flavonoids act as negative regulators of auxin transport in vivo in arabidopsis. *Plant physiology* 126, no. 2 (June): 524-35. doi:11402184.

Casimiro, Ilda, Tom Beeckman, Neil Graham, et al. 2003. Dissecting Arabidopsis lateral root development. *Trends in plant science* 8, no. 4 (April): 165-71.

Casimiro, Ilda, Alan Marchant, Rishikesh P Bhalerao, et al. 2001. Auxin transport promotes Arabidopsis lateral root initiation. *The Plant cell* 13, no. 4 (April): 843-52.

Celenza, John, P Grisafi, and Gerald R Fink. 1995. A pathway for lateral root formation in Arabidopsis thaliana. *Genes & development* 9, no. 17 (September 1): 2131-42.

Chen, Rujin, P Hilson, J Sedbrook, et al. 1998. The arabidopsis thaliana AGRAVITROPIC 1 gene encodes a component of the polar-auxin-transport efflux carrier. *Proceedings of the National Academy of Sciences of the United States of America* 95, no. 25 (December 8): 15112-7. doi:9844024.

Cholodny, N.G. 1927. Wuchshormone und Tropismen bei Den Pflanzen. *Biologisches Zentralblatt* 47: 604– 626.

Chomsky, Noam. 1956. Three models for the description of language. *IRE Trans. on Information Theory* 2: 113-124.

Ciesielski, Theophil. 1872. Untersuchungen über die Abwärtskrümmung der Wurzel. *Beitrage zur Biologie der Pflanzen* 1: 1–30.

Costes, E, E García-Villanueva, C Jourdan, J L Regnard, and Y Guédon. 2006. Co-ordinated growth between aerial and root systems in young apple plants issued from in vitro culture. *Annals of botany* 97, no. 1 (January): 85-96. doi:mcj003.

Covington, Michael F, and Stacey L Harmer. 2007. The circadian clock regulates auxin signaling and responses in Arabidopsis. *PLoS biology* 5, no. 8 (August): e222. doi:06-PLBI-RA-0645.

Darwin , C, and G Darwin . 1880. *The power of movement in plants.* New York, USA: Appleton-Century Inc.

Davies , P J. 1995. *Plant hormones: Physiology, biochemistry and molecular biology* . ed. Davies P.J. Dordrecht, The Netherlands: Kluwer Academic Publishers.

Davies , P J, and E K Mitchell. 1972. Transport of indoleacetic acid in intact roots of Phaseolus coccineus. *Planta* 105: 139-154.

De Koster, C G, and Aristid Lindenmayer. 1987. Discrete and continuous models for heterocyst difference in growing filaments of blue-green bacteria. *Acta Biotheorica* 36: 247-273.

De Smet, Ive, Takuya Tetsumura, Bert De Rybel, et al. 2007. Auxin-dependent regulation of lateral root positioning in the basal meristem of Arabidopsis. *Development (Cambridge, England)* 134, no. 4 (February): 681-90.

De Smet, Ive, Steffen Vanneste, Dirk Inzé, and Tom Beeckman. 2006. Lateral root initiation or the birth of a new meristem. *Plant molecular biology* 60, no. 6 (April): 871-87.

Delker, Carolin, Anja Raschke, and Marcel Quint. 2008. Auxin dynamics: the dazzling complexity of a small molecule's message. *Planta* 227, no. 5 (April): 929-41. doi:10.1007/s00425-008-0710-8.

Dolan, Liam, K Janmaat, V Willemsen, et al. 1993. Cellular organisation of the Arabidopsis thaliana root. *Development (Cambridge, England)* 119, no. 1 (September): 71-84.

Douady, and Couder. 1992. Phyllotaxis as a physical self-organized growth process. *PHYSICAL REVIEW LETTERS* 68, no. 13 (March 30): 2098-2101.

Drew, M.C. 1975. Comparison of the effects of a localized supply of phosphate, nitrate, ammonium and potassium. . *New Phytol.*, no. 75: 479-490.

Dubrovsky, J G, Peter Doerner, A Colón-Carmona, and T L Rost. 2000. Pericycle cell proliferation and lateral root initiation in Arabidopsis. *Plant physiology* 124, no. 4 (December): 1648-57.

Dubrovsky, J G, G A Gambetta, A Hernández-Barrera, S Shishkova, and I González. 2006. Lateral root initiation in Arabidopsis: developmental window, spatial patterning, density and predictability. *Annals of botany* 97, no. 5 (May): 903-15.

Dubrovsky, J G, T L Rost, A Colón-Carmona, and Peter Doerner. 2001. Early primordium morphogenesis during lateral root initiation in Arabidopsis thaliana. *Planta* 214, no. 1 (November): 30-6. doi:11762168.

Feugier, Francois G, Atsushi Mochizuki, and Yoh Iwasa. 2005. Self-organization of the vascular system in plant leaves: inter-dependent dynamics of auxin flux and carrier proteins. *Journal of theoretical biology* 236, no. 4 (October 21): 366-75. doi:S0022-5193(05)00126-8.

Feugier, François G, and Yoh Iwasa. 2006. How canalization can make loops: a new model of reticulated leaf vascular pattern formation. *Journal of theoretical biology* 243, no. 2 (November 21): 235-44. doi:S0022-5193(06)00220-7.

Fortin, M C, F J Pierce, and K L Poff. 1989. The pattern of secondary root formation in curving roots of Arabidopsis thaliana (L.) Heynh. *Plant, cell & environment* 12: 337-9. doi:11539812.

Friml, Jirí, Anne Vieten, Michael Sauer, et al. 2003. Efflux-dependent auxin gradients establish the apical-basal axis of Arabidopsis. *Nature* 426, no. 6963 (November 13): 147-53.

Friml, Jirí, Justyna Wiśniewska, Eva Benková, Kurt Mendgen, and Klaus Palme. 2002. Lateral relocation of auxin efflux regulator PIN3 mediates tropism in Arabidopsis. *Nature* 415, no. 6873 (February 14): 806-9.

Friml, Jirí, Xiong Yang, Marta Michniewicz, et al. 2004. A PINOID-dependent binary switch in apical-basal PIN polar targeting directs auxin efflux. *Science (New York, N.Y.)* 306, no. 5697 (October 29): 862-5.

Gälweiler, L, C Guan, A Müller, et al. 1998. Regulation of polar auxin transport by AtPIN1 in Arabidopsis vascular tissue. *Science (New York, N.Y.)* 282, no. 5397 (December 18): 2226-30. doi:9856939.

Gardner, M. 1970. Mathematical games: The fantastic combinations of John Conway's new solitaire game "life". *Scientific American* 223: 120-123.

---. 1971. Mathematical games: On cellular automata, self-reproduction, the Garden of Eden and the game "life". *Scientific American* 224: 112-117.

Geldner, Niko, Jirí Friml, York-Dieter Stierhof, Gerd Jürgens, and Klaus Palme. 2001. Auxin transport inhibitors block PIN1 cycling and vesicle trafficking. *Nature* 413, no. 6854 (September 27): 425-8. doi:11574889.

Giavitto, Jean-Louis. 2003. Collections, Transformations and their Application to the

Modeling and the Simulation of Dynamical Systems. In *RTA '03, 14th International Conference on Rewriting Techniques and Applications*. Valencia, Spain.

Giavitto, Jean-Louis, and Olivier Michel. 2003. Modeling the topological organization of cellular processes. *Bio Systems* 70, no. 2 (July): 149-63. doi:12915272.

Grieneisen, Verônica A, Jian Xu, Athanasius F M Marée, Paulien Hogeweg, and Ben Scheres. 2007. Auxin transport is sufficient to generate a maximum and gradient guiding root growth. *Nature* 449, no. 7165 (October 25): 1008-13. doi:nature06215.

Guilfoyle, Tom. 2007. Plant biology: sticking with auxin. *Nature* 446, no. 7136 (April 5): 621-2.

Guilfoyle, Tom, G Hagen, T Ulmasov, and Jane Murfett. 1998. How does auxin turn on genes? *Plant physiology* 118, no. 2 (October): 341-7. doi:9765520.

Guilfoyle, Tom, T Ulmasov, and G Hagen. 1998. The ARF family of transcription factors and their role in plant hormone-responsive

transcription. *Cellular and molecular life sciences : CMLS* 54, no. 7 (July): 619-27. doi:9711229.

Hallé, Francis, and R.A.A Oldeman. 1970. *Essai sur l'architecture et dynamique de la croissance des arbres tropicaux.* Paris: Masson and Co.

Hanan, James. 1992. Parametric L-systems and Their Application To the Modelling and Visualization of Plants. Ph. D. dissertation, University of Regina, June. http://algorithmicbotany.org/papers/hanan.dis1992.html.

Hangarter, R P. 1997. Gravity, light and plant form. *Plant, cell & environment* 20, no. 6 (June): 796-800.

Herman, G T, and G Rozenberg. 1975. *Developmental systems and languages.* North-Holland, Amsterdam.

Hodge, A. 2006. Plastic plants and patchy soils. *Journal of experimental botany* 57, no. 2: 401-11. doi:eri280.

Hofmeiester, wilhelm. 1868. Allgemeine morphologie der gewachse. In *Handbuch der Physiologischen botanik*, 2: W. hofmeister. Leipzig: W. Engelmann.

Imlau, A., E. Truernit, and N. Sauer. 1999. Cell-to-cell and long-distance trafficking of the green fluorescent protein in the phloem and symplastic unloading of the protein into sink tissues. *Plant Cell* 11, no. 3: 309-22.

Ivanchenko, Maria G, Gloria K Muday, and Joseph G Dubrovsky. 2008. Ethylene-auxin interactions regulate lateral root initiation and emergence in Arabidopsis thaliana. *The Plant journal : for cell and molecular biology* (April 24). doi:TPJ3528.

Jones, A M. 1998. Auxin transport: down and out and up again. *Science (New York, N.Y.)* 282, no. 5397 (December 18): 2201-3.

Jönsson, Henrik, Marcus G Heisler, Bruce E Shapiro, Elliot M Meyerowitz, and Eric Mjolsness. 2006. An auxin-driven polarized transport model for phyllotaxis. *Proceedings of the National Academy of Sciences of the United States of America* 103, no. 5 (January 31): 1633-8.

von Koch, H. 1905. Une méthode géométrique élémentaire pour l'étude de certaines questions de la théorie des courbes planes. *Acta mathematica* 30: 145-174.

Kramer, Eric M. 2001. A mathematical model of auxin-mediated radial growth in trees. *Journal of theoretical biology* 208, no. 4 (February 21): 387-97. doi:11222044.

---. 2002. A mathematical model of pattern formation in the vascular cambium of trees. *Journal of theoretical biology* 216, no. 2 (May 21): 147-58.

---. 2006. How far can a molecule of weak acid travel in the apoplast or xylem? *Plant physiology* 141, no. 4 (August): 1233-6.

---. 2007. Computer models of auxin transport: a review and commentary. *J Exp Bot* (April 12).

---. 2008. Computer models of auxin transport: a review and commentary. *Journal of experimental botany* 59, no. 1: 45-53. doi:erm060.

Kramer, Eric M, and Malcolm J Bennett. 2006. Auxin transport: a field in flux. *Trends in plant science* 11, no. 8 (August): 382-6.

Kramer, Eric M, Nicholas L Frazer, and Tobias I Baskin. 2007. Measurement of diffusion within the cell wall in living roots of Arabidopsis thaliana. *Journal of experimental botany* 58, no. 11: 3005-15. doi:erm155.

Kuderová, Alena, Ivana Urbánková, Martina Válková, et al. 2008. Effects of conditional IPT-dependent cytokinin overproduction on root architecture of Arabidopsis seedlings. *Plant & cell physiology* 49, no. 4 (April): 570-82. doi:pcn029.

Laplaze, Laurent, Eva Benkova, Ilda Casimiro, et al. 2007. Cytokinins act directly on lateral root founder cells to inhibit root initiation. *The Plant cell* 19, no. 12 (December): 3889-900. doi:tpc.107.055863.

Laskowski, M J, M E Williams, H C Nusbaum, and I M Sussex. 1995. Formation of lateral root meristems is a two-stage process. *Development (Cambridge, England)* 121, no. 10 (October): 3303-10.

Leyser, Ottoline. 2005. Auxin distribution and plant pattern formation: how many angels can dance on the point of PIN? *Cell* 121, no. 6 (June 17): 819-22.

---. 2006. Dynamic integration of auxin transport and signalling. *Current biology : CB* 16, no. 11 (June 6): R424-33.

Lindenmayer, Aristid. 1968. Mathematical models for cellular interaction in development. *Journal of Theoretical Biology* 18: 280-315.

---. 1971. Developmental systems without cellular interaction, their languages and grammars. *Journal of Theoretical Biology* 30: 455-484.

Ljung, Karin, Rishikesh P Bhalerao, and Göran K Sandberg. 2001. Sites and homeostatic control of auxin biosynthesis in Arabidopsis during vegetative growth. *The Plant journal : for cell and molecular biology* 28, no. 4 (November): 465-74. doi:11737783.

Ljung, Karin, Anna K Hull, John Celenza, et al. 2005. Sites and regulation of auxin biosynthesis in Arabidopsis roots. *The Plant cell* 17, no. 4 (April): 1090-104.

Lomax, T L, Gloria K Muday, and P H Rubery . 1995. Auxin transport. In *Plant hormones.*, 509–530. Davies PJ, Ed. Dordrecht: Kluwer.

Lucas, Mikaël, Christophe Godin, Christian Jay-Allemand, and Laurent Laplaze. 2008. Auxin fluxes in the root apex co-regulate gravitropism and lateral root initiation. *J. Exp. Bot.* (January): erm171. doi:10.1093/jxb/erm171.

Ludwig-Müller, Jutta. 2000. Indole-3-butyric acid in plant growth and development. *Plant Growth Regulation* 32, no. 2 (November 1): 219-230. doi:10.1023/A:1010746806891.

Luschnig, Christian, R A Gaxiola, P Grisafi, and Gerald R Fink. 1998. EIR1, a root-specific protein involved in auxin transport, is required for gravitropism in Arabidopsis thaliana. *Genes & development* 12, no. 14 (July 15): 2175-87. doi:9679062.

Malamy, Jocelyn, and Philip Benfey. 1997. Organization and cell differentiation in lateral roots of Arabidopsis thaliana. *Development (Cambridge, England)* 124, no. 1 (January): 33-44. doi:9006065.

Malamy, Jocelyn, and Katherine S Ryan. 2001. Environmental Regulation of Lateral Root Initiation in Arabidopsis. *Plant Physiol.* 127, no. 3 (November 1): 899-909. doi:10.1104/pp.010406.

Mandelbrot, B B. 1982. *The fractal geometry of nature.* San Francisco: W. H. Freeman.

Marchant, Alan, Rishikesh Bhalerao, Ilda Casimiro, et al. 2002. AUX1 promotes lateral root formation by facilitating indole-3-acetic acid distribution between sink and source tissues in the Arabidopsis seedling. *The Plant cell* 14, no. 3 (March): 589-97.

Mattsson, J, Z R Sung, and Thomas Berleth. 1999. Responses of plant vascular systems to auxin transport inhibition. *Development (Cambridge, England)* 126, no. 13 (July): 2979-91. doi:10357941.

Merks, Roeland M H, Yves Van de Peer, Dirk Inzé, and Gerrit T S Beemster. 2007. Canalization without flux sensors: a traveling-wave hypothesis. *Trends in plant science* 12, no. 9 (September): 384-90. doi:S1360-1385(07)00183-5.

Mitchison, G J. 1980. A model for vein formation inhigher plants. *Proceedings of the Royal Society B: Biological Sciences* 207: 79-109.

---. 1981. The polar transport of auxin and vein patterns in plants. . *Philosophical Transactions of the Royal Society B: Biological Sciences* 295: 461-471.

Moore, Ian. 2002. Gravitropism: lateral thinking in auxin transport. *Current biology : CB* 12, no. 13 (July 9): R452-4.

Müller, A, C Guan, L Gälweiler, et al. 1998. AtPIN2 defines a locus of Arabidopsis for root gravitropism control. *The EMBO journal* 17, no. 23 (December 1): 6903-11.

Murphy, A, W A Peer, and L Taiz. 2000. Regulation of auxin transport by aminopeptidases and endogenous flavonoids. *Planta* 211, no. 3 (August): 315-24. doi:10987549.

Negi, Sangeeta, Maria G Ivanchenko, and Gloria K Muday. 2008. Ethylene regulates lateral root formation and auxin transport in Arabidopsis thaliana. *The Plant journal : for cell and molecular biology* (May 20). doi:TPJ3495.

Nordström, Anders, Petr Tarkowski, Danuse Tarkowska, et al. 2004. Auxin regulation of cytokinin biosynthesis in Arabidopsis thaliana: a factor of potential importance for auxin-cytokinin-regulated development. *Proceedings of the National Academy of Sciences of the United States of America* 101, no. 21 (May 25): 8039-44. doi:15146070.

Okada, K., J. Ueda, M. K. Komaki, C. J. Bell, and Y. Shimura. 1991. Requirement of the Auxin Polar Transport System in Early Stages of Arabidopsis Floral Bud Formation. *The Plant cell* 3, no. 7 (July): 677-684. doi:12324609.

Okushima, Yoko, Hidehiro Fukaki, Makoto Onoda, Athanasios Theologis, and Masao Tasaka. 2007. ARF7 and ARF19 regulate lateral root formation

via direct activation of LBD/ASL genes in Arabidopsis. *The Plant cell* 19, no. 1 (January): 118-30.

Oparka, Karl J. 2005. *Plasmodesmata*. Blackwell Pub Professional.

Ottenschläger, Iris, Patricia Wolff, Chris Wolverton, et al. 2003. Gravity-regulated differential auxin transport from columella to lateral root cap cells. *Proceedings of the National Academy of Sciences of the United States of America* 100, no. 5 (March 4): 2987-91. doi:12594336.

Paciorek, Tomasz, Eva Zazímalová, Nadia Ruthardt, et al. 2005. Auxin inhibits endocytosis and promotes its own efflux from cells. *Nature* 435, no. 7046 (June 30): 1251-6.

Paponov, Ivan A, William D Teale, Martina Trebar, Ikram Blilou, and Klaus Palme. 2005. The PIN auxin efflux facilitators: evolutionary and functional perspectives. *Trends in plant science* 10, no. 4 (April): 170-7.

Perrin, Robyn M, Li-Sen Young, Narayana Murthy U M, et al. 2005. Gravity signal transduction in primary roots. *Annals of botany* 96, no. 5 (October): 737-43.

Pradal, Christophe, Frédéric Boudon, C Nouguier, Jérome Chopard, and Christophe Godin. 2008. PlantGL: a Python-based geometric librairy for 3D plant modelling at different scales. *Submitted to Graphical Model.*

Prusinkiewicz, Przemyslaw, Yvette Erasmus, Brendan Lane, Lawrence D Harder, and Enrico Coen. 2007. Evolution and development of inflorescence architectures. *Science (New York, N.Y.)* 316, no. 5830 (June 8): 1452-6. doi:1140429.

Prusinkiewicz, Przemyslaw, M Hammel, James Hanan, and R Měch. 1996. L-systems: from the theory to visual models of plants. In *Machine Graphic and Vision 5*, 365-392.

Prusinkiewicz, Przemyslaw, and Aristid Lindenmayer. 1990. *The Algorithmic Beauty of Plants*. Springer-Verlag.

Prusinkiewicz, Przemyslaw , and William R Remphrey. 2000. Characterization of architectural tree models using L−systems and Petri nets. In *L'arbre − The Tree 2000: Papers presented at the 4th International Symposium on the tree*, pp. 177−186. M. Labrecque (Ed.). http://www.cas.muohio.edu/~meicenrd/mudescd/Xidw/TreeForm/catm.tree2000.pdf.

Radoslaw, Karwowski. 2002. Improving the Process of Plant Modeling: The L+C Modeling Language. University of Calgary.

Reed, R C, S R Brady, and G K Muday. 1998. Inhibition of auxin movement from the shoot into the root inhibits lateral root development in Arabidopsis. *Plant physiology* 118, no. 4 (December): 1369-78. doi:9847111.

Reinhardt, D, T Mandel, and C Kuhlemeier. 2000. Auxin regulates the initiation and radial position of plant lateral organs. *The Plant cell* 12, no. 4 (April): 507-18.

Reinhardt, Didier, Eva-Rachele Pesce, Pia Stieger, et al. 2003. Regulation of phyllotaxis by polar auxin transport. *Nature* 426, no. 6964 (November 20): 255-60.

de Reuille, Pierre Barbier, Isabelle Bohn-Courseau, Christophe Godin, and Jan Traas. 2005. A protocol to analyse cellular dynamics during plant development. *The Plant journal : for cell and molecular biology* 44, no. 6 (December): 1045-53. doi:TPJ2576.

de Reuille, Pierre Barbier, Isabelle Bohn-Courseau, Karin Ljung, et al. 2006. Computer simulations reveal properties of the cell-cell signaling network at the shoot apex in Arabidopsis. *Proceedings of the National Academy of Sciences of the United States of America* 103, no. 5 (January 31): 1627-32.

Robinson. 1994. The response of plants to non-uniform supplies of nutrient. . *New Phytol.*, no. 127: 635-674.

Rolland-Lagan, Anne-Gaëlle, and Przemyslaw Prusinkiewicz. 2005. Reviewing models of auxin canalization in the context of leaf vein pattern formation in Arabidopsis. *The Plant journal : for cell and molecular biology* 44, no. 5 (December): 854-65.

Rozenberg, G, and A Salomaa. 1980. *The mathematical theory of L systems.* New York, USA: Academic Press.

Rubery, P H, and A R Sheldrakke. 1974. carrier-mediated auxin transport. *Planta* 118: 101-121.

Sabatini, Sabrina, Dimitris Beis, Harald Wolkenfelt, et al. 1999. An Auxin-Dependent Distal Organizer of Pattern and Polarity in the Arabidopsis

Root. *Cell* 99, no. 5 (November 24): 463-472. doi:10.1016/S0092-8674(00)81535-4.

Sachs, T. 1969. Polarity and the Induction of Organized Vascular Tissues. *Ann Bot* 33, no. 2 (March 1): 263-275.

---. 1984. Axiality and polarity in vascular plants. In *Positional Controls in Plant Development*, 193-224. PW Barlow, DJ Carr, eds. Cambridge, UK: Cambridge University Press.

Sack, F D, and J Z Kiss. 1989. Rootcap structure in wild type and in starchless mutant of Arabidopsis. *American Journal of Botany* 76, no. 3: 454-64.

Salisbury, Frances J, Anthony Hall, Claire S Grierson, and Karen J Halliday. 2007. Phytochrome coordinates Arabidopsis shoot and root development. *The Plant journal : for cell and molecular biology* 50, no. 3 (May): 429-38.

Salomaa, A. 1973. *Formal languages*. New York, USA: Academic Press.

Sauer, Jozef Balla, Christian Luschnig, et al. 2006. Canalization of auxin flow by Aux/IAA-ARF-dependent feedback regulation of PIN polarity. *Genes & development* 20, no. 20 (October 15): 2902-11.

Scheres, Ben, Philip Benfey, and Liam Dolan. 2000. *The Arabidopsis Book*. http://www.bioone.org/perlserv/?request=get-document&doi=10.1199%2Ftab.0101.

Scheres, Ben, H Wolkenfelt, Viola Willemsen, et al. 1994. Embryonic origin of the Arabidopsis primary root and root meristem initials. *Development*, no. 120: pp. 2475-2487.

Scheres, Ben, and Jian Xu. 2006. Polar auxin transport and patterning: grow with the flow. *Genes & development* 20, no. 8 (April 15): 922-6.

Schiefelbein, John, and Philip Benfey. 1991. The development of plant roots: new approaches to underground problems. *The Plant Cell* 3, no. 11 (November).

Scott, T K, and M B Wilkins. 1969. Auxin Transport in roots. Effects of light on IAA movement and geotropic response in Zea roots. *Planta*.

Skoog, Folke, and Kenneth V Thimann. 1934. FURTHER EXPERIMENTS ON THE INHIBITION OF THE DEVELOPMENT OF LATERAL BUDS BY GROWTH HORMONE. *Proceedings of the National Academy of Sciences* (July 2).

Smith, Richard S, Soazig Guyomarc'h, Therese Mandel, et al. 2006. A plausible model of phyllotaxis. *Proceedings of the National Academy of Sciences of the United States of America* 103, no. 5 (January 31): 1301-6.

Snow, M, and R Snow. 1962. A Theory of the regulation of phyllotaxis based on Lupinus albus. *Philosophical Transactions of the Royal Society of London* 244: 483-513.

Stieger, Pia A, Didier Reinhardt, and Cris Kuhlemeier. 2002. The auxin influx carrier is essential for correct leaf positioning. *The Plant journal : for cell and molecular biology* 32, no. 4 (November): 509-17. doi:12445122.

Swarup, Ranjan, and Malcolm Bennett. 2003. Auxin transport: the fountain of life in plants? *Developmental cell* 5, no. 6 (December): 824-6.

Swarup, Ranjan, Jirí Friml, Alan Marchant, et al. 2001. Localization of the auxin permease AUX1 suggests two functionally distinct hormone transport pathways operate in the Arabidopsis root apex. *Genes & development* 15, no. 20 (October 15): 2648-53.

Swarup, Ranjan, Joanna Kargul, Alan Marchant, et al. 2004. Structure-function analysis of the presumptive Arabidopsis auxin permease AUX1. *The Plant cell* 16, no. 11 (November): 3069-83.

Swarup, Ranjan, Eric M Kramer, Paula Perry, et al. 2005. Root gravitropism requires lateral root cap and epidermal cells for transport and response to a mobile auxin signal. *Nature cell biology* 7, no. 11 (November): 1057-65.

Swarup, Ranjan, Alan Marchant, and Malcolm J Bennett. 2000. Auxin transport: providing a sense of direction during plant development. *Biochemical Society transactions* 28, no. 4: 481-5.

Tan, Xu, Luz Irina A Calderon-Villalobos, Michal Sharon, et al. 2007. Mechanism of auxin perception by the TIR1 ubiquitin ligase. *Nature* 446, no. 7136 (April 5): 640-5.

Tanaka, H, P Dhonukshe, P B Brewer, and Jirí Friml. 2006. Spatiotemporal asymmetric auxin distribution: a means to coordinate plant development. *Cellular and molecular life sciences : CMLS* 63, no. 23 (December): 2738-54. doi:10.1007/s00018-006-6116-5.

The Arabidopsis Genome Initiative. 2000. Analysis of the genome sequence of the flowering plant Arabidopsis thaliana. *Nature* 408, no. 6814 (December 14): 796-815. doi:10.1038/35048692.

Thimann, Kenneth V. 1948. Plant Growth Hormones. In *The hormones*, 1: Pincus G, Thimann K, eds. New York, USA: Academic Press.

---. 1977. *Hormone action in the whole life of plants.* The University of Massachusetts Press. Amherst, MA.

Tsurumi, Seiji, and Y Ohwaki. 1978. Transport of 14C-labeled indoleacetic acid in Vicia root segments. *The Plant cell physiology* 19: 1195-1206.

Ulmasov, T, J Murfett, G Hagen, and Tom Guilfoyle. 1997. Aux/IAA proteins repress expression of reporter genes containing natural and highly active synthetic auxin response elements. *The Plant cell* 9, no. 11 (November): 1963-71. doi:9401121.

Utsuno, K, T Shikanai, Y Yamada, and T Hashimoto. 1998. Agr, an Agravitropic locus of Arabidopsis thaliana, encodes a novel membrane-protein family member. *Plant & cell physiology* 39, no. 10 (October): 1111-8. doi:9871369.

Vieten, Anne, Michael Sauer, Philip B Brewer, and Jirí Friml. 2007. Molecular and cellular aspects of auxin-transport-mediated development. *Trends in plant science* 12, no. 4 (April): 160-8.

Vieten, Anne, Steffen Vanneste, Justyna Wisniewska, et al. 2005. Functional redundancy of PIN proteins is accompanied by auxin-dependent cross-regulation of PIN expression. *Development (Cambridge, England)* 132, no. 20 (October): 4521-31.

Weyers, Jonathan D. B., Neil W. Paterson, Richard A'brook, and Zhi-Yong Peng. 1995. Quantitative Analysis of the Control of Physiological Phenomena by Plant Hormones. *Physiologia Plantarum* 95, no. 3 (March): 486-494. doi:10.1111/j.1399-3054.1995.tb00867.x.

Wisniewska, Justyna, Jian Xu, Daniela Seifertová, et al. 2006. Polar PIN localization directs auxin flow in plants. *Science (New York, N.Y.)* 312, no. 5775 (May 12): 883.

Wolfram, S. 1984. Computer software in science and mathematics. *Scientific American* 251: 188-203.

---. 1985. Some recent results and questions about cellular automata. In *Dynamical systems and cellular automata,*, 153-167. J. Demongeot, E. Goles, and M. Tchuente. London: Academic Press.

Woodward, Andrew W, and Bonnie Bartel. 2005. Auxin: regulation, action, and interaction. *Annals of botany* 95, no. 5 (April): 707-35.

Zhang, Hanma, and Brian G Forde. 2000. Regulation of Arabidopsis root development by nitrate availability. *J. Exp. Bot.* 51, no. 342 (January 1): 51-59. doi:10.1093/jexbot/51.342.51.

Zhang, Hanma, Andrea Jennings, Peter W Barlow, and Brian G Forde. 1999. Dual pathways for regulation of root branching by nitrate. *Proceedings of the National Academy of Sciences of the United States of America* 96, no. 11 (May 25): 6529-34.

Zhao, Yunde. 2008. The role of local biosynthesis of auxin and cytokinin in plant development. *Current opinion in plant biology* 11, no. 1 (February): 16-22. doi:18409210.

RESUME en français

Les plantes dépendent de leur système racinaire pour leur ancrage au substrat et leur nutrition hydrique et minérale. La bonne réalisation de ces fonctions dépend fortement de l'architecture du système racinaire dans son ensemble. Dans la plante modèle *Arabidopsis thaliana*, la ramification racinaire est la résultante d'événements d'initiation et d'émergence de nouvelles racines latérales, et présente un fort lien avec l'hormone végétale auxine. Le déroulement des événements d'initiation et d'émergence est aujourd'hui bien décrit aux échelles moléculaire et cellulaire, mais peu de données sont disponibles pour expliciter la régulation globale de ces événements. A l'aide d'une approche mêlant biologie, analyse mathématique et modélisation informatique, cette thèse s'est attachée à élucider les mécanismes de régulation de ces événements chez *Arabidopsis*, afin de proposer une vue intégrée de la ramification racinaire. Nous avons montré que la graviperception et l'initiation des racines latérales sont régulés par un même flux d'auxine, et qu'une gravistimulation peut induire l'initiation d'une nouvelle racine latérale. Nous avons mis en évidence l'existence d'un équilibre entre initiation et émergence basé sur une compétition pour les ressources. Enfin, nous avons développé un modèle macroscopique et un modèle cellulaire de flux d'auxine dans la racine, et avons analysé les propriétés respectives de ces deux modèles.

TITRE en anglais

Auxin Fluxes and Root Ramification in Arabidopsis thaliana: Toward a Virtual Root

RESUME en anglais

Plants depend on their roots for anchorage and nutrition. The architecture of thc root system a key factor for these two functions. In the model plant *Arabidopsis thaliana*, root branching is the composition of events of initiation and emergence of new lateral roots. While individual events of initiation and emergence are well described at the cellular and molecular level in *Arabidopsis* and are known to be linked with the plant hormone auxin, little is known about the precise mechanisms regulating those events. Using an approach combining biology, mathematical analyses and computer modelling, this thesis project aimed to elucidate those mechanisms, and to propose an integrated view of root branching. We showed that lateral root initiation and graviperception are co-regulated by the same auxin fluxes, and that gravistimulation induced the formation of new lateral root primordia. We demonstrated that the developing primordia interact with the initiation system through resource competition, and that it exist a balance between initiation and emergence. Finally, we developed macroscopic and cellular models of auxin fluxes within the root, and analyzed the specific properties of those models.

DISCIPLINE
Biologie végétale intégrative, Modélisation mathématique et informatique

MOTS-CLES
Français : Arabidopsis, racine, auxine, modèlisation, gravitropisme
English: Arabidopsis, root, auxin, modelling, gravitropism

INTITULE ET ADRESSE DE L'U.F.R. OU DU LABORATOIRE :

Equipe VirtualPlants - INRIA, UMR DAP, TA40/02, Cirad, Avenue Agropolis 34398 Montpellier cedex 5, France
Equipe Rhizogenèse - IRD, UMR DIA-PC, 911 avenue Agropolis, 34394 Montpellier cedex 5, France